United States
Environmental Protection
Agency

Environmental Sciences Research
Laboratory
Research Triangle Park NC 27711

EPA-600/4-78-049
August 1978

Research and Development

EPA

Select Research Group in Air Pollution Meteorolgy

Third Progress Report

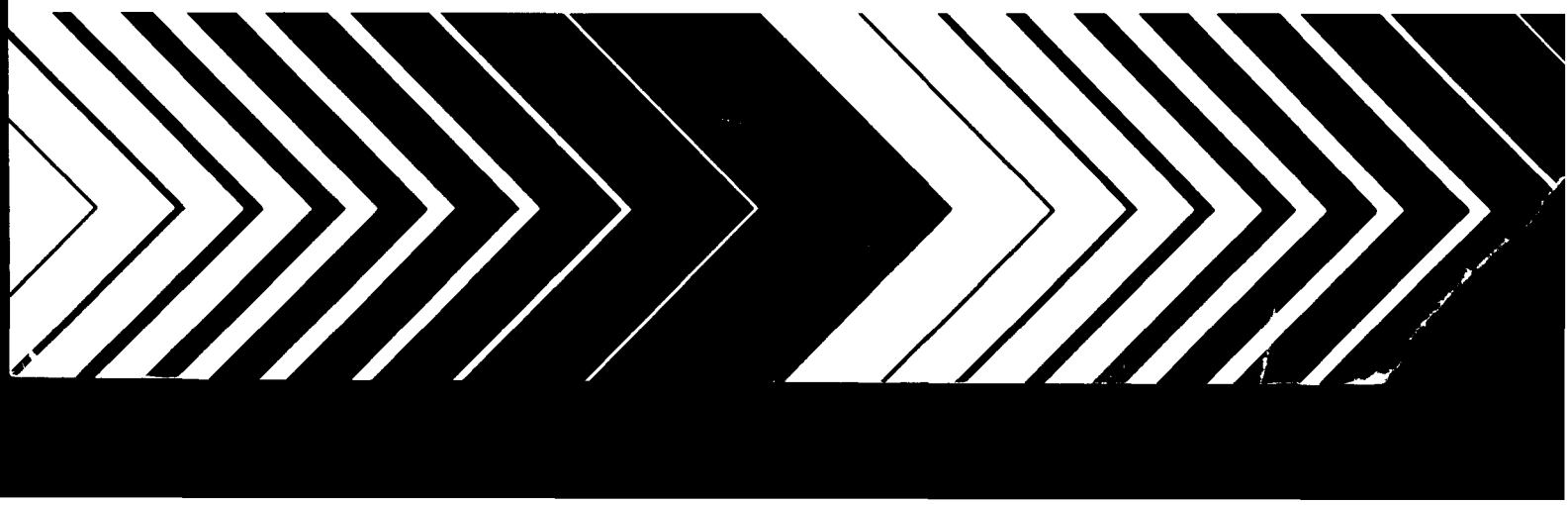

RESEARCH REPORTING SERIES

Research reports of the Office of Research and Development, U.S. Environmental Protection Agency, have been grouped into nine series These nine broad categories were established to facilitate further development and application of environmental technology Elimination of traditional grouping was consciously planned to foster technology transfer and a maximum interface in related fields The nine series are.

1 Environmental Health Effects Research
2 Environmental Protection Technology
3 Ecological Research
4. Environmental Monitoring
5 Socioeconomic Environmental Studies
6 Scientific and Technical Assessment Reports (STAR)
7 Interagency Energy-Environment Research and Development
8. "Special" Reports
9 Miscellaneous Reports

This report has been assigned to the ENVIRONMENTAL MONITORING series. This series describes research conducted to develop new or improved methods and instrumentation for the identification and quantification of environmental pollutants at the lowest conceivably significant concentrations It also includes studies to determine the ambient concentrations of pollutants in the environment and/or the variance of pollutants as a function of time or meteorological factors.

This document is available to the public through the National Technical Information Service, Springfield, Virginia 22161.

EPA-600/4-78-049
August 1978

SELECT RESEARCH GROUP IN AIR POLLUTION METEOROLOGY
THIRD ANNUAL PROGRESS REPORT

by

R. A. Anthes
A. K. Blackadar
R. L. Kabel
J. L. Lumley
H. Tennekes
D. W. Thomson

The Pennsylvania State University
University Park, Pennsylvania 16802

Grant No. R800397

Project Officer

Francis Binkowski
Meteorology Assessment Division
Environmental Sciences Research Laboratory
Research Triangle Park, North Carolina 27711

ENVIRONMENTAL SCIENCES RESEARCH LABORATORY
OFFICE OF RESEARCH AND DEVELOPMENT
U.S. ENVIRONMENTAL PROTECTION AGENCY
RESEARCH TRIANGLE PARK, NORTH CAROLINA 27711

DISCLAIMER

This report has been reviewed by the Environmental Sciences Research Laboratory, U.S. Environmental Protection Agency, and approved for publication. Approval does not signify that the contents necessarily reflect the views and policies of the U.S. Environmental Protection Agency, nor does mention of trade names or commercial products constitute endorsement or recommendation for use.

FOREWORD

The set of papers comprising this particular report by members of the Select Research Group (SRG) in Air Pollution Meteorology at the Pennsylvania State University was prepared at the request of K. Calder, the program's EPA project monitor.

After 3 years of research, the scientific results of the EPA-supported program at Penn State were clearly becoming evident in the air pollution meteorology research community. For example, at the Third Symposium on Atmospheric Turbulence, Diffusion and Air Quality held in Raleigh, North Carolina on 19-22 October 1976, ten scientific papers were presented by members of SRG. Numerous other publications are now in press or preparation for a variety of the regular air-pollution-related scientific journals.

Rather than duplicate publication of SRG's diverse scientific results, it was felt that the members would perform an important service by writing their views, principally in a review sense, on topics related to their project responsibilities. The following papers are the results of that exercise.

ABSTRACT

In lieu of a scientific report of the detailed investigations of the Select Research Group in Air Pollution Meteorology (SRG) (which are being published elsewhere), a series of reviews on topics of concern to SRG has been prepared at the request of the EPA scientific monitor. These reviews are presented in this report.

The overall problem of constructing a general, predictive air-quality model is considered in an article by R. A. Anthes. Emphasis is placed on the meteorological aspects of the modeling problem. A scale analysis of the pollutant conservation equation indicates that different physical processes are important on the urban, regional, and global scales of pollutant transport and diffusion. Therefore, different types of models are appropriate for these different scales. The physical and numerical aspects of predictive meteorological models on the regional scale are reviewed in detail. Next, some general classes of air pollution transport and diffusion models are discussed. Finally, an example of a simple combined meteorological air-quality model is given.

Most past attempts to model the distribution of meteorological quantities and mixing processes within the planetary boundary layer have featured a gradient- or K-type closure. A review of these closure specifications, particularly as they relate to the Richardson number, is given by A. K. Blackadar. The implications of second-order closure methods for K-type approximations are discussed, and a nocturnal boundary-layer model based on this approximation is presented.

H. Tennekes considers the question of how mixing-height variations affect the pollutant concentrations predicted by air-quality simulation models. It

is found that the variations of the mixing height have significant effects on the climatology of box models, and that the behavior of a box model during episodes of poor ventilation is modified profoundly by the amplitude of the diurnal cycle in the mixing height.

J. Lumley considers two types of urban air pollution models according to the way in which turbulent transport is simulated. It is shown that gradient transport models cannot predict the countergradient fluxes of heat and contaminants that are observed in convective situations. Second-order models are examined in detail, and recently raised questions regarding the accuracy requirements for these models are put to rest. The details and limitations of second-order models are discussed.

The importance of accounting for natural sources and sinks of atmospheric pollutants in air-quality simulation models is discussed by R. Kabel. Several removal processes are described and illustrated with examples from the literature. Emphasis is placed on those mechanisms active at the earth's surface. In particular, a brief evaluation of methods of predicting gas- and liquid-phase mass transfer coefficients for an atmosphere-water interface is attempted.

Alternative *in-situ* and remote-probing measurement techniques suitable for application to model validation studies are reviewed by D. W. Thomson. Locally applied inversion-rise, box, and Gaussian plume models may be verified using conventional micrometeorological measurements supplemented by acoustic sounder (sodar) observations. Definitive evaluation of urban- and regional-scale models will require a variety of special surface and aerological measurements.

CONTENTS

FIGURES

Number Page

HIGH-RESOLUTION MODELS OF THE PLANETARY BOUNDARY LAYER
A. K. Blackadar

TABLES

METEOROLOGICAL ASPECTS OF REGIONAL-SCALE AIR-QUALITY MONITORING

Richard A. Anthes
Department of Meteorology

INTRODUCTION

As urban industrial areas expand, air pollution problems extend farther from localized pollution sources and become regional, national, and even global in extent. The scientific, political, economic, and pathological aspects of large-scale pollution problems are enormously complex. Unlike local problems (in which those who do the polluting suffer diminished air quality), on the regional and larger scales individuals far downwind pay the price.

Besides the obvious economic, biological, and aesthetic penalties of increased regional pollution, the earth's climate may be vulnerable to increasing emissions of gases and particulates. One example is the documented (SMIC, 1971) increase in CO_2 over the last 20 years and the associated modifications to the global radiation balance. Another example currently receiving much attention is the emission of freon at the ground with subsequent diffusion to the stratosphere, where chlorine atoms formed by its photodissociation threaten the ozone layer (Basuk, 1975). On a smaller scale, there is growing concern that the use of cooling towers in giant energy parks may significantly affect the temperature, cloud cover, and precipitation for tens of kilometers around a site (Hanna and Gifford, 1975). Already, considerable evidence exists that warm-season rainfall is increased by as much as 30% within 50 km of major urban areas (Huff and Changnon, 1973; Semonin and Changnon, 1974). Harnack and Landsberg (1975) note cases wherein the urban thermal effect was the likely triggering mechanism for shower development over Washington, D.C.

The significance of possible changes to weather and climate and the association between decreasing air quality and increasing morbidity and mortality (e.g., Landsberg, 1969) demand quantitative studies of the fate of pollutants that have left a source. Such studies require models, since we wish to be able to predict future air quality from a given set of initial conditions, or to predict the outcome of a given pollution control strategy. Simply monitoring a given pollutant or atmospheric condition, while a necessary task in pollution control, does not permit predictions hours, days, or years in advance.

"Air-quality model" can describe many models of varying types and complexities. Even a qualitative assessment of meteorological conditions and their probable effect on pollutant transport and diffusion represents a simple model — an imprecise conceptual model built in the mind of the forecaster by prior experience. At the other end of the complexity scale, we can imagine an enormous mathematical, physical, and chemical model which predicts all scales of atmospheric motion affecting contaminant transport and diffusion (and the chemical reactions modifying each species). This model is well beyond our present scientific and computational skills. Still, there must be models that can provide acceptably accurate quantitative answers at reasonable cost.

This paper considers the overall regional-scale air-quality prediction problem and summarizes potential uses and limitations of various available mathematical models. Because the problem is very large, only a brief look at each modeling component is possible. (Many of the individual components are so complex as to deserve separate, detailed reviews.) After briefly enumerating some potential uses for accurate models, we discuss the general problem of forecasting the concentration of a contaminant at a given point. This forecast involves two major components: a meteorological model and a pollutant transport and diffusion model. The development of a realistic, predictive meteorological model is considered first. Modeling of pollutant transport and diffusion by the wind field is then discussed. A specific example (based on one aspect of current mesoscale modeling work at The Pennsylvania State University) of the combination of a time-dependent meteorological model and a transport and diffusion model to produce an air-quality model is presented.

POTENTIAL USES FOR PREDICTIVE AIR-QUALITY MODELS*

Before discussing the various types of air-quality models, it is useful to speculate on the potential uses of a truly predictive air-quality model — one which starts with an observed state of the atmosphere and, together with the proper boundary conditions (including known emission rates), accurately predicts the behavior of the pollutant in space and time. The question is not whether a perfect forecast of this type is possible; we know the answer to that question is no. The question is: How close, and at what cost, can we approach this ideal?

One of the most useful applications of a predictive air-quality model would be the prediction of the concentration of a particular pollutant at a receptor in order to provide a rational basis for an air pollution control strategy. Models for this purpose could be used in real time during air pollution episodes to regulate industrial and domestic uses of energy or on a long-term basis to study the consequences of proposed changes in pollutant emissions. Such a prediction on the regional scale demands an accurate accounting of contributions from possibly many sources upwind of the receptor. With the knowledge of a relative contribution from each source, the efficacy of a proposed control measure can be evaluated. An example of the use of an air-quality model to test particular emission control strategies for the New York City region is given by Slater (1974).

A second application of air-quality models is in land-use planning. As major new polluting sites are proposed, it may be possible to take advantage of local meteorological conditions to minimize the effect of emissions on the local population. Models may be used to determine which location of major transportation systems, fossil-fuel and nuclear power parks, or industries will least affect the environment. In some cases, models may indicate that the proposed construction should not proceed at all in the region, because the cost to the local air quality or climate would be too great. Obviously, the

---

*Fortak (1974) provides an excellent comprehensive discussion of the applications of air-quality modeling.

models whose results determine the fate of such million- or billion-dollar projects must be accurate. It is also obvious that, when changes to the micro- and mesoscale climate are considered, such as the possibility of dramatically increasing the frequency of winter fogs and summer thunderstorms by the construction of a major cooling tower complex (e.g., Hanna and Gifford, 1975), the models must be sufficiently general so as to handle the complicated feedback between the pollution and the atmosphere. It is in such problems associated with land-use planning and the preparation of environmental impact statements that the most complicated air-quality models will probably be most useful.

A third use of air-quality models is the real-time forecasting of air quality. Real-time forecasting of air quality can be useful to people planning outdoor activities and domestic chores even during relatively non-critical situations, as well as during the critical air pollution episodes when health warnings may become necessary. The benefits of accurate real-time forecasting in determining the impact of controls (such as a switch to cleaner fuels or a curtailment of industrial activities) have been discussed above.

Finally, a fourth potential use of air-quality models is the evaluation of a particular control strategy. In this role, the model may be utilized to determine whether the pollution problem has improved because of the controls or because of changing meteorological conditions.

An air-quality model that also includes time-dependent meteorological parameters can be very useful as a research tool to determine the minimum meteorological conditions for a given location that will ensure that concentrations do not exceed a prescribed standard. Thus, many experiments with a model under varying large-scale meteorological conditions may determine the necessary local conditions for a 3-hour average to exceed the standard for a given emission rate. For example, on a coastal city it might be found that for a standard to be exceeded it is necessary that all of the following occur:

(a) the large-scale geostrophic wind speed is less than 5 m/s;
(b) the lapse rate near the ground is less than 3 °C/km;
(c) the surface heat flux is less than 0.2 cal/cm^2 min.

Forecasting in real time would be greatly aided at a very low cost by statistical statements of this kind.

In a related example of the utility of a combined meteorological air-quality model, we consider the possibility of generating local climatological statistics in data-poor regions as a function of known, large-scale climatological parameters as measured by standard observing systems. In a related use, we might imagine "filling in" observations between stations through the use of the models. Such local meteorological statistics could then be used in simple air-quality models, such as the Gaussian model. Statistics of the type included in a stability wind rose (joint probability distribution of wind directions, speeds, and stability class) or which describe the mean afternoon mixing depth and mean depth of the nocturnal inversion could be generated by the model and used to provide estimations of annual average concentrations. The input would be derived from each possible large-scale condition; the output would be a probability distribution of the expected air quality.

Generalized Air-Quality Models

The general goal of an air-quality model is to forecast the concentration (in dimensions of mass per volume) of a contaminant, Q, over space and time given the initial conditions on the atmospheric structure and on the distribution of Q, and given the boundary conditions. For limited domains, the boundary conditions generally consist of the meteorological and concentration values on the upwind side of the domain (lateral boundary conditions), the conditions at the surface including surface heat, moisture and momentum fluxes, the emission rates in space and time over the domain, and appropriate upper boundary conditions. Mathematically, we wish to solve the equation for the time rate of change of $Q(x,y,z,t)$:

$$\frac{\partial Q}{\partial t} = - \underset{\sim}{V}_H \cdot \nabla Q - w \frac{\partial Q}{\partial z} - Q \nabla \cdot \underset{\sim}{V} - \nabla_H \cdot \overline{\underset{\sim}{V}'_H Q'} - \frac{\partial \overline{w'Q'}}{\partial z} \qquad \text{(Eq. 1)}$$

+ Sources + Sinks

given $Q(x,y,z,t_o)$, the time-dependent mean* horizontal and vertical velocities ($\underset{\sim}{V}_H$ and w), the horizontal and vertical eddy fluxes represented by $\nabla_H \cdot \overline{\underset{\sim}{V}'_H Q'}$ and $\frac{\overline{\partial w'Q'}}{\partial z}$, and the volume sources (emission rates) and sinks (e.g., deposition, rainout, reactions).

It is obvious from Equation 1 that the mean wind and the turbulent fluxes play a major role in determining the behavior of the concentrations. The truly predictive model will consist of forecast equations for these meteorological variables as well as the prediction of Q itself. For example, Pandolfo and Jacobs (1973) describe experimental forecasts of CO over the Los Angeles area utilizing a combined meteorological-pollutant model. However, solutions of Equation 1 alone for specified wind distributions may be of some use in strategy planning (for example, in answering "what if" questions, such as "What would the local concentration be if the wind behaved in a certain way?"). Real-time forecasting of particular pollution episodes, however, requires a predictive model for the meteorology as well as the pollutant.

Because it is possible and sometimes useful to utilize fairly sophisticated models to predict air quality without simultaneously predicting the meteorology (for example, by solving Equation 1 for specified or observed wind distributions), it is convenient to break the general air-quality model into two major components: the meteorological model and the pollutant model (Figure 1). The meteorological model, which may range in complexity from a simple empirical model to a vast, sophisticated, computer-oriented model, provides the meteorological variables that affect the transport, diffusion, and reaction of Q. These variables are then utilized in the pollutant model to forecast the advection and diffusion of Q. If Q is passive (that is, if its behavior does not appreciably affect the meteorology), the meteorological and pollutant models may be run in series. The meteorological model is run first; the appropriate data are stored and then used in the subsequent pollutant model.

---

*Here the mean refers to averages over appropriate space and time scales. In a grid-point numerical model, for example, the spatial average is the average over a single mesh volume; the time average is over one time step.

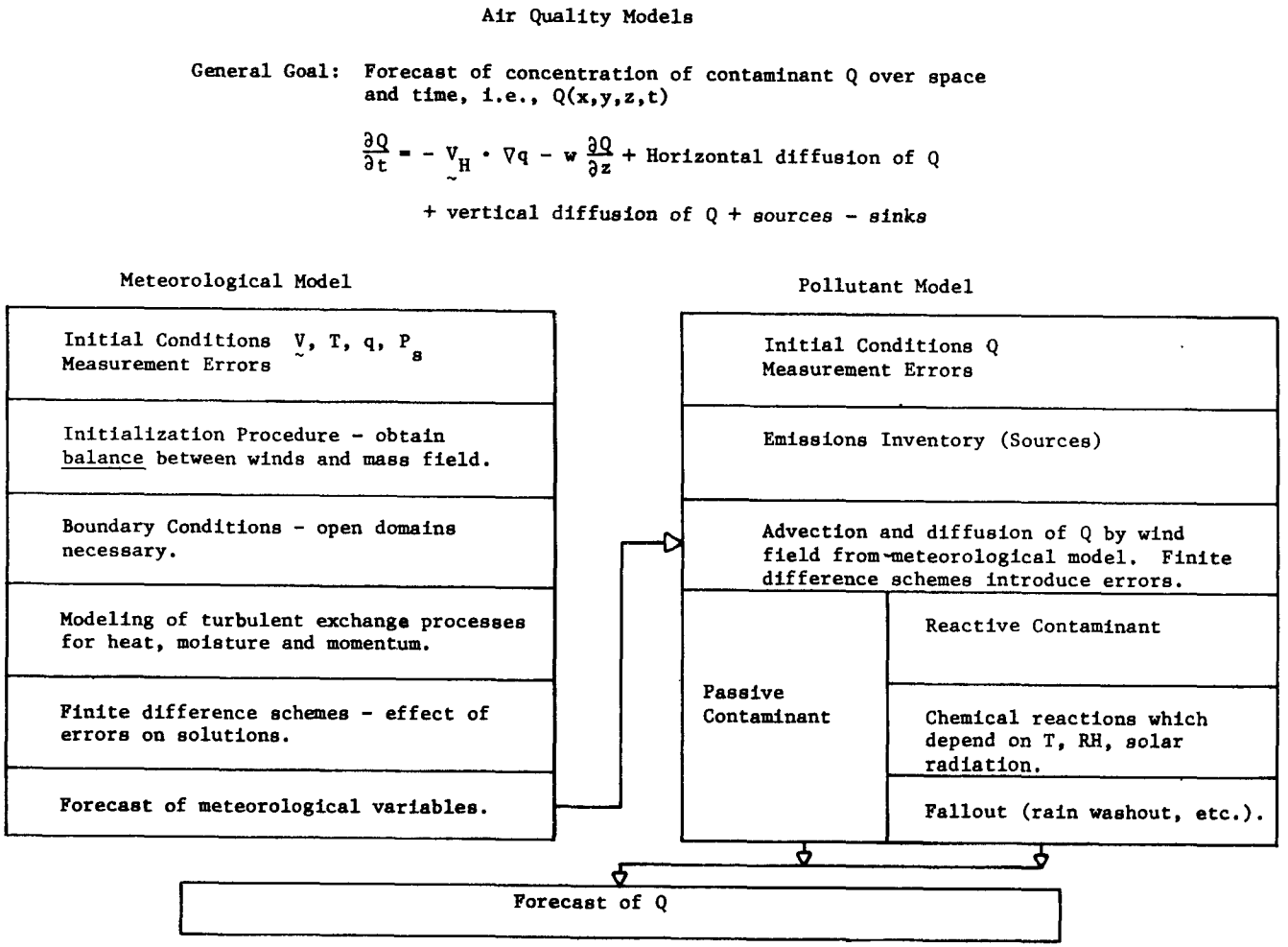

Figure 1. Schematic view of the components of a general air-quality model.

In the more difficult situation in which the pollutant affects the weather, both models must be run simultaneously. Fortunately, for many air pollution problems, the pollutant does not significantly affect the dynamics and thermodynamics on the regional scale. An important exception, however, occurs in the stratosphere, where several pollutants threaten the ozone layer.

The meteorological and pollutant components of the general air-quality model are discussed later in this paper. At this point we discuss the special requirements for air-quality models that arise on different scales of motion and for different meteorological conditions. This analysis demonstrates that different types of air-quality models are required for different conditions. Thus, in building air-quality models it is very useful for the modeler to know the specific requirements for the model, including the horizontal scale of interest, the length of the forecast, the pollutant to be modeled, the available input data, and the computation resources available. That is, the particular problem must be defined as precisely as possible.

Scale Analysis of the Pollutant Conservation Equation

Some of the fundamental differences between air-quality predictions on the regional (400 x 400 km), urban (5 x 5 km), and single-plume scales may be seen from a scale analysis of Equation 1. Grønskei (1974) has made a similar calculation. This analysis for the regional and urban scales assumes that the variation of the pollutant concentration is of the same scale throughout the domain and that the characteristic scale of variation is comparable to the size of the domain itself. In other words, the typical distance from a relative maximum in concentration to a relative minimum is of the same order of magnitude as the domain size. Thus this analysis does not apply to the problem of tracing an individual plume on the regional scale. This problem, which should be approached by a trajectory-diffusion model, is discussed in "A Combined Meteorological Air-Quality Model," below.

Without loss of generality, we may assume that the average v-component of the horizontal wind is 0 and combine the sources and sinks of Q into a single term, S. We then define the nondimensional variables:

$$
\begin{aligned}
Q' &= Q/\hat{Q} \\
u' &= u/\hat{u} \\
w' &= w/\hat{w} \\
x' &= x/L_x \\
y' &= y/L_y \\
z' &= z/L_z \\
t' &= t/T
\end{aligned}
\qquad \text{(Eq. 2)}
$$

where $\hat{u}$ and $\hat{w}$ are the magnitudes of the typical mean horizontal and vertical velocity components, $\hat{Q}$ is the amplitude of the variation in pollution concentration over the domain, L_x and L_y are the typical horizontal scales associated with the spatial variation of Q, L_z is the vertical scale of variation, and T is the time scale of the variation of Q. We also assume, for order of magnitude purposes, that the horizontal and vertical turbulent fluxes can be represented by gradient-transport or K theory, and that the term including the three-dimensional divergence is small compared to the advection terms. With these definitions and assumptions, Equation 1 may be written as

$$
\begin{aligned}
\frac{1}{T}\left(\frac{\partial Q'}{\partial t'}\right) = &- \frac{\hat{u}}{L_x}\left(u'\frac{\partial Q'}{\partial x'}\right) - \frac{\hat{w}}{L_z}\left(w'\frac{\partial Q'}{\partial z'}\right) + \frac{K_H}{L_x^2}\left(\frac{\partial^2 Q'}{\partial x'^2}\right) \\
&+ \frac{K_H}{L_y^2}\left(\frac{\partial^2 Q'}{\partial y'^2}\right) + \frac{K_z}{L_z^2}\left(\frac{\partial^2 Q'}{\partial z'^2}\right) + \frac{S}{\hat{Q}}
\end{aligned}
\qquad \text{(Eq. 3)}
$$

where K_H and K_z are the horizontal and vertical diffusivities, respectively. By the definition of the scaling parameters, all terms in parentheses are nondimensional and of order of magnitude one. Therefore, the relative importance of the horizontal and vertical advection, horizontal and vertical diffusion, and source/sink terms are given by the coefficients of the nondimensional terms. Furthermore, the time scales of each process are given by the inverse of the coefficients. Therefore, given certain space scales of variation and particular meteorological conditions, the importance of each process can be ascertained, and the overall time scale of the pollution fluctuation at a given point can be estimated.

We analyze Equation 3 for three space scales and six meteorological conditions. The three space scales are the regional, urban, and single-plume scales, summarized in Table 1. For the regional and urban scales, a uniform

square grid array of dimensions 40 x 40 is assumed to cover the domain. This array size, together with the size of the domain (given by L_x and L_y), determines the mesh size, Δs. For these horizontal scales, the vertical scale, L_z, is assumed to be equal to the mixing depth, H. The horizontal diffusion coefficient, K_H, is the most arbitrary and difficult-to-determine parameter. Here we relate K_H to a perturbation horizontal velocity, V' (arbitrarily set equal to 1 m/s), and a mixing length which is taken to be the grid size of the model:

$$K_H = V' \Delta s \qquad \text{(Eq. 4)}$$

For the single-plume scale, the horizontal dimension, L_x, along the direction of the flow is greater than the scale across the flow, and the vertical scale is usually smaller than the mixing depth (Gifford, 1973, p. 8). Furthermore, on this small scale the order of magnitude of the horizontal diffusivity is taken equal to the magnitude of the vertical diffusivity, K_z, which will be related to the meteorological parameters.

The six meteorological categories utilized in this analysis are listed in Table 2. Moderate wind conditions are represented by $\hat{u}$ equal to 4 m/s and $\hat{w}$ equal to 1 cm/s. The height of the mixed layer is 1 km, except for the stable categories, when it is reduced to 200 m.

The magnitude of the vertical diffusivity, K_z, is assumed to be equal to the vertical eddy coefficient for momentum. In the surface layer, under neutral conditions, K_z is given by

$$K_z = k\, u_* z \qquad \text{(Eq. 5)}$$

where k is the Kármán constant (~ 0.4) and u_* is the friction velocity,

$$u_*^2 = \tau/\rho \qquad \text{(Eq. 6)}$$

where τ is the surface stress and ρ is the density. The surface stress is usually related to the "anemometer-level" wind speed, $|\underset{\sim}{V}_s|$, by the relation

TABLE 1. SCALES OF AIR-QUALITY MODELS

	L_x	L_y	L_z	Δs	K_H
Regional	400 km	400 km	H	10 km	10^4 m^2/s
Urban	5 km	5 km	H	125 m	125 m^2/s
Plume	1000 m	100 m	100 m	---	K_z

TABLE 2. METEOROLOGY CLASSES USED IN SCALE ANALYSIS

	Approximate Pasquill (1961) Stability Class	$\hat{u}$(m/s)	$\hat{w}$(cm/s)	H (m)	K_z(m^2/s)
(a) typical: moderate wind, neutral stability	D	4	1	1000	25
(b) moderate wind, convective	B	4	1	1000	250
(c) light wind, convective	A	1	0.25	1000	250
(d) light wind, stable	F	1	0.25	200	1
(e) calm, convective	A	0	0	1000	250
(f) calm, stable	-----	0	0	200	1

$$\tau = \rho C_D |\underset{\sim}{V}_s|^2 \qquad \text{(Eq. 7)}$$

where C_D is the dimensionless drag coefficient which ranges from 1×10^{-3} over a smooth sea to 16×10^{-3} over thick grass (Sutton, 1953).

Equation 5 for K_z cannot hold as z becomes comparable to the height of the planetary boundary layer (PBL), since the size of the mixing eddies is ultimately limited by this depth. Thus K_z reaches a maximum somewhere near the middle of the PBL and decreases to a small value at the height h. For estimation of the order of magnitude of K_z under neutral conditions, Equation 7 is combined with Equations 6 and 5 and then evaluated at 100 m:

$$K_z(100\text{ m}) = 100\ k\ C_D^{\frac{1}{2}}\ |\underset{\sim}{V}_s| \qquad \text{(Eq. 8)}$$

With $k = 0.4$, $C_D = 10 \times 10^{-3}$, and $|\underset{\sim}{V}| = 4$ m/s, u_* equals 0.4 m/s and the value of K_z is 16 m^2/s. The maximum value of K_z in a PBL of 1-km depth is probably greater than this value. For example, Deardorff (1972), in his three-dimensional boundary-layer model, found the maximum value of K_z to be given by

$$K_z^{max} = .02\ \frac{u_*^2}{f} \qquad \text{(Eq. 9)}$$

where f equals the Coriolis parameter. For f equal to 10^{-4}/s and the above value of u_*, the maximum K_z is 32 m^2/s.

Based on the above estimates, a typical order of magnitude for K_z under condition (a) in Table 2 is 25 m^2/s. Under "convective" conditions of strong upward heat flux, K_z is increased by a factor of 10. This gives the same order of K_z found by Yamada and Mellor (1975) in their model of the afternoon of Day 33 of the Wangara Experiment. Under stable conditions (d and f), the vertical diffusivity is reduced to 1 m^2/s.

The results of the analysis are presented in Table 3. Because of the extreme variability in the source/sink term, we neglect this term in the

TABLE 3. RESULTS OF SCALE ANALYSIS

Scale and Synoptic Situation	$\frac{\bar{Q}}{L_x}$ s^{-1}	$\frac{\bar{Q}}{L_z}$ s^{-1}	$\frac{\bar{Q}}{H}$ s^{-1}	$\frac{K_H}{L_x^2}$ s^{-1}	$\frac{K_H}{L_y^2}$ s^{-1}	$\frac{K_z}{L_z^2}$ s^{-1}	$\frac{K_z}{H^2}$ s^{-1}	Horizontal Time Scale	Vertical Time Scale (Δt_v)	$\hat{u}\cdot\Delta t_v$	$\frac{\hat{u}\,\Delta t_v}{\Delta x}$
Regional											
(a) "typical"	1×10^{-5}	Same as	1×10^{-5}			Same as	2.5×10^{-5}	28h	11.1h	160km	16
(b) convective, mod. wind	1×10^{-5}	$\frac{\bar{Q}}{H}$	1×10^{-5}				25×10^{-5}	28h	1.1h	16km	1.6
(c) convective, light wind	0.25×10^{-5}		0.25×10^{-5}			$\frac{K_z}{2}$	25×10^{-5}	111h	1.1h	4km	0.4
(d) stable, light wind	0.25×10^{-5}		1.25×10^{-5}	6×10^{-8}	6×10^{-8}	H	2.5×10^{-5}	111h	11h	40km	4
(e) convective, calm	0		0				2.5×10^{-5}	28 weeks	1.1h	0	0
(f) stable, calm	0		0				2.5×10^{-5}	28 weeks	11h	0	0
ΔS = 10km											
Urban											
(a) "typical"	80×10^{-5}	Same as	1×10^{-5}			Same as	2.5x10-5	0.35h	11.1h	160km	1280
(b) convective, mod. wind	80×10^{-5}		1×10^{-5}				25.0×10^{-5}	0.35h	1.1h	16km	128
(c) convective, light wind	20×10^{-5}	$\frac{\bar{Q}}{H}$	0.25×10^{-5}			$\frac{K_z}{H^2}$	25.0×10^{-5}	1.4h	1.1h	4km	32
(d) stable, light wind	0		1.25×10^{-5}	5×10^{-6}	5×10^{-6}		2.5×10^{-5}	1.4h	11h	40km	320
(e) convective, calm	0		0				25×10^{-5}	56h	1.1h	0	0
(f) stable, calm			0				2.5×10^{-5}	56h	11h	0	0
ΔS = 125m											
Plume											
(a) "typical"	4×10^{-3}	1×10^{-4}	1×10^{-5}	2.5×10^{-5}	2.5×10^{-3}	2.5×10^{-3}	2.5×10^{-5}	400s	400s	1.6km	Not Applicable
(b) convective, mod. wind	4×10^{-3}	1×10^{-4}	1×10^{-5}	2.5×10^{-4}	2.5×10^{-2}	2.5×10^{-2}	2.5×10^{-4}	40s	40s	0.16km	
(c) convective, light wind	1×10^{-3}	0.25×10^{-4}	0.25×10^{-5}	2.5×10^{-4}	2.5×10^{-2}	2.5×10^{-2}	2.5×10^{-4}	40s	40s	0.04km	
(d) stable, light wind	1×10^{-2}	1.0×10^{-6}	1.0×10^{-6}	1.0×10^{-4}	1.0×10^{-4}	1.0×10^{-4}	2.5×10^{-5}	1000s	2.8h	10km	
(e) convective, calm	0	0	0	2.5×10^{-4}	2.5×10^{-2}	2.5×10^{-2}	2.5×10^{-4}	40s	40s	0	
(f) stable, calm	0	0	0	1.0×10^{-6}	1.0×10^{-4}	2.5×10^{-4}	2.5×10^{-5}	2.8h	2.8h	0	
ΔS = 0.25m											

general analysis and consider only the relative importance of horizontal and vertical transport and diffusion. For quasi-steady-state conditions, this term may be assumed to balance the largest terms in the equations.

On the regional scale, the horizontal time scale is greater than the vertical time scale for all meteorological situations. The next-to-the-last column, labeled "$\hat{u} \cdot \Delta t_v$," provides an estimate of the horizontal distance downwind from a source at which vertical mixing through the planetary boundary layer is essentially complete. For example, for case (a), the vertical mixing of a contaminant would be complete through a depth of 1 km at a distance of about 160 km downwind of a ground source. This result agrees with the downwind growth of the vertical dispersion coefficient, σ_z, in the Gaussian plume model discussed by Turner (1970, pp. 5-9) for a Pasquill stability class of D. The last column shows the ratio of this horizontal length to the horizontal grid size. For all meteorological classes except class "a" (moderate winds with typical vertical mixing), the vertical mixing may be considered complete (vertical distribution of Q uniform) beyond 4 grid lengths downwind of the source. Thus, for these conditions it is not necessary to include in the model a high vertical resolution of the PBL for the prediction of Q.

On the regional scale, horizontal diffusion by subgrid-scale eddies may be neglected (compared to horizontal advection) for all meteorological situations except perfectly calm, since the time scale for this process is about 28 weeks. However, the vertical transport by the mean vertical motion is of the same order as the horizontal transport, which indicates that vertical motions must be considered on this scale. These results are supported by the sensitivity experiments of Liu et al. (1974), who found vertical motions and vertical wind shear far more important than horizontal mixing in determining the accuracy of trajectory and grid models. Models which did not include vertical motions and vertical wind shear overpredicted ground-level concentrations by over 50 percent.

The data used by Nordlund (1975) in his study of SO_2 transport over northern Europe may be used as an example of the order of magnitude of the

source term, $S/\hat{Q}$, compared to the other terms in Equation 3 for the regional scale. Typical emissions of SO_2 into a volume 150 km x 150 km x 1 km are 5×10^5 ton/yr, or 1.4×10^4 g/s. A representative concentration over Europe in Nordlund's example is 30 $\mu g/m^3$. For these values, $\frac{S}{\hat{Q}}$ equals 2.1×10^{-5}/s, which is comparable in magnitude to the advective terms (Table 3).

The time scales for the variation of Q on the regional scale range from about a day (for moderate winds) to several days (for very light winds). Because these time scales are fairly long, there is a possibility of a deterministic prediction of air quality at a point under specific conditions. Also, the long time scales indicate that initial conditions must be specified accurately, as they will affect the predictions for long periods of time. Finally, steady-state conditions on this horizontal scale may be assumed for several hours, since the time scale of the variation is about a day.

On the urban space scale, the time scales of air quality variation in the horizontal become much shorter, on the order of an hour for all except perfectly calm conditions. The time scale for vertical diffusion exceeds the horizontal time scales, which indicates that a detailed vertical resolution of the PBL is necessary over the city. Complete vertical mixing, under most conditions, will not occur until tens of kilometers downwind of the urban area. This result helps explain why urban concentrations are poorly correlated with local mixing depths (Gifford, 1973, p. 7).

In contrast to the regional scale, mean vertical advection is negligible compared to horizontal advection on the urban scale. However, under some conditions vertical advection may produce an effect comparable to vertical mixing. Horizontal diffusion by subgrid-scale eddies is small compared to the advective effects, except under nearly calm conditions, a conclusion supported by Shir and Shieh's (1974, p. 190) results. Thus, for the urban scale, an approximate balance exists between horizontal advection, sources/sinks, and vertical diffusion.

A situation quite different from the regional and urban scales exists on the single-plume scale. As is well known, for the single plume, horizontal diffusion across the axis of the plume becomes important, and tends to balance horizontal advection from the plume's source and vertical diffusion. The mean vertical motion is negligible compared to these effects, as is the horizontal diffusion along the axis of the plume. This balance is the basis of Gaussian plume models. For example, in Roberts' (1923) model, the concentration is given by

$$Q = \frac{S}{4\pi x\,(K_H K_z)^{\frac{1}{2}}} \exp\left\{ -\frac{u}{4x}\left[\frac{y^2}{K_H} + \frac{z^2}{K_z}\right]\right\} \qquad \text{(Eq. 10)}$$

where S is the emission rate [mass time^{-1}]. Equation 10 is a solution to the steady-state equation,

$$u\frac{\partial Q}{\partial x} = K_H \frac{\partial^2 Q}{\partial y^2} + K_z \frac{\partial^2 Q}{\partial z^2} \qquad \text{(Eq. 11)}$$

Other empirically determined Gaussian plume models, which do not imply constant horizontal and vertical diffusivities, are available (e.g. Turner, 1970, p. 5).

The very short time scales of variations in the concentrations associated with single plumes indicate that deterministic forecasts — i.e., forecasts of instantaneous concentrations at a point — are impractical, if not impossible. Instead, therefore, time-averaged (typically 1-hour) estimates of Q are obtained at a point. Instantaneous values may easily differ by an order of magnitude or more from these average values.

In summary, the scale analysis has shown that different types of air-quality models are required for regional, urban, and single-plume predictions. For the regional scale, horizontal and vertical advection are important, and

vertical diffusion throughout the PBL is usually rapid enough so that a detailed vertical resolution of this process is often unnecessary. The time scales are long, so deterministic forecasts are practical. An accurate specification of the initial distribution of Q is necessary on this scale.

For the urban prediction problem, a detailed vertical resolution in a grid-point model is necessary, since the time scale of vertical diffusion is long compared to the horizontal transport time scale. Furthermore, turbulence models that are more accurate than K-theory models are needed to treat the general urban problem, since the size and structure of the turbulent eddies become important. The K-theory models become inadequate in the presence of buoyancy effects. Models that produce the same turbulent structure as the atmosphere (in a statistical sense) may be utilized to estimate the probability of a *local* (point-value) concentration exceeding a prescribed standard over a given time interval.

Because the horizontal time scales associated with urban pollution problems are of the order of an hour, initial conditions are of less importance than an accurate knowledge of the sources and the wind field; i.e., if the sources are known correctly and the winds forecast accurately, a correct forecast will evolve in roughly an hour, no matter what the initial conditions. This result was also found by Shir and Shieh (1974) in their urban model.

For the prediction of concentrations associated with a single plume, the time scales are so short that only time-averaged predictions are possible. The scale analysis indicates an approximate balance between horizontal advection, crosswind diffusion, and vertical diffusion, in agreement with the applicability of the Gaussian plume model.

The following section reviews the requirements of meteorological models on the regional scale and discusses some of the models currently under development.

METEOROLOGICAL MODELS ON THE REGIONAL SCALE

In this section, we discuss the most important aspects of predictive meteorological models on the regional scale. As shown in Figure 1, the components of a general meteorological model consist of (1) measuring initial values of the dependent variables, such as winds, surface pressure, temperature, and moisture, (2) analysis of these data to produce consistent three-dimensional initial fields, (3) treatment of boundary conditions on the edges of the domain, (4) modeling of important physical processes such as advection; turbulent fluxes of heat, moisture and momentum; radiation; and condensation; and (5) the numerical solution of finite difference equations that represent the processes in (4). Each of these component problems is complicated enough when considered by itself. When taken together in a complete model, as is necessary for a realistic treatment of general atmospheric conditions, the problem is truly enormous. It is therefore impossible in this brief review to give detailed descriptions of each component. Instead, the essential aspects of each component are introduced and references are given to other, more complete discussions.

The scale analysis of the preceding section indicated that pollutant variations on small space scales were associated with short time scales, so that deterministic predictions of instantaneous values of concentrations on horizontal scales of less than about 5 km were impractical. The same general rule is also true of the meteorological variables: small space scales are associated with very short time scales. Therefore, we restrict the following remarks to numerical models with horizontal resolutions of at least several kilometers which are capable of resolving the flow in a deterministic sense. For these models, the hydrostatic assumption is valid.

The basic set of equations utilized in time-dependent hydrostatic models (the so-called primitive equations) include the horizontal equation of motion,

$$\frac{\partial \underset{\sim}{V}}{\partial t} = (\underset{\sim}{V}\cdot\nabla)\underset{\sim}{V} - w\frac{\partial \underset{\sim}{V}}{\partial z} - \frac{1}{\rho}\nabla p - f\hat{k}\underset{\sim}{x}\underset{\sim}{V} + \underset{\sim}{F} \qquad \text{(Eq. 12)}$$

the thermodynamic equation,

$$\frac{\partial T}{\partial t} = - \underset{\sim}{V} \cdot \nabla T - w \frac{\partial T}{\partial z} + \frac{\omega}{\rho C_p} + \dot{Q} \qquad \text{(Eq. 13)}$$

the continuity equation,

$$\frac{\partial \rho}{\partial t} = - \nabla \cdot \rho \underset{\sim}{V} - \frac{\partial \rho w}{\partial z} \qquad \text{(Eq. 14)}$$

the hydrostatic equation,

$$\frac{\partial p}{\partial z} = - \rho g \qquad \text{(Eq. 15)}$$

the equation of state,

$$p = R T_v \rho \qquad \text{(Eq. 16)}$$

and the continuity equation for water vapor,

$$\frac{\partial q}{\partial t} = - \underset{\sim}{V} \cdot \nabla q - w \frac{\partial q}{\partial z} - C + E \qquad \text{(Eq. 17)}$$

where $\underset{\sim}{V}$ is the horizontal vector velocity, ρ is density, p is pressure, f is the Coriolis parameter, T is temperature, ω is $\frac{dp}{dt}$, C_p is the specific heat at constant pressure for day air, T_v is virtual temperature, g is the acceleration of gravity, and q is specific humidity.

The term $\underset{\sim}{F}$ in Equation 12 represents all frictional accelerations associated with turbulent motions; $\dot{Q}$ in Equation 13 represents diabatic effects, and C and E in Equation 17 represent condensation and evaporation, respectively. The modeling of these "sources and sinks" consists of relating these complicated processes to the dependent variables in the model. This modeling is often termed parameterization.

With the parametric modeling of the "source and sink" terms, the basic Equations 12-17 may be written in finite difference form and solved for future states of the atmospheric variables, subject to initial conditions over the

entire domain and time-dependent conditions on the vertical and horizontal boundaries of the domain.

Initialization of Mesoscale Regional Models

The relative importance to the forecast of the initial analyses of wind, temperature, and moisture compared to the other components of the meteorological model varies considerably with horizontal scale and the meteorological situation. A detailed representation of the initial conditions is most important on large scales and when the local forcing functions (represented by $\underset{\sim}{F}$, $\dot{Q}$, C and E in Equations 12, 13, and 17) are weak. Under these conditions, potential vorticity tends to be conserved and future states of the atmosphere are governed by a redistribution of the initial mass and momentum fields.

As the horizontal space scale decreases, a detailed representation of the initial conditions becomes somewhat less important. The specified conditions on the boundaries assume greater importance, since under all but very light wind conditions the variations associated with the initial conditions are advected away from the domain early in the forecast. Furthermore, the local forcing by terrain, frictional, and diabatic effects becomes more important on the smaller scales. On the urban scale, therefore, detailed initial conditions are unnecessary; the solutions will be determined almost entirely by the boundary conditions (possibly time-dependent) and the modeling of the local forcing functions. On the large regional scale (400 x 400 km or greater), however, the initial conditions must be resolved in some detail.

While initial three-dimensional analyses of wind, temperature, pressure, and moisture are required by the models, it is not necessary to measure all of these variables independently. For deep motions (vertical scales comparable to the tropopause height), the most important variable to measure and analyze accurately on the mesoscale is the horizontal wind. This result follows from adjustment theory (Rossby, 1938; Cahn, 1945; Økland, 1970), which states that on this scale the mass field (temperature and surface pressure) will quickly adjust through gravity waves to whatever initial wind field is provided. Thus it makes no sense to analyze extremely detailed temperature variations unless

a correspondingly detailed wind analysis is also provided. Warner (1976) has recently considered the transfer of initial errors between the mass and momentum variables in mesoscale models. He concluded that errors in the mass and momentum initial data are not strongly coupled, in the sense that there is very little transfer of error-related energy or uncertainty from one variable to another. Wind errors remain in the wind field while small mass field errors are removed through the adjustment process.

Although there is general agreement that the horizontal wind is the most important variable to initialize mesoscale models, it is not known how much of the mesoscale variability in the wind field must be included in the initial analysis for useful 12- to 24-hour mesoscale forecasts. It is the *hope* that the small-scale perturbations in the winds will evolve with time from the measured larger-scale circulations as a result of the physical forcing functions in the models.

Given the initial wind analysis, it is desirable to obtain a dynamically consistent temperature and surface pressure analysis. If the real atmosphere is balanced in a quasi-geostrophic sense, the temperature analysis may be obtained from a solution of the balance equation for geopotential height as a function of the winds (Fankhouser, 1969). Under some conditions, however, the atmosphere may not be balanced and the divergent and ageostrophic components of the wind may be significant. Solutions of a quasi-geostrophic 1-equation (e.g., O'Brien, 1970) to obtain the divergent component of the wind may not be applicable on the mesoscale. Therefore, iterative initialization methods which utilize the model's predictive equations themselves to produce a consistent analysis of all the variables may be necessary (Nitta and Novermale, 1969; Miyakoda and Moyer, 1968; Anthes and Warner, 1974; Rao and Fishman, 1975). The advantage of these schemes is their generality — all the physical processes in the model are incorporated into the initial analysis. The disadvantage is their cost — in some cases, the initialization process may consume a significant fraction of the total computer time required to make the forecast.

Lateral Boundary Conditions

The numerical treatment of the lateral boundaries is a difficult but very important aspect of a limited area forecast model. The problem on the interior of the domain is well posed only when the proper set of boundary conditions is prescribed. The solution on the interior may be completely different for apparently minor variations in the boundary conditions. Much discussion has appeared in the literature concerning the proper specification of variables on the open boundaries (Moretti, 1969; Shapiro, 1970). As discussed by Moretti, the only straightforward case occurs when the flow is supersonic, in which case the value on an inflow boundary may be arbitrarily specified, and the values on an outflow boundary obtained by a linear extrapolation outward from the interior of the domain.

In the subsonic case, however, waves may propagate upstream, so that values at inflow boundaries are partially dependent upon the flow on the interior of the domain. Thus the arbitrary specification of either constant or time-dependent boundary values may make the problem ill-posed. However, in the absence of proven computational methods to compute boundary variables correctly under general conditions, modelers are forced to take the pragmatic view that, if the lateral boundaries are located far enough away from the region of interest, the errors introduced at the boundaries will remain within some acceptable tolerance in the interior of the domain during the forecast period. We must therefore search for a set of conditions which minimizes the errors generated by the boundaries and their feedback into the interior.

Although it is normally recognized that a set of boundary conditions that minimizes the generation of high temporal and spatial frequency components to the numerical solution is desirable (if not absolutely necessary), it is less generally recognized that smoothly varying solutions near the boundary are not sufficient to guarantee accurate solutions on the interior of the grid. It is apparent that, as the size of the horizontal domain decreases, the specification of the velocity components and temperature along the boundaries affects the mean (wave number zero) values of these quantitites over the entire domain to an ever-increasing degree. Thus, on a mesoscale domain of 600 x 600 km, a

set of boundary conditions may be computationally "stable" and produce "smooth" results, but even small errors in the treatment of temperature or velocity may profoundly affect the mean kinetic and internal energy budgets over the domain.

The importance of specifying accurate values of temperature, surface pressure, and velocity components on the lateral boundaries of mesoscale models can be shown by considering the domain-averaged equation of motion (Anthes et al., 1974). Here, the approximate time rate of change of the average u-component of velocity (for frictionless flow) was shown to be

$$\frac{\partial \bar{u}^{D}}{\partial t} = - \frac{\overline{u_E^2 - u_W^2}^{L_y}}{L_x} - \frac{\overline{(uv)_N - (uv)_S}^{L_x}}{L_y} + f(\bar{v}_D^{D} - \bar{v}_g^{D}) \qquad \text{(Eq. 18)}$$

where the $(\bar{\ }^{D})$ operator denotes an average over the domain, the E, W, N, and S subscripts denote east, west, north and south boundaries respectively, and L_x and L_y are the lengths of the domains in the east–west and north–south directions.

The importance of the specification of the mass (given by the surface pressure and vertical temperature structure) appears in the term $f\bar{v}_g^{D}$, which is mainly determined by the difference in surface pressure and geopotential across the domain. As the domain size is decreased, the error in the mean geostrophic wind for a given temperature error increases rapidly. This point is illustrated in Figure 2, which shows the errors in the calculated geostrophic wind as a function of horizontal distance when a temperature difference error of 1° C is integrated hydrostatically over a 200-mb depth centered at the given pressure level. For synoptic scale domains (L >~ 3000 km), the error is about 1 m/s at all levels. The error increases rapidly as the domain size decreases below 1000 km. For a regional-scale model, with a domain size of 600 x 600 km, a 1° C temperature error on the lateral boundaries will produce large (~ 5 m/s) errors in the mean geostrophic wind across the grid, especially in the upper levels. These errors, if they persist in time,

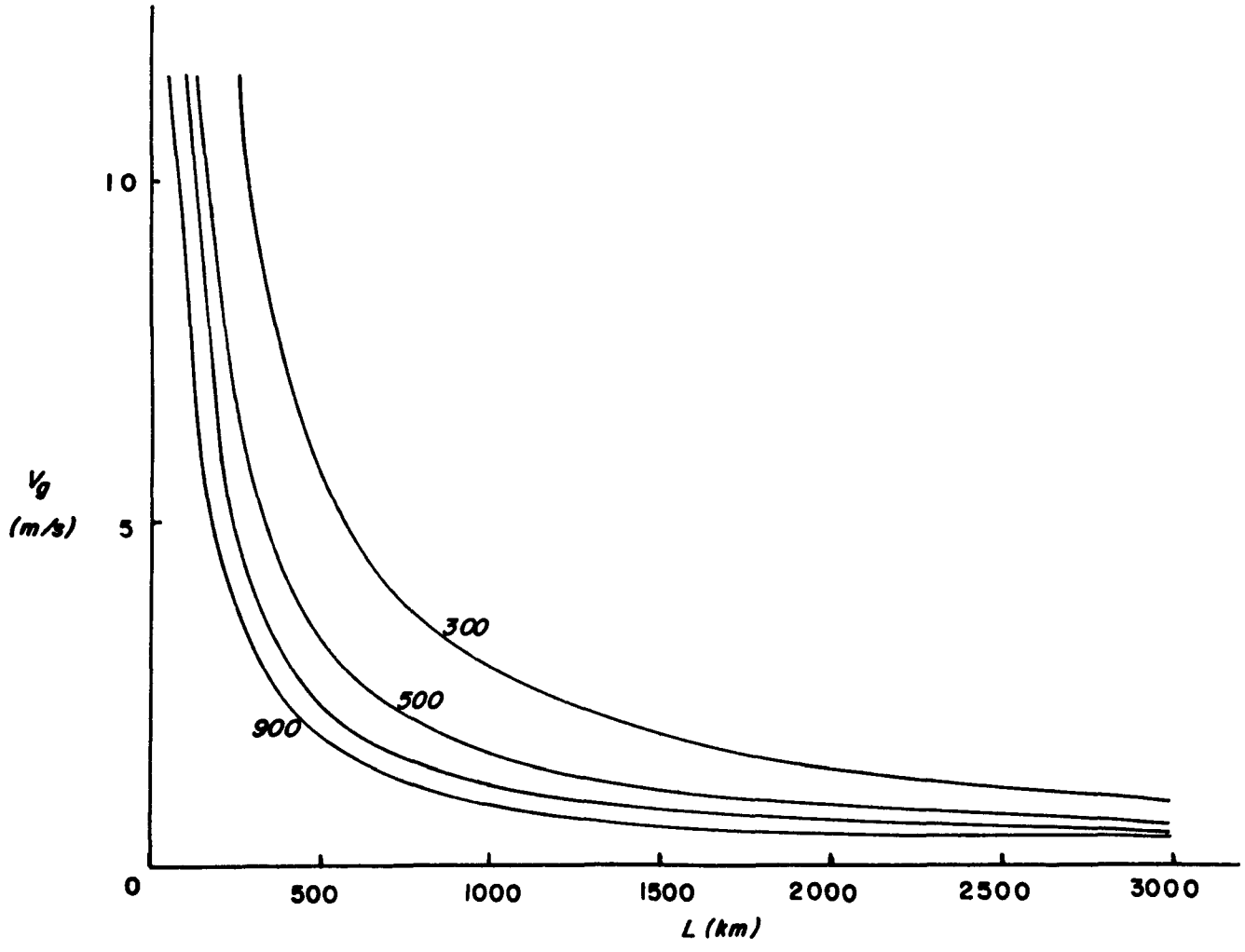

Figure 2. Error in the geostrophic wind as a function of horizontal interval produced when a temperature difference error of 1° C is integrated hydrostatically over a 200-mb depth centered at pressure levels of 300, 500, 700, and 900 mb.

may produce large erroneous accelerations of the mean motion over the domain. For example, with $f = 10^{-4}/s$, a 5 m/s error in geostrophic wind which persists for 6 hours would produce an erroneous change of 11 m/s in the *mean* velocity over the domain.

The preceding analysis indicates that, although it might be tempting for computational stability purposes to calculate the temperature on the lateral boundaries by some type of outward extrapolation from the interior of the domain, or a one-sided differencing scheme, the extreme sensitivity of the mean acceleration to small temperature errors leads us to reject these possibilities. Instead we conclude that, for mesoscale domains, it is preferable to specify the mass variables at *all* boundary points in a realistic and accurate way, in order to insure that the mean geostrophic wind and associated linear acceleration term remain accurate during the integration. This specification may come from a large-scale model (one-way interaction), or, in the research mode, from consistent analyses of observations.

The importance of accurately specifying the velocity components on the boundary is also discussed by Anthes et al. (1974). As the domain size becomes smaller than 1000 x 1000 km, net horizontal fluxes of momentum across the lateral boundaries may produce mean accelerations over the domain that are comparable in magnitude to the linear accelerations associated with the pressure gradient and Coriolis forces.

The preceding remarks indicate that the accurate calculation of lateral boundary conditions is a major component of the predictive mesoscale modeling problem. One attractive approach to the solution of this problem is to nest the fine-scale prediction model within a larger-scale prediction model. In a one-way interacting system, the large-scale model is integrated separately and provides time-dependent boundary conditions to the fine-mesh model. The forecasts on the fine mesh do not feed back into the large-scale model forecasts. Theoretical analyses (Phillips and Shukla, 1973), however, suggest that a better approach is to allow the two meshes to interact dynamically, which requires a simultaneous integration of the model equations on both meshes. An

example of a mesoscale forecast produced by such a two-way interacting system* is shown in Figure 3. Here a small-scale jet streak (local wind maximum), which is superimposed on a larger-scale jet stream, is forecast by a fine-mesh of 20-km horizontal resolution. The coarse mesh is 80 km. The isotachs (in m/s) are shown by solid lines; the temperature changes associated with vertical circulation in the vicinity of the jet are shown by dashed lines. This meteorological system consisting of strong winds normal to the lateral boundaries was chosen to provide a severe test of the numerical technique of meshing the two grid systems.

Finite Difference Schemes

Even if the initial and boundary conditions were known precisely and the forcing functions in Equations 12-17 represented by perfect mathematical models, the approximation of the partial derivatives in the governing equation would lead to errors in the forecasts. However, in contrast to the complicated feedbacks in the other components of the model that make a general analysis of errors very difficult, the errors introduced by the finite difference schemes are relatively well understood. There exist a vast number of temporal and spatial finite difference schemes to tempt the modeler. Many have special advantages in terms of accuracy, numerical stability, speed of computation, or simplicity in programming. In general, the most accurate schemes are the most complicated and time-consuming; the simple, fast schemes usually produce large truncation errors. For example, one of the simplest time and space differencing methods is the forward-in-time, upstream-in-space scheme, which may be illustrated for the simple advection equation

$$\frac{\partial Q}{\partial t} = - u \frac{\partial Q}{\partial x}, \qquad \text{(Eq. 19)}$$

by the finite difference approximation

*This forecast was produced by a nested grid version of the Penn State University mesoscale model (Anthes et al., 1974).

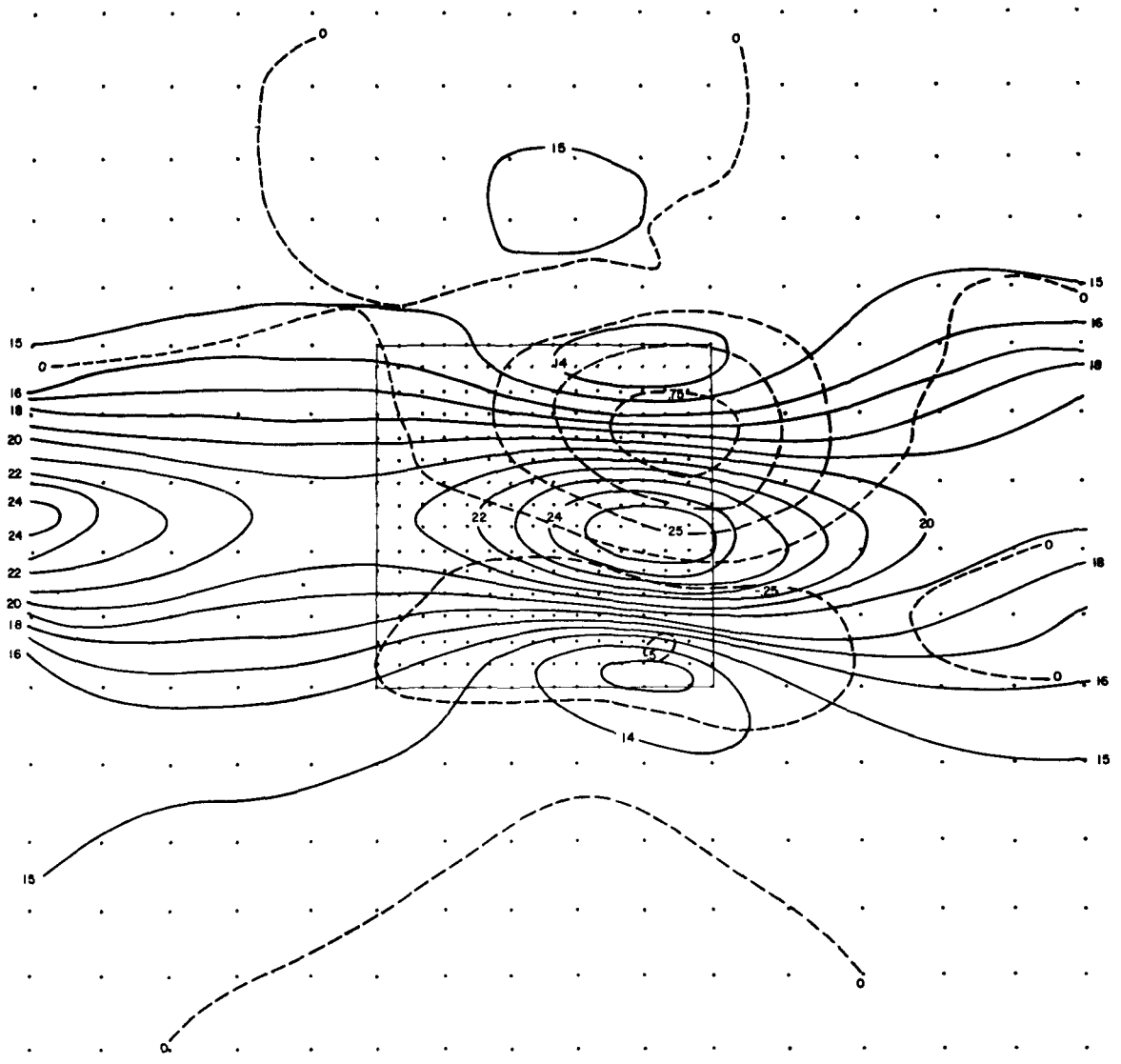

Figure 3. Temperature changes (dashed lines in °C) produced by vertical circulations associated with a propagating wind maximum (jet streak) at a level above the jet. The basic flow is from west to east (left to right in figure). Isotachs (solid lines) are labeled in m/s. The forecast was made on a two-way interacting nested grid.

$$\frac{Q_j^{n+1} - Q_j^n}{\Delta t} = - u_j^n \frac{(Q_j - Q_{j-1})}{\Delta x} \quad \text{for } u_j > 0$$

$$= - u_j^n \frac{(Q_{j+1} - Q_j)}{\Delta x} \quad \text{for } u_j < 0 \qquad \text{(Eq. 20)}$$

Here the n superscript denotes the time level ($t^n = n\Delta t$) and the j subscript indicates the horizontal position on the x axis ($x_j = j\Delta x$). This scheme is popular because it requires only two time levels of information and is very simple to use. However, as shown by Molenkamp (1968), the truncation errors associated with this scheme produce a strong false dispersion of Q. The computational pseudo-diffusion coefficient is

$$K = \frac{1}{2} |u| \left(1 - \frac{|u|\Delta t}{\Delta x}\right) \Delta x \qquad \text{(Eq. 21)}$$

where $\frac{|u|\Delta t}{\Delta x} \leq 1$. The magnitude of the horizontal mixing associated with this computational K usually exceeds the magnitude of the physical mixing process by an order of magnitude or more. For example, for a grid size of 5 km, a velocity of 5 m/s, and a ratio $\frac{u\Delta t}{\Delta x}$ equal to 1/2, the computational diffusion coefficient is 6.25×10^3 m^2/s. In the meteorological prediction equations, the use of such a damping integration scheme may be beneficial in maintaining numerically smooth and stable solutions. In modeling phenomena with strong local sources of energy, such as hurricanes (Rosenthal, 1970), cumulus clouds (Ogura, 1963), or sea breezes (Pielke, 1974), this scheme has produced useful results at a small cost. However, for less energetically active systems, and especially for predicting the transport of conservative quantities, more accurate schemes are necessary.

The forward-in-time, upstream-in-space finite difference scheme has only first-order accuracy in time and space (that is, the errors are proportional to the first powers of the time step, Δt, and grid spacing, Δx). More accurate finite difference schemes may be derived by including more terms in the Taylor's series expansions (e.g., Haltiner, 1971, p. 91). These higher-order schemes contain more points in the approximate expressions and require more computational time. Because the order of the finite difference equations is increased

beyond the order of the original partial differential equation, purely numerical modes may be introduced into the finite difference solutions. An example is the "computational mode" associated with the leapfrog (or centered in time and space) differencing scheme (e.g., Haltiner, 1971, p. 95). This particular mode of the numerical solution has no physical counterpart, and hence its amplitude must be controlled during the forecast.

The leapfrog scheme has second-order accuracy in space and time, which means that the errors in the differences are proportional to the second power of the step and grid size. Although these truncation errors are less than those associated with the first-order scheme, they do produce significant errors in the phase speed and rate of energy propagation of waves shorter than about $8\Delta x$. If advection or wave propagation is a dominant part of the meteorologically interesting portion of the solution, these errors will be significant, causing the short waves to propagate too slowly compared to their counterparts in the real atmosphere.

Other more accurate, finite difference schemes are available (e.g., Richtmyer and Morton, 1967; Crowley, 1968) at the expense of increased complexity. An increasingly popular scheme for evaluating space derivatives has fourth-order accuracy and was shown by Crowley (1968) to give superior results in the advection of a conservative quantity.

Because of the difficulty that traditional finite difference schemes have in reproducing faithfully the behavior of short wavelength features, alternative approaches are now receiving attention in research models. An example is the Galerkin method utilizing Chapeau basis functions for the independent variables (Long and Hicks, 1975). By expanding the variables in terms of the Chapeau functions, a more efficient finite difference scheme is generated. This scheme is able to resolve wavelengths as small as $4\Delta x$ with better accuracy than the conventional schemes. Use of these newer methods may make numerical models considerably more efficient in the future.

Parameterization of Physical Processes

One of the most important components of the meteorological model is the representation of physical processes in the atmosphere by mathematical relationships. These processes include:

(a) complex terrain effects,

(b) condensation heating and evaporative cooling,

(c) infrared and shortwave radiation,

(d) conduction of heat from the earth's surface to the air in the contact layer, and

(e) turbulent transfers of heat, moisture, and momentum through the boundary layer.

Complex terrain effects enter the mesoscale model as a lower boundary condition; the other processes involve models in themselves. These sub-models may become nearly as complex as the overall model and consume a major fraction of the computing time. Ideally, however, simple models which represent the essential physics associated with each process through parameterized relationships can be used to keep the model economically feasible. Although the details of the parameterization of physical processes may vary considerably among models, the concepts tend to be rather similar. This section reviews typical methods for representing the above physical processes in mesoscale models. The nature of these parameterizations and the model variables upon which they depend are given in Table 4. Blackadar (1978) presents a more complete review of the surface and boundary layer processes (d and e) which are most important to air-quality modeling.

Complex Terrain Effects--

Inhomogeneities at the earth's surface generate mesoscale and microscale circulations in a number of ways. Long, deep valleys tend to channel the surface wind, giving a strong bias to certain wind directions over the year. Differential heating of the sides of basins leads to oscillations in the surface winds (Staley, 1959). When statically stable air flows over ridges

TABLE 4. TYPICAL PARAMETERIZATION OF PHYSICAL PROCESSES IN MESOSCALE MODELS

Process	Important Parameters
Vertical flux of momentum, heat and moisture in PBL	H height of PBL
(a) Lower boundary condition (surface stress, surface heat flux, surface moisture flux)	$\bar{\theta}$ mean potential temperature in PBL $\bar{V}_a$ mean wind at anemometer level $\bar{V}$ mean wind in PBL C_D drag coefficient C_E heat transfer coefficient u_* friction velocity z_o roughness parameter θ_s average potential temperature at ground $R_{i_B} \simeq \frac{gH(\bar{\theta} - \theta_s)}{\bar{\theta}\,\lvert\bar{V}\rvert^2}$ bulk Richardson number $L = -u_*^3[k\frac{g}{\bar{\theta}}(\overline{w'\theta'})_a]$ Monin-Obukhov length
(b) profiles in surface layer (nominal depth ~ 100m)	z_o, L $-\overline{u'w'} \simeq K_m \frac{\partial \bar{u}}{\partial z}$
(c) fluxes from top of surface layer to top of PBL	$-\overline{w'\theta'} \simeq K_h (\frac{\partial \bar{\theta}}{\partial z} - \gamma_c)$ $-\overline{w'q'} \simeq K_q \frac{\partial \bar{q}}{\partial z}$ K_m, K_h, K_q may be formulated in a number of ways by relating them to (a) height of PBL (b) local vertical shear of wind averaged over area and time (c) local lapse rate, averaged over area and time (d) surface heat flux

(continued)

TABLE 4 (continued)

Process	Important Parameters
Cumulus convection (effect of cumulus clouds on environment)	vertical velocity: $\overline{w_c}$, $\overline{w_e}$ temperature: $\overline{T_c}$, $\overline{T_e}$ specific humidity: $\overline{q_c}$, $\overline{q_e}$ horizontal velocity: $\overline{V_c}$, $\overline{V_e}$ c subscript denotes cloud variable, e subscript denotes environmental value. $\overline{(\ )}$ represent average over lifetime of cloud (10-60 min.)
Radiation (shortwave)	surface albedo, percentage and type of clouds.
Radiation (longwave)	$\overline{T}(z)$ $\overline{q}(z)$ percentage and types of clouds (including heights). $\overline{(\ )}$ represents average over horizontal areas comparable to grid size
Terrain effects	height of terrain with wavelengths less than ~ $4\Delta x$ eliminated. Low-level stability, mean wind speed in PBL, and vertical profile of mean wind are important atmospheric parameters to define response of atmosphere to flow over rough terrain.

that are oriented more or less normally to the flow, a variety of gravity-wave phenomena are generated. Notable among these phenomena are the lee-slope windstorms that occur in the Rockies (Klemp and Lilly, 1975). However, mountains as high as the Rockies are not necessary to produce significant mesoscale perturbations; even hills of a few hundred meters in height can drastically modify the local rainfall distribution (Huff et al., 1975).

Under light prevailing winds, variations in terrain elevation produce elevated heat sources and sinks, which lead to vertical circulation on a small scale. Cold air at night drains down sloping surfaces and accumulates in valleys. This effect played a crucial role in the Donora, Pennsylvania disaster of 1948 (Williamson, 1973, p. 180). Knowledge of the frequency and intensity of these valley inversions, which can be monitored using indirect sensing techniques, would be extremely useful in land-use planning. Urban-scale models may be of some use here in real-time forecasting as well as in the research mode.

Gifford (1975) reviews some of the effects of rugged terrain on diffusion. In general, diffusion rates appear to be larger for a given meteorological situation than would be expected over homogeneous terrain. Differential heating and cooling, vortex shedding, and gravity waves are the probable mechanisms for increasing the diffusion rates.

Condensational Heating and Evaporational Cooling--

The treatment of the water cycle in a regional-scale model is important, both in the effect of condensation and evaporation on the dynamic and thermodynamic variables, and in the important role precipitation has in removing pollutants from the air. Even nonprecipitating clouds and fog greatly affect the surface heat flux and low-level stability. (Again, the Donora episode of 1948 may be cited; the formation of a deep fog layer prevented the solar radiation from burning off the nocturnal inversion.)

Cumulus and cumulonimbus convection, besides playing important roles in the energetics and dynamics of mesoscale systems, also act as very efficient

mixers of lower and upper tropospheric air. For example, it is common to observe "dirty plumes" in the otherwise clean upper tropospheric air over Miami where a cumulus cloud has dissipated. These links of the PBL with the middle and upper tropospheric layers are quite important in convective situations in determining the fate of pollutants on the regional scale.

Because the hydrostatic models cannot explicitly consider moist convective circulations, the cumulative effect of these cloud-scale motions on the temperature, moisture, and momentum structure of the mesoscale atmosphere must be related to the circulations that are resolvable by the model. Both theoretical and observational results indicate that the mesoscale horizontal convergence of water vapor is the most important parameter in determining when and where organized moist convection will occur (Hudson, 1971). Values of moisture convergence as high as 10^{-4} g/kg s may occur on the mesoscale.

The mesoscale moisture convergence over an area provides an integral constraint on the amount of precipitation and associated latent heating that is possible. The vertical distribution of the heat, moisture, and momentum fluxes by the convection is determined by the spectrum of clouds present. Current cumulus parameterization schemes vary from simple ones in which only a single cloud type is considered (e.g., Kuo, 1974) to more sophisticated ones in which a number of cloud types are permitted (Arakawa and Schubert, 1974; Ooyama, 1971).

Infrared and Shortwave Radiation--

Most mesoscale models do not yet contain the effects of radiation flux divergence in the free atmosphere; only the radiation budget at the ground is considered. This neglect is probably justified above the PBL for most mesoscale predictions because of the short time scales involved and the dominance of other physical processes in determining temperature changes in the free atmosphere. Radiation is probably most important in the evolution of the nocturnal PBL, although — in specific air pollution problems — attenuation of the daytime radiation by particles or other pollutants may also be important. Reasonably simple radiation models are available to treat this process (e.g.,

Sasamori, 1968). The most important variables that determine the longwave flux are cloud cover (depth and height) and the average vertical profiles of temperature and moisture.

The Planetary Boundary Layer--

Because knowledge of the time variation of the structure and height of the PBL is essential in the regional air pollution problem, the realistic parameterization of the PBL is of primary importance in the models. While the use of simple "mixed-layer" models (see, for example, "Transport and Diffusion Models," below) may be considered, a number of levels within the PBL may be necessary to resolve possible important vertical variations of momentum, moisture, and pollutants. With surface fluxes of heat, moisture, and momentum computed from a surface energy budget calculation and established similarity theory, vertical transfers of these quantities are calculated in most models by "K" theory, in spite of the nonrigorous nature of the flux-gradient relationship. The vertical mixing coefficients depend on such parameters as the height of the PBL, surface heat flux, and (locally) on the vertical wind shear and stability.

The predictive, as opposed to diagnostic, calculation of the surface fluxes of heat and moisture requires a simple energy budget which utilizes for input only external parameters such as time of day, year, latitude, and characteristics of the soil (Carlson, 1976). This budget is necessary to calculate the portion of the insolation that is utilized to evaporate surface moisture and heat the air in the contact layer. The surface flux of heat is necessary to calculate the Monin-Obukhov length, L, which is important in establishing the momentum and temperature structures in the surface layer. The surface flux of moisture is important in augmenting the water supply in the PBL, which in turn exerts a strong influence on the evolution of moist convection. Blackadar (1978) discusses the modeling of the PBL in greater detail.

TRANSPORT AND DIFFUSION MODELS

The second major component of the predictive air-quality model (Figure 1) is the transport and diffusion model, which utilizes the meteorological variables generated by the meteorological model to advect and diffuse a pollutant. This model may also calculate chemical reactions with other species or removal by such processes as washout or dry deposition. Some of these nonconservative aspects of the pollutant prediction problem are discussed by Kabel (1978).

Recently there have been numerous excellent reviews of the various transport and diffusion techniques that are utilized in air-quality models. Notable contributions are articles by Eschenroeder (1975), who gives 129 references, Hoffert (1972), Johnson (1972), Seinfeld (1970), and Lamb et al. (1973). Because of the existence of these comprehensive reviews, it would be redundant to give another detailed discussion of the various types of pollution transport and diffusion models. Instead, I will summarize the types of models available for this purpose and briefly discuss their relative strengths and weaknesses.

The general classes of air pollution transport and diffusion models are presented in Table 5, which gives a brief description of the important aspects of each model type, the horizontal scale of the model's applicability, an estimate of the computational expense in using the model (which is also a good measure of the model's complexity), and a single example. Eschenroeder (1975) gives many other examples and a more detailed description of each type of model.

BOX MODELS

The "box model" is one of the oldest air-quality models and is based on the assumption that the pollutant is uniformly mixed between the ground and a mixed layer depth, and that the area source rate and the wind speed are constant. These assumptions lead to very simple expressions for local concentrations, such as the model of Gifford and Hanna (1973):

TABLE 5. CLASSES OF DIFFUSION AND TRANSPORT MODELS

Type of model	Description and Basic Assumptions	Horizontal scale of applicability	Expense	Example
Box	Vertical mixing between ground and "lid", generally given by H, is complete, area emission rate constant; takes no account of wind direction variations. Inapplicable with near calm conditions.	urban	practically zero	Gifford and Hanna (1973)
Gaussian plume	Steady state; balance between horizontal advection, vertical and cross wind diffusion; no spatial or temporal variations in wind or atmospheric stability. Inapplicable with near calm conditions.	single plume	small	Turner (1970)
Langrangian puff	Source emissions treated as series of puffs, concentration within each puff is assumed Gaussian. Trajectory of puff is computed from space- and time-varying wind field. Applicable for tracing single puff; not very suitable for obtaining spatial variations of concentrations.	single source, urban or regional	moderate (for one puff)	Roberts et al. (1970)
Eulerian gridpoint	Time-dependent concentrations predicted over two- or three-dimensional array of points. May handle very wide range of conditions including large time and space variations in meteorological parameters as well as emission sources.	urban, regional	high	Pandolfo and Jacobs (1973)

(continued)

TABLE 5 (continued)

Type of model	Description and Basic Assumptions	Horizontal scale of applicability	Expense	Example
Particle-in-cell	Many particles, which represent mass or concentration of a pollutant, are advected by observed or predicted winds (specified on Eulerian grid). Concentration patterns on Eulerian grid obtained by interpolation from nearby particles. Pseudo-diffusion reduced compared to Eulerian grid calculation.	urban, regional	high	Sklarew et al. (1972)
Trajectory	Two- or three-dimensional trajectories are calculated from observed or predicted meteorological data to trace transport of a pollutant. May be utilized with puff models or K-theory diffusion models. Not very suitable for obtaining spatial variations of concentrations.	regional	moderate (for one trajectory)	Hall et al. (1973)
Quasi-Langrangian cell	Three-dimensional, material volumes (cells) of air are transported by observed or predicted winds. Cells deform with horizontal divergence or deformation in wind field. Emissions added to cells as they pass over source regions. Pollutants assumed well-mixed from ground to mixing height.	regional	moderate	Nordlund (1975)

$$Q = C \frac{S}{\tilde{V}} \qquad \text{(Eq. 22)}$$

where S is the area source rate (mass/area•time), and the value of C, a dimensionless parameter, depends on the city size and on the stability class. For typical city sizes and stabilities, C is about 250. In many tests of the performance of this simple model compared to other more complex models in predicting average concentrations over an area, the simple model generally does as well or better than the complex models in obtaining high correlation coefficients between observed and predicted averages. This fact should cause urban modelers to ask why a very simple model can perform, on the average, so well when compared to complex models, which are theoretically capable of treating more complicated episodes. The answer, I believe, lies simply in the relative importance of the terms in the general pollutant prediction equation. On the urban space and time scales, the dominant terms are the area sources, advection, and vertical mixing. The simple box model considers these effects, and (when they are known) good average predictions of Q result. However, such a simple model is incapable of treating situations in which large horizontal gradients of Q exist, or of treating the many complicated problems on the larger regional scale. Furthermore, the model breaks down as the wind speed approaches 0. Finally, a high correlation of observed and predicted values does not necessarily imply a good performance in individual cases, as shown by Anscombe (1973) and summarized by Eschenroeder (1975). Nevertheless, the practical utility of such simple models under the proper conditions is indisputable.

Gaussian Plume Models

The best known and most widely used air-quality models are variants of the Gaussian plume model. These models consider the vertical and cross wind dispersion of a single plume under steady-state conditions. Time-averaged (about 1 hour) concentrations downwind of a single source are obtained as functions of the mean wind speed and stability class. Multiple sources can be treated with Gaussian plume models by adding the plumes associated with separate sources. The concentrations from each plume are then combined in overlap

regions. Gaussian plume models are ideally suited for use with climatological data for producing annual estimates of concentrations near a particular source. Turner (1970) presents a user's workbook which describes the use of the Gaussian plume model. It is noteworthy that most Gaussian plume formulas are steady-state, empirical models based on the assumption of Gaussian distributions in the vertical and the horizontal. For example, a commonly used Gaussian plume model (Calder, 1970) is

$$Q = \frac{S \exp\left[-\tfrac{1}{2}\left(\frac{y^2}{\sigma_y^2} + \frac{Z_o^2}{\sigma_z^2}\right)\right]}{\pi U \sigma_y \sigma_z} \qquad \text{(Eq. 23)}$$

where S is the emission rate (mass/time) from a continuous point source at an elevation Z_o, U is the mean wind speed in the x-direction, and σ_y and σ_z are empirically-determined dispersion coefficients which depend on the distance, x, from the source and on the static stability. In many applications, the stability dependence of σ_y and σ_z is estimated in terms of the local meteorological conditions based on a scheme introduced by Pasquill (1961).

Lagrangian Puff Models

When the behavior of the pollutants emitted from a single source is over long periods of time (greater than 1 hour) or distances longer than those for which the Gaussian plume models are valid, a Lagrangian puff model becomes applicable. These models consider the behavior of a single "puff" of contaminated air after it leaves its source. The center of mass of the pollutant concentration is advected along a trajectory which may be computed from a three-dimensional wind field. The wind and stability along the trajectory may vary, and so the model is potentially applicable under a wide variety of meteorological conditions. The expansion and deformation of the puff and the diffusion within the puff by turbulence and wind shear may be computed as the puff moves along the trajectory. Because the downwind transport of the puff is accomplished by a Lagrangian calculation, there is no artificial diffusivity associated with the advection calculation. Although the puff model approach is most suitable for tracing individual emissions, a number of puffs

originating at different sources could be followed in order to obtain spatial variations at a later time. Examples of puff models are given by Roberts et al. (1970) and Sheih and Moroz (1972).

Eulerian Grid-Point Models

For forecasting temporal and spatial variations of pollutant concentrations over urban, regional, and larger scales, Eulerian grid-point models become useful, although three-dimensional models are quite expensive because they require large amounts of computer time. In the grid-point models, a finite-difference version of Equation 1 is solved as an initial-boundary value problem at many points over the domain of interest. The method is quite general, and may incorporate sources, sinks, and chemical reactions. The primary disadvantage, besides cost, lies in the truncation errors associated with the advection calculation and the resultant pseudo-diffusion (see "Meteorological Models on the Regional Scale," above; also, Liu and Seinfeld [1975]). However, this is an economic, not a theoretical difficulty. Finite difference methods of higher accuracy (Egan and Mahoney, 1972) and/or a larger number of grid points may be employed to reduce the truncation errors to any reasonably small value. An excellent example of the use of an Eulerian grid-point model is given by Shir and Shieh (1974), who solve the conservation equation for SO_2 over a three-dimensional array over the St. Louis area. The 30 x 40 horizontal array utilizes a constant mesh size of 1524 m along a side; the vertical structure of the model consists of 14 levels from the ground to the height of the mixed layer. Their results were better in general than those from the Gaussian plume model.

Particle-In-Cell (PIC) Models

An alternative to the Eulerian grid-point model which is also well suited for the time-dependent calculation of a pollutant concentration in three dimensions is the PIC model. In these models, particles represent a mass or a concentration of a species. These particles are transported by a specified wind field. In the absence of diffusion or other nonconservative

processes, the concentration or mass of a contaminant represented by a particle does not change; thus, the numerical diffusion associated with the advection calculation in a grid-point model is eliminated. However, for accurate resolution of gradients, a larger number of particles is necessary, which may make the PIC method more costly than grid-point models for a given accuracy. Nonconservative processes, usually defined at grid points, may modify the concentrations of nearby particles. Examples of the PIC technique are given by Sklarew et al. (1972) and Teuscher and Hauser (1974). An example of the PIC method used in conjunction with a mesoscale meteorological model is presented in this section.

Trajectory Models

Trajectory models are useful in tracing individual pollutants forward from their source to downwind receptors, or in identifying the sources of a given pollutant by computing backward trajectories from a particular receptor. When using real meteorological data, a wide variety of computational techniques is available to compute trajectories. These range from simple horizontal kinematic techniques in which an analyzed wind field on a constant level or constant pressure surface is used to compute successive positions of air parcels in space and time, to more complicated methods in which three-dimensional motions are considered. Because of the importance of vertical motions on the movement of air over periods of a day or more, trajectory models applied to these time scales must consider the three-dimensional atmospheric motions unless the pollutants are trapped under a well-defined mixed layer. The combination of typical synoptic-scale vertical motions (5 cm/s) in the presence of moderate vertical wind shear can lead to significant differences between horizontal and three-dimensional trajectories over 24 hours, especially when the wind changes direction with height. For example, let the wind change linearly from west at 10 m/s at a height of 1 km to east at 10 m/s at a height of 3 km. If the vertical velocity were constant at 2.3 cm/s during the 24-hour period, the parcel would rise from 1 km to 3 km in 24 hours. Its average east-west velocity during this period would be 0, and so its true horizontal

displacement would be 0. A constant-level trajectory, however, would erroneously place the parcel 864 km downwind! Utilizing real data, Danielsen (1961) has found similar errors.

The most accurate trajectory method in the free atmosphere for use with real data is probably some variation of the isentropic trajectory method. Very useful in tracing middle and upper tropospheric pollutants such as ozone, this method requires the computation of trajectories along isentropic — or constant potential temperature — surfaces (Danielsen, 1961; Bleck, 1968). Under adiabatic conditions, pollutants are confined to isentropic surfaces and vertical displacements are readily calculated from the displacements in the isentropes. Although some dynamical constraints may be incorporated into the basic kinematic calculation on isentropic surfaces, a comparison of three-dimensional trajectories computed from the more complicated methods showed no obvious improvement over the simple kinematic method (Hoke, 1973).

Quasi-Lagrangian Models

When a well-defined mixed-layer height exists over a regional domain, quasi-Lagrangian models are suitable for modeling the regional transport of pollutants. For example, Nordlund (1975) utilized this method to calculate the time-dependent behavior of SO_2 over northwestern Europe. Liu and Seinfeld (1975) compared the validity of Eulerian and Lagrangian models. In the quasi-Lagrangian cell model, the atmosphere from the ground to the mixed-layer height is divided into more or less rectangular cells, with horizontal sides of the order of 50 km. These cells represent material volumes of the atmosphere that are transported by the mean wind in the PBL. In the presence of horizontal divergence or deformation, the cells may shrink, expand, or become distorted in shape. However, because the transport is done in a Lagrangian rather than Eulerian framework, numerical diffusion is absent. As the cells pass over sources, they may be enriched by additional pollutants. Removal processes and chemical reactions may be calculated within the individual cells. The quasi-Lagrangian method becomes less applicable in situations in which a clearly defined mixed-layer top does not exist, because the pollutants are not

confined by an upper surface. Multi-level grid-point models or PIC models would be more appropriate under these conditions.

A Brief Look at the Accuracies of Air-Quality Models

The ultimate test of any air-quality model is how well it performs its assigned task. Because the assigned tasks may vary so much from one air-quality modeling problem to another (e.g., compare the problem of estimating annual average SO_2 concentrations at a stack base to the problem of modeling ozone transport and reactions), a general comparison of the models is impossible. Before a comparison is meaningful, the problem and the constraints must be precisely defined. Eschenroeder (1975) has summarized some comparisons between simple box models, PIC models, Eulerian grid-point models, and trajectory models. He emphasizes that simple statistics (such as temporal correlation coefficients) can be very misleading, and that prospective users must critically examine the model's output in many different individual situations, as well as the statistics, to judge fairly a model's utility.

Regarding the overall accuracy of air-quality models, it appears that the limiting variables in all the models are (1) the accuracy of the emissions inventory, (2) the accuracy of the meteorological variables, particularly the mesoscale wind field, (3) the accuracy of the parameterization of meteorological processes such as turbulent mixing, and (4) the accuracy of the representation of the chemical reaction processes. The computational difficulties associated with the grid-point and Lagrangian models can be eliminated immediately, if resources permit, by simply increasing the resolution or the efficiency of the numerical scheme. It is relatively straightforward to calculate the cost of reducing the numerical truncation errors by a given amount.

The problem of estimating and improving the accuracy of the emissions inventory is very important, but the solution appears to be mainly technical. The problem of calculating an accurate emissions inventory is mammoth; for example, Shenfield and Boyer (1974) estimated that 10,000 man-hours were required to obtain an inventory of 5 pollutants for Toronto. In spite of the

enormous amount of work required to establish accurate emissions inventory, this problem, like the accuracy of the computational scheme, is limited by lack of resources, not by a fundamental gap in basic knowledge.

In contrast to the problems of obtaining the emissions inventory and improving the numerical accuracy of the computation scheme (which are at least theoretically solvable), very basic questions remain concerning the limiting accuracy of modeled mesoscale meteorological processes and the models of the important chemical reactions. It is not known for certain that useful predictions are possible on the regional scale, much less the urban scale. In my opinion, therefore, the long-range improvements in *predictive* air-quality models will depend on progress in these two areas of research, including research in understanding the basic physical processes discussed above ("Meteorological Models on the Regional Scale"). These efforts will undoubtedly lead to more complicated models than some might wish, however. In the words of Shir and Shieh (1974), "After all, any attempt at research modeling should first aim toward understanding the overall phenomenon rather than emphasizing the simplicity and convenience of the model."

A COMBINED METEOROLOGICAL AIR-QUALITY MODEL

The problems associated with meteorological and air pollution modeling have been discussed very generally. In the balance of this paper, a specific example of how meteorological models and transport models may be combined to produce an air-quality model will be presented. The example uses one of the mesoscale meteorological models under development at The Pennsylvania State University.

While progress continues on the development of the general, multi-level hydrodynamic model described by Anthes et al. (1974), we realize that similar meteorological models of the planetary boundary layer would be useful in some air-quality modeling problems. Therefore, we have developed and are currently testing a relatively simple mixed-layer model which may have the potential of modeling mesoscale perturbations to larger-scale flows in the boundary layer.

This section describes the model, shows some of the results, and demonstrates how its meteorological output can be utilized for an air-quality prediction. This latter example illustrates the relative ease with which mesoscale meteorological models may be combined with transport and diffusion models to produce a completely time-dependent air-quality model.

Mesoscale Mixed-Layer Model

The disadvantage of any multi-level primitive equation model is its requirement for large amounts of computer time. It is, therefore, important to investigate the conditions under which simpler, more economic models can duplicate the main results from the more complicated models. Since the major mesoscale forcing occurs at the ground, it might be expected that under most conditions the mesoscale perturbations will have their greatest amplitude in the PBL. Thus it is tempting to consider mesoscale models of the PBL alone, assuming that the middle and upper tropospheric circulations are adequately predicted by large-scale models.

Lavoie (1972, 1974) developed a prototype model of the PBL which has been applied quite successfully to mesoscale studies of Great Lakes snowstorms and convective precipitation over Hawaii. Application of this mixed-layer model to two such diverse situations suggests that this type of model may have other applications to the modeling of low-level flows. Because of its simplicity, we wish to ascertain the meteorological conditions under which the simple model may be substituted for the complex model. With this in mind, we have modified Lavoie's model, which was originally designed with steady-state problems in mind, to more realistically accommodate time-dependent solutions. The major modifications include:

(a) Changing the first-order time and space differencing schemes, which heavily damp the solutions, to a conservative second-order scheme;

(b) Incorporation of a more realistic parameterization of entrainment at the top of the inversion;

(c) Modification of the parameterization of the response of the stable layer above the inversion.

The vertical structure of the mixed-layer model is shown in Figure 4. A thin (50 m) surface layer, which contains most of the vertical wind shear, follows the variable terrain. The next layer, which extends from Z_s equal to 50 m above the terrain to the base, h, of a stable upper layer, is assumed to be well mixed with nearly uniform horizontal winds and potential temperature, θ. The forecast equations for horizontal velocity, $\underset{\sim}{V}$, and θ apply to this layer. The layer above the PBL is approximated by a constant (in the vertical) lapse rate. This layer initially may contain synoptic-scale variations in temperature and wind. Later, the perturbations that develop in the PBL may produce perturbations in the upper stable layer which feed back into the PBL.

The height, h, of the PBL is assumed to be a material surface with the important exception that turbulent entrainment of mass, heat, and momentum may occur across h. This entrainment is related to the surface fluxes of heat and momentum.

The isentropic surfaces depicted in Figure 4 indicate possible variations in the thermal structure of the model. The θ_1 isentrope intersects the height of the PBL at a first-order discontinuity in potential temperature. The θ_2 isentrope intersects h at a zero-order discontinuity in θ. Mesoscale variations in potential temperature are possible within the PBL and between h and H, the undisturbed level. Above H, only synoptic-scale variations are permitted.

A Forecast of Boundary Layer Flow Over Complex Terrain

A preliminary experiment conducted with the mixed-layer model is discussed in this section to illustrate its potential. The model domain consists of a west-east cross section through the Appalachian mountains that extends over the Atlantic Ocean (Figure 5). To test the stability of the model under strong wind conditions, the initial conditions consist of a mean west wind of 30 m/s, a constant potential temperature of 290 K, and a stable layer with no large-scale temperature variations above h. The height of the inversion, h, is initially 1425 m.

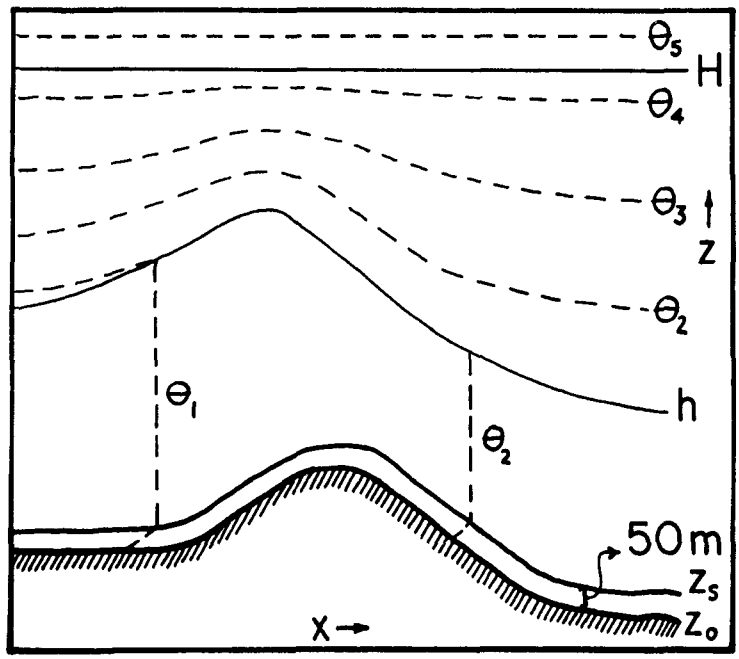

Figure 4. Structure of a mixed-layer model. The dashed lines are isentropes, the top of the mixed layer is denoted by h. Above the level H, the atmosphere is assumed to be undisturbed.

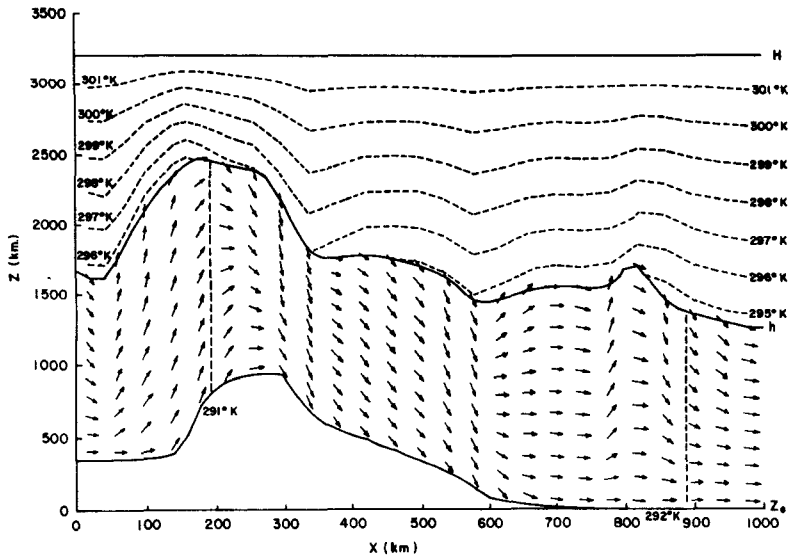

Figure 5. West-east cross section showing wind direction and potential temperature structure at 9 hours from the mixed-layer model.

The wind and temperature structure of the model after 9 hours is shown in Figure 5. The inversion has been lifted by air flowing over the mountains and to a lesser extent by entrainment due to mechanical mixing (the surface heat flux was 0 in this experiment). A perturbation exists near the coast (780 km) where the ground surface becomes suddenly smoother. Strong upward motion exists upwind of the mountains with downward motion extending to the lee.

The isentropic surfaces in the upper stable layer reflect the deformation of the PBL height. The perturbed surfaces show how significant vertical motions (and presumably clouds and precipitation) can be created in a deep layer above the PBL. Finally, entrainment has produced a downward heat flux at h, resulting in a maximum of 2° C warming in the PBL (note the 290 K and the 291 K isentropes).

A Particle-In-Cell Transport and Diffusion Model

Once the time-dependent meteorological fields are available, a transport and diffusion model is necessary to complete the prediction of a passive contaminant. As discussed in "Transport and Diffusion Models," above, the PIC model is one way of calculating regional-scale transports without large numerical diffusive effects. The transport model presented here treats the advection of a pollutant (SO_2 in this example) in a Lagrangian sense by adopting the PIC technique of Teuscher and Hauser (1974). Although the advection is a Lagrangian calculation, the effects of vertical diffusion, divergence, and deposition are calculated on an Eulerian grid. For this calculation, the concentrations represented by the particles are interpolated to the Eulerian grid where the appropriate contribution to the time rate of change of the concentration by each process is computed. These changes are then interpolated back to the particles. In the absence of nonconservative physical processes, the concentrations are preserved exactly as they move downwind. The computational details will be presented in future publications.

To resolve possibly important vertical variations in the pollutant concentrations, the vertical grid length in this experiment is 200 m. The meteorological data, however, are derived from the mixed-layer model described

earlier. These data are interpolated in the vertical as needed by the transport model. It is important to note that any model data (or observations) could be utilized in the transport model.

It may be argued that meteorological data from a mixed-layer model, which represent averages over the depth of the PBL, do not justify a high-resolution (in the vertical) transport model. While this is undoubtedly true for many meteorological situations in which the pollutant is uniformly mixed between the ground and the top of the PBL, the scale analysis (in "Potential Uses for Predictive Air-Quality Models," above) indicates that there are regional-scale meteorological situations in which pollution will not be mixed uniformly for a significant (100-200 km) distance downwind of the source. Another potential application of a high-resolution transport model in a meteorologically well mixed boundary layer is the prediction of low clouds. Treating water vapor as a "pollutant," a high-resolution transport model could be useful even within a fairly well mixed PBL to predict fogs, stratus, and stratocumulus clouds. In any case, the large number of layers here are included mainly for illustration purposes; simplificaion to a single uniformly mixed layer is quite simple.

The conservation equation for SO_2 solved in this experiment is

$$\frac{dQ}{dt} = - Q\nabla\cdot\underset{\sim}{V} - \frac{\partial F}{\partial z} \quad [\mu g\ m^{-3} s^{-1}] \qquad \text{(Eq. 24)}$$

where F is the vertical flux of Q in $\mu g/m^2 s$. The flux at the lower boundary (50 m in this experiment) is calculated from

$$F_{50m} = V_d\ (Q^b - Q_{50m}) + S \qquad \text{(Eq. 25)}$$

where V_d is the deposition velocity, Q^b is the "background" concentration, $Q_{50\ m}$ is the value of Q at 50 m, and S is an arbitrary source rate. The vertical flux at levels above 50 m is calculated from the expression

$$F = - K(z)\ \frac{\Delta Q}{\Delta z}$$

where K(z) is given by a parabolic expression

$$K(z) = \frac{4\ Kmax}{(h-Zo)}\ z\left(1 - \frac{z}{h-Zo}\right) \qquad \text{(Eq. 26)}$$

where Zo is the terrain elevation and Kmax is 20 m^2/s.

The meteorological data for the SO_2 prediction experiment were derived from a 12-hour forecast utilizing the mixed-layer model. The initial conditions for this forecast for horizontal velocity, u, and the height of the mixed layer are shown in Figure 6. The forecast data were interpolated linearly between stored values at 1-hour intervals for use in the transport model.

The hourly-averaged variations of u, w, and h between 5-6 hours and 11-12 hours are depicted in Figure 6. The conditions are fairly steady during the period. High wind velocities occur immediately downwind of the peak. The mixing depth tends to follow the terrain. Downward motion occurs over most of the domain.

The initial conditions for the SO_2 transport model consist of a uniform concentration of 50 $\mu g/m^3$. Particles which enter through the upstream boundary are assigned this value. In order to generate a plume, an upward flux of SO_2 of 35 $\mu g/m^2 s$ occurs throughout the forecast between 40 and 60 km (Figure 7).

Deposition velocities of SO_2 are of the order of 1 cm/s (Smith and Jeffrey, 1975; Rasmussen et al. 1975). There is evidence that the deposition velocities under some conditions are as much as an order of magnitude higher over water than land (Kabel, 1978). For this experiment, the deposition velocity is assumed to be 0 over land ($x < 280$ km) and 0.025 m/s over water ($x > 280$ km). The background concentration, Q^b, is taken to be 0.

Starting from homogeneous conditions at t - 0, a well developed plume is moving downwind at 3 h (Figure 7). The initially uniform mixed-layer height has quickly adjusted to the variable terrain. The advancing pollutant "front"

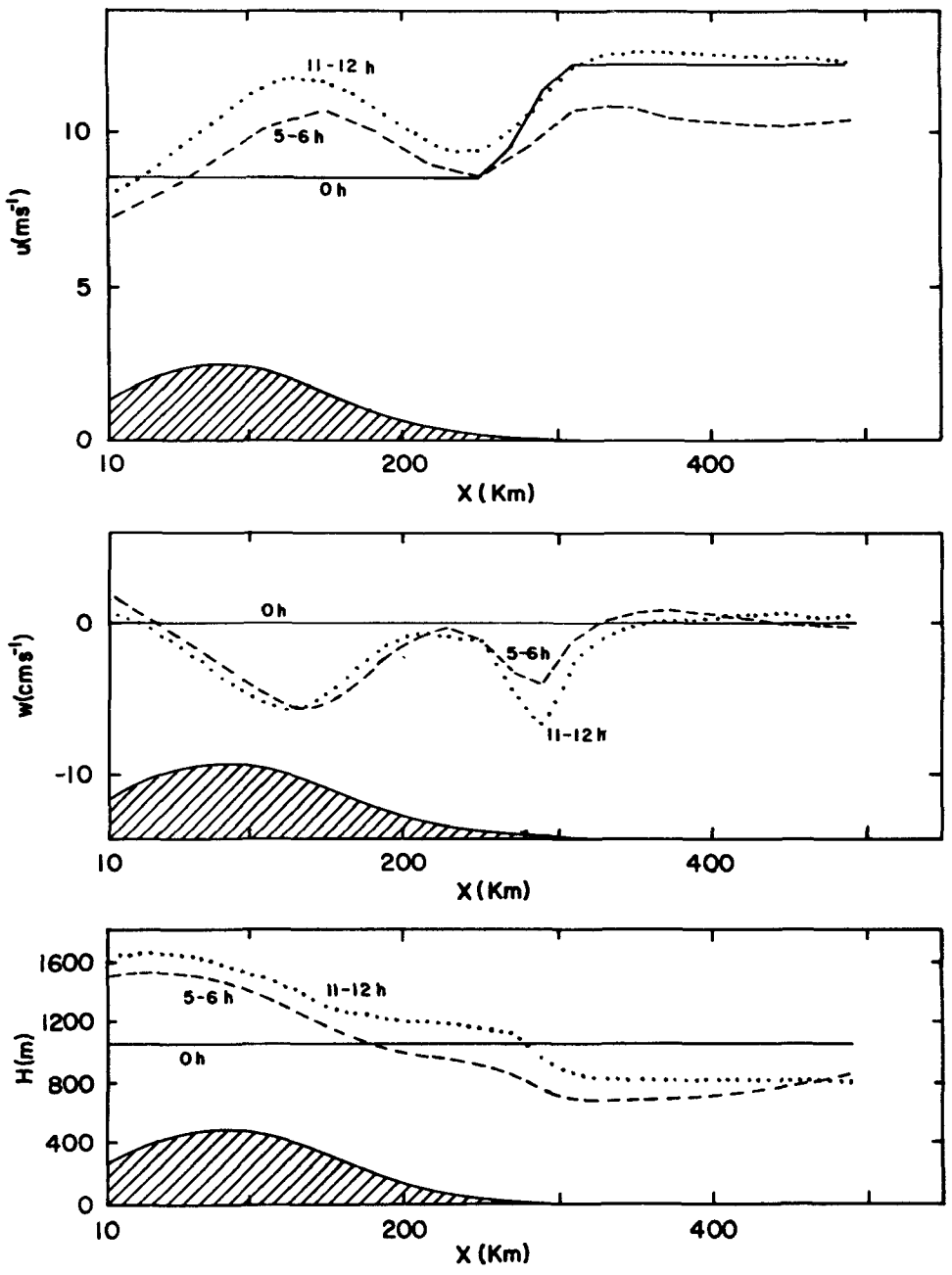

Figure 6. Horizontal profiles of the west-east component of velocity, u; vertical velocity, w, at the top of the mixed layer; and the height of the mixed layer at 0 hours (initial conditions), the 5- to 6-hour average, and the 11- to 12-hour average. These profiles were computed from the mixed-layer model.

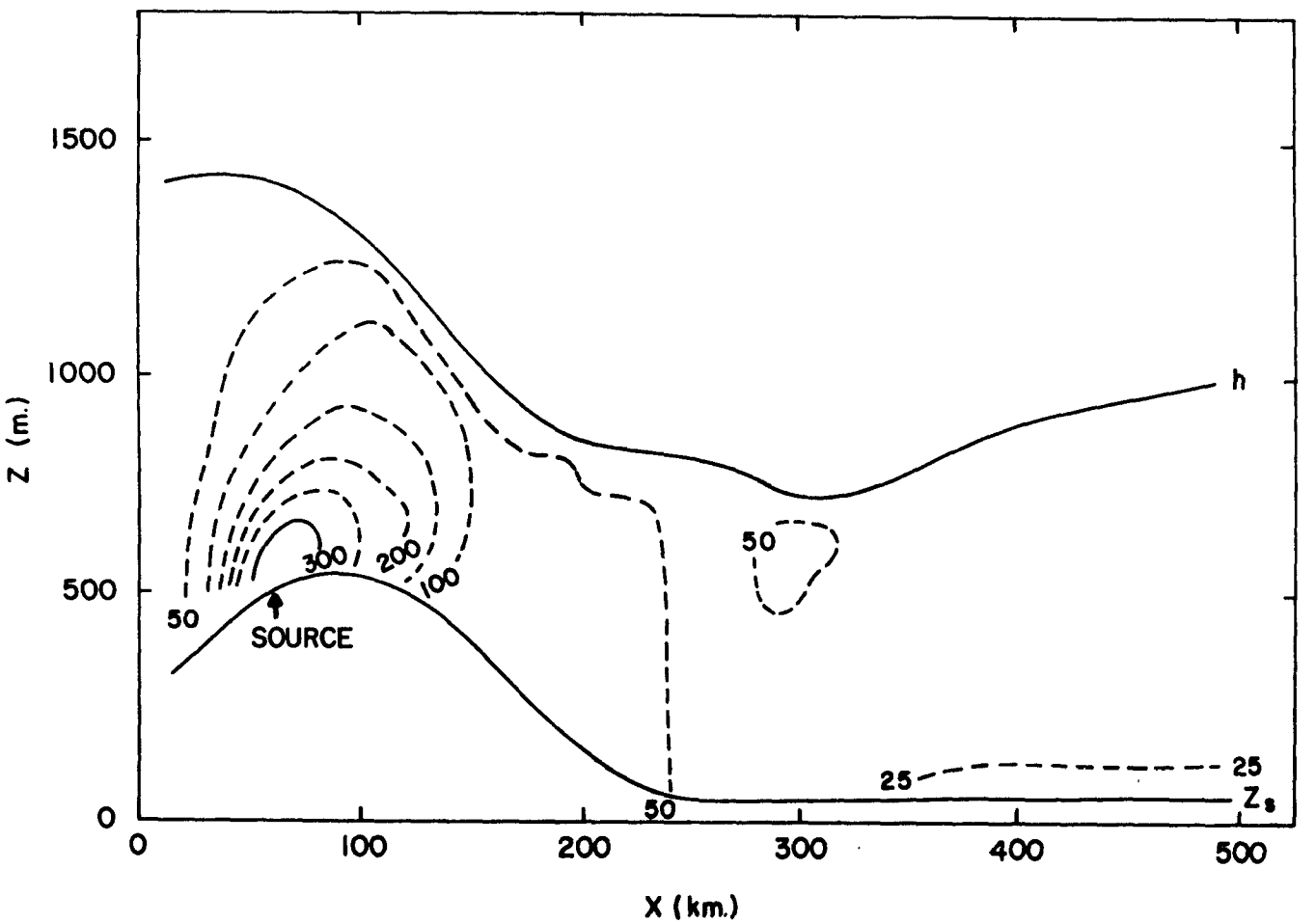

Figure 7. Forecast SO_2 concentrations after 3 hours using combined meteorological (mixed-layer) and particle-in-cell diffusion model. The initial concentration was 50 $\mu g/m^3$. A source of SO_2 occurs between 40 and 60 km. Deposition occurs over the water ($x \geq 280$ km) but not over the land ($x < 280$ km).

is nearly vertical, and deposition over the water has significantly reduced the initial concentration.

At 6 hours (Figure 8), the plume is advancing down the mountainside and starting to move out over the water. Very strong gradients of SO_2 are resolved near the source. Deposition over the water has caused a positive vertical gradient of SO_2 near the surface. A steady-state concentration, representing a balance between the emission rate, advection, and diffusion, has been reached near the mountain peak.

At 12 hours (Figure 9), the leading edge of the plume has moved off the domain. The deposition process has produced a weak minimum at the lower outflow corner of the domain. Particles in this area have had the largest trajectory in contact with the water surface. Vertical mixing of SO_2 by the turbulence parameterization is essentially complete throughout the mixed layer at a distance of 200 km (10 horizontal grid units) downwind of the source.

This hypothetical experiment illustrates the generality of the PIC modeling technique when utilized with a mesoscale meteorological model. Time-dependent winds, mixed-layer heights, and sources and sinks are easily combined to produce a completely predictive air-quality model if the initial and boundary conditions are known. The meteorological model of the PBL is relatively inexpensive (compared to multi-layer models) — the computation time for this 12-hour forecast on an IBM 370/168 was 18 s. For the two-dimensional version of this model on a 40 x 40 grid, the time for a 12-hour forecast would be about 8 min.

Future research should be directed toward improving the physics in the meteorological model and the parameterization of the reaction and sink processes in the pollutant model, and in the testing of both models against observations. For conditions in which the mixed-layer model is inapplicable, the pollutant transport model could obtain the data from more general, multi-level models.

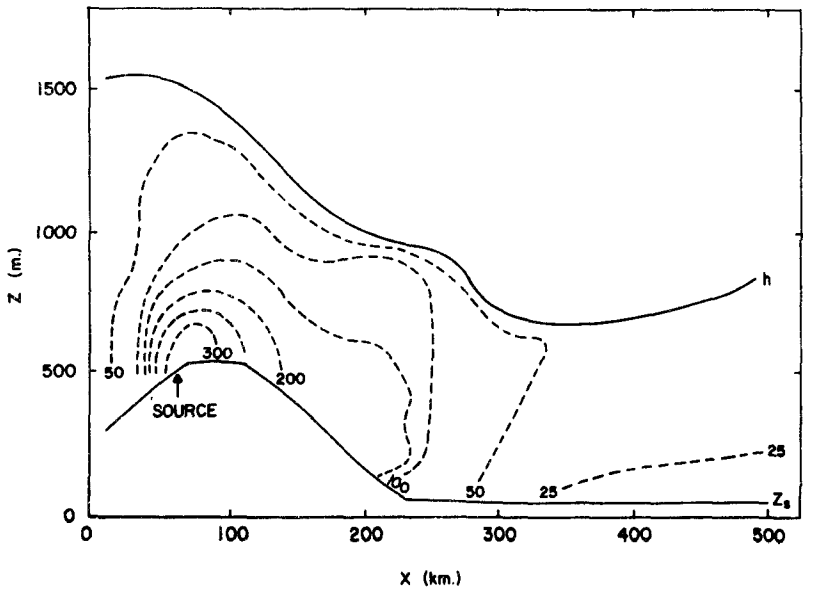

Figure 8. Forecast SO_2 concentrations after 6 hours in the experiment described in the text and in the caption for Figure 7. Note that the plume "front" is continuing its eastward advance (compare with Figure 7) while a steady-state concentration, representing a balance between source, advection, and diffusion, has been reached near the mountain peak.

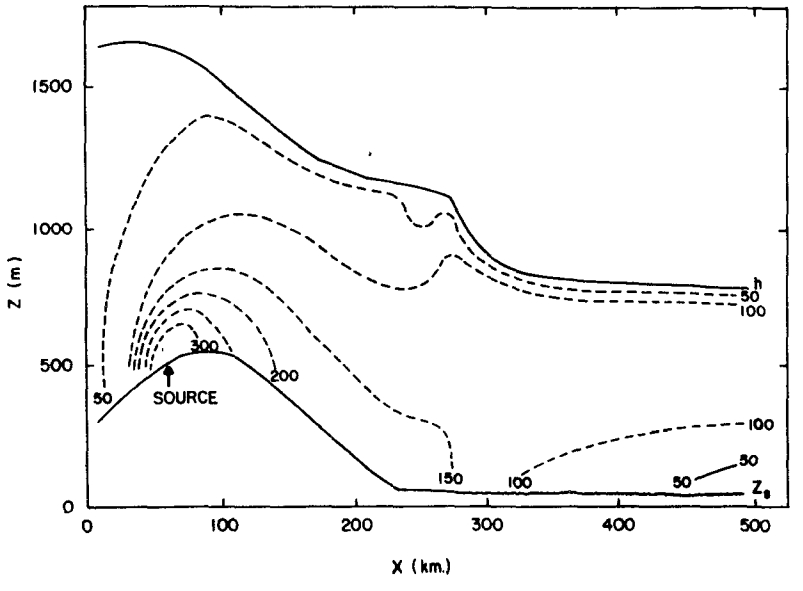

Figure 9. Forecast SO_2 concentration after 12 hours in the experiment described in the text and in the captions for Figures 7 and 8.

ACKNOWLEDGMENTS

Daniel Keyser contributed substantially to the mixed-layer model and to the PIC model. Joseph Sobel contributed the illustration of the meshed model results (Figure 3) from his work. Henk Tennekes and Dennis Thomson critically read the manuscript and made useful comments. Robert Kabel contributed to the modeling of the SO_2 deposition parameterization. Betty Bunnell typed the manuscript and Gary Fried drafted the figures. This work was supported by the U.S. Environmental Protection Agency through Grant R800397.

REFERENCES

Anscombe, F. J. 1973. Graphs in Statistical Analysis. American Statistician 27(1):17-21.

Anthes, R. A., N. Seaman, J. Sobel, and T. T. Warner. 1974. The Development of Mesoscale Models Suitable for Air Pollution Studies. In: Select Research Group in Air Pollution Meteorology, Second Annual Progress Report (Vol. 1). U.S. Environmental Protection Agency, Research Triangle Park, North Carolina. 271 pp.

Anthes, R. A., and T. T. Warner. 1974. Prediction of Mesoscale Flows over Complex Terrain. Research and Development Tech. Report ECOM-5532, Atmospheric Science Laboratory, White Sands Missile Range, New Mexico. 101 pp.

Arakawa, A., and W. Schubert. 1974. Interaction of a Cumulus Cloud Ensemble with the Large-Scale Environment, Part I. J. Atmos. Sci. 31:674-701.

Basuk, J. 1975. Freons and Ozone in the Stratosphere. Bull. Amer. Meteor. Soc. 56(6):589-591.

Blackadar, A. K. 1978. High-Resolution Models of the Planetary Boundary Layer. In: Select Research Group in Air Pollution Meteorology, Third Annual Progress Report. U.S. Environmental Protection Agency, Research Triangle Park, North Carolina.

Bleck, R. 1968. A Numerical Technique for Calculating Dry and Moist Adiabatic Trajectories in the Atmosphere. Ph.D. Thesis. Dept. of Meteorology, The Pennsylvania State University, University Park, Pennsylvania. 102 pp.

Cahn, A. 1945. An Investigation of the Free Oscillations of a Simple Current System. J. Meteor. 2:113-119.

Carlson, T. 1976. Personal communication.

Calder, K. L. 1970. Some Miscellaneous Aspects of Current Urban Pollution Models. In: Proceedings of the Symposium on Multiple-Source Urban Diffusion Models, A. C. Stern, ed. APCO Publication AP-86, U.S. Environmental Protection Agency, Research Triangle Park, North Carolina. pp. 4-1 - 4-13.

Crowley, W. P. 1968. Numerical Advection Experiments. Mon. Wea. Rev. 96:1-11.

Danielsen, E. F. 1961. Trajectories: Isobaric, Isentropic and Actual. J. Meteor. 18:479-486.

Deardorff, J. W. 1972. Numerical Investigation of Neutral and Unstable Planetary Boundary Layers. J. Atmos. Sci. 29:91-115.

Egan, B. A., and J. R. Mahoney. 1972. Numerical Modeling of Advection and Diffusion of Urban Area Source Pollutants. J. Appl. Meteor. 11:312-322.

Eschenroeder, A. 1975. An Assessment of Models for Predicting Air Quality. ERT Document ERTW-75-3. Environmental Research and Technology, Inc., Santa Barbara, California. 83 pp.

Fankhouser, J. C. 1969. Convective Processes Resolved by a Mesoscale Rawinsonde Network. J. Appl. Meteor. 8:778-798.3.

Fortak, H. 1974. Potential Applications of Mathematical-Meteorological Diffusion Models to the Solution of Problems of Air Quality Maintenance. In: Air Pollution: Proceedings of the Fifth Meeting of the Expert Panel on Air Pollution Modeling N.35, Danish Atomic Energy Commission, Roskilde, Denmark, 4-6 June. pp. 7-1 - 7-109.

Gifford, F. A. 1973. The Simple ATDL Urban Air Pollution Model. ATDL Contribution File No. 78 Revised, Air Resources Atmospheric Turbulence and Diffusion Laboratory, Oak Ridge, Tennessee. 17 pp.

Gifford, F. A. 1975. A Review of Turbulent Diffusion Typing Schemes. ATDL Contribution File No. 75/2, Air Resources Atmospheric Turbulence and Diffusion Laboratory, Oak Ridge, Tennessee. 55 pp.

Gifford, F. A., and S. R. Hanna. 1973. Modeling Urban Air Pollution. Atmos. Environ. 7:131-136.

Grønskei, K. E. 1974. Requirements of Air-Quality Models for Land Use Planning. In: Air Pollution: Proceedings of the Fifth Meeting of the Expert Panel on Air Pollution Modeling N.35, Danish Atomic Energy Commission, Roskilde, Denmark, 4-6 June. pp. 11-1 - 11-29.

Haltiner, G. J. 1971. Numerical Weather Prediction. Wiley, New York. 317 pp.

Hanna, S. R., and F. A. Gifford. 1975. Meteorological Effects of Energy Dissipation at Large Power Parks. Bull. Amer. Meteor. Soc. 56(10):1069-1076.

Harnack, R. P., and H. E. Landsberg. 1975. Selected Cases of Convective Precipitation Caused by the Metropolitan Area of Washington, D.C. J. Appl. Meteor. 14:1050-1060.

Hoffert, M. I. 1972. Atmospheric Transport, Dispersion, and Chemical Reactions in Air Pollution: A Review. AIAA J. 10(4):377-387.

Hoke, J. E. 1973. A Comparison of Three Methods for Computing Isentropic Trajectories. M.S. Thesis. The Pennsylvania State University, University Park, Pennsylvania. 83 pp.

Hudson, H. R. 1971. On the Relationship Between Horizontal Moisture Convergence and Convective Cloud Formation. J. Appl. Meteor. 10(4):755-762.

Huff, F. A., and S. A. Changnon, Jr. 1973. Precipitation Modification by Major Urban Areas. Bull. Amer. Meteor. Soc. 54(12):1220-1232.

Huff, F. A., S. A. Changnon, Jr., and D. M. A. Jones. 1975. Precipitation in the Low Hills of Southern Illinois: Part I. Climatic and Network Studies. Mon. Wea. Rev. 103(9):823-829.

Johnson, W. B. 1972. The Status of Air Quality Simulation Modeling. In: Proceedings of the Interagency Conference on the Environment, U.S. Atomic Energy Commission, Washington, D.C., October 1972. pp. 114-127.

Kabel, R. L. 1978. Natural Removal of Gaseous Pollutants. In: Select Research Group in Air Pollution Meteorology, Third Annual Progress Report. U.S. Environmental Protection Agency, Research Triangle Park, North Carolina.

Klemp, J. B., and D. K. Lilly. 1975. The Dynamics of Wave-Induced Downslope Winds. J. Atmos. Sci. 32(2):320-329.

Kuo, H. L. 1974. Further Studies of the Parameterization of the Influence of Cumulus Convection on Large-Scale Flow. J. Atmos. Sci. 31(5):1232-1240.

Lamb, D. V., F. I. Badgley, and A. T. Rossano, Jr. 1973. A Critical Review of Mathematical Diffusion Modeling Techniques for Air Quality with Relation to Motor Vehicle Transportation. Washington State Highway Dept. Research Report 12.1, Research Project Y-1540. University of Washington.

Landsberg, H. E. 1969. Weather and Health. Anchor Books (Doubleday and Company), Garden City, New York. 148 pp.

Lavoie, R. L. 1972. A Mesoscale Numerical Model of Lake-Effect Storms. J. Atmos. Sci. 29(6):1025-1040.

Lavoie, R. L. 1974. A Numerical Model of Trade Wind Weather on Oahu. Mon. Wea. Rev. 102(9):630-637.

Liu, M.-K., J. H. Seinfeld, and P. M. Roth. 1974. Assessment of the Validity of Airshed Models. Proceedings of the Fifth Meeting of the Expert Panel on Air Pollution Modeling N.35, Danish Atomic Energy Commission, Roskilde, Denmark, 4-6 June. pp. 34-1 - 34-16.

Liu, M.-K., and J. H. Seinfeld. 1975. On the Validity of Grid and Trajectory Models of Urban Air Pollution. Atmos. Environ. 9:555-574.

Long, P. E., Jr., and F. J. Hicks. 1975. Simple Properties of Chapeau Functions and Their Application to the Solutions of the Advection Equation. TDL Office Note 75-8, National Oceanic and Atmospheric Administration, National Weather Service, Techniques Development Laboratory, World Weather Building. 23 pp.

Miyakoda, K., and R. W. Moyer. 1968. A Method of Initialization for Dynamical Weather Forecasting. Tellus 20:115-128.

Molenkamp, C. R. 1968. Accuracy of Finite Difference Methods Applied to the Advection Equation. J. Appl. Meteor. 7(2):160-167.

Moretti, G. 1969. Importance of Boundary Conditions in the Numerical Treatment of Hyperbolic Equations. Physics of Fluids, Supplement 11:13-20.

Nitta, T., and J. B. Novermale. 1969. A Technique of Objective Analysis and Initialization for the Primitive Forecast Equations. Mon. Wea. Rev. 97:652-658.

Nordlund, G. G. 1975. A Quasi-Lagrangian Cell Method for Calculating Long-Distance Transport of Airborne Pollutants. J. Appl. Meteor. 14:1095-1104.

O'Brien, J. J. 1970. Alternative Solutions to the Classical Vertical Velocity Problem. J. Appl. Meteor. 9:197-203.

Ogura, Y. 1963. The Evolution of a Moist Convective Element in a Shallow, Conditionally Unstable Atmosphere: A Numerical Calculation. J. Atmos. Sci. 20:407-424.

Økland, H. 1970. On the Adjustment Toward Balance in Primitive Equation Weather Prediction Models. Mon. Wea. Rev. 99:271-279.

Ooyama, K. 1971. A Theory on Parameterization of Cumulus Convection. J. Meteor. Soc. Japan 49 (Special Issue):744-756.

Pandolfo, J., and C. Jacobs. 1973. Tests of an Urban Meteorological-Pollutant Model Using CO Validation Data in the Los Angeles Metropolitan Area, Vol. I. EPA-R4-73-025a, U.S. Environmental Protection Agency, Washington, D.C. 177 pp.

Pasquill, F. 1961. The Estimation of the Dispersion of Windborne Material. Meteor. Mag. 90(1063):33-49.

Phillips, N. A., and J. Shukla. 1973. On the Strategy of Combining Coarse and Fine Grid Meshes in Numerical Weather Prediction. J. Appl. Meteor. 12:763-770.

Pielke, R. A. 1974. A Three-Dimensional Numerical Model of the Sea Breezes over South Florida. Mon. Wea. Rev. 102:115-139.

Rao, G. V., and J. Fishman. 1975. An Iterative Initialization Scheme for Mesoscale Studies. Tellus 27(2):157-167.

Rasmussen, K. H., M. Taheri, and R. L. Kabel. 1975. Global Emissions and Natural Processes for Removal of Gaseous Pollutants. Water, Air, and Soil Pollution 4(1):33-64.

Richtmyer, R. D., and K. W. Morton. 1967. Difference Methods for Initial-Value Problems (2nd ed.). Interscience (Wiley), New York. 405 pp.

Roberts, O. F. T. 1923. The Theoretical Scattering of Smoke in a Turbulent Atmosphere. Proceedings of the Royal Society of London (Series A) 104: 640-654.

Roberts, J. J., E. S. Croke, and A. S. Kennedy. 1970. An Urban Atmospheric Dispersion Model. In: Proceedings of the Symposium on Multiple-Source Urban Diffusion Models, A. C. Stern, ed. APCO Publication AP-86, U.S. Environmental Protection Agency, Research Triangle Park, North Carolina. pp. 1-6 - 1-72.

Rosenthal, S. L. 1970. A Circularly-Symmetric Primitive Equation Model of Tropical Cyclone Development Containing an Explicit Water Vapor Cycle. Mon. Wea. Rev. 98:643-663.

Rossby, C. G. 1938. On the Mutual Adjustment of Pressure and Velocity Distribution in Certain Simple Current Systems. II. J. Marine Res. 1(3):239-263.

Sasamori, T. 1968. The Radiative Cooling Calculation for Application to General Circulation Experiments. J. Appl. Meteor. 7:721-729.

Seinfeld, J. H. 1970. Mathematical Models of Air Quality Control Regions. In: Development of Air Quality Standards, A. Atkinson and R. Gaines, eds. Charles E. Merrill, Columbus, Ohio. pp. 169-196.

Semonin, R. G., and S. A. Changnon, Jr. 1974. Metromes: Summary of 1971-1972 Results. Bull. Amer. Meteor. Soc. 55(2):95-100.

Shapiro, R. 1970. Smoothing, Filtering and Boundary Effects. Reviews of Geophysics and Space Physics 8(2):359-387.

Sheih, C. M., and W. J. Moroz. 1972. A Lagrangian Puff Diffusion Model. CAES Publication No. 273-72. Center for Air Environment Studies, The Pennsylvania State University, University Park, Pennsylvania. 47 pp.

Shenfield, L., and A. E. Boyer. 1974. The Utilization of an Urban Air Pollution Model in Air Management. In: Air Pollution: Proceedings of the Fifth Meeting of the Expert Panel on Air Pollution Modeling N.35, Danish Atomic Energy Commission, Roskilde, Denmark, 4-6 June. pp. 22-1 - 22-35.

Shir, C. C., and L. J. Sheih. 1974. A Generalized Urban Air Pollution Model and Its Applications to the Study of the SO_2 Distribution in the St. Louis Metropolitan Area. J. Appl. Meteor. 13(2):185-204.

Sklarew, R. C., A. J. Fabrick, and J. E. Prager. 1972. Mathematical Modeling of Photochemical Smog Using the PIC Method. J. Air Pollution Control Assoc. 22(11):865-869.

Slater, H. H. 1974. Application of Implementation Planning Program (IPP) Modeling Analysis to the New Jersey, New York, Connecticut Interstate AQCR. In: Air Pollution: Proceedings of the Fifth Meeting of the Expert Panel on Air Pollution Modeling N.35, Danish Atomic Energy Commission, Roskilde, Denmark, 4-6 June. pp. 9-1 - 9-56.

SMIC. 1971. Inadvertant Climate Modification. Report of the Study of Man's Impact on Climate (SMIC). MIT Press, Cambridge, Massachusetts. pp. 233-237.

Smith, F. B., and G. H. Jeffrey. 1975. Airborne Transport of Sulfur Dioxide from the U.K. Atmos. Environ. 9:643-659.

Staley, D. O. 1959. Some Observations of Surface Wind Oscillations in a Heated Basin. J. Meteor. 16(4):364-370.

Sutton, O. G. 1953. Micrometeorology. McGraw-Hill, New York. p. 258.

Teuscher, L. H., and L. E. Hauser. 1974. Development of Modeling Technique for Photochemical Air Pollution. EPA-650/4-74-003, U.S. Environmental Protection Agency, Research Triangle Park, North Carolina. 91 pp.

Turner, D. B. 1970. Workbook of Atmospheric Dispersion Estimates. PHS-999-AP-26, U.S. Environmental Protection Agency, Research Triangle Park, North Carolina. 88 pp.

Warner, T. T. 1976. The Initial Growth of Data-Related Errors in Mesoscale Numerical Weather Prediction Models. Ph.D. Dissertation. The Pennsylvania State University, University Park, Pennsylvania. 114 pp.

Williamson, S. J. 1973. Fundamentals of Air Pollution. Addison-Wesley Publishing Co., Reading, Massachusetts. 472 pp.

Yamada, T., and G. Mellor. 1975. A Simulation of the Wangara Atmospheric Boundary Layer Data. J. Atmos. Sci. 32:2309-2329.

HIGH-RESOLUTION MODELS OF THE PLANETARY BOUNDARY LAYER

Alfred K. Blackadar
Department of Meteorology

INTRODUCTION

It may be taken as axiomatic that all transport models used in air-quality simulation applications require a knowledge of the mean wind distribution within some portion of the boundary layer. The great number of air-quality simulation models that have evolved within the last few years differ rather fundamentally in the way this information is expected to become available. In the simplest class of models, it is merely assumed that the required wind distribution is provided directly from observations or less directly through some interpolative analysis of observations made at a number of places. The models comprising the most complicated class provide for the prediction of the complete mean wind distribution from an observed antecedent state and from boundary conditions based on predictable external physical features of the environment such as solar radiation, soil characteristics, and surface roughness. Between these two extremes lies an intermediate class of models characterized by a partially known wind and temperature field, consisting perhaps of only surface values. In this intermediate class, the dynamical equations are used primarily to enable the unknown portions of the three-dimensional field to be estimated.

Models are also required to give information about the diffusion of contaminants or other properties into or out of the path of the mean wind. The demands that must be met by models are of two different kinds: diffusion transports that are required for the determination of contaminant distributions, and those that are needed for the correct modeling and prediction of the mean wind distribution. Both demands must be kept in mind when planning how the boundary layer and the boundary conditions are to be treated. For example, a

knowledge of the mean wind and lapse rate near the ground may be all that is needed to estimate the concentration of contaminants downwind of an elevated point source; however, it is probably necessary to model the diffusion of heat and momentum in a fairly sophisticated way throughout the PBL in order to provide information about the surface wind distribution, if this needs to be known at some future time. The solar radiation that enters into the estimation of stability class needed for many diffusion estimates poses special problems for predictive models, for the state of cloudiness almost certainly is quite sensitive to the accumulations caused by the convergence fields of water vapor diffusion.

For many purposes, it is sufficient to predict the distribution of wind and turbulence in the lowest 100 m of the atmosphere. If this is the case, aerodynamic theory can provide the needed information if the surface fluxes of heat and momentum are predicted by the model. There are basically two ways of providing these fluxes. The first is to abandon a detailed description of the boundary layer in favor of parametric relations between the surface fluxes and a combination of free-atmosphere and surface variables. The second is to provide a sufficient number of levels in the boundary layer to resolve the significant features of the distributions of wind and temperature, and to deduce from these the resulting fluxes of physical quantities and changes of mean variables. The parametric treatment of the boundary layer is described by Tennekes (1978). The present report deals with the second approach. A more thorough discussion of recent work on second-order closure approximations in high-resolution treatment of the boundary layer is given by Lumley (1978).

EMPIRICAL METHODS

Although the incorporation of the boundary layer into simulation models of the atmosphere on various scales is a relatively new requirement, the theory on which modern solutions are based goes back to the early twentieth century. Not surprisingly, the fluxes of heat and momentum were patterned after the kinetic theory of gases which, during the latter half of the nineteenth century, had been triumphantly successful in explaining and predicting the molecular fluxes of heat and momentum in gases. Following the early theory of Ekman for

the current distribution in the surface layer of the ocean, and the adaptation of this theory by Taylor (1915) to the atmospheric boundary layer, it came to be realized that the effective viscosity of the atmosphere is not a property of the medium but of the state of turbulence and the size distribution of the turbulent eddies existing in the boundary layer.

Thus, at an early date the stage was set for the classical treatment of the fluxes, in which they are assumed to be determined by the gradients of the mean state variables, providing only that these variables are chosen to be represented in a form that is independent or conservative with respect to vertical motions. With considerable justification, the turbulent fluxes in horizontal directions have generally been assumed to be negligible in practical applications. Accordingly, the equations governing the variation of mean variables have been written as follows:

$$\frac{\partial U}{\partial t} + U\frac{\partial U}{\partial x} + V\frac{\partial U}{\partial y} + W\frac{\partial U}{\partial z} = -\frac{1}{\rho}\frac{\partial \bar{p}}{\partial x} + fV + \frac{\partial}{\partial z}K_m\frac{\partial U}{\partial z}$$

$$\frac{\partial V}{\partial t} + U\frac{\partial V}{\partial z} + V\frac{\partial V}{\partial y} + W\frac{\partial V}{\partial z} = -\frac{1}{\rho}\frac{\partial \bar{p}}{\partial y} - fU + \frac{\partial}{\partial z}K_m\frac{\partial V}{\partial z} \qquad \text{(Eq. 1)}$$

$$\frac{\partial \bar{\theta}}{\partial t} + U\frac{\partial \bar{\theta}}{\partial x} + V\frac{\partial \bar{\theta}}{\partial y} + W\frac{\partial \bar{\theta}}{\partial z} = -\frac{1}{c_p\rho}\frac{\partial R_N}{\partial z} + \frac{\partial}{\partial z}K_h\frac{\partial \bar{\theta}}{\partial z}$$

$$\frac{\partial U}{\partial x} + \frac{\partial V}{\partial y} + \frac{\partial W}{\partial z} = 0$$

$$\frac{\partial C_\alpha}{\partial t} + U\frac{\partial C_\alpha}{\partial x} + V\frac{\partial C_\alpha}{\partial y} + W\frac{\partial C_\alpha}{\partial z} = S_\alpha + \frac{\partial}{\partial z}K_\alpha\frac{\partial C_\alpha}{\partial z}$$

in which U, V, W, and $\bar{\theta}$, $\bar{p}$, and C_α are the mean velocity components, potential temperature, pressure, and pollutant concentrations, respectively; f is the Coriolis parameter; S_α is the source strength for the α pollution component; and K_m, K_h and K_α are the respective exchange coefficients for vertical turbulent transfer.

Although there is a great deal of interest and effort being placed in non-K-type theories at the present time (see Lumley, 1978), the proven and tested state of the art has not progressed much beyond K-type theories. The progress that has been made over the last 50 years has been mainly centered around methods of predicting the magnitude and distribution of the various K values either explicitly as a function of z or implicitly as a function of the distribution of mean quantities under the full range of meteorological conditions found in nature.

Completely explicit models of K_m were the first to be used and are still being used in some air-quality simulation models. An extensive bibliography of explicit treatments of K_m has been given by Wippermann (1973). Usually, the form of the vertical distribution is specified with a magnitude scale left to be determined in an appropriate way by meteorological conditions. Taylor's model consisted of the Ekman (constant K) layer matched to a surface layer in which the wind shear is parallel to the wind stress at the surface. From observations of the surface wind direction and height of the gradient wind level, Taylor determined that the value of K varies from 2.8 m^2/s during light wind conditions to 6.2 m^2/s in strong winds. Later models of the PBL in which a surface layer is matched to an upper layer with a prescribed K distribution have been studied by Rossby and Montgomery (1935), Yudin and Shvetz (1940), Ellison (1955), and Blackadar (1974a). Models such as these have been successful in relating the surface wind stress to the geostrophic wind speed and direction. They have thus contributed usefully to parametric (i.e., low-resolution) models of the boundary layer. Explicit constant K air pollution models have been formulated by Lee and Olfe (1974) and Yamada (1972).

O'Brien (1970) has proposed an explicit distribution for K that has been widely used in air-quality simulation models. It may be viewed as a cubic polynomial designed to satisfy the values of K and its derivative at key points:

$$K(z) = K_A + [(z - h^*)^2 / (h^* - z_B)^2] \times \{(K_B - K_{h^*}) + (z - z_B)[K_B' + 2(K_B - K_h^*)/(h^* - z_B)]\} \quad \text{(Eq. 2)}$$

In this equation, h* is the height of the top of the boundary layer, B refers to the surface layer, and the prime refers to the first derivative with respect to height. K_B and K_B' are assumed to be known from surface boundary-layer theory. The O'Brien distribution has been used by Bornstein (1972 and 1975) and by Pielke and Mahrer (1975). Of a similar nature but differing in detail is the distribution used by Shir and Shieh (1974):

$$K = u_* \, k \, z \, \exp(-4z/h^*) \qquad \text{(Eq. 3)}$$

where u_* is the friction velocity given by

$$u_* = \sqrt{\tau_o/p} \qquad \text{(Eq. 4)}$$

and k is von Kármán's constant. In a similar way, a trapezoidal function for K(z) was used by Bankoff and Hanzevack (1975). Although the use of explicit distributions of K has obvious advantages of simplicity, they must be scaled at the surface by parameters (K, u_*, etc.) that are known *a priori* at every time and place. This requirement tends to restrict their use to diagnostic models.

IMPLICIT K MODELS

Implicit models are designed to remove the necessity of making *ad hoc* assumptions about the distribution of K. Instead it is assumed that K should be determined by the distribution of wind shear and lapse rate. By introducing these relationships one can leave the model to generate the K distribution step by step in accordance with the evolving wind and temperature distributions. The method has the advantage that it is unnecessary to make *ad hoc* assumptions or definitions about the location and extent of the boundary layer. In a sense, the whole atmosphere becomes the boundary layer, and the model itself determines the domain where variables are influenced by the boundary conditions.

Implicit models are also useful for a different reason. It is almost impossible to determine the actual K distributions from observed velocity and temperature distributions, except in the lowest 100 m of the atmosphere. In

the case of the eddy viscosity, K_m, this situation results from the fact that, above a height of approximately 100 m, the deviation of the actual wind from the geostrophic wind vector becomes smaller in magnitude than the error of measuring the geostrophic wind itself. Empirical guidance about the actual distribution of K, especially with nonsimple distributions of wind and temperature, is not available, and observations are not sufficiently numerous and precise to verify the validity of assumed distributions. In this situation, the most reliable estimates result from an extrapolation of empirical relations that have been substantiated in the surface layer.

For the purpose of discussing the methods that have been used, it is convenient to recognize two different approaches. The first is almost totally empirical, and will be referred to as "the empirical method." The second is partly empirical and partly based on the turbulent energy equation. In accordance with Soviet usage, the second approach will be called "the semi-empirical method."

The empirical method attempts to predict the various K values using an expression of the form

$$K = \ell^2 s \cdot f(Ri) \qquad \text{(Eq. 5)}$$

where Ri is the Richardson number, s is the wind shear

$$s = \left[\left(\frac{\partial U}{\partial z} \right)^2 + \left(\frac{\partial V}{\partial z} \right)^2 \right]^{\frac{1}{4}} \qquad \text{(Eq. 6)}$$

and ℓ is a length that is presumed to characterize the energy-containing turbulence. Within the surface layer, ℓ is proportional to height:

$$\ell = kz \qquad \text{(Eq. 7)}$$

It is known that ℓ does not continue to increase linearly upward above the surface layer, but little is actually known about its distribution in the expanded atmospheric boundary layer. The most widely used distribution is that suggested by Blackadar (1962) on the basis of Mildner's Leipzig wind observations:

$$\ell = kz / (1 + kz/\lambda) \qquad \text{(Eq. 8)}$$

where

$$\lambda = .00027G/f \qquad \text{(Eq. 8a)}$$

or, as suggested more recently,

$$\lambda = .0063u_{*}/f \qquad \text{(Eq. 8b)}$$

and G is the geostrophic wind speed. This formulation has been used by Estoque and Bhumralkar (1970), Delage and Taylor (1970), Wagner and Yu (1972), Delage (1974), Lee and Olfe (1974), Gutman and Torrance (1975), Sheih and Moroz (1975), Yu and Wagner (1975), Torrance and Shum (1976), Yu (1976), and, with small modifications, by Fiedler (1972) and Mellor and Yamada (1974). Other explicit ℓ formulations which are, in effect, rather similar to the above have been suggested by Lettau (1962) and Appleby and Ohmstede (1964).

Not all authors have chosen to make ℓ independent of lapse rate, and from the point of view of Equation 7 it is immaterial whether the dependence of K on lapse rate is placed in ℓ or in f(Ri), or divided between them. However, for the present discussion, the work of the various contributors will be presented in such a way that the entire dependence on lapse rate is contained in f(Ri). We have chosen to present the discussion in terms of Richardson numbers rather than the similarity function z/L because the latter cannot as a rule be computed from model variables such as wind shear and lapse rate.

One of the simplest empirical determinations of f(Ri) follows from the work of Panofsky et al. (1960). Good agreement with observations was found over negative Richardson numbers for the equation

$$\phi_m^4 - 18 \frac{z}{L'} \phi_m^3 = 1 \qquad \text{(Eq. 9)}$$

in which

$$\phi_m = kzs/u_* \qquad \text{(Eq. 10)}$$

and

$$L' = \frac{\bar{\theta} u_* s}{kg\partial\bar{\theta}/\partial z} \qquad \text{(Eq. 11)}$$

Since K_m is by definition u^{*2}/s and since in these cases $\ell = kz$, one can easily show that

$$f_m(Ri) = \frac{K_m}{\ell^2 s} = (1 - 18Ri)^{\frac{1}{2}} \qquad \text{(Eq. 12)}$$

This function is shown in Figure 1 along with other formulations that have been suggested. Although the study discussed above was completed more than 15 years ago, it appears to be consistent with a great deal of data that have been collected since then, and may therefore be considered the best empirical basis for judging the validity of other functions that have been used. Also, as far as it is known at present, the function in Equation 12 has the correct asymptotic behavior for large negative Richardson numbers (though many uncertainties about this remain) and therefore represents the best basis for an empirical extrapolation into the extended planetary layer.

Under stable conditions the observations scatter so much that it is almost impossible to justify any particular empirical law. K_m should fall to 0 when the Richardson number approaches the critical value, but there is no agreement what this value is. The consensus favors a value in the range from 0.20 to 0.25. However, it must be kept in mind that, when the Richardson number is measured from observations that span an extended layer, the measured value is usually larger than the largest values occurring within the layer and larger even than the mean value of all the Richardson numbers occurring in the layer. Thus the "practical value" of the critical number may be larger than the value that would be appropriate if the fine structure of each layer could be determined.

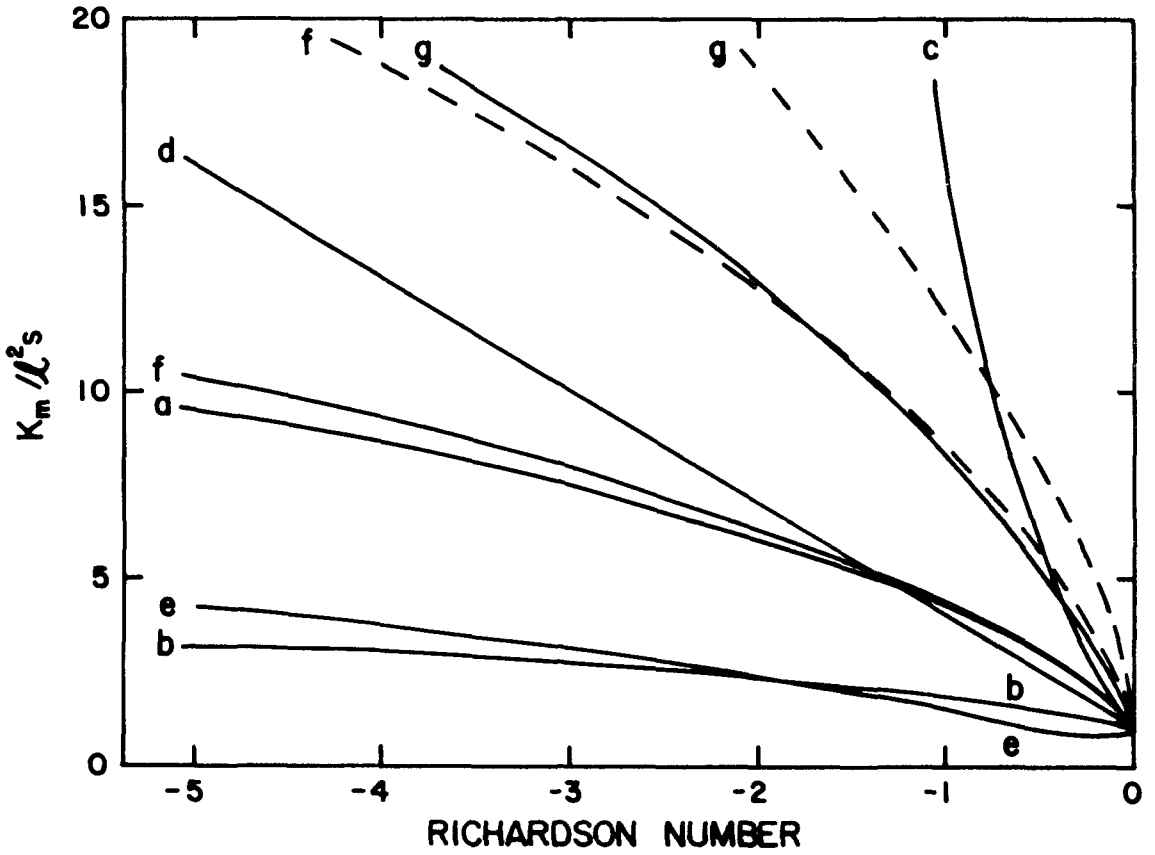

Figure 1. $K_m/\ell^2 s$ (solid lines) and $K_h/\ell^2 s$ (dashed lines) according to various formulations: *a*. Panofsky et al. (1960); *b*. Pandolfo et al. (1971); *c*. Estoque and Bhumralkar (1970); *d*. Gutman et al. (1973); *e*. Zilitinkevich and Laikhtman (1965); *f*. Blackadar Level 2 approximation; *g*. Mellor and Yamada (1974) Level 2 approximation. The simple energy equation method with $\alpha_T = 2$ gives a result that is indistinguishable from *b*.

The most thorough summary of all of the nighttime wind and temperature profiles available in published sources is that of Dyer (1974). His conclusion is that the universal function ϕ for all quantities is the same, implying the equality of the K values for all stable Richardson numbers. In this case, the adopted relation

$$\phi = 1 + 5z/L' \qquad \text{(Eq. 13)}$$

may be rewritten as

$$f(Ri) = (1 - 5Ri)^2 \qquad \text{(Eq. 14)}$$

implying a critical Richardson number of 0.20. This function is plotted in Figure 2.

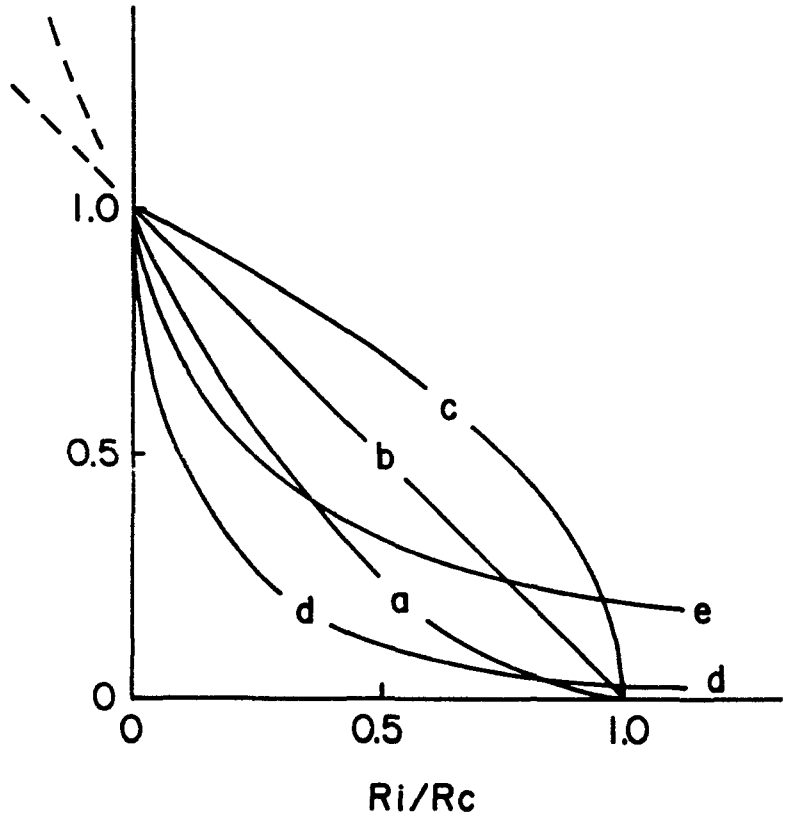

Figure 2. $K_m/\ell^2 s$ as function of Richardson number according to various formulations: *a*. empirical function following Dyer (1974); *b*. approximation adopted for the nocturnal boundary-layer model; *c*. energy equation with $\alpha_T = 1$; *d*. Estoque and Bhumralkar (1970) as corrected; *e*. Gutman et al. (1973).

With these empirically determined functions in mind, we may now look at some of the functions that have been used in boundary layer simulation models by various authors. The first is that of Estoque and Bhumralkar (1970). (Note that the equations that appear below are those that appear in corrected form in Gutman et al. [1973], rather than those given in the original article.)

$$\begin{aligned} K &= \ell^2 s\ (1 - 3\ Ri)^2 \text{ for } Ri \leq 0 \\ &= \ell^2 s\ (1 + 3\ Ri)^{-2} \text{for } Ri > 0 \end{aligned} \qquad \text{(Eq. 15)}$$

These equations are shown in Figures 1 and 2 as curves *c* and *d*, respectively. It is possible that these are not the functions that the authors intended to be used; in any event, they do not conform acceptably to the empirical functions. Several later papers by Wagner and Yu (1972), Gutman et al. (1973), Gutman and Torrance (1975), and Torrance and Shum (1976) employ what appear to have been the originally intended functions:

$$\begin{aligned} K &= \ell^2 s\ (1 - 3\ Ri) \quad \text{for} \quad Ri \leq 0 \\ &= \ell^2 s\ (1 + 3\ Ri)^{-1} \quad \text{for} \quad Ri > 0 \end{aligned} \qquad \text{(Eq. 16)}$$

These are shown as *d* in Figure 1 and *e* in Figure 2. They appear to give acceptable values for small positive and negative Richardson numbers but may not have the correct asymptotic behavior under very stable or very unstable conditions.

Pandolfo and his colleagues have published a number of model studies of the boundary layer. Of particular interest for air-quality simulation modeling is a study by Pandolfo, Atwater, and Anderson (1971). The forms used in this method are:

$$\begin{aligned} K_m &= \ell^2 s\ (1 - \alpha Ri)^2 \quad \text{for} \quad Ri > -0.48 \\ &= \ell^2 s\ \left(-\frac{h^4}{k^2} Ri\right)^{1/3} \quad \text{for} \quad Ri < -0.48 \end{aligned} \qquad \text{(Eq. 17)}$$

where α is the Monin-Obukhov constant (the value of which is in the range of 3 to 5) and h is Priestley's constant (with a value close to unity). The function for the stable case corresponds exactly with the empirical function shown

as a in Figure 2. Pandolfo, however, did not allow K to fall below the value 1 m^2/s. For negative Richardson numbers, the function falls far below the empirical values. The systematic error is offset by the fact that Pandolfo's ℓ increases linearly upward throughout the entire boundary layer instead of approaching a constant (as it is usually treated in other models).

In the semi-empirical method of Zilitinkevich and Laikhtman (1965), it is assumed as a starting point that

$$K_m = c_1 \ell_z q \quad , \quad K_h = \alpha_T K_m \qquad \text{(Eq. 18)}$$

where ℓ_z is a length to be discussed later and

$$q^2 = u'^2 + v'^2 + w'^2 \qquad \text{(Eq. 19)}$$

The quantity q is determined from the turbulent energy equation which, for stationary homogeneous turbulence without turbulent transport of energy, may be written

$$K_m s^2 - \alpha_T K_m \frac{g}{\theta} \frac{\partial \bar{\theta}}{\partial z} - \varepsilon = 0 \qquad \text{(Eq. 20)}$$

The dissipation rate ε is assumed to be given by

$$\varepsilon = c_3 q^3 / \ell_z \qquad \text{(Eq. 21)}$$

Substitution gives the result

$$K_m = \ell_z^2 s \, (1 - \alpha_T \, Ri)^{\frac{1}{2}} \qquad \text{(Eq. 22)}$$

after absorbing the ratio c_1^3/c_3 into definition of ℓ_z. If ℓ_z is defined in the customary way (so as to be independent of the stratification), this result falls very close to curve b in Figure 1 and c in Figure 2. In the latter case, the implied critical Richardson number is unity — a value that is almost certainly too large. In the unstable case, α_T has a value that ranges from about 1.3 to a limiting value of a little over 2 for indefinitely large negative

values of Ri. Comparison with the empirical equation (Equation 12) reveals that the energy equation yields the correct form for $f_m(Ri)$, but the constant is too small. This fact was first pointed out by Panofsky (1961), who explained that the large constant in the empirical equation apparently results from the high sensitivity of K to thermally induced motions, both because of their large size and their vertical orientation.

The method of Zilitinkevich and Laikhtman (1965) is interesting also because of the implicit method of determining ℓ_z:

$$\ell_z \equiv -2k\Psi / \frac{d\Psi}{dz} \qquad \text{(Eq. 23)}$$

where

$$\Psi \equiv s^2 - \alpha_T \frac{g}{\bar{\theta}} \frac{\partial \bar{\theta}}{\partial z} = s^2(1 - \alpha_T Ri) \qquad \text{(Eq. 24)}$$

The method may be viewed as an extension of von Kármán's expression

$$\ell = - ks / \frac{ds}{dz} \qquad \text{(Eq. 25)}$$

to nonneutral layers. ℓ_z is a function of Richardson number, and before comparison with other methods can be accomplished it is necessary to evaluate ℓ_z in terms of the usually defined ℓ that is equivalent to kz in the surface layer. This has been done, assuming (as did Zilitinkevich and Laikhtman) that $\alpha_T = 1$, and assuming that ϕ_m satisfies the KEYPS equation

$$\phi_m^4 - \frac{\gamma z}{L} \phi_m^3 = 1 \qquad \text{(Eq. 26)}$$

in which L is the Monin length defined by

$$L = - \bar{\theta} c_p \rho u_*^3 / kgH_o \qquad \text{(Eq. 27)}$$

H_o is the surface turbulent heat flux, and γ is a constant equal to about 12.

With these assumptions, one can obtain the result

$$f_m(Ri) = \frac{(1 - Ri)^{5/2} \left(1 - \frac{3}{4}\gamma Ri\right)^2}{\left(1 - \tfrac{1}{2}Ri\right)^2 \left(1 - \gamma\ Ri\right)^2} \qquad \text{(Eq. 28)}$$

This function appears in Figure 1 as curve *e*. Although the result does not compare favorably with the empirical curve *a*, the difference is offset in the planetary boundary model by the fact that ℓ is kz and thus increases linearly upward throughout the entire boundary layer. This method was broadened to include the effects of the turbulent diffusion of turbulent energy and applied to the entire planetary boundary layer by Bobileva et al. (1965). The predicted geostrophic drag coefficients and surface wind directions appear to display the same systematic errors that led Blackadar (1962) to reject Equation 25 for ℓ in favor of Equation 8.

Another implicit formulation of ℓ has been suggested by Wippermann (1971) on the basis of the vertical distribution of stress.

Rossby number similarity demands that — in a stationary, homogeneous, neutral atmosphere — ℓ should be scaled by the length u*/f. This view is compatible with both Equations 8 and 11. The view has recently come to be widely accepted that, as the atmosphere becomes increasingly convective, the appropriate scale length shifts rapidly from u*/f to the actual depth of the mixed layer. A few authors, including Busch et al. (1976), have actually used such a specification for ℓ in convective cases. There is no agreement on how to treat the nighttime stable layer; logical possibilities include some adaptation of Equation 8 and a shift toward the Monin length L as the length scale.

APPROXIMATIONS BASED ON A SECOND-ORDER CLOSURE

Recently, a number of authors, including Donaldson (1973), Deardorff (1973), Mellor (1973), Lewellen and Teske (1973), Lumley and Kajeh-Nouri (1973), Blackadar (1974b), Yamada and Mellor (1975), and Wyngaard and Coté (1974) have applied second-order closure methods to simulation models of the atmospheric boundary layer. A review of the development of these methods is presented by

Lumley (1978). The methods are still experimental in nature, but they have nevertheless led to considerable success in deriving relationships within the surface boundary layer that had previously only been known from observational experience. In this section, we shall make inferences about the fluxes of heat and momentum by applying to the respective equations approximations of horizontal homogeneity and stationarity as they are usually applied in boundary-layer models.

The nature of the closure approximations that have been applied to the equations for the turbulent fluxes has been described by Donaldson (1973) and Deardorff (1973). Mellor and Yamada (1974) have considered the relative order of magnitude of the terms in these equations and have shown that three levels of approximation can be achieved in a systematic way. We shall base the ensuing discussion on the Level 2 approximation, which is achieved by disregarding advective and diffusive terms in the equations for the second moments of the turbulent fluctuations. The equations as written below apply to the situation in which all of the mean quantitites are functions of height only — conditions which are generally assumed to be acceptable for the purpose of calculating fluxes in boundary-layer models:

$$C_m \ell^{-1} \sigma_w \overline{wu} = - \alpha_m \sigma_w^2 \frac{\partial U}{\partial z} + \frac{g}{\bar{\theta}} \overline{U\theta'} \qquad \text{(Eq. 29)}$$

$$C_m \ell^{-1} \sigma_w \overline{wv} = - \alpha_m \sigma_w^2 \frac{\partial V}{\partial z} + \frac{g}{\bar{\theta}} \overline{V\theta'} \qquad \text{(Eq. 30)}$$

$$C_m \ell^{-1} \sigma_w (\sigma_w^2 - 1/3q^2) = \frac{4}{3} \frac{q}{\theta} \overline{w\theta'} + 2/3 \left(\overline{wu} \frac{\partial V}{\partial z} + \overline{wv} \frac{\partial V}{\partial z}\right) \qquad \text{(Eq. 31)}$$

$$C_h \ell^{-1} \sigma_w \overline{u\theta'} = - \overline{w\theta'} \frac{\partial U}{\partial z} - \overline{wu} \frac{\partial \bar{\theta}}{\partial z} \qquad \text{(Eq. 32)}$$

$$C_h \ell^{-1} \sigma_w \overline{v\theta'} = - \overline{w\theta'} \frac{\partial V}{\partial z} - \overline{wv} \frac{\partial \bar{\theta}}{\partial z} \qquad \text{(Eq. 33)}$$

$$C_h \ell^{-1} \sigma_w \overline{w\theta'} = \alpha_h \frac{g}{\bar{\theta}} \overline{\theta'^2} - \sigma_w^2 \frac{\partial \bar{\theta}}{\partial z} \qquad \text{(Eq. 34)}$$

$$C_E \ell^{-1} \sigma_w \, q^2 = \frac{g}{\theta} \overline{w\theta'} - \left(\overline{wu} \frac{\partial U}{\partial z} + \overline{wv} \frac{\partial V}{\partial z} \right) \qquad \text{(Eq. 35)}$$

$$C_\theta \ell^{-1} \sigma_w \overline{\theta'^2} = - \overline{w\theta'} \frac{\partial \bar{\theta}}{\partial z} \qquad \text{(Eq. 36)}$$

In obtaining these equations from the Mellor and Yamada Level 2 approximation, we have made certain changes that appear to improve their usefulness. Using what is essentially the Level 3 approximation, which includes the diffusive terms, Lewellen and Teske (1973) achieved Monin-Obukhov similarity when the equations were applied to a surface-layer model. With the Level 2 approximation, however, Monin-Obukhov similarity cannot be achieved, because q/σ_w cannot be eliminated from the equations and, as is well known, q/σ_w does not obey Monin-Obukhov similarity in the surface layer. As has been shown by Blackadar (1974b), Monin-Obukhov similarity is restored by writing the equations in the above form, making them equivalent to the Mellor-Yamada equations if the following substitutions are made for the original length scales ℓ_1, ℓ_2, Λ_1, and Λ_2:

$$\ell_1 = \frac{q}{3\sigma_w} \frac{\ell}{C_m} \qquad \Lambda_1 = \frac{q}{\sigma_w} \frac{\ell}{C_E}$$

$$\ell_2 = \frac{q}{3\sigma_w} \frac{\ell}{C_h} \qquad \Lambda_2 = \frac{q}{\sigma_w} \frac{\ell}{C_\theta} \qquad \text{(Eq. 37)}$$

We have also put

$$\alpha_m \equiv \left(1 - C_1 \frac{q^2}{\sigma_w^2} \right) \qquad \text{(Eq. 38)}$$

The quantities α_m and α_h originate from the effects of vortex stretching and buoyancy adjustment on the pressure correlation terms. Under isotropic conditions they have the values 2/5 and 2/3, respectively. Under boundary-layer conditions the turbulence is not (in general) isotropic; therefore, these quantities must be determined empirically. Mellor and Yamada did not include the effects of buoyancy adjustment; therefore, in their equations α_h is replaced by unity.

The eight equations represent a closed set that may be solved algebraically to obtain explicit relations between the fluxes and the gradients of mean quantities. We note that Equations 6 and 8 together yield a gradient-type heat flux such that

$$\frac{K_h}{\sigma_w \ell} = k_h = \left(C_h + \frac{2\alpha_h \mu}{C_\theta}\right)^{-1} \qquad \text{(Eq. 39)}$$

where

$$\mu \equiv \frac{\ell^2 s^2}{\sigma_w^2} \, Ri \qquad \text{(Eq. 40)}$$

Similarly, Equations 1 and 4 or 2 and 5 together yield flux-gradient expressions for the momentum flux components with an effective exchange coefficient given by

$$\frac{K_m}{\ell \sigma_w} = K_m = (C_h \alpha_m - k_h \mu) \; / \; (C_m C_h + \mu) \qquad \text{(Eq. 41)}$$

Finally, an independent expression relating μ and Ri is obtained by eliminating q between Equations 3 and 7 and then eliminating σ_w using Equation 12. This equation is quadratic in form:

$$(a_1 Ri - a_2)\, \mu^2 + (b_1 Ri - b_2)\, \mu + CRi = 0 \qquad \text{(Eq. 42)}$$

where a_1, a_2, b_1, b_2, and C are positive functions of C_m, C_h, C_E, C_θ, α_h, and α_m.

Certain properties are easily seen from these expressions. First, when the Richardson number is 0, μ is also 0; thus σ_w (though indeterminate in Equation 12) is not necessarily 0 in neutral conditions. The solution further shows that μ always has the same sign as the Richardson number. Second, as μ becomes infinitely positive, the Richardson number approaches a limiting value. This is the critical Richardson number, and its value is given by

$$Ri_c = \frac{a_2}{a_1} = \frac{(C_m - 2c_E)\,(2\alpha_h \alpha_m C_h - C_\theta)}{6\alpha_h C_E C_m + C_\theta\,(C_m + 4C_E)} \qquad \text{(Eq. 43)}$$

The values of C_m, C_h, C_θ, and C_E are easily derived from neutral surface-layer observations if α_m is known; their values are independent of the value of α_h. Using published results of the 1968 Kansas field experiment, Blackadar (1974b) determined the values

$$\begin{aligned} C_m &= 0.52 \\ C_h &= 1.10 \\ C_\theta &= 0.19 \\ C_E &= .10 \end{aligned} \qquad \text{(Eq. 44)}$$

assuming

$$\begin{aligned} \alpha_m &= .40 \\ k &= .40 \\ \ell &= kz \end{aligned} \qquad \text{(Eq. 45)}$$

He also showed that these values give excellent predictions of the asymptotic relations for free convection if α_h in this case approaches the value 1.

The set of Equations 11 through 14 allows K_h, K_m, and σ_w to be completely determined from the Richardson number, wind shear s, and an appropriate length ℓ if α_m and α_h can be assumed to be fixed. Although the value of α_h near the neutral state has not been determined, its effect in this part of the range is minimal. The relationships for the unstable (negative) range of Richardson numbers are given in Figure 1. The curves are well represented by the functions

$$\begin{aligned} K_m/\ell^2 s &= (1 - 21\ Ri)^{\frac{1}{2}} \\ K_h/\ell^2 s &= (1 - 87\ Ri)^{\frac{1}{2}} \end{aligned} \qquad \text{(Eq. 46)}$$

The predicted curve for K_m is very close to the empirical function, as may be seen from Equation 12.

The fact that α_h appears to approach unity in free convection is consistent with the hypothesis that buoyancy compensation becomes negligible as the vortices become greatly elongated in the vertical. Buoyancy compensation arises

when temperature anomalies set up a gradient of the pressure anomaly that opposes the buoyant acceleration. With chimney-type convection, it is reasonable to believe that these opposing forces are at a minimum. By the same reasoning, it should be expected that, with stable stratification and the strong tendency for vertical motions to be suppressed, the buoyancy compensation would be enhanced and that α_h should accordingly become quite small.

We can make an inference about the behavior of α_h under stable stratification in the following way. Experience has shown that under very stable conditions K_h and K_m approach equality. If we invoke this requirement on Equations 11 and 13 as μ tends to infinity, we obtain the condition

$$\alpha_m \alpha_h = C_\theta / C_h$$

The quantity α_m does not appear to change over the entire range of negative Richardson numbers; therefore, we might reasonably expect that it is also invariant under stable conditions. Using the value 2/5 for α_m in Equation 46 results in the estimate of 0.437 for α_h which, as expected, is smaller than the theoretical value of 0.667 for isotropic conditions. Putting this value into Equation 43 leads to a predicted value of the critical Richardson number equal to 0.207, which is almost exactly the value that was determined from the Kansas field program observations. Again, we do not know how α_h varies with Richardson number over the whole stable range, but we are aided by the fact that the distributions of K_h, K_m, and σ_w in the vicinity of the neutral state are completely independent of α_h. Accordingly, we may hope to obtain a reasonable prediction of the distributions of these quantitites by holding α_h fixed over the entire range. The resulting predictions of the distributions of these quantities are given in Figures 3 and 4. It may be noted that, with negligible error over the range of positive and slightly negative Richardson number, K_h and K_m are given quite well by the simple formulas:

$$K_m = K_h = 1.1 \left(\frac{Ri_c - Ri}{Ri_c} \right) \ell^2 s \quad \text{if } Ri \leq Ri_c \qquad \text{(Eq. 47)}$$

$$= 0 \quad \text{if } Ri \geq Ri_c$$

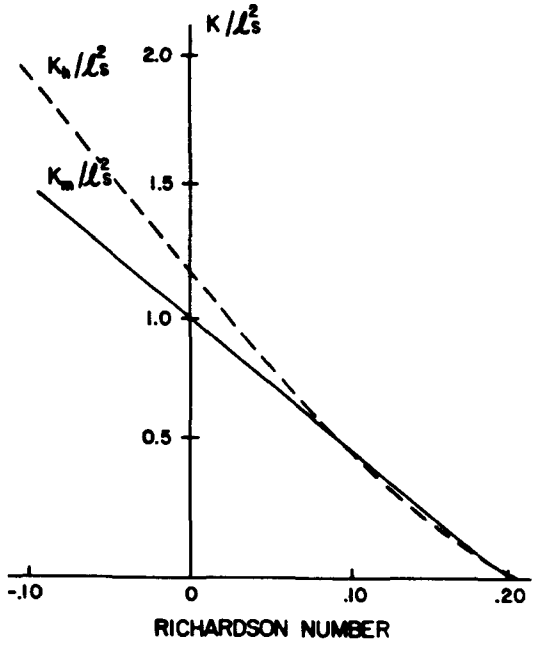

Figure 3. Level 2 approximation for K_m and K_h for positive Richardson numbers.

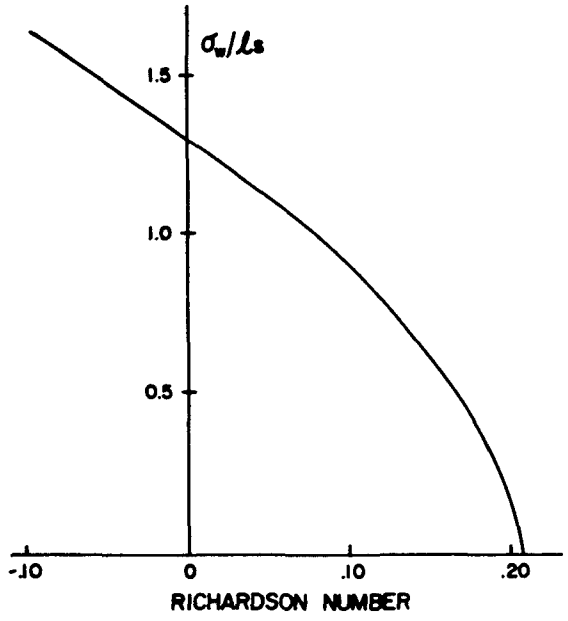

Figure 4. Level 2 approximation for positive Richardson numbers.

Unfortunately, the approximations of the second-order equations that have been used do not give any insight as to how the value of ℓ is to be found in the higher portions of the boundary layer where the size distribution of the eddies ceases to be determined by the distance to the ground. We are thus forced to rely on empirical evidence for this length as in the more primitive K theories. One hypothesis is that, under stable conditions, ℓ might reasonably be identified with the Monin length, which typically has a magnitude of the order of 10 to 50 m. Since this is of the same order as the typical free-atmospheric value of ℓ under neutral conditions, one might expect that ℓ is not strongly affected by the stability over most of the stable range.

Up until now we have considered only the solutions leading to the calculation of the fluxes of heat and momentum. It needs only to be pointed out that, as soon as these fluxes have been determined, one can return to Equations 32, 33, 35, and 36 to determine the remaining statistical quantities. The application in the surface boundary layer has given good results in the prediction of $\overline{\theta'^2}$, and — if the extended boundary-layer models are also at least moderately successful in the application of this equation — will be of great interest for the interpretation of accoustic sounding observations. Equation 35 has not been very successful in the surface layer for predicting q, apparently because of the strong influence of the neglected diffusion term. The importance of the diffusion terms away from the immediate influence of the boundary and, consequently, the ability of Equation 35 to produce acceptable results in the extended layer are not known.

PREDICTIVE MODELING OF THE NOCTURNAL BOUNDARY LAYER

The model that has been developed for insertion into the regional-scale three-dimensional model has had as its goal the achievement of maximum simplicity consistent with the requirements of predicting the distributions of wind, temperature, and other mean quantities relevant to air-quality simulation. The accuracy required for the predicted distributions does not need to be greater than that which is generally available for verification. By the same token, the accuracy need not eliminate the likely effects (on the solution) of uncertainties in the initial state and boundary conditions. The effect of such

uncertainties has not been quantitatively determined, and one of the important applications of our predictive model will be to determine its sensitivities to such uncertainties.

The requirements of a predictive model demand that the soil heat budget be included, for only in this way can the interactions of the predictable long-wave and shortwave radiation fluxes at the surface with the lower atmosphere be properly taken into account. Normally, models designed to include the soil heat budget have had to incorporate a considerable number of levels within the soil. From the point of view of predicting the interactions with the atmospheric layer, however, it is necessary only to know the soil surface temperature as a function of time. As a result, it is possible to reduce the number of levels very greatly; in fact, we have shown that — for a pure sinusoidal heat input at the surface — the surface temperature amplitude and phase can be exactly calculated with a simple model consisting of a uniform slab resting on a substrate of constant temperature. This analysis is given in the Appendix.

Let θ_g be the surface temperature of the soil, which is also the uniform temperature of the slab. We shall designate the heat capacity per unit area of the slab by C_g. It is shown in the Appendix that the appropriate value of C_g is given by

$$C_g = 0.95 \sqrt{\lambda C_s / 2\omega} \qquad \text{(Eq. 48)}$$

where λ is the thermal conductivity of the soil, C_s the heat capacity of the soil per unit volume, and ω is the angular velocity of the earth's rotation. If θ_m is the temperature of the substrate, the rate of heat transfer from the substrate to the slab is given by $\kappa_m C_g (\theta_m - \theta_g)$, where κ_m is shown in the Appendix to be appropriately given by

$$\kappa_m = 1.18\ \omega \qquad \text{(Eq. 49)}$$

The heat budget of the slab then yields an equation for the soil surface temperature:

$$\frac{\partial \theta g}{\partial t} = \frac{1}{C_g} (I_s + I\downarrow - \sigma\theta_g^4 - H_o) - \kappa_m (\theta_g - \theta_m) \qquad \text{(Eq. 50)}$$

where I_s is the solar insolation absorbed in the surface, $I\downarrow$ is the longwave back radiation from the atmosphere, σ is the Sefan-Boltzmann constant, and H_o is the heat flux carried away from the surface by turbulence. The value to be used for θ_m is the mean temperature of the slab (and thus of the surface air) during the most recent past.

For computational purposes, we divide the domain of the atmosphere to be modeled into layers of thickness Δz. The average properties of each layer are designated by an odd value of the index i, as shown in Figure 5:

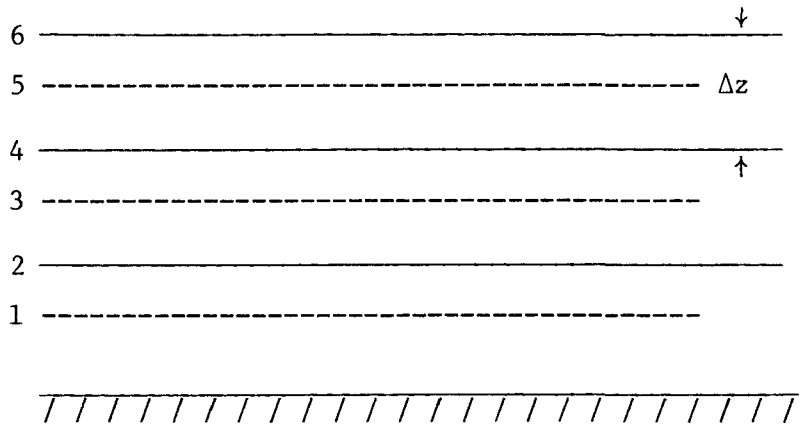

Figure 5. Atmospheric layers and grid nomenclature for the nocturnal boundary-layer model.

Quantities such as the Richardson number

$$Ri_i = \frac{g}{\bar{\theta}\Delta z} \left(\frac{\theta i+1 - \theta i-1}{s_i^2} \right) \qquad \text{(Eq. 51)}$$

where

$$s_i^2 = [(V_{i+1} - V_{i-1})^2 + (V_{i+1} - V_{i-1})^2] / (\Delta z)^2 \qquad \text{(Eq. 52)}$$

will normally be calculated only at even-numbered values of i. The equations for the mean velocity and the mean potential temperature are applied at each odd numbered value of i greater than or equal to 3. We assume that the mean vertical velocity is 0.

$$\frac{\partial U_i}{\partial t} + U_i \frac{\partial U_i}{\partial x} + V_i \frac{\partial U_i}{\partial y} = f(V_i - V_{gi}) + \frac{K_{m(i+1)}}{\Delta z^2}(U_{i+2} - U_i) - \frac{K_{m(i-1)}}{\Delta z^2}(U_i - U_{i-2})$$

$$\frac{\partial V_i}{\partial t} + U_i \frac{\partial V_i}{\partial x} + V_i \frac{\partial V_i}{\partial y} = -f(U_i - U_{gi}) + \frac{K_{m(i+1)}}{\Delta z^2}(V_{i+2} - V_i) - \frac{K_{m(i-1)}}{\Delta z^2}(V_i - V_{i-2})$$

$$\frac{\partial \theta_i}{\partial t} + U_i \frac{\partial \bar{\theta}_i}{\partial x} + V_i \frac{\partial \bar{\theta}_i}{\partial y} = \frac{K_{H(i+1)}}{\Delta z^2}(\bar{\theta}_{i+2} - \bar{\theta}_i) - \frac{K_{H(i-1)}}{\Delta z^2}(\bar{\theta}_i - \bar{\theta}_{i-2}) \qquad \text{(Eq. 53)}$$

Generally in the stable nocturnal model, it has been assumed that K_m and K_h are equal and are given by the Richardson number using Equation 47 obtained by the second-order Level 2 approximation. The latter approximation gives no basis for predicting ℓ; trial solutions suggest that a constant value of 28 to 40 m gives good results. The value of K is never allowed to fall below 0; when the Richardson number exceeds the critical value, K is arbitrarily set equal to 0. In all of the cases treated so far, the value of 1/4 has been used for the critical value of the Richardson number. Possibly a value of 1/5 would be better in view of the indications of the second-order closure predictions. However, the Richardson number calculated by finite differences tends to be systematically greater than the mean of the Richardson numbers within the layer. Therefore, it should not be too surprising if even larger critical values would be found to work best in certain applications, particularly if large values of Δz are used.

The lowest layer must be treated differently from the rest because there is no turbulent exchange through the underlying surface; we must use the

surface fluxes, which have yet to be determined. Since the layer thickness Δz is normally kept rather small (50 m has typically been used) it is reasonable to assume that the wind direction does not change between the ground and $z_1 = \Delta z/2$. The surface stress is then in the same direction as the wind at z_1. Thus the equations for the lowest layer are:

$$\frac{\partial U_1}{\partial t} + U_1 \frac{\partial U_1}{\partial x} + V_1 \frac{\partial U_1}{\partial y} = f(V_1 - V_{g1}) + K_2 \left(\frac{U_3 - U_1}{\Delta z^2}\right) - \frac{u_*^2 U_1}{\Delta z W}$$

$$\frac{\partial V_1}{\partial t} + U_1 \frac{\partial V_1}{\partial x} + V_1 \frac{\partial V_1}{\partial y} = -f(U_1 - U_{g1}) + K_2 \left(\frac{V_3 - V_1}{\Delta z^2}\right) - \frac{u_* 2 V_1}{\Delta z W} \qquad \text{(Eq. 54)}$$

$$\frac{\partial \theta_1}{\partial t} + U_1 \frac{\partial \theta_1}{\theta x} + V_1 \frac{\partial \theta_1}{\partial y} = K_2 \left(\frac{\theta_3 - \theta_1}{\Delta z^2}\right) + \frac{H_o}{C_p \rho \Delta z}$$

where

$$W \equiv (U_1^2 + V_1^2)^{\frac{1}{2}} \qquad \text{(Eq. 55)}$$

In order to solve the atmospheric equations it is necessary to have, in addition to the initial and boundary conditions, the components of the geostrophic wind as function of height and time at each place. After insertion of the boundary-layer model into the three-dimensional regional-scale model, this information will be available; when used as a one-dimensional model, the boundary-layer model must rely on observations to estimate the geostrophic wind. In a similar way, the back radiation from the atmosphere, which is needed in Equation 50, will eventually be calculated from the temperature and water vapor distributions provided by the model.

The final requirement of the model is to specify how the surface fluxes of heat and momentum are to be calculated from the variables of the model. In the past, modelers have generally solved this problem by assuming that the lowest layer satisfies Monin-Obukhov similarity. The wind and temperature profiles are then specified according to empirical equations in terms of the

boundary fluxes, which are determined by fitting the profiles at the levels where the temperature and velocity components are known — usually at the nominal surface z_o and at the first level z_1. This is the procedure that was followed by Pandolfo et al. (1971) and by Yu and Wagner (1975). The procedure is open to some question, however, particularly at night, because it is known that — as one approaches the surface — the processes dominating the temperature distribution change quite rapidly from turbulent exchange to radiation. Thus, extrapolations of the Monin-Obukhov temperature profiles to the surface (which may have a different z_o from that applicable to the wind) may lead to a gross error in the estimate of the ground surface temperature, an error that is difficult to verify observationally because of the notorious difficulty of measuring the actual air temperature at the ground surface.

For the purposes of our model, we assume that the temperature profile is dominated by turbulence and therefore obeys Monin-Obukhov similarity throughout the first layer down to a level a_a, which has a nominal height of 1 m and which may be identified with the height of the thermometer in an ordinary instrument shelter. Below z_a, we assume that temperature changes are determined by the radiative flux divergence as well as the turbulent flux convergence. For the calculation of the wind distribution, we assume that the wind profile follows Monin-Obukhov similarity down to the height z_o, where the wind speed is 0.

As far as we are aware, satisfactory empirical equations for the radiative and turbulent flux divergences in the surface layer have never been determined. We have adopted a suggestion by Sellers (1965, p. 234) that the radiative cooling rate is proportional to $(\theta_a - \theta_g)$ and that, in the equilibrium case, this cooling rate is compensated by the effects of turbulent flux convergence. The latter is assumed to be proportional to H_o. This view of the operation of these flux divergences appears to be supported by the observation of Rider and Robinson (1951) that the radiative flux divergence tends to increase with the amount of turbulent mixing near the surface. Accordingly, the "surface" air temperature is governed by the equation

$$\frac{\partial \theta_a}{\partial t} = a\,(\theta_g - \theta_a) - b\,H_o \,/\, c_p\,\rho\,z_a \qquad \text{(Eq. 56)}$$

The behavior of this equation is such that the existence of turbulence at night causes the surface air temperature to be elevated above the ground surface temperature; when the wind becomes calm, the surface air temperature decays exponentially to the ground temperature. Sellers, using data of Rider and Robinson, suggests a coefficient that would make $a = 3.6 \times 10^{-4}$/s. We have experimented with a variety of values and have adopted $a = 8.3 \times 10^{-4}$/s and $b = 0.200$.

Since we are assuming that Monin-Obukhov similarity prevails in the lowest layer, well known laws would permit $(\theta_1 - \theta_a)$ and W_1 to be determined from $T_* = -H_o/c_p k \rho u_*$ and from u_*. In principle, the problem can be inverted; in practice, this is infeasible due to the nature of some of the functions involved in the relationship. Fortunately, the problem is simplified by the fact that good initial estimates of u_* and T_* are available from the previous time step and a double iteration routine is sufficient to produce accurate updated values. The first step in this routine is to estimate the bulk Richardson number

$$B = \frac{g}{\bar{\theta}} \frac{z_1}{W_1^2} \left[(\theta_1 - \theta_a) + T_* \ln \frac{z_a}{z_o}\right] \qquad \text{(Eq. 57)}$$

using the most recently available values of θ_1, θ_a, W_1, and T_*. The form of the profile equations varies according to the value of B, and three possibilities exist. The first case occurs when B is positive and exceeds the value 1/5. In this case the lowest layer becomes nonturbulent, and (even though the wind at the level z_1 is not 0) the momentum and heat fluxes at the surface are set equal to 0. The second case is the stable case in which $0 \leq B \leq 1/5$. Here we proceed to calculate the Monin length L from the formula

$$\frac{1}{L} = \frac{1}{z_1} \ln \frac{z_1}{z_o} \left[\frac{B}{1-5B}\right] \qquad \text{(Eq. 58)}$$

and then derive u_* and T_* from

$$u_* = kW_1 \; / \; (\ln \frac{z_1}{z_o} - \Psi_m) \qquad \text{(Eq. 59)}$$

$$T_* = (\theta_1 - \theta_a) \; / \; (\ln \frac{z_1}{z_a} - \Psi_h) \qquad \text{(Eq. 60)}$$

in which

$$\Psi_m = \Psi_h = -5 \; z_1 \; / \; L \qquad \text{(Eq. 61)}$$

In the unstable case, $B \leq 0$ is not so likely to occur at night. When it occurs, the following routine is executed. Using the last estimate of the Monin length L, one determines

$$x = (1 - 16 \frac{z_1}{L})^{1/4} \qquad \text{(Eq. 62)}$$

and then proceeds, in sequence, to obtain

$$\Psi_h = 2 \ln \frac{1+x^2}{2} \qquad \text{(Eq. 63)}$$

$$\Psi_m = (\frac{\Psi h + \pi}{2}) + 2 \ell n (\frac{1 + x}{2}) - 2 \tan^{-1} x \qquad \text{(Eq. 64)}$$

$$u_* = kW_1 \; / \; (\ln \frac{z_1}{z_o} - \Psi_m) \qquad \text{(Eq. 65)}$$

$$T_* = (\theta_1 - \theta_a) \; x \; (\ln \frac{z_1}{z_a} - \Psi_h) \qquad \text{(Eq. 66)}$$

$$\frac{1}{L} = \frac{B}{z_1} \left[\frac{(\ln \frac{z_1}{z_o} - \Psi_m)^2}{(\ln \frac{z_1}{z_o} - \Psi_h)} \right] \qquad \text{(Eq. 67)}$$

The functions in Equations 63 and 64 were derived by Paulson (1970).

Having thus arrived at new values of u_* and T_*, one may return to recalculate B (and so forth) as many times as desired. A single reiteration has proved to be entirely satisfactory in our one-dimensional model experiments. Having obtained acceptable values of u_* and T_*, one obtains H_o from

$$H_o = -k \; c_p \; \rho u_* \; T_* \qquad \text{(Eq. 68)}$$

To ensure computational stability, it is necessary at all times to satisfy the inequality

$$\frac{2\,K\,\delta t}{(\Delta z)^2} < 1 \qquad \text{(Eq. 69)}$$

To choose a time step that is small enough to ensure that this inequality is always satisfied would be unnecessarily expensive in computer time. Ordinarily, a 2-min time step is sufficient for the level of accuracy demanded of the model. To cope with occasional situations where shorter time steps are needed, provision is made for a variable time step to be calculated from the equation

$$\delta t = m\,\frac{(\Delta z)^2}{K_{max}} \qquad \text{(Eq. 70)}$$

where m is less than 1/2 and K_{max} is the largest value of K found during the previous time step. A value of m = 1/4 has performed very well. The variable value thus calculated is used only if it is less than 2 min.

The remainder of this report will deal with several experiments that have been performed with the model. In the first of these, the atmosphere was initially set at a constant potential temperature of 25° C, and the same temperature was assigned to θ_g and θ_m. I_s, $I\downarrow$, and σ were all set equal to 0. Thus, there was no heating or cooling throughout the experiment and the stability was neutral. The geostrophic wind was set equal to 20 m/s parallel to the x-axis, and the wind was set equal to the geostrophic value at every level. The model, of course, constrains the wind at the ground to 0, and (since there is a momentum flux at the surface) a boundary layer grows rapidly upward. The model was allowed to run for a period equivalent to about 2 pendulum days, at which time the solution had nearly approached a steady state. The resulting wind hodograph and the vertical distribution of K_m are shown in Figures 6 and 7. It is possible that the distribution of K is affected by the upper boundary. Although the wind is not constrained at the top level, the momentum flux has been arbitrarily made equal to 0 there. The small value of K, however, results mainly from the fact that the shear is approaching 0 as one ascends to greater heights. The spiral and the K distribution agree at least qualitatively with what is normally observed in neutral barotropic boundary layers.

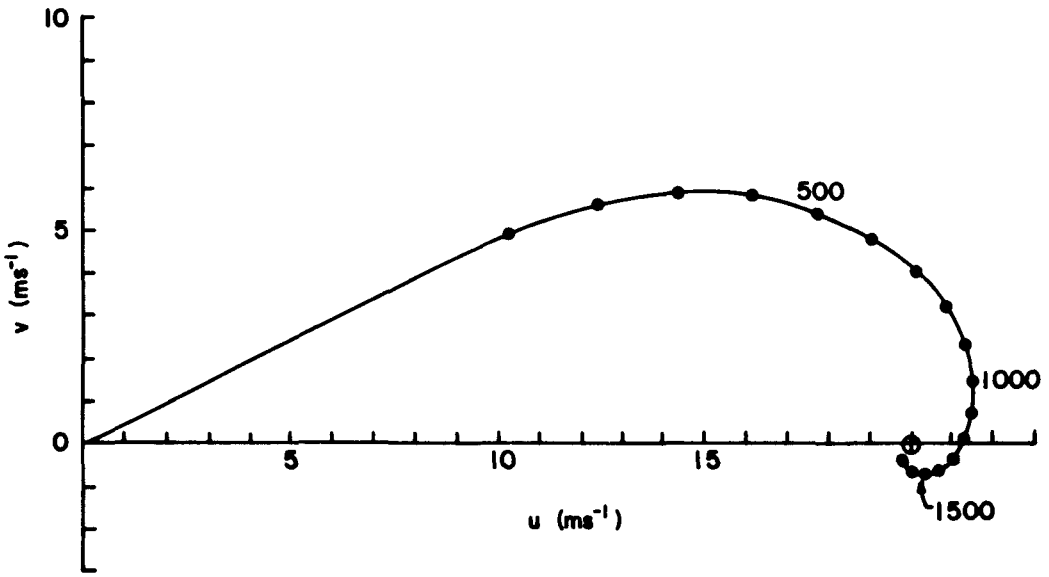

Figure 6. Spiral wind hodograph for a steady-state neutral simulation.

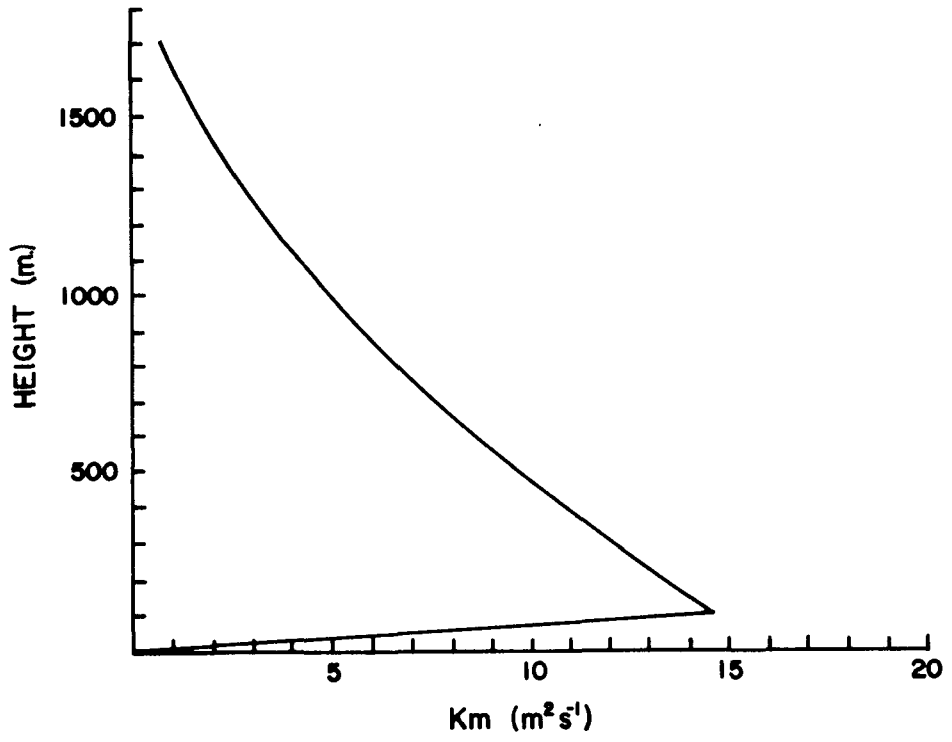

Figure 7. Vertical distribution of K_m for a steady-state neutral simulation.

The second experiment attempted to predict the evolution of wind and temperature distributions observed at O'Neill, Nebraska during the Great Plains Field Observation Program in 1953. The data used for the initial condition and for the verification were from the 1st, 3rd, 6th, and 7th general observation periods. A composite formed from the average of the four observations was used. Averages of U, V, and θ were tabulated from the surface up to 2000 m above the surface, at 2-hour intervals from 1835 CST to 0635 CST. The advective terms in the equations were all set equal to 0, and the ground slab characteristics were determined from the published measurements (Lettau and Davidson [1957]). The geostrophic wind was held fixed during the period of integration. The components adopted at 1500 m were those estimated by Lettau and Davidson, but the geostrophic magnitude at the surface had to be increased from 10.8 to 14.5 m/s to obtain satisfactory agreement between predicted and observed changes. A comparison of the observed and predicted wind speed and temperature profiles is shown in Figure 8. Figure 9 shows a comparison of the predicted ind observed values of "surface" air temperature θ_o. The poor performance of the measured geostrophic winds is a serious problem in the prediction of the boundary layer evolution from observed conditions, just as it has always rendered determination (in practice) of the vertical distribution of stress and exchange coefficient by the geostrophic departure method nearly impossible.

In the third experiment, the integration was begun at 1600 Local Apparent Time with a neutral equilibrium wind distribution calculated from a simple two-layer model. θ_g and the potential temperature of all layers of the atmosphere were initially set equal to 25° C. The values of other important parameters are given in Table 1. Solar heating was calculated at each time step from the hour angle and declination of the sun using an atmospheric transmission coefficient of 0.8 and a surface albedo of 0.20. Although the solar zenith angle is increasing, the surface heating is still sufficiently strong (initally) to cause the entire layer to become unstable; there is an immediate and rapid adjustment of all of the variables during the first hour or so. Thereafter, all quantities are evolving slowly and smoothly. The results are shown for three runs. Runs 1 and 2 differ only in the value of the roughness of the surface; Runs 2 and 3 differ only in the geostrophic wind. Figures 10 and 11

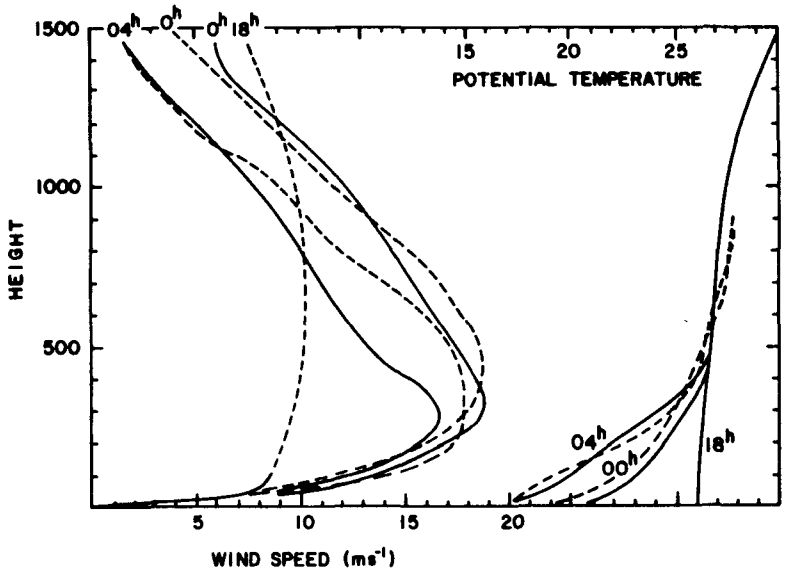

Figure 8. Predicted (solid lines) and observed (dashed lines) wind speed and potential temperature profiles at O'Neill, Nebraska. The observations pertain to a composite of four different nights.

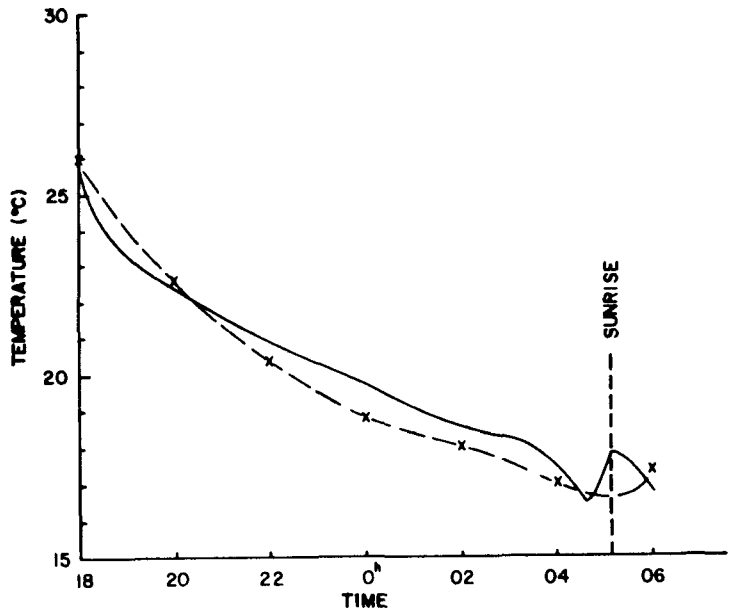

Figure 9. Predicted (solid line) and observed (dashed line) surface air temperatures as a function of time for the O'Neill composite.

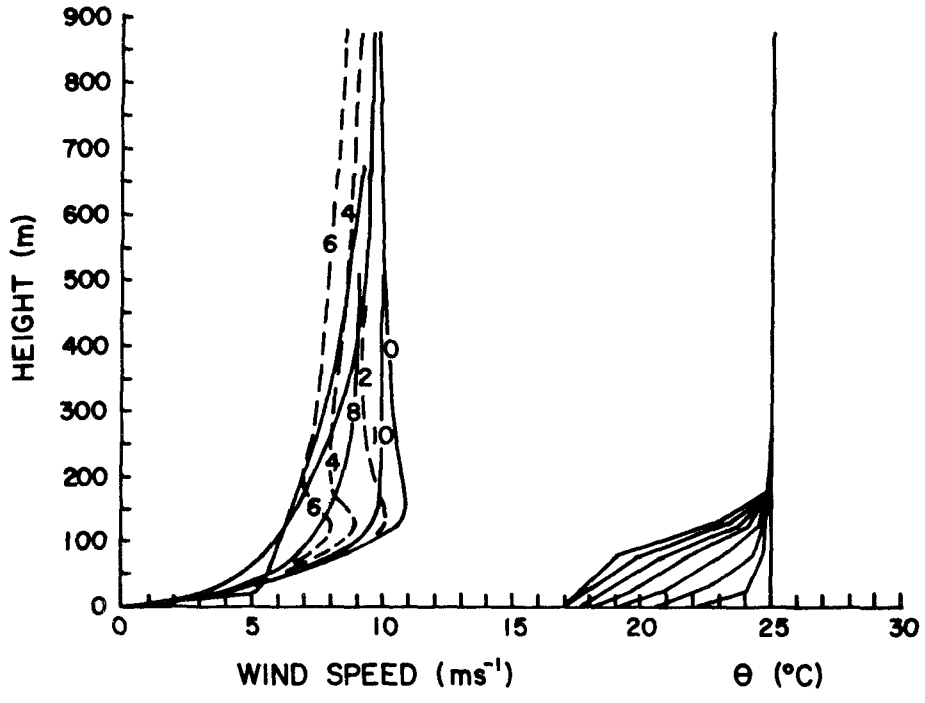

Figure 10. Evolution of wind speed and potential temperature profiles for conditions listed in Table 1; roughness parameter 0.1 m and geostrophic wind speed 8.0 m/s.

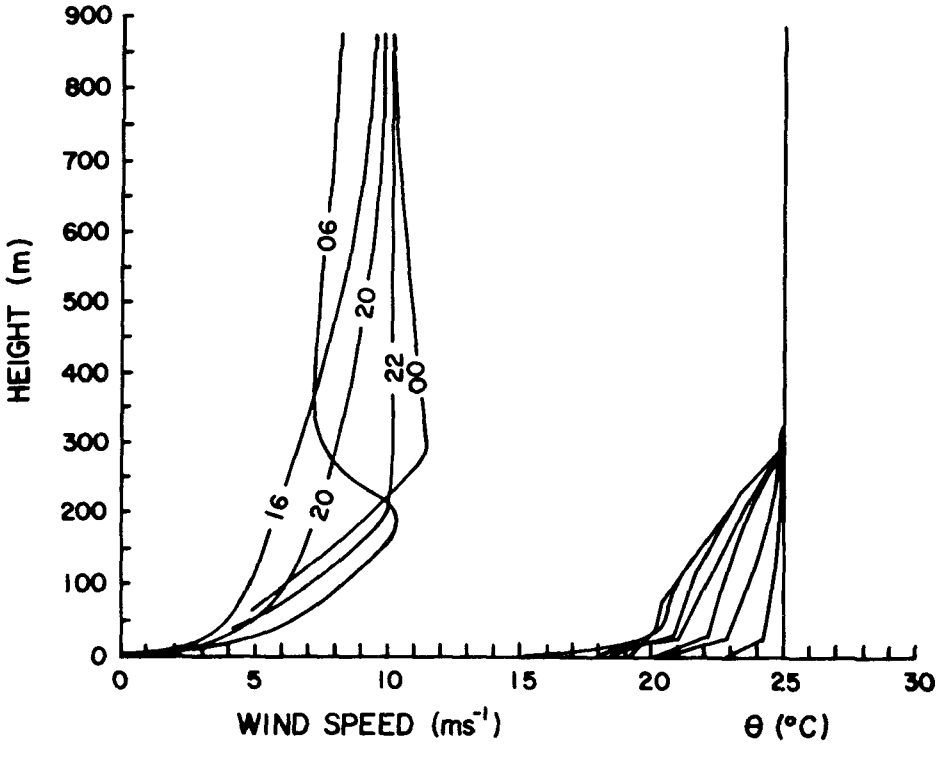

Figure 11. Evolution of wind speed and potential temperature profiles for conditions listed in Table 1; roughness parameter 1.0 m and geostrophic wind speed 8.0 m/s.

TABLE 1. PARAMETERS AND INITIAL CONDITIONS USED IN THE THIRD EXPERIMENT

	Run 1	Run 2	Run 3
Downward longwave radiation I (ly/min)	0.42	0.42	0.42
Roughness parameter z_o (m)	0.10	1.0	1.0
Geostrophic wind U_g (m/s)	8.0	8.0	9.4
V_g (m/s)	0.0	0.0	0.0
Substrate Temp. θ_m (°C)	20	20	20
Latitude	45N	45N	45N
Solar declination	+10°	+10°	+10°
$C_g/C_p \rho$ (m)	221	221	221
Critical Richardson number	0.25	0.25	0.25
ℓ (m)	71	71	71

show very clearly how an increase of the surface roughness from 0.1 to 1.0 m increases the height of the layer of mixing during the night. There is also a slight increase of wind at 0 hours at the upper levels due to the fact that, with the larger roughness, the initial wind at these levels is more greatly retarded from the geostrophic wind, and consequently the amplitude of the inertia oscillation is increased. Comparison of Figures 12 and 13 shows a still greater growth of the depth of the mixed layer caused, in this case, by an increase of the geostrophic wind from 8.0 to 9.4 m/s. Figure 13 shows an example of the vector variation of the wind during the night at a level near the top of the mixed layer; the vector wind hodograph at 03 hr is interesting in that (rather typically) it bears a resemblance to a wind spiral, even though the wind is not in equilibrium.

Figures 14, 15, and 16 show the course of the "surface" air temperature and u_* during the night for each of the three runs. The most rapid cooling

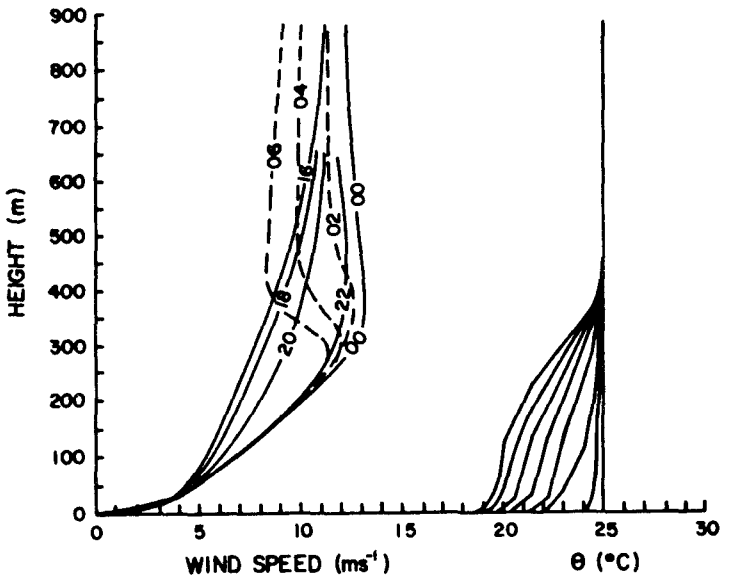

Figure 12. Evolution of wind speed and potential temperature profiles for conditions listed in Table 1; roughness parameter 1.0 m and geostrophic wind speed 9.4 m/s.

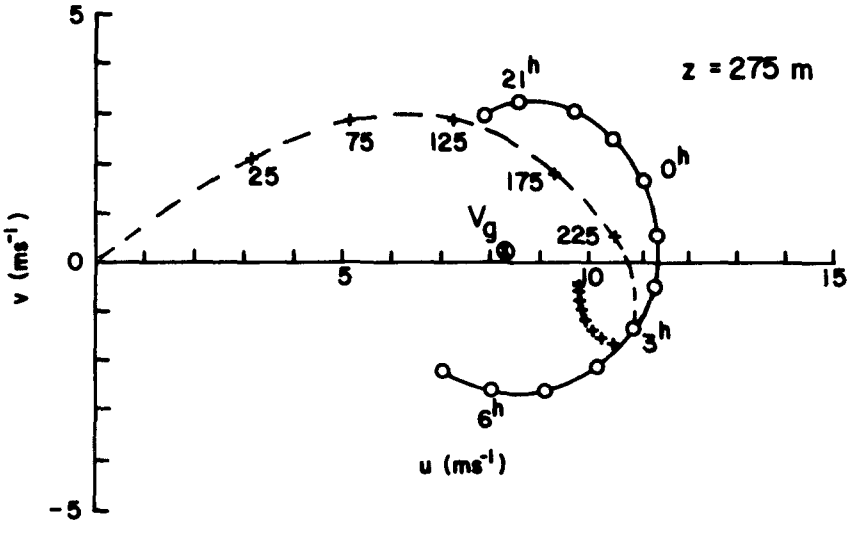

Figure 13. Wind vector hodograph calculated for Run 2 in Table 1. Dashed line shows the wind vector variation with height at 0300 Local Apparent Time. Solid line shows the wind vector variation with time at a height of 275 m.

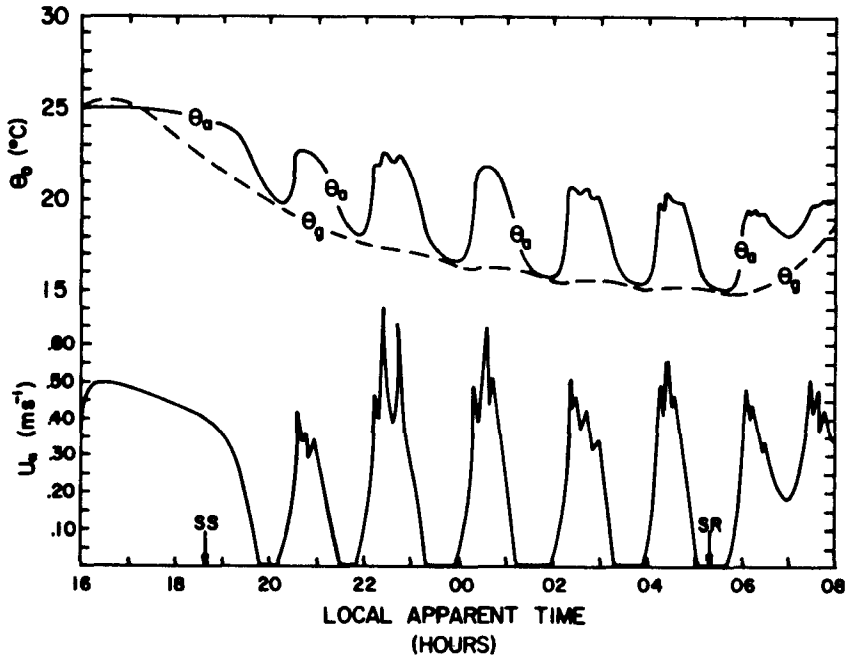

Figure 14. θ_a and u_* as function of time during the night for conditions listed in Table 1; roughness parameter 0.1 m and geostrophic wind speed 8.0 m/s.

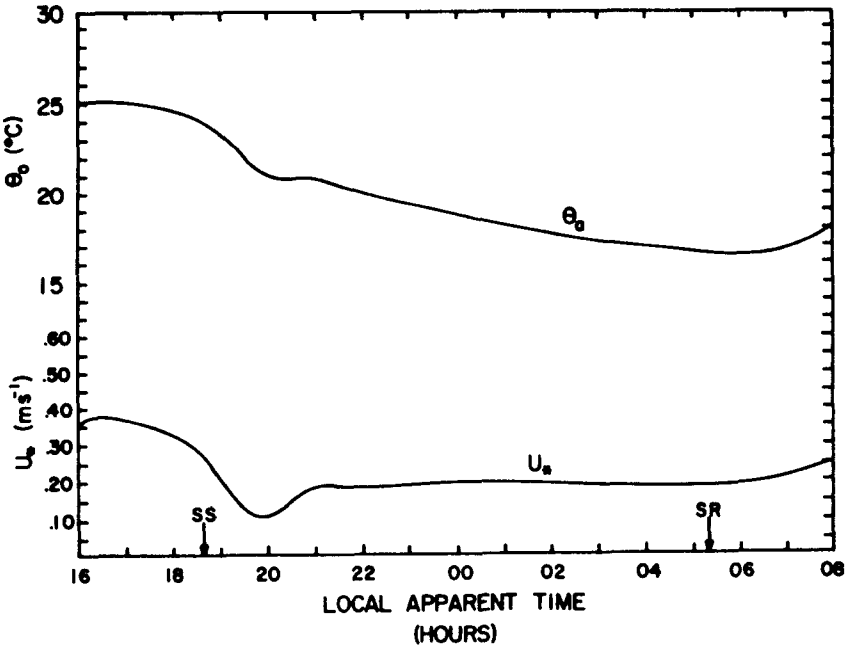

Figure 15. θ_a and u_* as function of time during the night for conditions listed in Table 1; roughness parameter 1.0 m and geostrophic wind speed 8.0 m/s.

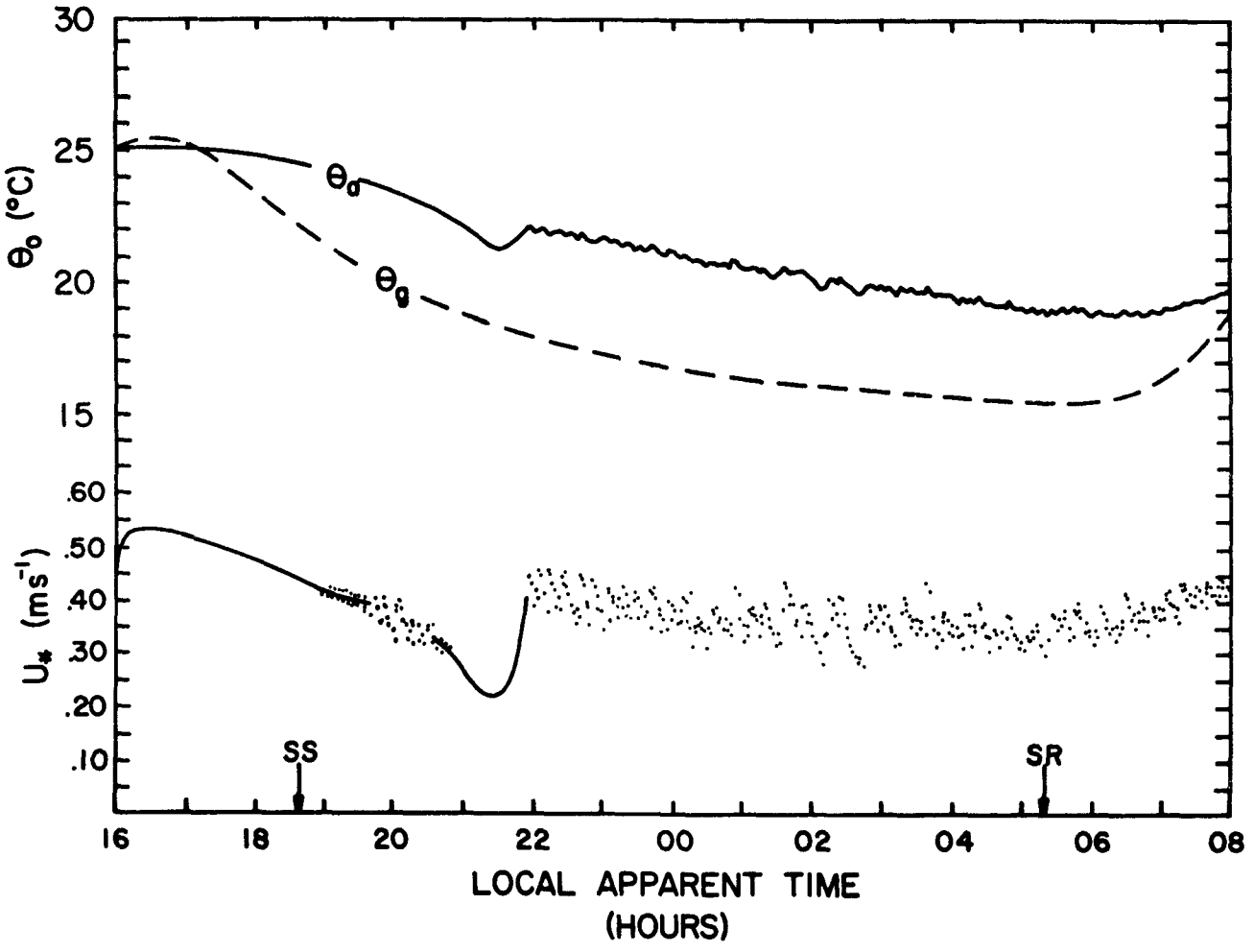

Figure 16. θ_a and u_* as function of time during the night for conditions listed in Table 1; roughness parameter 1.0 m and geostrophic wind speed 9.4 m/s.

occurs immediately after sunset, in accordance with what is most often actually observed. The rapidity of cooling at this time is partly associated with the fact that the upper level winds have not had time to accelerate, and (accordingly) the wind shear and turbulent mixing in the ground-based nocturnal inversion are still weak. Later, the increasing wind shear causes a higher level of turbulence to prevail, thus lifting the inversion and maintaining a higher u_* at the surface and a somewhat reduced surface cooling rate. In the case of the second run, the particular combination of parameters results in the occurrence of a remarkable series of alternations between calm and turbulent episodes. During the calm episodes, the "surface" air temperature decays to the ground temperature. Initially, the result is to increase the Richardson number aloft and thus to reduce the downward flow of heat and momentum. At the same time, however, the dynamical terms are increasing the shear aloft, thus tending to reduce the Richardson number. Because the latter process has a time scale that is controlled by the Coriolis parameter, however, the onset of the subcritical Richardson number is delayed. When it does happen, there is a catastrophic breakdown of several levels almost simultaneously. The event is followed by several minutes of warmer temperatures and gusty winds at the surface. Such turbulent episodes were first observed and discussed by Durst (1933). A well observed case has also been given by Gifford (1952). It is a curious fact that, in spite of the increased roughness of the second run, the minimum "surface" air temperature was less than in the first run; the average "surface" air temperature, however, was increased. In the case of the third run, the higher geostrophic wind did not permit the wind to become completely calm at the surface. Once the higher wind shear aloft became established, the surface winds remained fairly strong and gusty throughout the night, and the minimum "surface" air temperature stayed quite high.

REFERENCES

Appleby, J. F., and W. D. Ohmstede. 1964. Numerical Solution of the Distribution of Wind and Turbulence in the Planetary Boundary Layer. Meteor. Res. Note No. 8, Meteor. Dept., USAERDA, Fort Huachuca, Arizona. 47 pp.

Bankoff, S. G., and E. L. Hanzevack. 1975. The Adaptive-Filtering Transport Model for Prediction and Control of Pollutant Concentration in an Urban Airshed. Atmos. Environ. 9:793-808.

Blackadar, A. K. 1962. The Vertical Distribution of Wind and Turbulent Exchange in a Neutral Atmosphere. J. Geophys. Res. 67:3095-3102.

Blackadar, A. K. 1974a. Implications of a Simple Two-Layer Model of the Diabatic Planetary Boundary Layer. Izvestiya Acad. Sci. U.S.S.R., Atmospheric and Oceanic Phys. 10:663-664 (English edition, Amer. Geophys. Union, 10:409-410).

Blackadar, A. K. 1974b. Experiments with Simplified Second-Moment Approximations for Use in Regional Scale Models. In: EPA-650/4-74-045, Select Research Group in Air Pollution Meteorology, Second Annual Progress Report. U.S. Environmental Protection Agency, Research Triangle Park, North Carolina. pp. 234-271.

Bobileva, I. M., S. S. Zilitinkevich, and D. L. Laikhtman. 1965. Turbulent Exchange in the Thermally Stratified Planetary Boundary Layer of the Atmosphere. International Colloquium on Fine-Scale Structure of the Atmosphere, Moscow.

Bornstein, R. B. 1972. Two-Dimensional Non-Steady Numerical Simulations of Nighttime Flow of a Stable Planetary Boundary Layer Over a Rough Warm City. Paper presented at Conference on Urban Environment and Second Conference on Biometeorology, Philadelphia, Pennsylvania, 31 Oct. - 2 Nov.

Bornstein, R. D. 1975. The Two-Dimensional URBMET Urban Boundary Layer Model. J. Appl. Meteor. 14:1459-1477.

Busch, N. E., S. W. Chang, and R. A. Anthes. 1976. A Multi-Level Model of the Planetary Boundary Layer Suitable for Use with Mesoscale Dynamic Models. J. Appl. Meteor. 15:909-919.

Deardorff, J. W. 1973. Three-Dimensional Numerical Modeling of the Planetary Boundary Layer. In: Workshop on Micrometeorology, D. A. Haugen, ed. American Meteorological Society, Boston. pp. 271-311.

Delage, Y. 1974. A Numerical Study of the Nocturnal Atmospheric Boundary Layer. Quarterly J. Royal Meteor. Soc. 100:351-364.

Delage, Y., and P. A. Taylor. 1970. Numerical Studies of Heat-Island Circulations. Boundary Layer Meteor. 1:201-226.

Donaldson, C. du P. 1973. Construction of a Dynamic Model of the Production of Atmospheric Turbulence and the Dispersal of Atmospheric Pollutants. In: Workshop on Micrometeorology, D. A. Haugen, ed. American Meteorological Society, Boston. pp. 313-392.

Durst, C. S. 1933. The Breakdown of Steep Wind Gradients in Inversions. Quarterly J. Royal Meteor. Soc. 59:131-136.

Dyer, A. J. 1974. A Review of Flux-Profile Relationships. Boundary Layer Meteor. 7:363-372.

Ellison, T. H. 1955. The Ekman Spiral. Quarterly J. Royal Meteor. Soc. 81: 637-638.

Estoque, M. A., and C. M. Bhumralkar. 1970. A Method for Solving the Planetary Boundary Layer Equations. Boundary Layer Meteor. 1:169-194.

Fiedler, F. 1972. The Effect of Baroclinicity on the Resistance Law in a Diabatic Ekman Layer. Beitr. Phys. Atmos. 45:164-173.

Gifford, F. A. 1952. The Breakdown of a Low-Level Inversion Studied by Means of Detailed Soundings with a Modified Radiosonde. Bull. Amer. Meteor. Soc. 33:373-379.

Gutman, D. P., and K. E. Torrance. 1975. Response of the Urban Boundary Layer to Heat Addition and Surface Roughness. Boundary Layer Meteor. 9:217-233.

Gutman, D. P., D. E. Torrance, and M. A. Estoque. 1973. Use of the Numerical Method of Estoque and Bhumralkar for the Planetary Boundary Layer. Boundary Layer Meteor. 5:341-346.

Lee, R. L., and D. B. Olfe. 1974. Numerical Calculations of Temperature Profiles Over an Urban Heat Island. Boundary Layer Meteor. 7(1):39-52.

Lettau, H. H. 1962. Theoretical Wind Spirals in the Boundary Layer of a Barotropic Atmosphere. Beitr. Phys. Atmos. 35:195-212.

Lettau, H., and B. Davidson, eds. 1957. Exploring the Atmosphere's First Mile (2 vols.). Vol. I, Instrumentation and data evaluation. Vol. II, Site description and data tabulation. Pergamon Press, New York. 578 pp.

Lewellen, W. S., and M. Teske. 1973. Prediction of the Monin-Obukhov Similarity Functions from an Invariant Model of Turbulence. J. Atmos. Sci. 30:1340-1345.

Lumley, J. L. 1978. Simulating Turbulent Transport in Urban Air Pollution Models. In: Select Research Group in Air Pollution Meteorology, Third Annual Progress Report. U.S. Environmental Portection Agency, Research Triangle Park, North Carolina.

Lumley, J. L., and B. Kajeh-Nouri. 1973. Computational Modeling of Turbulent Transport. Paper presented at Second IUTAM - IUGG Symposium on Turbulent Diffusion in Environmental Pollution, Charlottesville, Virginia, 8-14 April.

Mellor, G. L. 1973. Analytical Prediction of the Properties of Stratified Planetary Surface Layers. J. Atmos. Sci. 30:1061-1069.

Mellor, G. L., and T. Yamada. 1974. A Hierarchy of Turbulence Closure Models for Planetary Boundary Layers. J. Atmos. Sci. 31:1791-1806.

O'Brien, J. J. 1970. A Note on the Vertical Structure of the Eddy Exchange Coefficient in the Planetary Boundary Layer. J. Atmos. Sci. 27:1213-1215.

Pandolfo, J. P., M. A. Atwater, and G. E. Anderson. 1971. Prediction by Numerical Models of Transport and Diffusion in an Urban Boundary Layer. Vol. 1 of Final Report to Environmental Protection Agency (Contract No. CPA 70-62), Center for Environment and Man, Inc., Hartford, Connecticut. 139 pp.

Panofsky, H. A. 1961. An Alternative Derivation of the Diabatic Wind Profile. Quarterly J. Royal Meteor. Soc. 87:109-110.

Panofsky, H. A., A. K. Blackadar, and G. E. McVehil. 1960. The Diabatic Wind Profile. Quarterly J. Royal Meteor. Soc. 86:390-398.

Paulson, C. A. 1970. The Mathematical Representation of Wind Speed and Temperature Profiles in the Unstable Atmospheric Surface Layer. J. Appl. Meteor. 9:857-861.

Pielke, R. A., and Y. Mahrer. 1975. Representation of the Heated Planetary Boundary Layer in Mesoscale Models with Coarse Vertical Resolution. J. Atmos. Sci. 32:2288-2308.

Rider, N. E., and G. D. Robinson. 1951. A Study of the Transfer of Heat and Water Vapor Above a Surface of Short Grass. Quarterly J. Royal Meteor. Soc. 77:375-401.

Rossby, C. G., and R. B. Montgomery. 1935. The Layer of Frictional Influence In Wind and Ocean Currents. Papers in Physical Oceanography and Meteorology (Massachusetts Institute of Technology and Woods Hole Oceanographic Institute) 3(3). 101 pp.

Sellers, W. D. 1965. Physical Climatology. University of Chicago Press, Chicago, Illinois. 272 pp.

Sheih, C. M., and W. J. Moroz. 1975. Mathematical Modelling of Lake Breeze. Atmos. Environ. 9:575-586.

Shir, C. C., and L. J. Shieh, 1974. A Generalized Urban Air Pollution Model and Its Application to the Study of SO_2 Distributions in the St. Louis Metropolitan Area. J. Appl. Meteor. 13:185-204.

Taylor, G. I. 1915. Eddy Motion in the Atmosphere. Phil. Trans. Royal Society of London (Series A) 215:1-26.

Tennekes, H. 1978. The Effects of Mixing-Height Variability on Air-Quality Simulation Models. In: Select Research Group in Air Pollution Meteorology, Third Annual Progress Report. U.S. Environmental Protection Agency, Research Triangle Park, North Carolina.

Torrance, K. E., and J. S. W. Shum, 1976. Time Varying Energy Consumption as a Factor in Urban Climate. Atmos. Environ. 10:329-337.

Wagner, N. K., and T-w. Yu. 1972. Heat Island Formation: A Numerical Experiment. In: Preprints, Conference on Urban Environment and Second Conference on Biometeorology (American Meteorological Society), Philadelphia, Pennsylvania, 31 Oct. - 2 Nov. pp. 83-88.

Wippermann, F. 1971. A Mixing-Length Hypothesis for the Planetary Boundary Layer Flow in the Atmosphere. Beitr. Phys. Atmos. 44:215-226.

Wippermann, F. 1973. The Planetary Boundary Layer of the Atmosphere. Deutscher Wetterdienst, Offenbach a. M., West Germany. 346 pp.

Wyngaard, J. C., and O. R. Coté. 1974. Evolution of a Convective Planetary Boundary Layer: A High-Order Closure Model Study. Boundary Layer Meteor. 7:289-308.

Yamada, T. 1972. Urban Heat Island Effects on Air Pollution. In: Preprints, Conference on Urban Environment and Second Conference on Biometeorology (American Meteorological Society), Philadelphia, Pennsylvania, 31 Oct. - 2 Nov. pp. 99-105.

Yamada, T., and G. L. Mellor. 1975. A Simulation of the Wangara Atmospheric Boundary Layer Data. J. Atmos. Sci. 32:2309-2329.

Yu, T. W. 1976. Numerical Studies of Atmospheric Boundary Layer with a Turbulent Energy Closure Scheme. In: Proceedings, Third Symposium on Atmospheric Turbulence, Diffusion, and Air Quality, Raleigh, North Carolina, 19-22 October. pp. 53-59.

Yu, T. W., and N. K. Wagner. 1975. Numerical Study of the Nocturnal Urban Boundary Layer. Boundary Layer Meteor. 9:143-162.

Yudin, M. I., and M. E. Shvetz. 1940. Statsionarnaya Model Raspredeleniya Vetra s Vysotoi v Turbulentnoi Atmosfere (A Stationary Model for the Distribution of Wind with Height in a Turbulent Atmosphere). Trud. Glav. Geofiz. Obs. 31(8):42-52. (Transl. Feb. 1959, Tech. Inf. and Libr. Serv., Ministry of Supply. ASTIA AD 215818.)

Zilitinkevich, S. S., and D. L. Laikhtman. 1965. Turbulent Regime in the Surface Layer of the Atmosphere. Izv. Akad. Nauk SSSR, Ser. fiz. atm. i okean. 1:150-156.

APPENDIX: SOIL SLAB MODEL

Statement of Problem

Given a soil slab of uniform properties exposed to a periodic input of heat from above given by

$$H = (I_s + I\downarrow - \sigma\theta_g^4 - H_o) = \hat{H} \cos \omega t \qquad \text{(Eq. A1)}$$

and in thermal contact with a heat reservoir at constant temperature θ_m below, we seek to determine the values of C_g and κ_m in the equation

$$C_g \frac{\partial \theta_g}{\partial t} = H_o - \kappa_m C_g (\theta_g - \theta_m) \qquad \text{(Eq. A2)}$$

that will enable the amplitude and phase of the slab temperature θ_g to be identical to the surface temperature of a real soil layer of uniform thermal conductivity λ and heat capacity per unit volume C_s. The outcome of this analysis is (1) to show that the slab model is capable of providing a ground surface temperature that imitates the real soil temperature, and (2) to enable C_g and κ_m to be calculated from ω, λ, and C_s.

Actual Temperature Distribution Within the Soil

Let T represent the temperature as function of depth -z and time t in the soil layer. The Fourier heat equation governing the temperature distribution is

$$\frac{\partial T}{\partial t} = \frac{\lambda}{C_s} \frac{\partial^2 T}{\partial z^2} \qquad \text{(Eq. A3)}$$

We require that at infinite depth the temperature approaches a constant value T_o and that at z = 0 the heat flux is continuous. Thus we have

$$\left(\lambda \frac{\partial T}{\partial z}\right)_{z=0} = \hat{H} \cos\omega t \qquad \text{(Eq. A4)}$$

The trial solution

$$T = T_o + \hat{T}e^{\beta z}\cos\ (\omega t - \partial + \nu z) \qquad \text{(Eq. A5)}$$

satisfies the boundary condition at infinite depth and also satisfies Equation A3 provided

$$\nu = \beta = \sqrt{C_s \omega\ /\ 2\lambda} \qquad \text{(Eq. A6)}$$

Negative values of ν and β are ruled out by the boundary conditions.

Substitution of the solution into Equation A4 places an additional constraint on the solution, which may be expressed in the form

$$\hat{H}\cos\omega t \equiv \lambda\hat{T}\beta\ [(\sin\delta + \cos\delta)\cos\omega t + (\sin\delta - \cos\delta)\sin\omega t] \qquad \text{(Eq. A7)}$$

Since the coefficient of sin ωt must be identically 0, we have

$$\delta = \pi/4$$

Thus the surface temperature peaks at 1/8 period after the peak heat flux at the surface. Equating coefficients of the cos ωt term gives

$$\hat{T} = \hat{H}\ /\ \sqrt{\lambda\ C_s\ \omega} \qquad \text{(Eq. A8)}$$

Requirements of the Slab Model

The slab model is not intended to provide any information about the temperature or heat flux distribution within the soil. Its only function is to present the atmosphere with a surface temperature θ_g that has the same amplitude and phase as the actual soil temperature at z = 0. Accordingly, it is required that

$$\theta_g = T_o + \frac{\hat{H}}{\sqrt{\lambda\ C_s\ \omega}}\ \cos\ (\omega t - \frac{\pi}{4}) \qquad \text{(Eq. A9)}$$

be a solution of Equation A2. Substitution gives

$$-C_g \frac{\hat{H}}{\sqrt{\lambda C_s \omega}} \sin\left(\omega t - \frac{\pi}{4}\right) \equiv \hat{H} \cos \omega t + \kappa_m C_g \theta_m - \kappa_m C_g T_o \qquad \text{(Eq. A10)}$$

$$-C_g \kappa_m \frac{\hat{H}}{\sqrt{\lambda C_s \omega}} \cos\left(\omega t - \frac{\pi}{4}\right)$$

which must be satisfied for all values of t. One requirement is

$$\theta_m = T_o \qquad \text{(Eq. A11)}$$

With this substitution and further expansion one obtains the equation

$$\frac{C_g \omega \hat{H}}{\sqrt{2\lambda C_s \omega}} (\cos\omega t - \sin\omega t) \equiv \hat{H} \cos\omega t - \frac{\kappa_m C_g \hat{H}}{\sqrt{2\lambda C_s \omega}} (\cos\omega t + \sin\omega t) \qquad \text{(Eq. A12)}$$

which is satisfied identically only if

$$\kappa_m = \omega \qquad \text{(Eq. A13)}$$

and if

$$C_g = \sqrt{\lambda C_s / 2\omega} \qquad \text{(Eq. A14)}$$

In reality, the forcing function H is not a simple cosine function (as assumed here). However — since the equations are linear — we can represent the functions H and T as a Fourier series, each mode of which satisfies the above sets of equations individually, with an appropriate multiple of ω in place of the fundamental. These considerations suggest that it is possible to choose C_g and κ_m in such a way as to give a perfect representation of any single desired mode, but no single values of C_g and κ_m can give a perfect realization of all of the modes together. Presumably, the best performance of the slab model results if one uses an average value of these parameters weighted in proportion to the energy contained in the various modes comprising the forcing

function. The solar insolation at the time of the equinoxes, normalized by its midday value, is well represented by the series

$$\frac{R_s}{R_{noon}} = .3183 + .5000 \cos \omega t + .2122 \cos 2\omega t - .0424 \cos 4\omega t$$

$$+ .0182 \cos 6 \omega t - .0101 \cos 8 \omega t + .0064 \cos 10 \omega t - \ldots$$

When weighted by the squares of the coefficients of each harmonic, the values of the parameters become

$$\kappa_m = 1.18 \quad \omega$$

$$C_g = 0.95 \sqrt{\lambda C_s / 2 \omega} \qquad \text{(Eq. A15)}$$

Since these so closely approximate the values applicable to a pure cosine forcing, and since the actual heating function is somewhat purer than that of the insolation, it is to be expected that the slab model will imitate the actual soil surface with acceptable accuracy.

THE EFFECTS OF MIXING-HEIGHT VARIABILITY ON AIR-QUALITY SIMULATION MODELS

Henk Tennekes
Department of Aerospace Engineering

INTRODUCTION

The structural properties of the atmospheric boundary layer and the turbulent motion occurring within it determine the vertical transport of momentum, heat, moisture, and pollutants to and from the earth's surface. It is evident that the height to which turbulent mixing processes extend is a key parameter in air pollution meteorology. For example, seasonally averaged values of pollutant concentration depend on seasonal averages of the mixing height over the geographical region concerned. Some of the parameters involved in the computation of plume dispersion from "point" or "line" sources are related to the mixing height; convective activity in a shallow boundary layer, for example, is less vigorous than that in a deep one with the same surface heat flux. Since the dispersion of pollutants is controlled not only by diffusion but also by advection, air-quality simulation models depend on accurate forecasts of the flow field. Mixing-height parameterization is an integral part of the boundary-layer and cumulus-cloud parameterization schemes needed in advanced numerical weather predictions on regional and synoptic scales (Deardorff, 1972; Arakawa and Schubert, 1974).

The mixing height does not play a major role in the prediction of pollutant dispersion over relatively short distances. As long as the pollution from surface sources and sources in the lower part of the boundary layer does not reach the inversion that normally caps the atmospheric boundary layer, the influence of the "lid" on vertical dispersion is relatively small. A rough estimate (Deardorff and Willis, 1975) for the horizontal distance covered be-

before pollution from a ground source first reaches the top of a convective boundary layer is:

$$x = hU/\sigma_w \qquad \text{(Eq. 1)}$$

where h is the mixing height, U is the wind speed, and σ_w is the vertically averaged standard deviation of the vertical velocity fluctuations. If, for example, σ_w = 0.2 m/s, U = 2 m/s, and h = 1000 m, then pollutants released at the surface travel 10 km downwind before they reach the top of the boundary layer, and probably another 10 or 20 km are required before the vertical concentration distribution becomes reasonably uniform. It is, therefore, not surprising that the air-quality index in urban environments is rather poorly correlated with the mixing height (Eschenroeder, 1975). However, that conclusion is valid only for average conditions over a medium-size urban area; it cannot, and should not, be applied to the regional scale or to stagnation episodes on the urban scale.

The mixing height limits vertical dispersion over distances that are long compared to those given by Equation 1. The effects of an inversion lid can be studied best if an air-quality simulation model that includes the mixing height as an explicit variable is used. A box model for pollution in a large urban area with distributed sources appears to be ideally suited for this purpose. This paper explores some of the problems associated with the effects of mixing-height variations on box models. It is not our intent to replace the detailed numerical computations that are needed for accurate predictions of pollutant concentrations. Instead, we wish to demonstrate the impact of mixing-height variations on average concentration levels and on the concentration levels encountered in severe pollution episodes. In this way, we illustrate the sensitivity of air quality to the probability distribution of the mixing height in any given geographical area, and call attention to some of the statistical measurement problems caused by the interplay among diurnal, synoptic, and seasonal variability of the parameters involved.

INVERSION-RISE PARAMETERIZATION

We begin our analysis with a brief review of the state of the art in inversion-rise parameterization. For many years, maximum-temperature forecasts and forecasts of the mixing height at sunset have been based on the premise that the total amount of heat added to the atmosphere between sunrise and sunset modifies the vertical temperature distribution in such a way that heat is conserved while the lapse rate in the daytime mixed layer remains adiabatic. Writing this conservation statement in the form of a differential equation, we obtain

$$\frac{1}{2}\gamma\frac{dh^2}{dt} = \frac{H_s}{\rho c_p} \qquad \text{(Eq. 2)}$$

where γ is the lapse rate of potential temperature in stable air just above the top of the mixed layer ($z \geq h$), and H_s is the surface heat flux. The corresponding potential temperature in the mixed layer is taken to be equal to the potential temperature of the sunrise (or midnight) sounding at the height $z = h$.

The current generation of inversion-rise models takes the effect of entrainment at the top of the boundary layer into account (Betts, 1973; Carson, 1973; Deardorff, 1972; Tennekes, 1973). In convective conditions, the differential equation governing inversion rise is surprisingly similar to Equation 2:

$$\frac{1}{2}\gamma\frac{dh^2}{dt} = (1 + \varepsilon)\frac{H_s}{c_p} \qquad \text{(Eq. 3)}$$

Here, ε depends on the efficiency of the conversion of turbulent kinetic energy to potential energy. The most commonly used value of ε is 0.4, corresponding to conditions in which the downward heat flux at the inversion base is 20% of the upward heat flux from the surface. Note that $\varepsilon = 0.4$ corresponds to a 40% increase in the rate of growth of h^2 over that predicted by Equation 2; the effect on h itself is only 20%.

Expressions such as Equation 3 must be modified if there is substantial mechanical production of turbulent kinetic energy (as in high wind conditions); estimates for the required correction term have appeared in the literature (e.g., Tennekes, 1973). Corrections are also needed in case large-scale subsidence and/or advection of horizontal changes in mixing height are present. These effects require information from numerical prognostic models of the three-dimensional low-level wind field (Anthes, 1978). The correction terms in the mixing-height parameterization, however, are quite straightforward (Deardorff, 1972); they need not concern us at this point.

In the present context, the accuracy and reliability of forecasts based on Equation 3 and its generalizations are of great importance. The accumulated experience of the last 3 years indicates that current inversion-rise models perform exceedingly well. They predict the daytime temperature cycle to within 2° C, and the mixing height at noon to within 100 m or so (Tennekes and Van Ulden, 1974); they are used for regional pollution-index forecasts for the greater London area (Pasquill, 1974); and they are supported by field and laboratory data from a wide variety of sources. Detailed and comprehensive research by Zeman (1975) and Stull (1975) suggests that the current generation of inversion-rise parameterization schemes successfully handles all of the conditions that occur in practice. Thus, for most practical purposes the inversion-rise problem may be regarded as solved. We can move on to the next problem.

As a preliminary, we need to derive the steady-state advective counterpart of Equation 3. If an urban heat island is surrounded by rural areas with negligible heat flux, and if the wind speed over the region is U, Equation 3 becomes

$$\frac{1}{2}\gamma U \frac{\partial h^2}{\partial x} = \frac{1.4H_s}{\rho c_p} \qquad \text{(Eq. 4)}$$

We have used $\varepsilon = 0.4$. The mixing height thus increases as

$$h(x) = (2.8H_s/\rho c_p \gamma U)^{1/2} x^{1/2} \qquad \text{(Eq. 5)}$$

where x is the distance from the upwind edge of the city. If the diameter of the urban area is D, the mixing height at the downwind edge of the heat island is given by

$$h(D) = \left(\frac{2.8H_s}{\rho c_p \gamma U}\right)^{1/2} D^{1/2} \qquad \text{(Eq. 6)}$$

This may be regarded as an updated version of Summers' (1965) heat-island formula. As the analysis in the next section will show, steady-state expressions (such as Equation 6) are virtually useless in stagnation episodes because the dynamic response of the pollutant concentration under the inversion lid is quite sluggish if the wind speed is small.

If the population density of urban areas is roughly independent of the diameter D, then the total population N is proportional to D^2. The mixing height over urban heat islands thus is proportional to the 1/4 power of the population, clearly a rather weak dependence (Panofsky, 1976). Since the mixing height tends to increase with city size, the parameter h/D occurring in the steady-state solution of box-model equations will tend to depend only weakly on size. This factor contributes to the poor correlation between pollutant concentration and mixing height over most cities (Gifford and Hanna, 1973). However, as Gifford has pointed out repeatedly (e.g., Gifford, 1973), the *principal* reason that urban ground-level concentration is poorly correlated with mixing height is that urban receptors perceive mainly nearby sources. The effective diffusion height of pollution from sources that are capable of influencing a particular receptor is almost always small compared to the mixing height.

THE DYNAMICS OF BOX MODELS

Box models are formulated in such a way that the effective height of vertical pollutant dispersion appears as an explicit parameter. We have to make a clear distinction between the two major types of urban box models. If the area concerned is not too large, if it is not walled in by topographical obstructions, and if the wind speed is not too small, then vertical dispersion

is limited by the finite diffusivity of the turbulence in the mixed layer. In that case, pollutants are unlikely to disperse to the top of the mixed layer before they are carried out of the box by the wind. The mixing height consequently plays no explicit role in the formulation of the problem under these conditions. It does play an implicit role, however, because the average turbulent diffusivity in the boundary layer depends on the integral scale of the turbulent motion (which, obviously, is larger if the boundary layer is thick) and on the turbulence intensity (which, at least in convective conditions, is also a function of the boundary-layer thickness). In these cases, the proper procedure for formulating the problem is to define the upper boundary of the box as a sloping surface corresponding to the effective height of turbulent dispersion (Gifford and Hanna, 1973; Hanna, 1975). For a variety of reasons, some of which have been mentioned above, the effective dispersion height at the downwind edge of the area concerned tends to be roughly proportional to its diameter, so that it is not useful to make a major issue of possible scale effects (Gifford and Hanna, 1973; Gifford, 1973).

Diffusion-limited box models become rather cumbersome if time-dependent phenomena have to be studied, because the upper boundary then has to be regarded as a function both of position and of time. Fortunately, as we shall see shortly, the concentration in a diffusion-limited box model tends to be very close to its moving equilibrium value (except in stagnation conditions), so that a quasi-steady analysis often suffices.

The other major class of box models is that in which vertical dispersion is limited by an inversion lid. If the wind speed is low, if the area concerned is very large, or if the ventilation is limited by mountains, we may assume that turbulent dispersion is so rapid that the vertical concentration distribution becomes roughly uniform a short distance from the upwind side of the city. Inversion-limited box models thus are appropriate for the study of severe air pollution episodes over very large urban areas. This is the problem we investigate below.

We consider a shallow box over a large urban area covered by uniformly distributed surface sources of pollution. The source strength per unit area

is denoted by q (kg/m^2 s). The box is square; the length of each side is D. The upper boundary of the box is at the current mixing height h; we take the inversion lid to be independent of position. The wind speed is U; since the ventilation cross section is hD, the pollutant flux out of the downwind side of the box is cUhD (c is the average pollutant concentration [kg/m^3] in the box). The average pollutant concentration left above the current mixing height by the mixed layer from previous days is denoted by c_*. Clearly, $c_* = 0$ if there is adequate ventilation, or if the current mixing height happens to be larger than the sunset values of the last few days. We assume that there is sufficient mixing within the box to make the concentration inside essentially uniform. Since D is large, we ignore turbulent diffusion out of the lateral sides of the box. We also ignore the background concentration outside the box, because it is advected through the area without change and thus adds nothing to the dynamics of the problem.

The conservation equation for the total amount of pollution inside the box now may be written as

$$\frac{d}{dt}(chD^2) = qD^2 - UDhc + c_* \frac{dh}{dt} D^2$$

Dividing this by D^2, we obtain

$$\frac{dch}{dt} = q - \frac{Uhc}{D} + c_* \frac{dh}{dt} \qquad \text{(Eq. 7)}$$

or

$$h\frac{dc}{dt} = q - \frac{Uhc}{D} \quad (c - c_*) \frac{dh}{dt} \qquad \text{(Eq. 8)}$$

These equations are not valid if $dh/dt < 0$ for causes other than subsidence, because the pollutants deposited at higher levels by a daytime mixed layer are left there when the mixing height collapses around sunset.

Equation 8 is quite similar to the one proposed by Lettau (1970). The principal difference is that the last term of Equation 8 is a parameterized

version of the corresponding term in Lettau's equation. The term at issue is the turbulent pollutant flux $\overline{w'c'}$ caused by entrainment at the inversion lid. The parameterization involved in the last term of Equation 8 is identical to that employed for the turbulent fluxes of heat, moisture, and momentum in inversion-rise models. A straightforward application of those ideas gives

$$(\overline{w'c'})_{z=h} = (c - c_*)\frac{dh}{dt} \qquad \text{(Eq. 9)}$$

Our model thus is consistent with Lettau's. Through Equation 9, the box model now is linked directly to the inversion-rise models discussed in "Inversion-Rise Parameterization" (above).

The time required to ventilate an urban area of size D with a wind speed U is equal to D/U. This is the principal time constant in the differential Equation 8; we shall call it the "ventilation time." If the last term of Equation 8 happens to be negligible, the ventilation time is equal to the reciprocal of Lettau's "flushing frequency." We are reluctant to call D/U the "ventilation period" because it does not relate to cyclic phenomena, but to the response time (effective memory interval) of the box model. The response modes of the box model tend to be exponentially decaying ones, as we shall see shortly.

The ventilation time is a function of size and wind speed; it is altogether independent of the mixing height and should not be confused with the "ventilation index" hU. If an urban area is relatively small, it seems likely that the ventilation time is almost always (except for occasional true stagnation episodes, presumably a set of measure 0) less than half a day. In that case, we can be sure that the pollution left at elevated levels by today's mixed layer will have been advected out of the control box before sunrise tomorrow. Tomorrow's mixed layer then grows into clean ambient air (we are reflecting the background concentration, as it is merely advected through the box). In these circumstances, Equation 8 can be integrated starting at sunrise (subscript r); this yields

$$ch - c_r h_r = \left(\frac{qD}{U} - c_r h_r\right)\left\{1 - \exp\left(-\frac{Ut}{D}\right)\right\} \qquad \text{(Eq. 10)}$$

where t is counted from sunrise. At sunset (subscript s) that same day, Equation 10 gives

$$c_s h_s - c_r h_r = \left(\frac{qD}{U} - c_r h_r\right)\left\{1 - \exp\left(-\frac{UT}{2D}\right)\right\} \qquad \text{(Eq. 11)}$$

where T is 24 hours (we are taking days and nights of equal duration). These equations demonstrate the effect of the ventilation time D/U: the exponential decay in Equations 10 and 11 is measured in ventilation units. The equations also suggest that there is little advantage to be gained by incorporating the inversion-rise term into the definition of "flushing frequency," as proposed by Lettau (1970). We note further that the integration cannot be continued beyond sunset because the mixing height rapidly decreases as the surface heat flux changes sign, so that the upper boundary of the box has to be relocated at a height appropriate to nighttime conditions.

The behavior of Equation 1 also shows under what kind of conditions the pollutant conservation equation may be approximated by its steady-state form. If UT/2D >> 1, so that it takes much less than 12 hours to ventilate the urban area, the effects of transients in the variables involved are damped out very quickly. The actual concentration at all times, then, is very close to its moving equilibrium value:

$$c = qD/hU \qquad \text{(Eq. 12)}$$

The quasi-steady approximation is also valid if the effective turbulent dispersion height is used instead of the mixing height; the only important restriction is that UT/2D must be large. Clearly, this condition is satisfied more easily in a diffusion-limited box model. Formally, there is also a restriction on high-frequency components or transients in the emission rate q; in practice, however, that is of no real concern.

Unfortunately, Equation 12 cannot be used in stagnation episodes with severe pollution accumulation. In fact, the nature of Equations 8 and 10 and the observation that yesterday's pollution carries over into today if $UT/2D < 1$ suggest that a stagnation episode may be defined as one in which $UT/2D < 1$ (that is, one in which the region concerned cannot be fully ventilated in half a day). In a stagnation episode, it will be necessary to use differential equations (such as Equation 8) because the ventilation is so slow that temporary storage effects become of key importance.

A deeper appreciation for these effects can be obtained by examining the frequency response of a box with fixed lid ($h = H$), constant wind speed, and sinusoidal forcing. The appropriate equation is

$$H\left\{\frac{dc}{dt} + \left(\frac{U}{D}\right)c\right\} = q_1 + q_2 \sin \omega t \qquad \text{(Eq. 13)}$$

The phase lag of the oscillations in c is then given by

$$\tan \phi = \omega D/U \qquad \text{(Eq. 14)}$$

and the amplitude of the concentration oscillations is attenuated relative to that of the emission cycle by a factor A, given by

$$A = \{1 + (\omega D/U)^2\}^{-\frac{1}{2}} \qquad \text{(Eq. 15)}$$

Examples are given in Tables 1 and 2.

TABLE 1. AMPLITUDE ATTENUATION AND PHASE LAG FOR A DIURNAL EMISSION CYCLE ($\omega = 2\pi/T$)

D/U (hours)	24.0	12.0	6.0	3.0
ϕ (hours)	5.5	4.8	3.8	2.5
A(n/d)	0.16	0.30	0.54	0.79

TABLE 2. AMPLITUDE ATTENUATION AND PHASE LAG FOR A SEMIDIURNAL EMISSION CYCLE ($\omega = 4\pi/T$)

D/U (hours)	24.0	12.0	6.0	3.0
ϕ (hours)	2.9	2.7	2.4	1.9
A(n/d)	0.08	0.16	0.30	0.54

These data show clearly that the amplitude of the concentration fluctuations is severely attenuated if the ventilation time D/U is large. The storage of pollution inside the box in cases with poor ventilation almost completely suppresses diurnal and semidiurnal concentration fluctuation. The amplitude of the concentration cycle is cut roughly in half (compared to that of the emission cycle) when the latter is diurnal and the ventilation time is 6 hours, or when it is semidiurnal and the ventilation time is 3 hours. The corresponding phase lags are about 4 hours and 2 hours, respectively.

A typical emission pattern would be one with a diurnal cycle having a maximum at noon and a semidiurnal cycle that peaks at sunrise and sunset. This gives an emission curve that peaks at the morning and afternoon rush hours (Figure 1). The corresponding concentration curves, for a ventilation time D/U = 6 hours, show that the effect of the morning rush hour is partially canceled by the phase delay in the diurnal concentration cycle, causing a shallow concentration maximum between 10 and 11 a.m. The highest concentration is reached in the early evening, when the concentration increase due to the afternoon rush traffic adds to the delayed maximum in a diurnal cycle. A similar example is given by Lettau (1970). If a complicated emission cycle is expanded in a Fourier series, Equations 14 and 15 can be used to calculate the Fourier coefficients of the concentration cycle. Such an extension is straightforward but of limited practical use, because the wind speed is unlikely to remain constant over extended periods of time.

The response time of the box model equals the ventilation time, and the latter is large in stagnation episodes. This means that emission control measures (such as the reduction of SO_2 emissions from fossil-fuel-burning

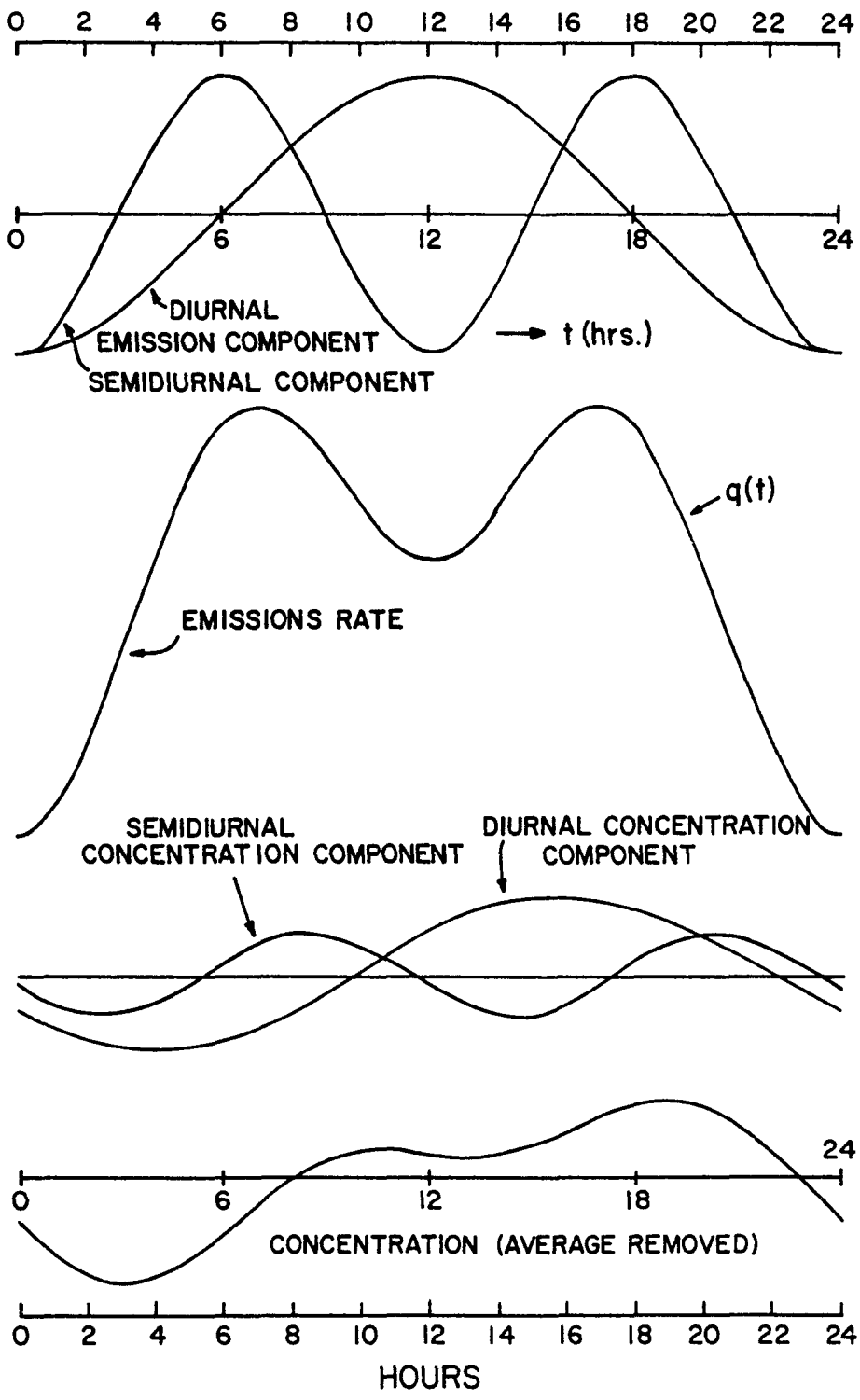

Figure 1. Typical 1-day emission curve and associated concentration curves.

power plants) must *anticipate* a stagnation episode by a time interval comparable to the critical ventilation time. If the ventilation time of a large urbanized region gradually increases to several days as the center of a high-pressure system approaches, emissions have to be decreased *before* the ventilation time becomes too large. This conclusion is obvious enough; the point is that the box model equation demonstrates it so clearly.

If, for example, U decreases as

$$U = U_o(1 - t/S) \qquad \text{(Eq. 16)}$$

then the solution of the homogeneous box model equation under a fixed lid is, for $t \leq S$,

$$c = c_o\{\exp - \frac{U_o t}{D} \quad (1 - \frac{1}{2} \quad \frac{t}{S})\} \qquad \text{(Eq. 17)}$$

Let us apply this to a case in which emissions are cut back to 0 when the ventilation time becomes 12 hours. We take S = 48 hours. Twenty-four hours after the control measures $U_o t/D = 2$, but the factor in the parentheses becomes 3/4, so that the concentration decay factor c/c_o is not 0.13 but 0.22. Forty-eight hours later, the decay factor is not 0.02 but 0.13. If the emission control during the same episodes is delayed by 12 hours, the ventilation time at the time of cutback has increased to 16 hours and S has decreased to 36 hours. The concentration decay factor at the time the wind speed becomes 0 is then 0.32. Since c_o was allowed to increase by a factor of approximately 16/12, the final concentration is 0.43 of the concentration corresponding to D/U = 12 hours. The 12-hour control delay thus increases the final concentration (at t = S) by a factor of 3.

Again, in an episode with S = 48 hours and D/U_o = 24 hours, the concentration decay factor is 0.46 after 24 hours and 0.37 after 48 hours (when U becomes 0). Obviously, control measures have to be taken well before the ventilation time becomes too large. In this last case, the concentration at t = S is comparable to that in a steady-state situation with D/U = 12 hours.

We have used S = 48 hours as a typical example. If the wind speed decreases more rapidly, early emission control measures are even more urgent. It goes without saying that a thorough study of box models with parametric excitation in wind speed and mixing height would be of substantial interest.

The examples given above support our definition of stagnation episodes as periods in which the ventilation time exceeds 12 hours. For a town 6 mi in diameter, the corresponding wind speed is 0.5 mi/hour; for a metropolis with a diameter of 24 mi, the critical wind speed is 2 mi/hour. If the probability distribution of the wind speed is known, it is not difficult to compute the frequency of occurrence of stagnation episodes. The box model gives simple but profound answers to urban air pollution problems. The model cannot become confused by details of source distributions and turbulent dispersion patterns, for it does not allow those complications to enter into the governing equation. Of course, the model can handle only one class of problems; it is of no use, for example, when the impact of a strong isolated source (such as a power plant or energy park) must be evaluated.

The dominant role of the advective time constant in the dynamic response of the box model resembles that in hot-wire anemometry (Hinze, 1975) and in the theory of the Eulerian time spectrum of turbulence (Tennekes, 1975).

We now turn to the qualitative study of the effects of inversion rise. This is accomplished conveniently by writing Equation 8 in the form:

$$\frac{h}{c}\frac{dc}{dt} = \frac{q}{c} - \frac{Uh}{D} - \frac{c - c_*}{c}\frac{dh}{dt} \qquad \text{(Eq. 18)}$$

One effective way to store pollution without rapidly increasing concentration levels is to increase the height of the mixed layer. If $c_* = 0$, this makes clean air available for dilution at a speed dh/dt; this may compare favorably with the equivalent ventilation speed Uh/D, especially if the size D of the area concerned is very large. Unfortunately, this mechanism, which is potentially quite effective, is virtually useless in stagnation episodes, because after one or two stagnation days the air above the mixed layer is just as polluted as the air inside it.

It is also instructive to nondimensionalize Equation 18 with the period T/2 of the semidiurnal cycle. This yields

$$\frac{T}{2c}\frac{dc}{dt} = \frac{qT}{2hc} - \frac{UT}{2D} - \frac{c - c_*}{c}\frac{T}{2h}\frac{dh}{dt} \qquad \text{(Eq. 19)}$$

The left-hand side of Equation 19 is the fractional increase in c in diurnal time units. The factor (T/2h) dh/dt is of order 1 if the mixing height increases by 1000 m from sunrise to sunset, with an average value of 500 m. These numbers are typical of summer conditions; they demonstrate that the contribution made by inversion rise can be comparable to that of a wind speed barely capable of ventilating the box in half a day. For an urban area with D = 40 km, the corresponding wind speed is 1 m/s. The effects of dh/dt on episodes with relatively poor ventilation thus should not be neglected, but we must remember that recapture of polluted air from above does tend to diminish the beneficial effects of inversion rise in stagnation episodes lasting several days.

Since the wind speed is a function of time, and since the response of the box model depends on the wind speed, it seems natural to normalize the time t with the current flushing frequency. The normalized clock then runs slow if the flushing frequency is small, and fast when the latter is large. Lettau (1970) approaches this issue by writing Equation 8 as

$$\frac{dc}{dt} = \frac{q}{h} - \omega_f c \qquad \text{(Eq. 20)}$$

where the flushing frequency ω_f is defined by

$$\omega_f = \frac{U}{D} + \frac{c - c_*}{c}\frac{dh}{dt} \qquad \text{(Eq. 21)}$$

Here we have used the parameterized form of Lettau's flux term given by Equation 9. Entrainment at the rising inversion lid increases the effective flushing frequency. However, we prefer not to follow Lettau's example on this point, because the entrainment term in Equation 21 contains a combination of dependent and independent variables. The rate at which normalized time advances then is a function of the unknown concentration; that seems a major disadvantage.

We propose instead to use the product $\phi = ch$ as the principal output variable (h, of course, is an input variable, but that should cause us no confusion). The value of ϕ corresponding to the quasi-equilibrium solution of the box-model equation will be denoted by ϕ_s:

$$\phi_s \equiv (ch)_s = qD/U \qquad \text{(Eq. 22)}$$

This quasi-steady solution is a simple algebraic function of the input variables. The time increment dz on the normalized clock is defined by

$$d\tau = (U/D)dt \qquad \text{(Eq. 23)}$$

Rewriting Equation 7 in terms of $\phi(\tau)$, we obtain

$$\frac{d\phi}{d} + \phi = \phi_s + c_* \frac{dh}{d\tau} \qquad \text{(Eq. 24)}$$

In this equation, ϕ_s (the value of ch corresponding to an exact balance between emission and ventilation at all times) serves as an equivalent source strength. The normalized recapture term, $c_*\ dh/d\tau$, is best interpreted as an additional source term; it is 0 most of the time (whenever $TU/2D > 1$) but makes occasional brief contributions during stagnation episodes.

If c_* happens to be 0, Equation 24 can be integrated (Lettau, 1970) to yield

$$\phi = \phi_o \exp(-\tau) + \int_0^\tau \exp(\tau' - \tau)\phi_s(\tau')d\tau' \qquad \text{(Eq. 25)}$$

Since the mixing height is discontinuous around sunset, the maximum permissible integration period is from just after sunset today to sunset tomorrow (we take h to have a small constant value during the night). This restriction severely limits the range of applications of a formal solution such as Equation 25. Still, this equation very clearly demonstrates the memory effects inherent in the box model. The effects of the initial condition ϕ_o are completely negligible after $\tau = 3$, and the effective integration interval in the second term

of Equation 25 is a few units of normalized time before the current time τ. The box has a "fading memory;" in normalized time units, the time constant of the memory equals 1.

More detailed and comprehensive studies of the dynamics and statistics of box models probably should include an analysis of the practical benefits of working with normalized time. In this context, it seems worthwhile to discuss some of the major properties of the ventilation clock. The time τ on that clock is obtained by integrating Equation 26, yielding

$$\tau = \frac{1}{D}\int_o^\tau U\, dt = \frac{\bar{U}t}{D} + \frac{1}{D}\int_o^\tau u'dt \qquad \text{(Eq. 26)}$$

We have written the wind speed U as the sum of its long-term average value $\bar{U}$ and the fluctuations u'. The latter represent diurnal and synoptic oscillations; turbulent wind fluctuations have been removed in the way the box model was defined (the ventilation speed is the average wind speed over the ventilation cross section).

Equation 26 contains the integral of a stationary random function with 0 mean. The second term of Equation 26 thus becomes a Gaussian random variable after sufficient time has passed (Lumley, 1970; Tennekes and Lumley, 1972). For time values which are large in comparison to 1 (in ventilation units), Equation 26 behaves as

$$\tau = \frac{\bar{U}t}{D} + \frac{\sigma_u}{D}(2t\tau)^{\frac{1}{2}}f(t) \qquad \text{(Eq. 27)}$$

Here, f(t) is a normalized Gaussian variable, σ_u is the standard deviation of the wind speed fluctuations, and τ is the time integral scale associated with the correlation function $\rho u(t - t') = u'(t)u'(t - t')/\sigma_u^2$ (Tennekes and Lumley, 1972, Chapter 6). In the long run, the ventilation clock thus runs at a rate proportional to the mean wind (seasonal or longer average), but it has Gaussian "jitter" whose amplitude increases as $t^{1/2}$ as time proceeds. This property may be useful in studies of the climatology of box models; we have not yet explored that possibility.

Another interesting property of τ is that it increases quite slowly during stagnation episodes. The time series of the concentration c, taken as a function of normalized time, thus tends to have a brief spike of very large amplitude whenever stagnation conditions occur. Such an "intermittent" time series provides opportunities for certain simplifications; a related example is given in the next section.

Expressions such as Equations 24 and 25 provide a basis for studies of the interactions between the dynamical and statistical (climatological) features of box models. For example, the memory integral in Equation 25 presumably reduces the variance of ϕ relative to that of the equilibrium solution ϕ_s, and increases the integral scale (correlation period) of the former compared to that of the latter. Further exploration of these issues, however, would carry us far beyond the scope of this paper. This does not mean that the climatology of box models is of no importance. Quite on the contrary, a close look at some key statistical features of box models is of considerable interest. That is the subject of the next section.

Let us recapitulate. Through a variety of examples we have illustrated the potential of a box model that takes inversion rise and response times into account. We have seen that the use of a differential equation is essential during stagnation episodes because the model responds so slowly; control measures during stagnation episodes thus cannot be based on the quasi-steady solution (Equation 12). It appears that a detailed comparison of the model with actual air pollution episodes over urban areas would be a worthwhile exercise. The box model, of course, would be used in conjunction with the inversion-rise models discussed in "Inversion-Rise Parameterization" (above).

THE CLIMATOLOGY OF BOX MODELS

Over sufficiently long time periods, a box model has to maintain a balance between emission and ventilation. This is true both for diffusion-limited box models and for inversion-limited ones. The statistical analysis presented in this section applies to both types, though details of the interpretation differ.

We begin our analysis by considering an urban area in which UT/2D >> 1 most of the time during the course of a year. To be specific, we assume that stagnation episodes (in which the equilibrium solution of the box model equation is not valid) constitute a set of measure 0. This implies that stagnation episodes do not have a significant impact on the statistics of the problem. We further assume that the effects of sunset discontinuities in the effective ventilation height h are negligible. With these restrictions (which we shall relax shortly), we can write

$$qD = Uhc \qquad \text{(Eq. 28)}$$

and assume it will be valid almost all of the time. As we have seen before, the applicability of the equilibrium solution is not restricted to inversion-limited box models. Indeed, the height h in Equation 28 may be taken as the mixing height or as the effective dispersion height, whichever is smaller. A box model for any given area is diffusion-limited most of the time, but inversion-limited during stagnation episodes. If the urbanized area is large, or happens to have a high incidence of low inversion lids, the fraction of time spent in the inversion mode is relatively large. That issue is discussed in "Mode-Switching Problems" (below).

We now take a long-term average of Equation 28. This could be a monthly average, a seasonal or annual mean, or a formal climatological average. The only restriction is that the averaging time should be long enough to produce stable statistics. We obtain

$$\begin{aligned}\overline{qD} &= \overline{Uhc} \\ &= \bar{U}\,\bar{h}\,\bar{c} + \bar{U}\,\overline{h'c'} + \bar{h}\,\overline{u'c'} + \bar{c}\,\overline{u'h'} + \overline{c'h'u'}\end{aligned} \qquad \text{(Eq. 29)}$$

In order to simplify the discussion, we ignore the triple correlation in Equation 29 and assume that mixing-height variations are uncorrelated with wind speed variations. Both of these assumptions should be experimentally tested. The parameters h, c, and U all are positive, and are likely to have strongly skewed probability distributions. Triple correlations, therefore,

may not be negligible. The wind speed spectrum tends to have a peak corresponding to the synoptic cycle (3-5 days), while the mixing-height variations occur mostly on a diurnal cycle. This would make the correlation $\overline{h'u'}$ small. However, in areas with sea or lake breezes, the wind speed does have a significant diurnal cycle which would be well correlated with the mixing-height variations. Furthermore, the effective dispersion height during diffusion-limited periods depends on the Richardson number (stability category); the correlation between the dispersion height and u, therefore, is not likely to be negligible.

With the simplifying assumptions outlined above, Equation 29 becomes

$$\overline{qD} = \bar{U}\,\bar{h}\,\bar{c} + \bar{U}\,\overline{h'c'} + \bar{h}\,\overline{u'c'} \qquad \text{(Eq. 30)}$$

We introduce the correlation coefficients r_h and r_u, which are defined by

$$\overline{h'c'} = -r_h \sigma_h \sigma_c \qquad \text{(Eq. 31)}$$

$$\overline{u'c'} = -r_u \sigma_u \sigma_c \qquad \text{(Eq. 32)}$$

Minus signs are used in order to make $r_h > 0$ and $r_c > 0$ (clearly, the two correlations involved are negative, because $c' > 0$ if $u' < 0$ or $h' < 0$). In order to facilitate comparison with the Gifford-Hanna (1973) model, we define the reference height h_R by

$$\overline{qD} = \bar{U} h_R \bar{c} \qquad \text{(Eq. 33)}$$

Substituting Equations 31, 32, and 33 into Equation 29, we obtain

$$\overline{qD} = \bar{U} h_R \bar{c} = \bar{U}\,\bar{h}\,\bar{c} - \bar{U} r_h \sigma_h \sigma_c - \bar{h} r_u \sigma_u \sigma_c \qquad \text{(Eq. 34)}$$

This yields

$$\frac{h_R}{\bar{h}} = 1 - r_h \frac{\sigma_h \sigma_c}{\bar{h}\,\bar{c}} - r_u \frac{\sigma_u \sigma_c}{\bar{U}\,\bar{c}} \qquad \text{(Eq. 35)}$$

Let us apply this relation to diffusion-limited box models. The reference height h_R implied in the Gifford-Hanna model is seen to be considerably smaller than the mean vertical dispersion height at the downwind edge of the urban area (which itself is smaller than the average mixing height in a diffusion-limited box model). Obviously, one of the strong points of the Gifford-Hanna scheme is that it avoids the issue of fluctuations and their correlations altogether by simply using an empirically determined value of h_R/D, without bothering about the actual statistics of h.

We have been unable to find reliable data on the correlation coefficients and standard deviations occurring in Equation 35. The discussion by Eschenroeder (1975) suggests that $r_h \sim 0.2$ and $r_u \sim 0.6$. We anticipate that $\sigma_c/\bar{c} \sim 1$, while $\sigma_h/\bar{h}$ and $\sigma_u/\bar{u}$ are likely to be about 0.5. In that case, $h_R/\bar{h}$ is about 0.6; clearly, the effects are significant. It would be of considerable interest to collect such statistical data, if only to determine if there are any systematic trends depending on the size D of the urban area. For example, it is conceivable that $\sigma_c/\bar{c}$ decreases with city size; if that were the case, h_R would tend to increase with D, making the constant $K = D/h_R$ in the Gifford-Hanna expression less dependent on the scale of the urban area. Very large urban areas are always somewhat polluted; this tends to increase $\bar{c}$ without a corresponding increase in σ_c.

The value of $K = D/h_R$ proposed by Gifford and Hanna (1973) is 225 for cities ranging from about 15 to 48 km in diameter. The corresponding values of h_R are in the vicinity of 100 m. Clearly, this is much smaller than the actual mean mixing height over the urban areas concerned. This confirms the hypothesis that urban box models are, statistically speaking, almost always (but not in stagnation episodes!) diffusion-limited. Climatological applications of a ventilation index or "flushing factor" based on seasonal averages of the mixing height thus make little sense for most cities.

The value of h_R corresponding to a large metropolis is about 200 m. The numbers given above suggest that the corresponding average dispersion height at the downwind side might be about 400 m. This value is fairly close to typical mixing heights; it is, in fact, larger than the mixing height one

might encounter on clear nights with little wind. The box model for a large urbanized region thus operates fairly frequently in the inversion-limited mode. This implies that climatological studies of urban box models will have to deal with the problem of switching from one mode to the other. That problem is discussed in "Mode-Switching Problems" (below).

Since the mean concentration $\bar{c}$ in an urban area is adversely affected by the correlations that occur in Equation 35, we must raise the issue of how these correlations might be determined in an observational program. Clearly, the measurement of a correlation requires spectral fidelity in the frequency ranges that contribute most to the covariance. Now, h has a spectral peak at the diurnal cycle, while much of the variance of U is associated with the typical 3- or 4-day period of synoptic variability. This implies that the variance of c has significant contributions at both these frequencies, and suggests that a sampling interval of half a day might be sufficient to obtain accurate values of the two correlation coefficients. It should be noted that daily mean values are altogether inadequate, because they would correspond to severe aliasing (Nyquist folding) of the spectra involved. The problem, however, is very much complicated by the fact that the ventilation height tends to decrease rather abruptly around sunset each day. As the convective activity in the afternoon's mixed layer dies out because the surface heat flux changes sign, the ventilation height reestablishes itself at a much smaller value, appropriate to nighttime conditions. The pollutants brought to higher levels by the mixed layer in the afternoon are left behind and may contribute to tomorrow's pollution if the ventilation time is large. Since all of this typically happens within the 1-hour period preceding sunset, it adds high-frequency components to the time series of the dispersion height. Often, these changes in h are accompanied by an equally rapid change in U, because the downward transport of geostrophic momentum also virtually ceases when convective mixing stops as day changes into night.

Similar considerations apply to the sampling rate needed to determine the statistics of q. The emission rate obviously exhibits diurnal and seasonal cycles, but it also has significant variance at periods corresponding to the length of the morning and afternoon traffic rush hours. Clearly, hourly mean

values would be most suitable for an analysis of this sort. Since the 2 hours around sunset are crucial, it might be sufficient to sample every hour around sunset, and every 3 or 4 hours at all other times. The time series then can be filled in by linear interpolation for all hours during which no data are taken. Still, time series consisting of sets of hourly means would be preferable. It is evident that this leads to a potentially valuable application of acoustic sounders: remote sensing of h(t) by acoustic radar is relatively cheap and convenient; in conjunction with hourly observations of c and U, this would yield extremely valuable information for air pollution climatology.

We note, in passing, that adequate time series of all parameters involved also would provide an opportunity to study the statistical relations between the variances of those parameters. We have refrained from writing a formal equation for σ_c^2 because of the large number of correlations involved, but it is clear in principle that adequate time series would allow a thorough study of the effects of the variability of h and U on the variability of c. The issues involved are related to exceedance statistics: how likely is it that c exceeds $\bar{c}$ by a factor of 10, say?

We now turn a statistical analysis of box models in which the pollutant concentration c_* above the current mixed layer cannot be ignored. This is not just a matter of poor ventilation, because the air above the thin mixed layer in the early evening is always polluted, even if the wind speed is relatively large. At sunset the daytime mixed layer collapses, leaving a concentration c_s in a layer whose depth h_s is often appreciably larger than that of the nighttime mixed layer. If we call the latter h_n, we have a layer of depth $h_s - h_n$ filled with a pollutant concentration c_*. The initial value of c_* is c_s; the concentration c_* decreases during the night as ventilation carries it out of the layer above the nighttime box. We define

$$h_s - h = h_* \qquad \text{(Eq. 36)}$$

so that the rate at which the remnants of daytime pollution are carried off by ventilation equals $h_* c_* U_*$. We allow U_* to be different from U; the wind speed

inside the mixed layer may differ from that above it, especially during stagnation episodes. The term $h_* c_* U_*$ makes a significant contribution to the overall ventilation rate in the early evening hours, even if there is adequate ventilation. If UT/2D >> 1, that contribution is different from 0 only during a small fraction of each diurnal cycle. Therefore, it tends to be quite intermittent, being equal to 0 most of the time. In episodes with poor ventilation, however, the contribution made by $h_* c_* U_*$ is appreciable during the entire night and well into the morning hours of the next day. If the long-term average concentration is constant, the balance between emission and mean ventilation now is given by

$$\overline{qD} = \overline{hUc} + \overline{h_* U_* c_*} \qquad \text{(Eq. 37)}$$

The influence of the second term (which we propose to call the "sunset detrainment effect") is most important during nights with poor ventilation, because h_* then is large compared to h, while c_* remains comparable to c over an extended period of time (in particular, when the emission rate at night is small compared to that in the daytime).

Applying the same averaging methods that were used for Equation 28, and making the same assumptions about the various triple correlations and the correlation between wind speed and mixing height, we obtain

$$\overline{qD} = \overline{U}\,\overline{h}\,\overline{c} + \overline{U}\,\overline{h'c'} + \overline{h}\,\overline{u'c'} + \overline{U_* h_* c_*} + \overline{U_*}\,\overline{h'_* c'_*} + \overline{h_*}\,\overline{u'_* c'_*} \qquad \text{(Eq. 38)}$$

The variable c_* is equal to 0 most of the time if the urban area is well ventilated on the average, and different from 0 mainly in the early evening hours. If non-0 values are encountered over a small fraction, say ε, of the entire averaging period (ε includes both the early evening hours of each day and the stagnation episodes), then

$$\overline{c_*} = \tilde{c}_* \varepsilon \qquad \text{(Eq. 39)}$$

where $\tilde{c}_*$ is the mean value of c_* for the periods in which it is not negligible (presumably, comparable to $\overline{c}$). The fluctuations c'_* then are given by

$$c_*' = c_* - \bar{c}_* = c_* - \tilde{c}_s\varepsilon \qquad \text{(Eq. 40)}$$

so that the variance becomes

$$\overline{(c_*')^2} = \sigma_{c*}^2 = \overline{c_*^2} - \overline{2c_*\tilde{c}_*\varepsilon} + \tilde{c}_*^2\varepsilon^2 = \overline{c_*^2} - \tilde{c}_*^2\varepsilon^2 \qquad \text{(Eq. 41)}$$

Because c_*^2 equals 0 most of the time, but is appreciable for a time fraction ε, we put

$$\overline{c_*^2} = (\tilde{c}_*^2)\varepsilon \qquad \text{(Eq. 42a)}$$

where $\tilde{}$, as before, refers to an average taken during the periods when c_* is significantly different from 0.

Since $\varepsilon << 1$, the variance given in Equation 41 may be approximated by

$$\sigma_{c_*}^2 = (\tilde{c}_*^2)\varepsilon = \tilde{c}_*^2(1 + k)\varepsilon \qquad \text{(Eq. 42b)}$$

where k represents the contribution made to the total variance by the c_*-fluctuations during the early evening hours.

We conclude that

$$\sigma_{c_*} = \tilde{c}_*(1 + k)^{\frac{1}{2}}\varepsilon^{\frac{1}{2}} \qquad \text{(Eq. 42c)}$$

which is considerably larger than $\overline{c_*}$, because ε is small and $\overline{c_*}$ is proportional to ε itself. This suggests that the ventilation term $\bar{U}_*\bar{h}_*\bar{c}_*$ is small compared to the corresponding correlation terms, unless the correlation coefficients involved also happen to be small.

It seems probable that $\overline{h_*'c_*'}$ is extremely small, because the presence of large values of c_* in elevated layers depends primarily on the absence of

adequate ventilation and not on the difference between the mixing heights of today and yesterday.

Contributions to $\overline{u_*'c_*'}$ are made by the strong negative correlation between u_*' and c_*' during stagnation episodes, but also by the well-ventilated periods, because the mean value of u_*' is larger than 0 if stagnation periods are excluded.

How large is ε? If an urban area is well ventilated on the average ($\bar{U}T/D >> 1$), the time D/U it takes to remove c_* by ventilation in the early evening corresponds to a fraction D/UT of each diurnal cycle (T = 24 hours). The average value of this fraction is proportional to the average value of the reciprocal wind speed. Therefore, the value of ε for a well ventilated urban area is given by

$$\varepsilon = D\overline{(U^{-1})}/T \tilde{=} D/\bar{U}T \qquad \text{(Eq. 43)}$$

The ventilation terms involving c_* thus are proportional to the average ventilation time of the area concerned. Their contributions to Equation 38 cannot be neglected if a city is very large or is located in a region with a low average wind speed. This is a rather surprising conclusion; intuitively, one would not expect that the climatological features of a box model are dependent on the response time. Clearly, the dynamical properties of box models are related to their climatology in unforeseen ways, and the effects of mixing-height variability require careful study. Further analysis of these issues appears to be worthwhile; however, that is beyond the scope of these exploratory investigations.

MODE-SWITCHING PROBLEMS

The box model for a typical urban area functions in the diffusion-limited mode most of the time. The corresponding values of UT/D are typically rather large; the analysis given in the preceding section has shown that quasi-steady solutions of the governing equations tend to be adequate in these circumstances.

During stagnation episodes, however, the box model switches to an inversion-limited mode; since the corresponding values of UT/D are less than 2 (recall that we have defined a stagnation episode as one in which UT/2D < 1), the behavior of the box then generally cannot be approximated with the aid of equilibrium solutions. Roughly speaking, the box model is either in a quasi-steady diffusion-limited mode or in a slowly responding inversion-limited mode.

We need to investigate under what conditions the box model switches from one kind of behavior to the other. On the average, the effective dispersion height z at the downwind edge of a diffusion-limited box model is about twice the reference height h_R of the Gifford-Hanna model (see "The Dynamics of Box Models," above). Therefore, the mean value of z/D is about 0.01. We now assume that z/D is proportional to the relative turbulence intensity σ_w/U, and that the average value of the latter is about 0.02 (corresponding roughly to neutral conditions). This implies that

$$z/h = \frac{1}{2} (\sigma_w/U)D/h \qquad \text{(Eq. 44)}$$

which is consistent with the estimate given in the Introduction to this report.

The ratio of interest is z/h, where h is the mixing height; it is given by

$$z/D = \frac{1}{2} \sigma_w/U \qquad \text{(Eq. 45)}$$

Whenever z/h exceeds 1, the ventilation term in the box model equation is proportional to the actual mixing height. This occurs when σ_w/U is relatively large (convective conditions), when h/D is relatively small (as in an episode with appreciable subsidence, or on clear nights with low wind speeds), or when D/U is relatively large (stagnation periods). If z < h, the box model is diffusion-limited, and z has to replace h in the ventilation term of the governing equation.

For very large urbanized areas, the ventilation cross section is limited by an inversion lid much of the time. This does not mean that no correction is needed for the effective volume of the box. Near the leading edge of the area, the effective height z of the box is a function of x; with the aid of Equation 44 we may approximate this dependence as

$$z(x) = \frac{1}{2} (\sigma_w/U)x \qquad \text{(Eq. 46)}$$

The effective lid reaches the inversion lid at a distance x_h, such that

$$x_h = 2h(\sigma_w/U)^{-1} \qquad \text{(Eq. 47)}$$

The nominal volume of the box (hD^2) is thus greater than the effective volume by an amount equal to

$$\frac{1}{2} x_h hD = h^2 D\ U/\sigma_w \qquad \text{(Eq. 48)}$$

and the ratio of the effective volume V_e to the nominal one becomes

$$\frac{V_e}{hD^2} = 1 - \frac{h}{D} \frac{U}{\sigma_w} \qquad \text{(Eq. 49)}$$

Whenever necessary, this correction term can be included in the left-hand side of the differential equation for the box model. However, Equation 49 is quite simple; the correction term will not complicate matters very much. It should be noted also that the volume of the box does not enter into the equilibrium solution of the box model equation. The latter depends only on the ventilation cross section hD.

In this context, it is of interest to realize, again, that the response time of the box model equals the ventilation time D/U. Our discussion points to applications over very large urbanized areas with large response times. This means that transient effects are likely to be quite important, and that the equilibrium solution of the box model equation is not going to give an adequate description of the pollutant concentration in the box. Thus a thorough study of the dynamic equation previously discussed ("The Dynamics of Box

Models") cannot be avoided. By way of illustration, consider an area with D = 60 km, over which the annual mean wind speed is 5 km/hour. Such an area has a mean response time of 12 hours, so that it will have a relatively high frequency of stagnation episodes (recall that we have defined a stagnation episode as one in which the pollution in the thick mixed layer at sunset today is not flushed away by tomorrow morning).

CONCLUSIONS

The box model is one of the simplest conceivable air-quality simulation models. We agree with Gifford (1973) that "simple" is the antonym of "complex," not of "sophisticated." The antonym of "sophisticated" is "naive," and the box model is ideally suited for the study of simple, sophisticated questions about pollution control during stagnation episodes and about many aspects of air pollution climatology and environmental impact assessment.

The analysis presented in this paper suggests that the time has come for a marriage between box models and inversion-rise models. Both are simple, reliable, and frugal with computer time; used together with appropriate observational programs, they appear to be ideal vehicles for exploratory studies of key issues related to air pollution control strategies for large cities and urbanized regions.

One of the principal conclusions that can be drawn from the results presented here is that Lettau's "flushing frequency" is indeed a key parameter in urban air pollution meteorology. It is no exaggeration to claim that the ventilation time D/U is, in many ways, of much greater importance than the ventilation index hU. The "flushing factor" is a steady-state concept, which seems rather inappropriate in stagnation episodes (because transient effects are quite large if the wind speed is small).

We have repeatedly drawn attention to the consequences of the sunset collapse of the mixing height. This effect leaves pollution (which may be entrained — recaptured — again during the next day in a stagnation episode) behind at elevated levels, and leads to additional terms in the climatological

balance equation for the box model. Thus, the behavior of the mixing height around sunset must be answered in the design of observational programs, the maximum permissible integration time for the differential equation involved is limited, there are severe restrictions on studies of the statistical effects of parametric excitation, and so on. At sunset, the mixed layer has to be redefined; in effect, the problem has to be restarted every day.

Lettau's box model contains a term representing the turbulent flux of pollution at the top of the box. In this paper, that term has been replaced by a parameterized one, borrowed directly from the "jump conditions" employed in the current generation of inversion-rise models. In this way, we have forged a strong and direct link between inversion-limited box models and inversion-rise models, and paved the way for further studies of box model dynamics.

ACKNOWLEDGMENTS

An early draft of this paper was read by F. A. Gifford, D. W. Thomson, and R. A. Anthes. Their comments helped to clarify several issues. (It is rather ironic that I managed to become confused by a simple model; I hate to think what I might have done with a complicated one!)

This research was supported by the U.S. Environmental Protection Agency under Grant No. R800397 with The Pennsylvania State University, and by the Atmospheric Sciences Section of the U.S. National Science Foundation through Grant DES75-13357.

REFERENCES

Anthes, R. A. 1978. Meteorological Aspects of Regional-Scale Air-Quality Monitoring. In: Select Research Group in Air Pollution Meteorology, Third Annual Progress Report. U.S. Environmental Protection Agency, Research Triangle Park, North Carolina.

Arakawa, A., and W. H. Schubert. 1974. Interaction of a Cumulus Cloud Ensemble with the Large-Scale Environment, Part I. J. Atmos. Sci. 31:674-701.

Betts, A. K. 1973. Non-precipitating Cumulus Convection and its Parameterization. Quarterly J. Royal Meteor. Soc. 99:178-196.

Carson, D. J. 1973. The Development of a Dry, Inversion-Capped, Convectively Unstable Boundary Layer. Quarterly J. Royal Meteor. Soc. 99:450-467.

Deardorff, J. W. 1972. Parameterization of the Planetary Boundary Layer for Use in General Circulation Models. Mon. Wea. Rev. 100:93-106.

Deardorff, J. W., and G. E. Willis. 1975. A Parameterization of Diffusion into the Mixed Layer. J. Appl. Meteor. 14:1451-1458.

Eschenroeder, A. 1975. An Assessment of Models for Predicting Air Quality. ERT Document ERTW-75-3. Environmental Research and Technology, Inc., Santa Barbara, California. 83 pp.

Gifford, F. A. 1973. The Simple ATDL Urban Air Pollution Model. ATDL Contribution File No. 78 Revised, Air Resources Atmospheric Turbulence and Diffusion Laboratory, Oak Ridge, Tennessee. 17 pp.

Gifford, F. A., and S. R. Hanna. 1973. Modeling Urban Air Pollution. Atmos. Environ. 7:131-136.

Hanna, S. R. 1975. Urban Diffusion Models. ATDL Contribution File No. 75-8, Air Resources Atmospheric Turbulence and Diffusion Laboratory, Oak Ridge, Tennessee.

Hinze, J. O. 1975. Turbulence (2nd ed.). McGraw-Hill, New York.

Lettau, H. H. 1970. Physical and Meteorological Basis for Mathematical Models of Urban Diffusion Processes. In: Proceedings of the Symposium on Multiple-Source Urban Diffusion Models, A. C. Stern, ed. APCO Publication AP-86, U.S. Environmental Protection Agency, Research Triangle Park, North Carolina.

Lumley, J. L. 1970. Stochastic Tools in Turbulence. Academic Press, New York.

Panofsky, H. A. 1976. Personal communication.

Pasquill, F. 1974. Atmospheric Diffusion (2nd ed.). John Wiley and Sons, New York.

Stull, R. B. 1975. Temperature Inversions Capping Atmospheric Boundary Layers. Ph.D. Dissertation. University of Washington, Seattle, Washington.

Summers, P. 1965. An Urban Heat Island Model. Paper presented at the First Canadian Conference on Micrometeorology, Toronto, 12-14 April.

Tennekes, H. 1973. A Model for the Dynamics of the Inversion above a Convective Boundary Layer. J. Atmos. Sci. 30:558-567.

Tennekes, H. 1975. Eulerian and Lagrangian Time Microscales in Isotropic Turbulence. J. Fluid Mech. 67:561-567.

Tennekes, H., and J. L. Lumley. 1972. A First Course in Turbulence. MIT Press, Cambridge, Massachusetts.

Tennekes, H., and A. P. van Ulden. 1974. Short-Term Forecasts of Temperature and Mixing Height on Sunny Days. In: Preprints, Symposium on Atmospheric Diffusion and Air Pollution (American Meteorological Society), Boston, Massachusetts, Sept.

Zeman, O. 1975. The Dynamics of Entrainment in the Planetary Boundary Layer: A Study in Turbulence Modeling and Parameterization. Ph.D. Dissertation. The Pennsylvania State University, University Park, Pennsylvania.

SIMULATING TURBULENT TRANSPORT IN URBAN AIR POLLUTION MODELS

John L. Lumley
Department of Aerospace Engineering

INTRODUCTION

An urban air pollution model is made up of many things: specification of emissions, with regard to type, strength, and distribution in time and space; specification of surface absorptivity and washout for the various pollutants; modeling of chemical reactions; and specification of the flow field, including the turbulent transport of the various pollutants. We intend here to limit our attention to the last aspect, turbulent transport. In view of the uncertainties of the first three aspects in present models, it is legitimate to ask whether there is any point in giving detailed consideration to turbulent transport.

Although crude transport models may be satisfactory for many purposes at the present state of development, we may hope that there will be a continual upgrading in all aspects of urban air pollution modeling, and that before too long we will reach a stage in which better models of the transport will be desirable. There is, in addition, evidence that the crude models used at present are inadequate in certain situations even by present standards, although this tends to be obscured because model predictions are not compared with well documented experimental data.

In what follows, we will examine the problem of modeling turbulent transport as though the other aspects of the air pollution modeling problem did not exist, and we will attempt to establish a general program for the development of an ideal model. Needless to say, real models in use at any

stage will be only crude approximations to such an ideal model, but the existence of the ideal may help us to avoid some of the more serious pitfalls in cruder models.

CLASSIFICATION OF URBAN POLLUTION MODELS

Urban pollution models may be conveniently classified by the way in which they treat the turbulent transport of contaminant and any other quantities which appear in the equations used. Turbulence, of course, is characterized by its enhanced transport (Tennekes and Lumley, 1972), and the proper treatment of this phenomenon is vital to the success of a model.

The majority of pollution models in use at the present time employ some form (more or less disguised) of gradient transport of contaminant. By this we mean that the predicted concentration distributions could be obtained from solution of a diffusion equation with variable diffusivities, whether in practice they are or not. The existence of a diffusion equation is evidence that a gradient-transport assumption has been made for the turbulent transport. The straightforward K-theory models (Turner, 1964; Lamb and Neiburger, 1971), of course, are of this type. Typically, in such a model the mean winds, diffusivities, and height of the inversion base are direct inputs, or must be predicted from relatively simple equations in which complex dynamical effects are parameterized. The specification by whatever means of the vertical and horizontal diffusivities always presents a problem; many semi-empirical ways of specifying the variation with height exist in the literature (Jaffe, 1967; Agee et al., 1973). None of these is completely satisfactory; in particular (as will be shown later), it is possible in convective situations to have countergradient flux of contaminant which cannot be described by these simple theories. A more fundamental problem, though less easy to document, is the fact that diffusivities *per se* are only appropriate to a homogeneous situation (Tennekes and Lumley, 1972). When terrain is changing rapidly in the wind direction, it is unlikely that any specification of the diffusivities will be satisfactory. It is only fair to say that these models have the advantage of conceptual and computational simplicity; their accuracy

is probably not too bad after dispersion has continued long enough for the contaminant to uniformly fill the mixed layer (although this does not occur on the urban scale as a general rule — this phase is more appropriate to a regional model such as that of Bowne, 1968). In the earlier phases, before the contaminant has filled the mixed layer (particularly in the presence of multiple sources), it is probably not possible to get closer than a factor of 2 to observed contaminant levels with this type of model (Turner, 1964). In addition, of course, the quantities which gradient-transport models can predict are limited. Essentially, they can predict only mean concentration, whereas we would like very much to predict, for example, concentration fluctuation variance, so as to be able to say something about the likelihood of maxima exceeding predetermined levels. Although we will probably continue to rely on this type of model for some time, particularly with better parameterizations of such quantities as inversion rise (Tennekes and Zeman, 1975), it is clear that it is nevertheless desirable to replace these models (if possible) with one which predicts more and which does not require such extensive parameterization and/or empirical input. We feel that the second-order models generally fall into this category.

The Gaussian plume technique (Pasquill, 1961) is a variant of gradient-transport modeling, in an indirect way. As it is usually applied, the user never comes in contact with the basic equations. However, the prototypical Gaussian plume is a solution of a diffusion equation with variable diffusivities. Hence, the Gaussian plume technique will have the same basic limitations as any other gradient-transport technique — primarily, poor prediction of the diffusivities in nearly windless convection. In addition, as applied in practice, the diffusivities are often allowed to vary in such a way that the resulting plume is not the solution of *any* reasonable equation; hence, it may not do as well as a more rational gradient-transport model. Overlooking this aspect, the Gaussian plume may be regarded in general as a solution appropriate to a homogeneous turbulent field; the Gaussian plume approach for multiple sources patches together homogeneous solutions to construct a solution in an inhomogeneous situation. This technique is valid if the scales of the inhomogeneity are large relative to the scales of the plumes (i.e., in

quasi-homogeneous situations). The Gaussian plume approach, of course, has numerous computational advantages in certain simple situations (particularly those with isolated sources).

The Lagrangian approach derives from Lamb and his co-workers (e.g., Lamb and Seinfeld, 1973). The techniques discussed above are Eulerian; that is, they describe events at a fixed point in space, past which matter is swept by the moving air. The entire turbulent transport problem can, of course, be cast in Lagrangian terms (that is, following individual particles). The prediction of the mean concentration then hinges on knowing the transition probabilities (see Tennekes and Lumley, 1972). Although this method is potentially exact if one knows the transition probabilities, in practice these are far more difficult to predict than diffusivities. Essentially, one always ends by assuming Gaussian transition probabilities. Gaussian transition probabilities correspond to a kinetic-theory type of situation (Lumley, 1975) and imply gradient transport; that is, they imply homogeneity and equilibrium, implying that time and length scales of the turbulence are small relative to those of the mean motions. In fact, Lamb (1974) has shown that the Lagrangian technique with Gaussian transition probabilities produces a Gaussian plume. Thus, the method reduces to an elegant and complicated version of the gradient-transport approach. Gifford (1973) comments on the desirability of sophisticated (rather than naive) models, and points out that this variable is not necessarily well correlated with the simple-complex variable. It is possible to be sophisticated only about things with which one has a great deal of experience. If a model is cast in terms which are unfamiliar, one runs the risk of having naive assumptions hidden by the unfamiliarity. We feel that the Lagrangian models as used are as naive as any other gradient-transport model, the appearance of sophistication being due to complexity.

It can hardly be emphasized too strongly that how a particular model is applied in practice (i.e., whether a diffusion equation actually appears and is solved explicitly) is irrelevant; if the model satisfies a diffusion equation, then it suffers from the inadequacies detailed above.

The only models which do not suffer from the defects touched on above, and which show promise of being able to calculate a greater range of quantities in more extreme (less homogeneous) situations, are the so-called second-order models. In these, no attempt is made to close the equations for the mean quantities by relating the second-order quantities to the mean quantities (the process which results in gradient transport in its many variants). The second-order quantities, of course, are the variances and the fluxes of momentum, heat, and contaminant. Instead, the equations for the second-order quantities are used, and closure assumptions are made regarding the third-order quantities which appear in the equations. These quantities are the fluxes of the variances and fluxes, and the terms which interchange kinetic energy among components, as well as the terms which describe the maintenance of the rate of destruction of the variances. Thus, the closure assumptions are made at a level that is one order higher. These second-order methods were first developed by Donaldson; for the elaboration to atmospheric flows, see Donaldson (1973). There are now many workers in the field (see Reynolds, 1976, for a partial list). The differences among these workers lie in the closure assumptions. There is no reason *a priori* to expect a closure assumption made at third order to be better than one made at second order, except for an unjustified hope that if the assumption is made at a sufficient remove from the quantities in which one is interested, it will do less harm. In fact, however, it turns out that — although the third-order closure assumptions are also elaborations of gradient transport, or kinetic theory approximations — there are various approximations which can legitimately be made at third order, but not at second, so that the closure assumptions are much better at third order. The second-order models result generally in a collection of several tens of nonlinear partial differential equations, first order in time, which can be solved with appropriate boundary conditions by time-stepping. In other words, when the values of all the field variables at an instant are known, the equations can be used to predict the values at the next instant. These techniques were not, of course, developed in the first instance for urban pollution predictions; rather, they were developed for prediction of flows of technological importance. Thus, the meteorological community benefits from about a decade of development of models for the turbulent momentum flux.

In the next section, we examine more closely some of the ways in which the gradient-transport models may fail (considering K theory, Gaussian plume, and Lagrangian transport together with Gaussian transition probabilities).

DRAWBACKS OF GRADIENT-TRANSPORT MODELS

The ways in which gradient-transport models fail are well known (see Tennekes and Lumley, 1972, Sections 2.3-2.5, 3.4). Generally speaking, gradient-transport models assume that the length and time scales of the turbulence are small relative to the length and time scales of the mean motion; that is, that there is a spectral gap (Lumley and Panofsky, 1964). This, of course, is rarely the case in a turbulent flow, where the length and time scales of the turbulent motion are usually of the same order as the length and time scales of the mean motion. Nevertheless, there are situations where gradient-transport ideas do work; it turns out that these are situations in which there is locally only one length and time scale in the flow, so that the flux must be proportional to the gradient (and to anything else which has the same dimensions). Hence, we may expect gradient-transport ideas to break down in situations in which we have several length or time scales; typically, this means that we have several physical effects going on simultaneously. We would consequently expect violations of gradient transport not only in situations which are rapidly changing in the streamwise direction (introducing another scale, the rate of change of the surface conditions), but in convective situations, in which buoyancy as well as wind shear is important. The failures in the former case are well documented (Kline et al., 1969). In the latter situation, simple examples have been worked out (Tennekes and Lumley, 1972, p. 101). We will present two examples of the latter situation, the first taken from Zeman (1975). Figure 1a shows the vertical distribution of vertical variance and turbulent energy in a convectively driven atmospheric mixed layer, together with the vertical fluxes of vertical variance and energy and the divergence of the flux of turbulent energy. The vertical turbulent transport of turbulent energy must remove turbulent energy from the region near the surface, and transport it to the vicinity of the inversion base. It is this process that is responsible for the growth in thickness of the surface mixed

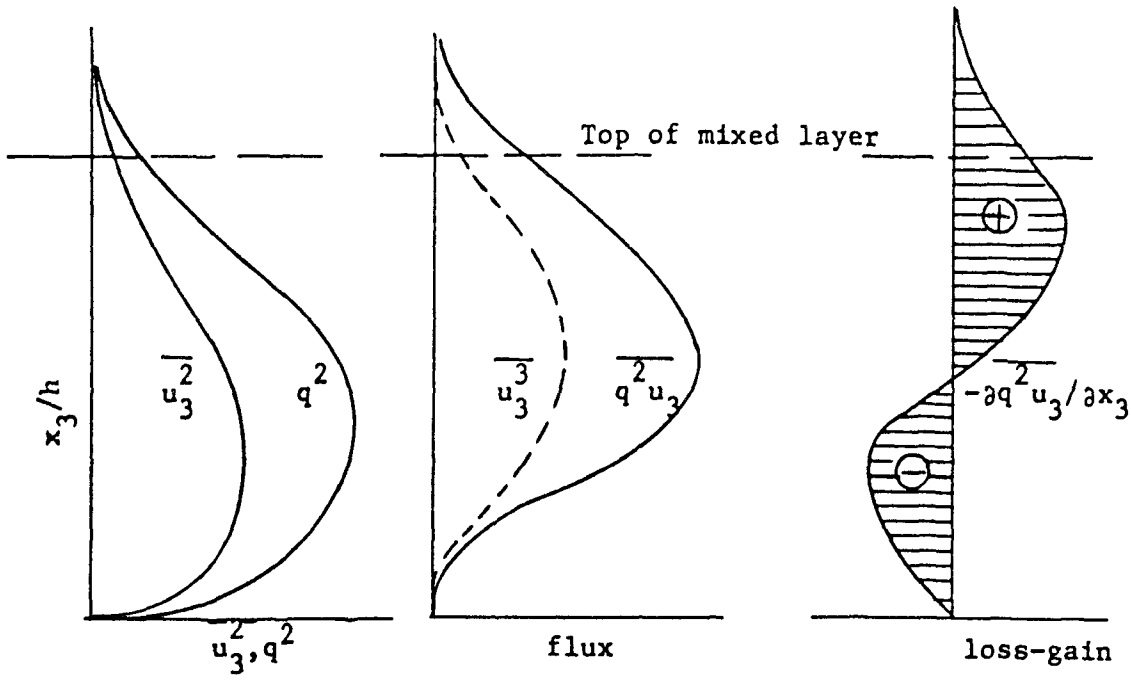

Figure 1a. Observed profiles of turbulence quantities in buoyancy-driven mixed layers (Zeman, 1975).

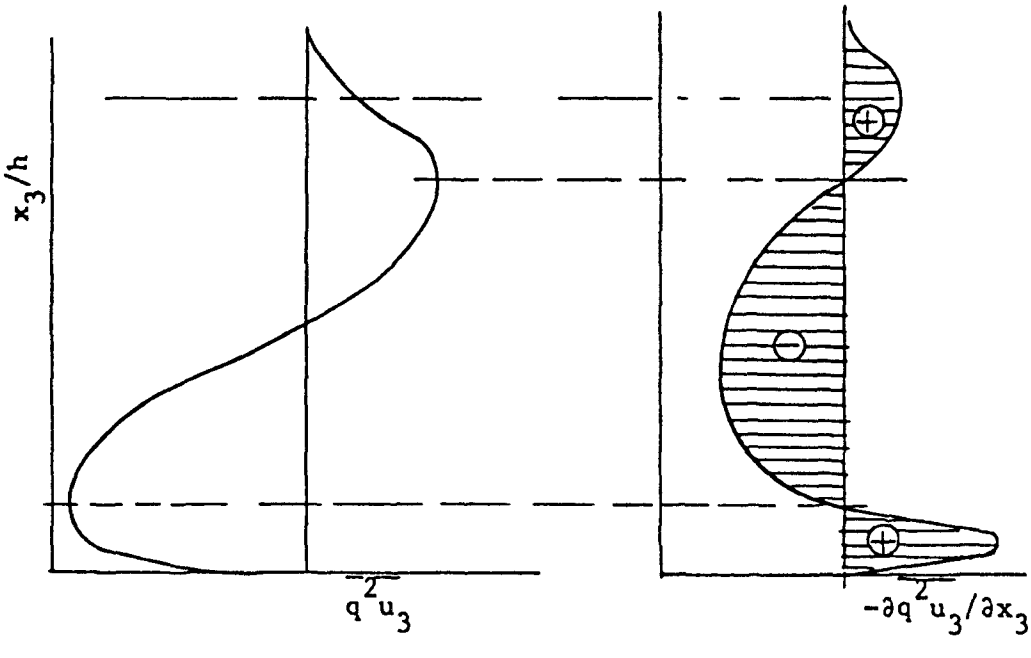

Figure 1b. The fluxes $\overline{q^2 u_3}$ and $-\partial \overline{q^2 u_3}/\partial x_3$ as calculated by a scalar transport model (Zeman, 1975).

layer, and for the entrainment of stable overlying fluid. Figure 1b illustrates the form of the divergence of turbulent energy flux which would be produced by a gradient-transport model. Energy is now removed from the center of the layer, and only a fraction is sent up to the inversion base, the remainder being sent down to the surface. Since — in a surface mixed layer driven entirely by convection — the vertical transport of turbulent energy (and temperature variance, and other second-order quantities) is entirely responsible for the dynamics, a layer powered by a gradient-transport model cannot behave properly (in fact, the rise of the inversion base is very poorly predicted, while the vertical distribution of turbulent energy is wildly in error).

We turn now to a somewhat more familiar situation that was discussed first by Priestley and Swinbank (1947) and later by Deardorff (1966, 1972). This is the matter of the countergradient vertical heat flux. Deardorff (1972) finds that, with negligible vertical wind shear, the vertical heat flux is related to the vertical potential temperature gradient by a form like

$$\overline{w\theta} = -K_h(\partial\theta/\partial z - \alpha g\overline{\theta^2}/\theta_o\overline{w^2}) \qquad \text{(Eq. 1)}$$

There is a certain amount of disagreement about the constant before the second term, although most authors would accept a number between 2/3 and 4/5 (see Lumley, 1975). Here w is the fluctuating vertical velocity, θ is the fluctuation in potential temperature, K_h is an eddy diffusivity for heat, θ_o is the mean potential temperature, $\partial\theta/\partial z$ is an average potential temperature through the layer in question, and g is the acceleration of gravity. Hence, if the vertical gradient of potential temperature is small and positive, the second term in parentheses can become more important, resulting in a positive (countergradient) heat flux. It has recently been pointed out (Warhaft, 1976) that the same effect takes place for a passive contaminant. Proceeding in exactly the same way as Deardorff (1972), we can obtain

$$\overline{wc} = -K_h(\partial C/\partial z - \alpha g\overline{\theta c}/\theta_o\overline{w^2} \qquad \text{(Eq. 2)}$$

where c and C are the fluctuating and mean values of a passive scalar contaminant. We may expect the $\overline{\theta c}$ correlation to be positive if both $\overline{\theta w}$ and $\overline{wc}$ are positive, so that the behavior of the term will be approximately the same as that of Equation 1. Since $\overline{\theta c}$ can reverse sign in other situations, the behavior in general is somewhat more complicated than that of Equation 1. It is difficult to make general statements about the effects of such a form as Equation 2, beyond saying that it will — in circumstances of intense fluctuations of potential temperature and concentration and relatively weak concentration gradients — cause an *intensification* of the gradient (due to the countergradient flux) resulting in higher concentration levels in certain regions than would be predicted by simple gradient-transport techniques.

From the point of view of urban air pollution modeling, it is legitimate to ask whether the failure of gradient-transport models in convective situations matters. That is, are urban pollution episodes associated with convective conditions? Urban pollution episodes do not often occur in the bright, sunny conditions ordinarily associated with convection. They are usually associated with a relatively low inversion base, and hence weak mixing and entrainment. They are associated, however, with relatively low wind, which would otherwise flush the volume. Hence, the mixing that does occur is primarily driven by convection, and not by wind shear. Other cases are easy to find: in the morning, in summer, during the commuting hours, the relevant turbulent transport will often be almost entirely convective, even under circumstances which may not constitute a pollution problem later in the day; at night, in the inner city, what transport exists will be driven by convection induced by the urban heat island. Thus, we must conclude that the ability to predict turbulent transport under conditions dominated by convection is a very important property of an urban air pollution model.

It might be suggested that a countergradient flux could be produced within the framework of conventional gradient transport by consideration of negative diffusivities. Unfortunately, negative diffusivities are violations of the second law of thermodynamics, and are violently unstable both analytically and numerically. The slightest irregularities in an initial profile are amplified rapidly, producing catastrophic breakdown of the calculations.

Equations 1 and 2 were generated by using a rudimentary form of second-order model. The type of effect represented (as well as other, less familiar effects) is incorporated automatically in the second-order models. Let us turn now to a more detailed examination of these models.

THE SECOND-ORDER MODELS: STABILITY CONSIDERATIONS

Smith and Pasquill (1974) have raised some questions about second-order modeling *per se*. They point out that one is frequently computing a situation which is nearly stationary. Let us consider the equation for the vertical heat flux:

$$\partial\overline{w\theta}/\partial t = K - U \qquad \text{(Eq. 3)}$$

K stands for the various terms which are known on the right-hand side, while U stands for the unknown terms that must be modeled. Smith and Pasquill (1974) reason that, if the time derivative on the left-hand side is 10^{-3} of the magnitude of K, then U must be modeled to an accuracy of 10^{-3} for the equation to balance.

If this were true, of course, second-order modeling would be a lost cause; there is no hope of modeling the various third-order terms to such accuracy. Fortunately, the difficulty is a chimera. Let us consider a simplified situation:

$$df/dt = A - Bf \qquad \text{(Eq. 4)}$$

This equation has the steady-state solution f = A/B. Suppose that we are interested in an almost-steady-state situation. We could simply neglect the time derivative and use the steady-state solution as an approximation: if A and B are known to within 5%, then the value of f will be within 10%. This is essentially what was done in analyzing the countergradient heat flux (Deardorff, 1972). One of the unknown terms on the right-hand side of Equation 3 is modeled as proportional to the heat flux; if the time derivative is

neglected, one can solve for the heat flux. This sort of approach is not seen by Pasquill (1975) to raise doubts to nearly the same extent.

Certainly, if it is only the steady state that interests one, this approach seems simplest at first glance. However, one is often interested in situations in which the time derivative is small, but not negligible. In addition, since one is in reality usually dealing with a large set of nonlinear equations which are extensively cross-coupled (even if only the steady state is of interest), it may be simpler to solve the system of equations as differential equations in time, allowing the system to approach its steady state if it will, putting in current values of all the variables on the right-hand side, and obtaining the new values from the time derivatives. If the system approaches a steady state, the values obtained will stop changing.

Let us see how this would work for the model Equation 4. We can write the solution in time as

$$f = f_o e^{-Bt} + (1 - e^{-Bt})A/B \qquad \text{(Eq. 5)}$$

where f_o is the initial value chosen. Let us suppose that $B > 0$ (we will consider the opposite case later). Then f will approach A/B for long time, no matter what the value of f_o, and will have covered 99% of the distance between f_o and A/B by $Bt = 4.61$. Of course, the final value will again be within 10%. What happens, of course, is that — the initial choice of $f = f_o$ being very much in error — the time derivative of f is initially not small. During a dimensionless time of 4.61, the value of f adjusts itself to bring the equation back in balance. The accuracy of the final value is of the order of the accuracy of the individual terms; in terms of Equation 3, neither the known nor the unknown terms have precisely the right values, but the values of all the variables have been adjusted to bring the equation into balance, and the amount they have had to be adjusted is of the order of the inaccuracy of the modeled terms.

The time required in this simple case is about 5 characteristic times to arrive within 1% of the answer. Although the real situation is much more

complicated, the behavior is in fact quite similar. The second-order equations are characterized by a time scale of roughly $q^2/3\varepsilon$, where q^2 is the turbulent mean square fluctuating velocity, and ε is the mean rate of dissipation of turbulent kinetic energy per unit mass. Any given problem, of course, may have other time scales, although there is a tendency for all time scales in a turbulent problem to become comparable as time goes on. Zeman (1975) uses h_o/w_{*o} as his time scale for modeling inversion rise, where h is the initial height of the mixed layer, and w_{*o} is the scaling velocity for vertical fluctuating velocity determined from the surface heat flux. This is approximately equal to the scale given above, and Zeman finds that the initial transient is no longer perceptible after 3 characteristic times. The disparity between 3 and 5 probably only indicates that the eye cannot discern departures of much less than 5%. Pasquill (1975) estimates a "settling-down" time of some tens of minutes in a practical situation. This is a little long; our criterion above would suggest 10 min for convergence to within 5%, 15 min for convergence to within 1%. This is probably just short enough to give some assurance that the solution will have "settled down" during the transit time over an area source of pollution of typical size. Pasquill (1975) suggests that the "settling-down" time may be improved by better modeling; from our discussions above, this is clearly not the case. The only thing that would reduce the "settling-down" time would be a better initial guess at the solution, even if the terms were all modeled perfectly. Since we may presume that a perfect initial guess at the solution is too much to hope for (obviating the necessity for a prediction scheme), we must learn to live with the "settling-down" time.

It is instructive to consider the case of B negative. Here, even though Equation 4 has a steady-state solution A/B, the solution will not approach this value for any positive time (in fact, f would go to this value only if time could go backward). If the initial value of f were precisely equal to A/B, f would remain at that value; practically, of course, the slightest difference from A/B would be amplified, and f would diverge to positive or negative infinity. The equation is now unstable. In modeling, it is of the utmost importance to be sure that the form of the modeled terms produces a stable set

of equations, in order to benefit from the behavior described earlier. If a term which has a destabilizing effect is inadvertently introduced, the system will immediately diverge and will not approach a steady state (even if one exists). Common sense is often a good guide in this; for example, it is clear in Equation 4 (even without the analysis) that B must be positive for relaxation; in systems of equations, however, the situation is not so clear if the term to be added contains a variable from another equation. The instability may become evident only by careful analysis of several of the equations taken together.

This discussion would be precisely the same if one were discussing mesoscale modeling or global-scale weather forecasting. The assumptions, the parameterization, and the modeling of various terms would be different, but the behavior of sets of partial differential equations of this type would be the same. The discussion above is also independent of the differencing scheme employed; there will be separate stability problems associated with the differencing scheme, which must be dealt with in the usual manner (Roache, 1972).

SECOND-ORDER MODELING TECHNIQUE AND PITFALLS

The heart of the second-order modeling problem is the modeling of the various unknown third-order terms in the equations. Two examples of these are $\overline{u_j \partial p/\partial x_i}$ and $\overline{\theta \partial p/\partial x_i}$ (these are designated as third-order terms because the pressure is quadratic in the velocity; see Tennekes and Lumley, 1972). Donaldson (1972) was the first to suggest that such terms be represented by tensorially and dimensionally correct combinations of second-order variables, which are (potentially) known. For this reason, second-order modeling is often called (as Donaldson suggested) "invariant" modeling, suggesting that the terms be modeled in a tensorially invariant form (wherein the model adopted retains its correctness regardless of the coordinate system). This is a requirement that has been applied in many other fields (and in fact is not optional; if an equation is correct, it must be independent of the coordinate system). The field to make greatest use of the idea is probably continuum mechanics; there one searches for a constitutive relation (relating stress and deformation

history) for various materials. Requiring that the relation in question be tensorially invariant under certain transformations has shed light on the possible forms of relations.

In second-order modeling, we attempt to do the same thing. We are not relating stress and deformation history, but we are relating physically meaningful tensors of various kinds. In addition to being tensorially and dimensionally correct, these relations must also satisfy various other requirements: they must have the right limiting values for large and small Reynolds numbers, for large and small anisotropy, and so forth. From a stability point of view, they must satisfy certain requirements, sometimes called realizability conditions (Schumann, 1976). An example of the latter is the requirement that the various terms modeled in the equations for the variances of the turbulent velocities do not permit negative variance values. That is, if the variance is 0, the time derivative of the variance must be 0 also (so that the variance cannot cross over to negative values). This is not always easy to arrange. One is inclined to feel that it is physically unlikely that the variance of a component will vanish, and that a model which is satisfactory for ordinarily observed values of the variances will therefore suffice; experience indicates, however, that (particularly during the convulsive recovery from a set of unrealistic initial conditions) if the equations are capable of producing nonphysical values of the variables, there is a chance that they will.

The literature abounds with examples of requirements that have not been met. Since the modeling was originally conceived as invariant modeling, all of the models are properly invariant in some sense. Thus, all models proposed for $\overline{p\partial u_i/\partial x_j}$ are second-rank tensors with zero trace (since $\overline{p\partial u_i/\partial x_i}$ must vanish within the Boussinesq approximation [Lumley and Panofsky, 1964]). Rotta (1951) showed that this term may be split into several parts, one of them corresponding to the interaction of the turbulence with itself (referred to as "nonlinear scrambling" or "return to isotropy," because this is the effect of the term), and others proportional to the mean velocity gradient, the buoyancy, and the Coriolis parameter. The latter are linear in the turbulent fluctuating velocity. They have the property of being anisotropic even

in an isotropic turbulence (Lumley, 1975). To illustrate, imagine a completely isotropic velocity and temperature field. At t = 0, apply a strong velocity gradient (or gravitational field, or Coriolis acceleration). Anisotropy of the velocity and temperature fields will immediately begin to develop. It is surprising, however, that these linear parts of the pressure (and hence of its correlations with other quantities) are *immediately* anisotropic while the velocity field is still isotropic (no development time is required). Hence, a model for $\overline{p\partial u_i/\partial x_j}$ which vanishes when the turbulence is isotropic is not likely to be satisfactory. This was recognized by Rotta (1951), and various models for these parts have been suggested (Hanjalic and Launder, 1972). However, there are authors who continue to suppress these parts (Lewellen, 1975). The experience of most authors is that it is impossible to reproduce the rate of increase of momentum or heat flux in rapidly changing situations without these terms. The effect of these contributions to the pressure is to partially cancel terms present in the equations (Lumley, 1975). Thus, the buoyant contribution to the pressure has the effect of reducing the buoyant contribution in the vertical energy and heat flux equations, while introducing terms in vertical heat flux in the horizontal energy equations. The terms thus redistribute some of the production, so that it is less anisotropic. These buoyant terms (and their analogs in contaminant concentration) are, however, neglected by some authors.

In the past, some authors did not use a complete set of equations; that is, the number of variables was greater than the number of equations, so that at least one variable had to be specified as input. The variable in question was usually a length scale, or some other quantity equivalent to a length scale. Lewellen and Teske (1973), Donaldson (1972), and Mellor (1973) all input a distribution for the length scale. This has proved quite satisfactory in well-understood situations, which are the kind usually employed in the testing of models (i.e., in horizontally homogeneous boundary layers). In these cases, one can easily predict a realistic distribution of length scale. There are, in fact, more than enough data to predict a realistic distribution of all the variables. Applied to the kind of situations that are of practical interest, however (with strong horizontal inhomogeneity of skin friction and

surface heat flux), it is not clear that one can so easily guess at a length scale distribution. Considerable effort on the part of many workers has gone into the development of a satisfactory equation for a length scale or equivalent quantity (and this effort continues); for a discussion, see Reynolds (1976). Use of a length scale equation (or equivalent) is now almost universal; Lewellen (1975) now uses a variant of the length scale equation used by other workers.

The dissipation term in the Reynolds stress tensor equations $\overline{\nu(\partial u_i/\partial x_k)(\partial u_j/\partial x_k)}$ has been modeled by some authors as proportional to $\overline{u_i u_j}$ (Daly and Harlow, 1970; Donaldson, 1972, 1973). However, from Kologorov's ideas of local isotropy (see Tennekes and Lumley, 1972), the off-diagonal terms must vanish as the Reynolds number becomes large (see Corrsin, 1972). That is, at very large Reynolds numbers, there must be a dissipation term in the component energy equations but not in the equation for the Reynolds stress $\overline{uw}$. The inclusion of such a term creates serious difficulties requiring compensation elsewhere in the equation. Most authors now realize this, and use a form for this term which will become diagonal as the Reynolds number goes to infinity (Lewellen, 1975).

There are probably almost as many forms for the turbulent transport terms as there are authors. We are considering here the turbulent transport of the variances and fluxes, typically $\overline{u_i u_j u_k}$. As we have seen earlier, simple gradient-transport ideas for these quantities are unlikely to work in situations that are dominated by buoyancy; such models do not transport the variances and fluxes in the right direction or to the right place, where they are needed dynamically. As an example, Lewellen (1975) uses transport models for $\overline{u_i u_j}$ and $\overline{u_i \theta}$ which are proportional to the gradients of these quantities. Such models are appropriate to turbulence which is nearly isotropic and in which buoyancy effects are negligible. To our knowledge, there is only one model for the turbulent transport terms which will work when buoyancy is dominant (Zeman, 1975).

The moral to be drawn from all of these examples is that modeling of the third-order terms is a very sophisticated business. It is not enough to

devise a model that is dimensionally and tensorially correct; it is necessary to consider the detailed dynamical behavior of the model vis-a-vis real turbulence, under a range of parameter values, for all physical phenomena present one at a time and in various combinations. Turbulence is, after all, a complicated phenomenon capable of behavior of almost infinite variety; it is too much to expect to construct in a naive way a model that behaves even approximately like it.

VERIFICATION OF SECOND-ORDER MODELS

In continuum mechanics, the behavior of a material is determined by the partial differential equation describing the conservation of momentum. This equation relates the variables describing the motion in the neighborhood of any point. In order to determine the flow field in a particular situation, this equation must be solved together with a set of boundary and initial conditions. Similar to the situation in turbulence, the differential equation for conservation of momentum is not closed, but contains the stress, which must be related to the other flow variables. Such a relation is termed a constitutive relation. When dealing with a new material, one formulates a constitutive relation connecting stress and deformation history in a properly invariant way, identifies in this general relationship certain invariant functions which define its behavior, and devises experiments which will permit measurements of these invariant functions. An invariant function is a function of tensorial invariants which is consequently the same in every coordinate system. The type of experiment usually devised is the simplest flow which will permit the function in question to be measured without the interference of other phenomena extraneous to the measurement. These flows are usually called viscometric, and great pains are taken to eliminate secondary flows, lack of two-dimensionality, nonuniform temperature, and so forth, so that one effect can be examined at a time.

We feel it is appropriate to do the same thing with the second-order models. The sets of differential equations for the second-order quantities play the role of the momentum equation for a material. Like that equation,

they are not closed, and relations must be found connecting the unknown functions appearing in the equations to the second-order quantities; these relations play the role of the constitutive relations. When these relations have been found, the equations can be solved in a particular domain with boundary and initial conditions to predict the behavior of the turbulence. In order to determine the constitutive relations, sets of viscometric experiments must be devised. In other words, we feel that no effort should be made to reproduce field data until each physical phenomenon has been examined alone and in combination with others in simple, well documented (laboratory) flow situations, over a range of parameter values. It is clear that any laboratory experiment that elucidates a phenomenon which occurs in the atmosphere is relevant to meteorology. One should not think only in terms of laboratory experiments which reproduce at once *all* major phenomena which occur in the atmosphere. Such experiments are not only difficult (Synder, 1972) (perhaps impossible) to perform, but they are seldom as useful as carefully defined experiments which display in isolated form a single phenomenon at a time.

Calibration of a model from an experiment in which several phenomena are present at once is dangerous; the modeling of several terms will be in question, corresponding to the several phenonmena, and the wrong term may be adjusted to bring the results of the model into agreement with the data. For example, suppose that, with a given set of coefficients, the model predictions do not match the measurements. Is this because of the effect of buoyancy on the transport, or anisotropy? Or has the passive scalar transport (as distinct from the effect of buoyancy) been modeled incorrectly? Suppose, by fiddling, we manage to adjust the coefficients so that the model predictions match the measurements; we still have no assurance that the values obtained are universal, and will work under different circumstances. We may have matched the data by putting in too much buoyant transport and not enough passive transport. In a situation in which these are in different ratio, the model will no longer match the data.

It is also important to calibrate the model against several similar flows that differ only in the various parameter values. Consider, for example, the

Reynolds number. In the atmosphere, the Reynolds number may be considered to be infinite; in the laboratory, it is finite. For this reason, any laboratory flow must be carried out for at least two values of the Reynolds number so that, with the help of theoretical insight on the behavior of the various terms with increasing Reynolds number (usually not too difficult to acquire), one may extrapolate to infinite Reynolds number. If an external influence is applied to a flow (such as the application of mean velocity gradient), the external influence may introduce a new scale (a time scale, in the case of the mean velocity gradient). The ratio of this scale to that of the turbulence, say, becomes a new variable, and it is important that several experiments be considered in order to determine the influence of this variable. If possible, it is also desirable, after considering each phenomenon separately, to consider the phenomena together in various combinations, since turbulence is far from linear and the various phenomena may combine in unforeseen ways.

Thoughout all of this, we are assuming that turbulence can be adequately described by a finite set of differential equations plus boundary and initial conditions. That is to say, the behavior of turbulence can be described in terms of relations among several variables in a neighborhood, plus conditions on the boundaries in space and time. If this were not true, there would be nothing universal about information obtained from a given experiment; i.e., the *relations* among the variables in a neighborhood (as opposed to the details of the flow field) would depend on the boundary conditions. Certainly this assumption is not exactly true for turbulence anywhere, and in particular near a boundary in space or time (Lumley, 1970). That it is true to a sufficient approximation away from boundaries in flows that do not vary too abruptly in space or time is the central assumption of second-order modeling, and this has been borne out by experience in modeling the various flows. In other words, in the progress made thus far, relations determined from one viscometric flow have been satisfactory in another with different boundary conditions. There is no reason to expect this assumption to be violated in the future; hence, we may have a certain amount of confidence that, if a set of viscometric flows exemplifying the various phenomena can be devised, the relations we find will be universal.

Let us consider the phenomena occurring in turbulent flows for which we need calibrating experiments (see Table 1). Turbulence decays; anisotropic turbulence becomes more isotropic; scalar fluctuations are produced from gradients; turbulence can be stretched, which alters its dynamics; the stretching can be combined with rotation, which is even more complicated; in inhomogeneous situations, transport occurs; the transport may be influenced by buoyancy. This listing is not yet sufficiently precise; for example, the separate effects of temperature fluctuations or concentration fluctuations must be examined. Thus, the observation that "turbulence decays" requires further investigation: turbulent *velocity* fluctuations decay, and turbulent *temperature* fluctuations decay. Do they decay at the same rate in a non-buoyant isotropic situation? How is the decay rate of the temperature fluctuations influenced by anisotropy of the velocity field? A time scale can be defined for the velocity field, and a similar one for the temperature field. Do these time scales tend to relax toward each other?

In this way, each entry in the list of phenomena can be broken down, forming, finally, a collection of definitive experiments. It is important to remember that each experiment is not of interest for its own sake, but rather as a paradigm of a particular phenomenon which occurs in the atmosphere (but in combination with so many other phenomena that we cannot separate effects). In just this way, a laboratory experiment designed to measure normal stresses in polyisobutylene may seem rather esoteric, but is essential to predict the behavior of STP in an engine bearing. Table 1 presents a final list of the various phenomena and some experiments to elucidate them. An X in the left-hand column denotes that the phenomenon is displayed in the experiment listed at the right. These experiments have, for the most part, been carried out over the last 20 years with the purpose of shedding light on turbulence dynamics (not for the calibration of any particular model).

It may be asked whether the phenomena listed are exhaustive. Is turbulence capable of other types of behavior overlooked here? There is no way to guarantee that none have been overlooked; the phenomena listed represent the consensus of the turbulence community at the present time. However, it is not

TABLE 1. EXPERIMENTS THAT ELUCIDATE PHENOMENA OF TURBULENCE

Phenomenon										
Velocity fluctuations	Temperature fluctuations	Anisotropy	Heat flux	Mean strain rate	Mean vorticity	Mean temperature gradient	Transport	Buoyancy		Experiment and Investigator(s)
X									(1)	Decay of isothermal, isotropic turbulence - Comte-Bellot and Corrsin (1966)
X	X								(2)	Decay of temperature fluctuations in isotropic turbulence - Mills et al. (1958); Lin and Lin (1973); Yeh and Van Atta (1973)
X		X							(3)	Return to isotropy - Uberoi (1956, 1957); Mills and Corrsin (1959)
X	X	X							(4)	Decay of temperature fluctuations in anisotropic turbulence - Mills and Corrsin (1959)
X	X	X	X						(5)	Decay of heat flux - No experiment exists
X	X					X			(6)	Production of temperature fluctuations from a uniform gradient by isotropic turbulence - Wiskind (1962); Alexopoulos and Keffer (1971)
X		X		X					(7)	Homogeneous strain of isothermal turbulence - Marechal (1972); Tucker and Reynolds (1968)
X	X	X		X		X			(8)	Homogeneous strain of turbulence with a mean temperature gradient - No experiment exists
X	X	X		X	X				(9)	Homogeneous shear - Rose (1966); Champagne et al. (1970)
X		X		X	X		X		(10)	Two-dimensional wake - Townsend (1956)
X	X	X	X			X	X	X	(11)	Convectively driven mixed layer - Willis and Deardorff (1973); Lenschow and Johnson (1968); Lenschow (1970, 1974); Telford and Warner (1964); Rowland (1973)
X	X	X	X	X	X	X	X		(12)	Two-dimensional hot non-buoyant wake - Mimaud-Lacoste (1972); Freymuth and Uberoi (1971)
X	X	X	X	X	X	X	X	X	(13)	Two-dimensional thermal plume - W. K. George (experiment presently under way)

likely that any more will be found, or — if some are — that they will be of great importance.

Experiment 5 requires some explanation. In order to measure the strength of the tendency to return to isotropy, we can produce an anisotropy of the velocity field (say, by stretching) and permit this to decay. This is equivalent to inducing a Reynolds stress and permitting it to decay, since the Reynolds stress tensor may be diagonalized. (That is to say, if at a point we have a Reynolds stress and various intensities, there is always another set of orthogonal axes through the same point in which the cross-correlations vanish, leaving only unequal intensities.) In exactly the same way, we should produce a heat flux representing an anisotropy of the combined fields and allow it to decay without the presence of a temperature gradient. One of the interesting and unanswered questions is whether the heat flux and the Reynolds stress would decay at the same rate. The problem lies in creating a heat flux without a temperature gradient or in removing the gradient after the heat flux has been set up. This could be done with a grid of small heated jets, so that an excess velocity would be associated with an excess temperature (initially). Such questions are not academic; in this case, the answer determines the turbulent Prandtl number (the ratio K_m/K_h) in homogeneous situations, and hence equilibrium levels of heat flux.

Experiment 8 also has not been accomplished. When turbulence is stretched, one must consider whether the stretching would change the value of the heat flux if a mean temperature gradient were present. If it changed, how would the change depend on the rate of stretching? This experiment would be a very simple modification of Experiment 6. One would simply add a mean temperature gradient (by heating the grid bars), first in the direction of positive strain rate and then in the direction of negative strain rate.

Where existing experiments have been suggested in Table 1, they have usually been picked for several values of the relevant parameters. In Experiment 7, for example, there are two quite different values of the ratio of turbulent time scale to time scale of the strain rate.

In several cases, the experiments mentioned are, in one respect or another, far from definitive. For example, the investigations listed under Experiment 2 display three separate evolutions of the ratio of thermal to mechanical time scale. We are currently carrying out this experiment in an effort to obtain more precise values. The two investigations mentioned under Experiment 3 show two opposite responses of the decay of dissipation to anisotropy; presumably, both are not correct. A third experiment is needed to settle the matter. Of course, the reason for these conflicting results is the fact that experiments are difficult to accomplish and, despite the greatest care, still retain a certain imprecision. This serves to underline why it is of the greatest importance that the model be calibrated against laboratory data, and not against field data. If laboratory data can still be ambiguous after the greatest care has been taken to define experimental situations, consider the ambiguity in field data, where so many variables are not under control! Unfortunately, in field data the ambiguity is not evident even when the data of different experiments are compared, since the experiments are typically not even nominally comparable.

There are several experiments not appearing in Table 1 which might have been listed under "Hard to Classify." First, there is the vital question of the response of anisotropic turbulence to changes in mean conditions. Experiments such as 6 and 9 always start with a grid-produced turbulence, which is approximately isotropic, and then apply a distorting mean velocity or temperature field. It is equally important to determine how a turbulence which has been subject to a certain mean field (and has, in consequence, acquired a certain structure) reacts to the sudden application of a quite different distorting mean field. This corresponds much more closely to nature, and it is essential to know if a model reproduces this behavior properly. Examples abound, the most common being the response of the surface mixed layer to a sudden change of terrain: the structure has come to equilibrium with particular conditions of surface roughness and heating, producing characteristic values of heat flux and anisotropy; following a change of terrain, the layer must accommodate itself to new values of roughness and heating. An experiment suitable for the nonthermal aspects of this might begin like Experiment 6, with a constant area

duct exponentially growing in one cross-stream direction and exponentially shrinking in the other. The duct would be elliptical at first and would become circular, and — in the classical experiment — would become elliptical in the orthogonal direction. By a suggestion of J. Mathieu (private communication), however, the duct could be cut at the circular section and rotated 45° so that the strain rate field applied in the second half of the duct would be at 45° to that applied during the first half. The ability to predict such a flow would be a very critical test of a model.

Second under "Hard to Classify" is the problem of the presence of a surface. It is not difficult to show (Lumley, 1970) that what we are trying to do with second-order modeling is only possible sufficiently far from a surface, or sufficiently long after initiation of a flow. That is, we are assuming that the distributions of the mean quantities through second order in a region uniquely determine the values of the mean quantities of third order. We can demonstrate that this is not the case one order lower by considering the relation of Reynolds stress to mean velocity profile; it is possible to have the same mean velocity profile with and without the presence of a wall, with two quite different Reynolds stress distributions. Presumably the same thing is true at all levels, so that we may expect our modeling of various terms to break down in the vicinity of a surface. The efforts of various workers to take account of this are described in Reynolds (1976); the matter is far from settled. Most of the work to date has been applied to the Reynolds stress (in particular, the pressure-strain correlation) and to the equation for the dissipation of turbulent kinetic energy, with very little applied to the thermal equations. That there is a problem here is evident, since in the neighborhood of a wall one customarily measures the ratio of streamwise to vertical heat flux near -3 (Monin and Yaglom, 1971); nearly the same ratio is measured for the ratio of streamwise to vertical turbulent energy flux (Schon, 1974). On the other hand, in homogeneous situations (Webster, 1964) one measures a value much nearer to unity, and this is approximately what the various current models predict with nearly any closure assumptions. Hence, it is clear that — after all relevant physical phenomena have been satisfactorily modeled away from a surface — some major modifications to the models will be required to account for the presence of a surface.

It seems likely that the majority of these modifications will consist of correctly taking into account the effect of the reduced Reynolds number on the return to isotropy near the wall, as well as including in the pressure gradient correlations terms corresponding to the surface integrals (resulting from the solution of the Poisson equation for the pressure). There may, however, be other, more subtle, effects.

Third under "Hard to Classify" are inhomogeneity and three-dimensionality. At this point (after all the flows of Table 1 have been modeled), the model will have been calibrated against a collection of flows which represent (at most) inhomogeneity in one direction at a time, and parallel flow. In every case, the modeling of the various terms is inherently three-dimensional; nevertheless, there will be constants that cannot be unambiguously determined by calibration against such simple flows. We will need well documented laboratory flows embodying change of direction with altitude and streamwise inhomogeneity. Snyder (1972) has discussed the modeling of the former. For this purpose, a flow such as the mixing layer formed by the interaction of two orthogonal streams of uniform mean velocity profile would be suitable. Such a flow was set up by Bradshaw a number of years ago (private communication) but the results have not appeared in the literature to the best of my knowledge. Streamwise inhomogeneity might be examined by attempting to predict the flows discussed by Tani (1969) for the isothermal case (corresponding to a change of surface roughness), or the flow of Johnson (1959) corresponding to a sudden change of surface heating.

At the present time, nine of the flows in Table 1 have been more or less satisfactorily matched; it is anticipated that substantial progress on the remaining four (plus the "Hard to Classify" problems) will be made in the next several years. This should not by any means imply that all problems will be resolved. In many cases, it will be necessary to bypass a problem, temporarily adopting a theoretical estimate, to return later to resolve the issue definitively. This is certainly the case with the resolution of the third problem (above), Experiments 7 and 8, and the question of the response of anisotropic turbulence to a distorting field, all of which require the results of difficult, carefully done experiments.

Of course, we cannot wait even a few years for a substantially resolved model. There is a present and continuing need for practical models, and it is possible to meet this need within the framework outlined in this paper. That is, so long as one is aware of the basic problem (of simulating a particular type of behavior), one can adopt engineering approximations appropriate to particular situations, while awaiting better models. This is the usual approach of all workers in the field. The Rotta (1951) model for the return to isotropy is such an approximation, for example; it has been used with more or less satisfactory results since the beginning of modeling efforts, although users have been aware of limitations in various circumstances. Many of the simulations used by Zeman (1975) are such engineering approximations. Only recently have more evolved models been suggested (Lumley, 1976). Even relatively simple models, if applied judiciously, can provide very satisfactory results in many situations (Lewellen and Teske, 1975).

We have made no mention of contaminant; however, temperature in a non-buoyant situation is the same as a passive contaminant. Chemically active contaminants are another matter, and a very complicated one. In principle, the behavior of chemically reacting species can be modeled using the same concepts that we have described above. However, there is relatively little good experimental information for calibration of the model, and only sparse theoretical guidance. The development of satisfactory models for chemically reacting species will be a long struggle. Incorporation of particles with finite terminal velocity, radiation, absorbing boundary conditions, and the like do not represent a problem, although there is again little experimental information, and time will be required.

WHAT CAN WE EXPECT FROM SECOND-ORDER MODELS?

Second-order models have certain basic limitations — certain things that cannot be expected of the models no matter how much time and effort are expended. First, models of this sort presume certain things — principally, that the length and time scales of the turbulence are small relative to the length and time scales characterizing the distributions of the mean quantities (Lumley, 1970); that is, that the situation is quasi-steady and quasi-homogeneous.

This is not as serious a limitation as it sounds; while the equations are an expansion (keeping first-order terms only) about the homogeneous, steady state, we can actually go fairly far from this state before serious error develops. Thus, in modeling decaying flows, or wakes, very satisfactory results are achieved when the scale ratios are between 1/2 and 1. This covers very many situations of practical interest, but probably not all. We must always bear in mind that the errors are likely to get worse with more abrupt changes or larger spatial gradients.

The model is restricted by the length and time scales of the region in which it is applied. That is, we envision applying the model in a region 20 km on a side, and 2 km high; it is presumed that the boundary conditions on the sides and top of the box are given by a mesoscale prediction program, of which this is one grid square (and in which all these complex effects are parameterized). Certainly the model cannot predict diffusivities corresponding to length scales larger than the box or to time scales longer than the transit time across the box. This is a limitation on the application of any model in this situation. Mesoscale variability must be introduced by variation of the boundary conditions. The second-order model can respond realistically to time-varying boundary conditions so long as the time scale of their variation is not less than three to five times the turbulence time scales (the situation is essentially the same as that discussed in connection with the time-to-recover from a poor initial condition).

Treating mesoscale variability by variation of boundary conditions is essentially the same as arbitrarily dividing atmospheric motions into "weather" and "turbulence," and suffers from some of the same problems. This can be unambiguously done when there is a spectral gap (Lumley and Panofsky, 1964), and corresponds to the time scale restriction just given. If there is significant energy near the spectral cut (within a factor of 2 on either side), then there will be additional interaction terms, and the effect of the "turbulence" on the "weather" will not be simply a Reynolds stress. However, it must be admitted that other approximations which (supposedly) are subject to this restriction behave well even when the restriction is fairly seriously violated. For example, the Navier-Stokes equations are based on the assumption

that the time scale of the motion described is long compared to the time between molecular collisions, so that the molecular velocity distribution will have time to come to equilibrium. For this reason, these equations should break down above a Mach number of the order of 2. Nevertheless, they work well to Mach numbers of the order of 10. The Heisenberg approximation for the turbulent spectrum (Monin and Yaglom, 1971) is based on cutting the spectrum at an arbitrary wave number, where no gap at all exists, and representing the effect of the small scales on the large by a Reynolds stress; despite the absence of a gap, the results are excellent in most respects. Hence, it is quite possible that handling mesoscale variability by variation of boundary conditions will be satisfactory to a value of the time scale ratio considerably smaller than the suggested safe value of 3 to 5. It is important to remember, however, that there is no fundamental reason to expect this to be so.

Within these very general limitations, a good second-order model is capable of very realistic predictions. In a homogeneous turbulence, without wind shear or buoyancy, a second-order model predicts that a continuous point source produces a Gaussian plume far downstream; the dispersion of the plume corresponds to an exponential Lagrangian correlation. The initial spread is linear and the later spread parabolic (as it should be). As time grows and the integral takes in more of the correlation, longer and longer time scales are responsible for the spread, corresponding to the classical description of dispersion (Corrsin, 1962). In the early stages of dispersion, the plume cross section is not Gaussian, but goes to 0 faster at the edges. If this were all the second-order model were capable of, it would hardly be an improvement on the Gaussian plume model, or the other gradient-transport models. The true merits of the second-order models only become evident when one considers an inhomogeneous multiple source situation, with buoyancy and wind shear; then diffusion coefficients and length scales are all automatically predicted. In fact, the entire turbulent field is predicted, together with the distribution of wind and temperature, as well as mean concentrations and fluxes and variances of concentration, and all from first principles (in the sense that the behavior of the model has been calibrated against the behavior of real turbulence in prototypical situations) without the necessity of intervention by the operator.

ACKNOWLEDGMENTS

This research was supported by the U.S. Environmental Protection Agency under Grant No. R800397 with The Pennsylvania State University, and by the Atmospheric Sciences Section of the U.S. National Science Foundation through Grant DES75-13357.

REFERENCES

Agee, E. M., D. E. Brown, T. S. Chen, and K. E. Dowell. 1973. Height Dependent Model of Eddy Viscosity in the Planetary Boundary Layer. J. Appl. Meteor. 12(2):409-412.

Alexopoulos, C. C., and J. F. Keffer. 1971. Turbulent Wake in a Passively Stratified Field. Physics of Fluids 14(32):216-224.

Bowne, N. E. 1968. Simulation Model for Air Pollution over Connecticut. Proceedings, Air Pollution Control Association, 61st Annual Meeting (St. Paul, Minnesota, 23-27 June) 2:68-80.

Champagne, F. H., V. G. Harris, and S. Corrsin. 1970. Experiments on Nearly Homogeneous Turbulent Shear Flow. J. Fluid Mech. 41:81-139.

Comte-Bellot, G., and S. Corrsin. 1966. The Use of a Contraction to Improve the Isotropy of Grid Generated Turbulence. J. Fluid Mech. 25:657-682.

Corrsin, S. 1962. Theories of Turbulent Dispersion. In: Mecanique de la Turbulence. Editions du CNRS, Paris. pp. 27-52.

Corrsin, S. 1972. Comment on "Transport Equations in Turbulence." Physics of Fluids 16:157-158.

Daly, B. J., and F. H. Harlow. 1970. Transport Equations in Turbulence. Physics of Fluids 13:2634-2649.

Deardorff, J. W. 1966. The Countergradient Heat Flux in the Lower Atmosphere and in the Laboratory. J. Atmos. Sci. 23:503-506.

Deardorff, J. W. 1972. Theoretical Expression for the Countergradient Vertical Heat Flux. J. Geophys. Res. 77(30):5900-5904.

Donaldson, C. DuP. 1972. Calculation of Turbulent Shear Flows for Atmospheric and Vortex Motions. AIAA J. 10:4-12.

Donaldson, C. DuP. 1973. Atmospheric Turbulence and the Dispersal of Atmospheri Pollutants. EPA-R4-73-016a. ARAP, Princeton, New Jersey.

Freymuth, P., and M. S. Uberoi. 1971. Structure of Temperature Fluctuations in the Heated Wake Behind a Circular Cylinder. J. Fluid Mech. 14(12): 2574-2580.

Gifford, F. A. 1973. The Simple ATDL Urban Air Pollution Model. ATDL Contribution File No. 78 Revised, Air Resources Atmospheric Turbulence and Diffusion Laboratory, Oak Ridge, Tennessee. 17 pp.

Hanjalic, K., and B. E. Launder. 1972. A Reynolds Stress Model of Turbulence and Its Application to Thin Shear Flows. J. Fluid Mech. 52:609-638.

Jaffe, S. 1967. Three-layer Diffusion Model as Applied to Unstable Atmospheric Conditions. J. Appl. Meteor. 6(2):297-302.

Johnson, D. S. 1959. Velocity and Temperature Fluctuation Measurements in a Turbulent Boundary Layer Downstream of a Stepwise Discontinuity in Wall Temperature. J. Appl. Mech. 3:325.

Kline, S. J., M. V. Morkovin, G. Sovran, and D. J. Cockrell. 1969. Proceedings, Computation of Turbulent Boundary Layers - 1968: AFOSR-IFP-Stanford Conference, Vol. 1. Thermosciences Division, Department of Mechanical Engineering, Stanford University.

Lamb, R. G. 1974. Lagrangian Analysis of a Passive Scalar in Turbulent Fluid. Part 1: General Theory. J. Fluid Mech. (submitted for publication).

Lamb, R. G., and M. Neiburger. 1971. An Interim Version of a Generalized Urban Air Pollution Model. Atmos. Environ. 5:239-264.

Lamb, R. G., and J. H. Seinfeld. 1973. Mathematical Modeling of Urban Air Pollution: General Theory. Environ. Sci. Tech. 7(3):253-261.

Lenschow, D. H. 1970. Airplane Measurements of Planetary Boundary Layer Structure. J. Appl. Meteor. 9:874-884.

Lenschow, D. H. 1974. Model of the Height Variation of the Turbulent Kinetic Energy Budget in the Unstable Planetary Boundary Layer. J. Atmos. Sci. 31:465-474.

Lenschow, D. H., and W. B. Johnson. 1968. Concurrent Airplane and Balloon Measurements of Atmospheric Boundary Layer Structure over a Forest. J. Appl. Meteor. 7:79.

Lewellen, W. S. 1975. Use of Invariant Modeling. Report No. 243, ARAP, Princeton, New Jersey.

Lewellen, W. S., and M. Teske. 1973. Prediction of the Monin-Obukhov Similarity Functions from an Invariant Model of Turbulence. J. Atmos. Sci. 30(7):1340-1345.

Lewellen, W. S., and M. Teske. 1975. Turbulence Modeling and Its Application to Atmospheric Diffusion, Parts I and II. EPA-600/4-75-01a and b.

Lin, S. C., and S. C. Lin. 1973. Study of Strong Temperature Mixing in Subsonic Grid Turbulence. Physics of Fluids 16(10):1587-1598.

Lumley, J. L. 1970. Toward a Turbulent Constitutive Relation. J. Fluid Mech. 41:413-434.

Lumley, J. L. 1975. Prediction Methods for Turbulent Flows: Introduction. Von Karman Institute Lecture Notes.

Lumley, J. L. 1976. The Return to Isotropy of Homogeneous Turbulence. To be submitted to J. Fluid Mech.

Lumley, J. L., and H. A. Panofsky. 1964. The Structure of Atmospheric Turbulence. Interscience (Wiley), New York.

Marechal, J. 1972. Etude Experimentale de la Deformation Plane d'une Turbulence Homogene. J. Mecanique 11:263-294.

Mellor, G. L. 1973. Analytic Prediction of the Properties of Stratified Planetary Surface Layers. J. Atmos. Sci. 30:1061-1069.

Mills, R. R., and S. Corrsin. 1959. Effect of Contraction on Turbulence and Temperature Fluctuations Generated by a Warm Grid. Memo 5-5-59W, NASA.

Mills, R. R., A. L. Kistler, V. Obrien, and S. Corrsin. 1958. Turbulence and Temperature Fluctuations Behind a Heated Grid. NACA TN 4288.

Mimaud-Lacoste, F. 1972. An Experimental Study of the Measurement of Fluctuating Temperature. M.S. Thesis. Department of Aerospace Engineering, The Pennsylvania State University, University Park, Pennsylvania.

Monin, A. S., and A. M. Yaglom. 1971. Statistical Fluid Mechanics. J. Lumley, ed. M.I.T. Press, Cambridge, Massachusetts.

Pasquill, F. 1961. The Estimation of the Dispersion of Windborne Material. Meteor. Mag. 90:33-49.

Pasquill, F. 1975. Some Topics Relating to Modeling of Dispersion in Boundary Layer. EPA-650/4-75-015.

Priestley, C. H. B., and W. C. Swinbank. 1947. Vertical Transport of Heat by Turbulence in the Atmosphere. Proceedings of the Royal Society of London (Series A) 189:543-561.

Reynolds, W. C. 1976. Computation of Turbulent Flows. In: Annual Review of Fluid Mechanics, Vol. 8. Annual Reviews, Palo Alto, California. pp. 183-208.

Roache, P. J. 1972. Computational Fluid Dynamics. Hermosa Publishers, Albuquerque, New Mexico.

Rose, W. G. 1966. Results of an Attempt to Generate a Homogeneous Turbulent Shear Flow. J. Fluid Mech. 25:97-120.

Rotta, J. C. 1951. Statistische Theorie Nichthomogener Turbulence, 1 & 2. Z. Phys. 129:547-572, 132:51-77.

Rowland, J. R. 1973. Intensive Probing of a Clear-Air Convective Field by Radar and Instrumented Drone Aircraft. J. Appl. Meteor. 12:149-155.

Schon, J. P. 1974. Contribution a l'Etude des Couches Limites Turbulentes Stratifies en Temperature. Thesis, Docteur es Sciences. l'Universite Claude Bernard de Lyon, France.

Schumann, U. 1976. Realizability of Reynolds Stress Turbulence Models. Physics of Fluids (submitted).

Smith, F. B., and F. Pasquill. 1974. Some Views on Modeling Dispersion and Vertical Flux. In: Air Pollution: Proceedings of the Fifth Meeting of the Expert Panel on Air Pollution Modeling N.35, Danish Atomic Energy Commission, Roskilde, Denmark, 4-6 June.

Snyder, W. H. 1972. Similarity Criteria for the Application of Fluid Models to the Study of Air Pollution Meteorology. Boundary Layer Meteor. 3(1): 113-134.

Tani, I. 1969. Review of Some Experimental Results on the Response of a Turbulent Boundary Layer to Sudden Perturbations. In: Proceedings: Computation of Turbulent Boundary Layers - 1968; AFOSR-IFP-Stanford Conference. Thermosciences Division, Mechanical Engineering Department, Stanford University. pp. 483-494.

Telford, J. W., and J. Warner. 1964. Fluxes of Heat and Vapor in the Lower Atmosphere Derived from Aircraft Observation. J. Atmos. Sci. 43:539-548.

Tennekes, H., and J. L. Lumley. 1972. A First Course in Turbulence. M.I.T. Press, Cambridge, Massachusetts.

Tennekes, H., and O. Zeman. 1975. Progress in Inversion Rise Parameterization. Bull. Amer. Meteor. Soc. 56(9):1045.

Townsend, A. A. 1956. The Structure of Turbulent Shear Flow. Cambridge University Press, London and New York.

Tucker, N. J., and A. J. Reynolds. 1968. The Distortion of Turbulence by Irrotational Plane Strain. J. Fluid Mech. 32:657-673.

Turner, D. E. 1964. A Diffusion Model for Urban Areas. J. Appl. Meteor. 3:83-91.

Uberoi, M. S. 1956. Effect of Wind Tunnel Contraction on Free Stream Turbulence. J. Aeronautical Sci. 23:754-764.

Uberoi, M. S. 1957. Equipartition of Energy and Local Isotropy in Turbulent Flows. J. Appl. Physics 28:1165-1170.

Warhaft, Z. 1976. Heat and Moisture Flux in the Stratified Boundary Layer. Quarterly J. Royal Meteor. Soc. 102:703-707.

Webster, C. A. G. 1964. An Experimental Study of Turbulence in a Density Stratified Shear Flow. J. Fluid Mech. 19:221.

Willis, G. E., and J. W. Deardorff. 1974. A Laboratory Model of the Unstable Planetary Boundary Layer. J. Atmos. Sci. 31:1297-1307.

Wiskind, H. K. 1962. A Uniform Gradient Turbulent Transport Experiment. J. Geophys. Res. 67(8):3033-3048.

Yeh, T. I., and C. W. Van Atta. 1973. Spectral Transfer of Scalar and Velocity Fields in Heated Grid Turbulence. J. Fluid Mech. 58:233-261.

Zeman, O. 1975. The Dynamics of Entrainment in the Planetary Boundary Layer: A Study in Turbulence Modeling and Parameterization. Ph.D. Dissertation. The Pennsylvania State University, University Park, Pennsylvania.

NATURAL REMOVAL OF GASEOUS POLLUTANTS

Robert L. Kabel
Department of Chemical Engineering
Center for Air Environment Studies

INTRODUCTION

From 1973 to the present there has been an increasing awareness of the importance of incorporation of natural processes for pollutant removal in air-quality simulation models. This awareness has developed as air pollution considerations have expanded from local to regional and even global scales. Another major stimulus came with the recognition that transport and deposition of atmospheric constituents could significantly pollute bodies of water. A corollary is that natural sources of atmospheric pollutants (and potential water pollutants) can be expected to be included in quantitative models along with man-made emissions in the near future.

For perspective, we might consider the estimated emissions from natural and anthropogenic sources for various gaseous pollutants. It is known that the combustion of fossil fuels produces far more SO_2 than the natural volcanic source. On the other hand, natural sources (especially biological decay) of a reduced form of sulfur, H_2S, far outweigh the anthropogenic sources. Of course, the H_2S is readily oxidized to SO_2 in the atmosphere, giving an approximate balance between natural and anthropogenic sulfur in the atmosphere. We might also consider the background concentrations and major identified sinks of the various pollutants. The largest background concentrations occur for those constituents which are chemically most inert and least water soluble. The importance of these concepts will become more evident as this paper progresses. Detailed discussion of this background material is given by Rasmussen et al. (1974, 1975).

NATURAL REMOVAL PROCESSES

In this section, the natural processes by which tropospheric pollutants are eliminated or converted are considered. Discussion of each kind of removal process is given and the limitations of the paper are more fully defined.

Table 1 indicates the various removal processes:

TABLE 1. REMOVAL PROCESSES

Interfacial	Bulk
Vegetation	Atmospheric Reactions
Soil	Precipitation Scavenging
Water Bodies	Dry Deposition
Stone	Aerosol Scavenging
Tropopause	

There are two main categories of removal processes. Interfacial processes occur at a boundary of the troposphere. By contrast, the bulk processes occur within the troposphere and have a more volumetric character.

Bulk Processes

Atmospheric Reactions--

Probably the best known removal process, chemical reaction in the atmosphere, is also a generation process. The oxidation of H_2S to SO_2 mentioned earlier is a simple case. Because of the photochemical smog problem, an entire literature has evolved from 25 years of intense research. Altshuller and Bufalini reviewed the literature in 1971. Hecht and Seinfeld (1972) have proposed an 81-step reaction mechanism for photochemical smog formation as well as a simplified 15-step version. Smog is by no means the only important consequence of atmospheric reactions. Each case is rather special, and no attempt will be made here to deal with this massive topic.

Precipitation Scavenging--

Two mechanisms of precipitation scavenging exist. In the first, the pollutant is incorporated into the droplets and/or particles during the nucleation and growth phases of cloud formation. The pollutant may even contribute to this process; for example, see Twomey (1971). Second, when the solid or liquid precipitation falls, gases and particles are collected during vertical passage through the polluted region. The relative importance of these two scavenging mechanisms is not well defined. But the phenomenon of acid rain is well known. Cogbill and Likens (1974) provide excellent perspective on the causes, nature, and impact of this phenomenon. At present, the pollution of surface regions (especially water bodies) via precipitation is receiving extensive attention. A case in point is Murphy's (1975) report on measured phosphorous input by rainfall into Lake Michigan. Thus, precipitation scavenging is observed to be an effective cleanser of the air and polluter of the water, at least for certain contaminants.

Predictive tools are also becoming available. A comprehensive analysis of reversible interaction of raindrops with atmospheric contaminants has been presented by Hales (1972). Further study by Hales et al. (1973) has led to the development of a mathematical model for predicting ground level washout fluxes and average concentrations in the rain as a function of location beneath a plume. The above references deal with liquid precipitation, which is surely the more important case. However, some serious attention has been given to scavenging by snow (Forland and Gjessing, 1975). The theory of precipitation scavenging is perhaps rather well advanced in comparison to its practical application. Measurement programs are now being conducted in all parts of the world. In this paper, we will not be concerned further with the subject.

Dry Deposition--

The term "dry deposition" has been used mainly to imply all removal processes at the earth's surface except precipitation scavenging. Such a characterization is so general as to be almost useless for modeling purposes. Accordingly, several processes usually lumped under this heading will be treated in detail elsewhere in this paper. There is, however, one bulk process which might be accurately called dry deposition. Consider the following simple but

important mechanistic illustration. A common air pollutant, sulfur dioxide, is oxidized and absorbed in a water droplet to give sulfuric acid. The oxidation can and does occur either before or after the absorption. The resulting acidic droplet is a natural site for the absorption of ammonia, another common and inherently basic pollutant. Since ammonia is very soluble in water, its absorption can also precede that of the sulfur dioxide. In either case, the result is that the uptake of one component is enhanced by the uptake of the other. If the water in the droplet now evaporates (ammonium sulfate is not particularly hygroscopic), a dry particle of ammonium sulfate remains and can eventually work its way to the ground. The chemistry and importance of such processes for the above case are well presented by Miller and de Pena (1972).

Aerosol Scavenging--

The previous illustration shows how ammonia can be scavenged by a sulfuric acid aerosol. Of course, the aerosol need not be an aqueous solution of an absorbed gas. The potential variety of particles is staggering. A good review of aerosol scavenging as a removal process is given by Hidy (1973). Because particle deposition will not be examined further in this paper, attention is called to some recent and valuable research by Sehmel (1975) on experimental measurements and predictions of particle deposition and resuspension rates.

Interfacial Processes

Tropopause--

The tropopause can be thought of as the upper edge of the troposphere and hence as an interface. At the present time, this interface is involved in a dramatic controversy. Man-made chlorofluorocarbons are introduced into the troposphere in a variety of ways. Because of their extreme chemical inertness, these pollutants eventually diffuse through the troposphere into the stratosphere. There, it is postulated, they participate in a series of reactions which lead to ozone depletion (Molina and Rowland, 1974). The ozone layer may also be affected by pollutants of natural origin. Nitrous oxide is produced in tremendous amounts by biological decay and is also quite inert in the near-earth region. Accordingly, it too may reach the stratosphere with results similar to those postulated for the chlorofluorocarbons (Friend, 1976).

Thus pollutant removal from the troposphere at its upper "boundary" can take on real importance in special cases. Although the tropopause can be thought of as a boundary of the troposphere, the passage of material through it is really a matter of atmospheric diffusion. This is the subject of a completely separate literature.

The greatest attention in this paper will be given to the earth interface processes. First, some illustrations of the removal mechanisms discussed earlier will be presented. Then the matter of quantitative modeling of such processes will be taken up. It should be realized that the matter addressed here is the effect of things (vegetation, soil, water, and stone) on pollution, and not the effect of pollutants on things (which has received so much attention).

Vegetation--

The ability of plants to exchange large quantities of gaseous materials with their surroundings is dramatically evidenced by the photosynthetic process involving carbon dioxide and oxygen and by evapotranspiration of water. A whole body of literature exists with respect to these compounds. The most prominent research on uptake of ordinary pollutants has been conducted by Hill (1971) and continued in collaboration with other workers. Some of Hill's early results are shown in Table 2. A striking trend of increasing uptake rate with increasing pollutant solubility in water is evident. Bennett et al. (1973) have developed a quantitative model for gaseous pollutant sorption by leaves. They emphasize the importance of estimating the internal solute concentration. The prediction of pollutant uptake by vegetation is still in an uncertain state; however, a good beginning has been made. The extensive literature on plant physiology offers promise for rapid progress in this area.

Soil--

Soil can be a very effective sink for atmospheric pollutants, especially if the soil is moist and the pollutants are water soluble. However, carbon monoxide is virtually insoluble in water and yet is taken up in huge quantities by the soil as a result of microbiological activity. The discovery of this

TABLE 2. SOLUBILITY IN WATER AND UPTAKE RATE OF POLLUTANTS

Pollutant	Uptake Rate in Alfalfa* (mol/m^2 s) x 10^9	Solubility at 20° C g/100 g
CO	0.0	0.00234
NO	2.1	0.00625
O_3	34.7	0.052
NO_2	39.6	decomposes
SO_2	59.0	10.8

*Concentration of the gas in the chamber was 2 x 10^{-6} mol/m^3.

massive sink for CO only a few years ago resulted in a reduction in the estimate of the residence time of carbon monoxide in the atmosphere from 3 to 0.1 yr. This illustrative case of the importance of an overlooked natural removal process in estimating global budgets is considered in detail by Ingersoll (1972). Quite a number of experimental studies on pollutant uptake by soils have been conducted. But the variety and complexity of soils, complicated especially by their biologic character, makes controlled experimentation difficult and quantitative modeling an awesome objective.

Water--

Water is surely a critical factor in almost all pollutant removal processes. It also plays a major role via the direct absorption of water soluble pollutants in the three-quarters of the earth's surface which is covered by water. Ammonia is chosen to illustrate this removal mechanism because of its high solubility (about six times that of SO_2; see Table 2). Cattle feedlots put large amounts of ammonia into the air. Of this, Hutchinson and Viets (1969) showed that the amount of NH_3 removed by the atmosphere by precipitation was "insignificant compared to the amount absorbed directly from the air by aqueous surfaces in the vicinity of cattle feedlots."

In an attempt to quantify the removal of ammonia released from a point source (such as from a plume produced by a sewage treatment plant) by an aqueous

surface, Calder (1972) developed a simple mathematical model which takes into consideration the atmospheric transport and diffusion of the plume as well as a characterization of the removal process. His conclusion was that 20% of the ammonia could be removed from the plume in passing over a 30-km-long lake at a wind velocity of 5 m/s. Because of the importance of aqueous sinks (large lakes, oceans), this paper will deal with this interfacial process in much greater detail at a later point.

Stone--

Sulfur dioxide in the atmospheric environment has caused inestimable damage to frescoes, monuments, and other edifices throughout the world. The damage is a result of enhanced weathering rates caused by the attack of sulfuric acid ($SO_2 + 1/2\ O_2 + H_2O \rightarrow H_2SO_4$) on the carbonate matrix of limestone and sandstone. Spedding (1969) showed that the SO_2 uptake rate is dependent upon the moisture level in the atmosphere. The H_2SO_4 reacts with the carbonate matrix to form gypsum as follows:

$$CaCO_3 + H_2SO_4 + H_2O \rightarrow CaSO_4 \cdot 2H_2O + CO_2$$

Because the resulting salt is more soluble in water than the carbonate, the gypsum would be more readily leached out from the stone. The stone would also be subject to physical disintegration because of the volume expansion that accompanies the mineral change (Luckat, 1973).

Luckat and Spedding provide values for SO_2 removal by stone of 6 to 200 and 50 to 200 mg/m^2 day, respectively. Luckat's data were obtained in highly industrial sections of Germany and Spedding had a concentration of 360 μg SO_2/m^3 (100 times the worldwide background level) in his experiments. Taking 5 mg/m^2 day as the lower limit of these data, the total earth's surface of 5×10^{14} m^2, and an estimate that 1% of the earth's surface is stone capable of removing SO_2, the annual removal rate is calculated to be 4.5×10^9 kg SO_2/yr. This rate is 5 to 20 times smaller than any of the estimated rates for other natural SO_2 sinks. More details on this calculation and comparison are given by Rasmussen et al. (1974). Clearly this process could be

modeled by applying the theory of adsorption and reaction rates to this heterogeneous reaction system. However, detailed analysis is not warranted because of the minor impact of this removal process on global budgets. Indeed, it is doubtful if it could even be of much consequence on a local scale.

PRINCIPLES

The remainder of this paper will be dedicated to describing principles and methods for quantitative modeling of the transfer of mass at the atmosphere-earth interface. The existence of atmospheric transport models which provide information on temperature, pressure, humidity, winds, pollutant concentrations, etc. is presumed. Of course, many models exist; see Anthes (1978). However, most do not incorporate removal at the earth's surface. Consider a recent model by Shir and Shieh (1975) which has been prepared to be compatible with the ongoing Regional Air Pollution Studies in the St. Louis area: "Many model options are provided which enable users to study conveniently the significant effects which these options have on the final concentration distributions." Unfortunately, the options do not include allowance for a finite pollutant flux at the surface. Shir and Shieh explain that "absorption of the SO_2 by the ground surface is neglected because it requires data describing the surface properties and their absorption rate." They call for investigation of the surface absorption rate. Allowance for a finite surface flux manifests itself simply as a boundary condition on any properly constructed atmospheric transport model.

Interfacial Flux Calculation

The calculation of the downward flux of a pollutant at a point on the earth's surface can be accomplished if the concentrations and eddy diffusivities are known as functions of height either by prediction or measurement. The product of the vertical concentration gradient and the eddy diffusivity is the flux at any height. Such fluxes can be extrapolated to the interface to find the desired surface flux. This is easier said than done, because eddy transport coefficients are not easily determined and the vapor phase concentrations (especially near the interface) are seldom accurately known. Thus this microscopic approach, even when used with parameterized turbulent transport coefficients, has not proved very useful in practical calculations. A macroscopic

approach which has found widespread application in chemical engineering, meteorology, and other fields is described below.

The vertical flux of a material in a gas phase, $F_g(0)$, can be represented by the equation

$$F_g(0) = k_g(z) \, [C_g(z) - C_g(0)] \qquad \text{(Eq. 1)}$$

The flux is proportional to a concentration driving force $[C_g(z) - C_g(0)]$ in which $C_g(z)$ is the pollutant concentration at some height z above the surface; and $C_g(0)$ is the concentration in the gas phase right at the interface. The coefficient of proportionality, $k_g(z)$, is called the gas phase mass transfer coefficient. The indicated z dependence implies that the coefficient must be selected to be consistent with the height at which the pollutant concentration is to be measured. The choice is quite arbitrary, although 1 and 10 m are commonly used in presenting meteorological data. If the gas phase concentration is known by measurement or model prediction at some height and the gas phase mass transfer coefficient is obtained for the same height from a correlation, the surface flux can be calculated if the interfacial concentration is known. Sometimes $C_g(0)$ is taken to be 0. However, this implies that the nonatmospheric side of the interface has an infinite capacity for the material and offers no resistance to the rate of mass transfer. In the case of uptake by rock, soil, and/or vegetation, neither of these assumptions is likely to be valid. Indeed, it may be the atmospheric phase resistance which is negligible. These solid phases may have to be characterized by a complex series of resistances according to their individual peculiarities.

By contrast, an aqueous phase (such as a lake or ocean) can be dealt with similarly to the gas phase. The flux equation is

$$F_\ell(0) = k_\ell(z') \, [C_\ell(0) - C_\ell(z')] \qquad \text{(Eq. 2)}$$

where $C_\ell(0)$ is the pollutant concentration in the liquid phase right at the interface; $C_\ell(z')$ is the concentration at some depth z'; and $k_\ell(z')$ is the liquid phase mass transfer coefficient corresponding to the depth at which the

pollutant concentration is known. Again, $C_\ell(z')$ is obtained by measurement or prediction and $k_\ell(z')$ from a correlation. Correlations for the gas and liquid phase mass transfer coefficients are the subject of later parts of this paper. In general, the interfacial concentration $C_\ell(0)$ is not easily obtained.

At steady state, there is continuity in the transfer of mass across the interface. That is, the flux of pollutant through the gas must be equal to the flux of pollutant through the liquid:

$$F_g(0) = F_\ell(0) \qquad \text{(Eq. 3)}$$

Equating Equations 1 and 2 leaves only two unknowns, the gas and liquid interfacial concentrations. A relationship between them is supplied by the postulate that phase equilibrium exists right at the interface. The validity of this postulate of interfacial equilibrium is well documented for numerous cases. For any particular case solution, thermodynamics can be used to obtain a quantitative expression such as

$$C_g(0) = f\,[C_\ell(0)] \qquad \text{(Eq. 4)}$$

An example of a rigorous calculation is given for SO_2 in equilibrium with fresh water and with seawater (Rasmussen et al., 1974). A commonly seen form of Equation 4 is $C_g(0) = H\,C_\ell(0)$, known as Henry's Law.

The calculative procedure is as follows:

a. $C_g(z)$ and $C_\ell(z')$ must be known or specified,

b. $k_g(z)$ and $K_\ell(z')$ must be predicted, and

c. Equations 1 through 4 are solved simultaneously for $C_g(0)$, $C_\ell(0)$, and $F(0)$, the interfacial compositions and the desired absorption flux.

Deposition Velocity

Equation 1, which effectively defines the gas phase mass transfer coefficient, will be recognized as being conceptually identical to Chamberlain's (1953) original formulation of the now-familiar deposition velocity. Because the interfacial concentration was usually not known, researchers over the years have made the perfect sink, $C_g(0) = 0$, assumption. Thus, the deposition velocity has come to be defined as

$$v_g \equiv F(0)/C_g \qquad \text{(Eq. 5)}$$

often without attention to its height dependence. Although (obviously) one can calculate a deposition velocity for any flux and concentration measurement, the values obtained have not been successfully correlated in a general sense (Chamberlain, 1975). The principal flaw has surely been in the ignoring of the role of the nonatmospheric phase.

Part of the charm of the deposition velocity is that it has units of velocity and can be applied to solid particles as well as gases. The easy visualization of falling particles encourages one to conceive of gases moving downward with a velocity v_g. Indeed, diffusional theory (Bird et al., 1960) gives

$$n_A = C_A v_A \qquad \text{(Eq. 6)}$$

where n_A is the mass flux of A with respect to stationary coordinates, C_A is the concentration of component A, and v_A is the velocity of species A with respect to stationary coordinates. Comparing Equations 5 and 6, it appears that v_A and v_g could be identical if C_A and C_g were taken at the same location. However, all terms in Equation 6 have point values only. Thus n_A would be the vertical flux at the point where C_A was measured, whereas $F(0)$ is the vertical flux at the surface. Hence v_g is not the same as v_A and is, in fact, only a ratio between two measured quantities, without physical significance except as a coefficient of proportionality.

Although the deposition velocity is firmly entrenched in the meteorology literature, use of the mass transfer coefficient formalism is strongly urged for the following reasons:

a. Equation 1 will surely be more successful in correlating surface fluxes (deposition) than Equation 5.

b. Misleading physical significance is less likely to be attached to $k_g(z)$ than to v_g.

c. Mass transfer coefficients have been shown to be useful in characterizing nonatmospheric phases. The nomenclature given in Equation 2 for the aqueous phase is in widespread use in the oceanography literature.

Need for Data

Equations 1 and 2 are guides to the experimental determination of the gas and liquid phase mass transfer coefficients, $k_g(z)$ and $k_\ell(z')$. For complete specification of $k_g(z)$, the flux through the interface and the gas phase concentrations at the interface and at some known height must be measured. Better still, vertical profiles of concentration could be measured. This provides one way of determining the interfacial concentration. For carefully specified circumstances, the interfacial gas phase concentration can be obtained from knowledge of the liquid phase characteristics. An analogous procedure will suffice for finding $k_\ell(z')$. Much of the data presently available are incomplete in some way. The height or depth of concentration measurement is unspecified, an interfacial concentration (usually 0) has been chosen without verification, and/or the flux has been obtained from an eddy diffusion model rather than measured directly. Unless all factors are measured, it is like using one model to develop another. As adequate data become available, correlations based on fluid-mechanical and physical-chemical considerations (such as those described below) will provide reliable estimates of the mass transfer coefficients for use in the boundary conditions on air-quality simulation models.

GAS PHASE MASS TRANSFER COEFFICIENT

In the calculation of deposition of a pollutant from the atmosphere to any medium at the earth's surface, it is necessary to quantify the mass transfer

through the air near the surface. As described earlier, this can be achieved if the gas phase mass transfer coefficient can be predicted.

Conceptually, the starting point is the Reynolds analogy, which expresses a similarity among mass, heat, and momentum transfer. One expression for the Reynolds analogy is

$$k_g(z) = C_D\, u(z) = u_*^2/u(z) \qquad \text{(Eq. 7)}$$

This expression says that the mass transfer coefficient, $k_g(z)$, is linearly proportional to the horizontal velocity, $u(z)$, which in turn is a function of height, z, and that the coefficient of proportionality is the familiar drag coefficient, C_D. Noting that $C_D = [u_*/u(z)]^2$, Equation 7 can be expressed as shown in terms of the friction velocity, u_*. The chemical engineering literature contains many modifications of the Reynolds analogy. One of the best known is the Chilton-Colburn (1934) equation, which allows for variation among chemical species by inclusion of the Schmidt number ($Sc = \mu/\rho D$):

$$k_g(z) = \frac{u_*^2}{u(z)\ Sc^{2/3}} \qquad \text{(Eq. 8)}$$

Owen and Thomson's (1963) research on heat transfer provides a somewhat different correction to allow for the fact that different species may diffuse at different rates, and (especially) to allow for the fact that surfaces may exhibit a bluff body character not accounted for by the Reynolds analogy. Their equation is

$$\frac{1}{k_g(z)} = \frac{1}{u_*}\left|\frac{u(z)}{u_*} + B^{-1}\right| \qquad \text{(Eq. 9)}$$

In all of these equations, u_* is the familiar friction velocity, which is related to the shear stress at the surface by $u_* = \sqrt{\tau_o/\rho}$.

Owen and Thomson's Equation 9 has been accepted by many investigators who have then tried to obtain correlations for B^{-1}. One such correlation is suggested by Dipprey and Sabersky (1963):

$$B^{-1} = 10.25\ Re_o^{0.2}\ Sc^{0.44} - 8.5 \qquad \text{(Eq. 10)}$$

The Reynolds number in Equation 10 is the roughness Reynolds number, $Re_o = u_* z_o/\nu$, where ν is the kinematic viscosity and z_o is the so-called roughness height. Sutton (1953) has tabulated values for z_o for various types of underlying surfaces. Charnock (1955) has developed the following correlation for a water surface:

$$z_o = b\ u_*^2/g \qquad \text{(Eq. 11)}$$

where g is the gravitational acceleration and b is a constant for which various values have been given. One more relationship is required and is provided for neutral conditions by the logarithmic velocity profile:

$$\frac{u(z)}{u_*} = \frac{1}{k}\ \ln\left(\frac{z}{z_o}\right) \qquad \text{(Eq. 12)}$$

In this equation, k is the von Kármán constant, usually given a value of 0.4. For nonneutral conditions, corrections can be made to Equation 12 as required (Panofsky, 1963).

To obtain a value of the gas phase mass transfer coefficient, the calculation proceeds as follows: From a value of wind speed u(z) at a single height z, Equations 11 or 13 and 12 can be solved for z_o and u_*. Note that this allows specification of the vertical velocity profile via Equation 12. A method for obtaining u_* directly for airflow over water is provided by Hicks (1973):

$$C_D = \left|\frac{u_*}{u(10)}\right|^2 = [0.65 + 0.07\ u(10)] \times 10^{-3} \qquad \text{(Eq. 13)}$$

Knowing the appropriate physical properties for the air and the pollutant of interest, the correction factor B^{-1} can be obtained from Equation 10. From the known velocity profile, Equation 12, and the calculated values of u_* and

B^{-1}, the mass transfer coefficient can be determined from Equation 9 for whatever height the pollutant concentration is known.

The above development is only illustrative, as many of the ideas have reached far more sophisticated levels and almost classic form in a variety of special applications. On the other hand, generalization is lacking when it comes to predicting B^{-1} and hence k_g. Figure 1 shows the mass transfer coefficient as a function of the roughness height for a variety of correlations, including the Reynolds analogy. A neutral atmosphere with a wind velocity at 10 m of 10 m/s was chosen, with SO_2 as the diffusing gas. For smooth surfaces (low z_o) the correlations are in rather good agreement. However, they diverge sharply as roughness increases. To date, proper interpretation of adequate data has not occurred to reconcile the discrepancies.

LIQUID PHASE MASS TRANSFER COEFFICIENT

The kind of data analysis and correlation evaluation recommended in the previous section has recently been completed by Brtko (1976) for the liquid phase. This paper presents only the major features of his work.

Researchers in chemical engineering, oceanography, and other fields have measured liquid phase mass transfer coefficients. Most often the data have been interpreted in terms of the thickness of a hypothetical stagnant film and thus have resisted successful correlation. Danckwerts (1951) proposed a surface renewal theory which is conceptually attractive but contains a surface renewal rate parameter which has proved hard to predict *a priori*. Recently, Fortescue and Pearson (1967) and Lamont and Scott (1970) have proposed roll cell mass transfer models based on different characterizations of the turbulence in the liquid phase.

Brtko and Kabel (1976) have adapted the two models to the situation where the roll cells are the result of wind-induced turbulence in the liquid phase. The result for the more successful of the two models is

$$k_\ell(z') = 0.4\ Sc^{1/2} \left[\frac{\nu u_*^3}{kz'} \left(\frac{\rho_a}{\rho_w} \right)^{3/2} \right]^{1/4} \qquad \text{(Eq. 14)}$$

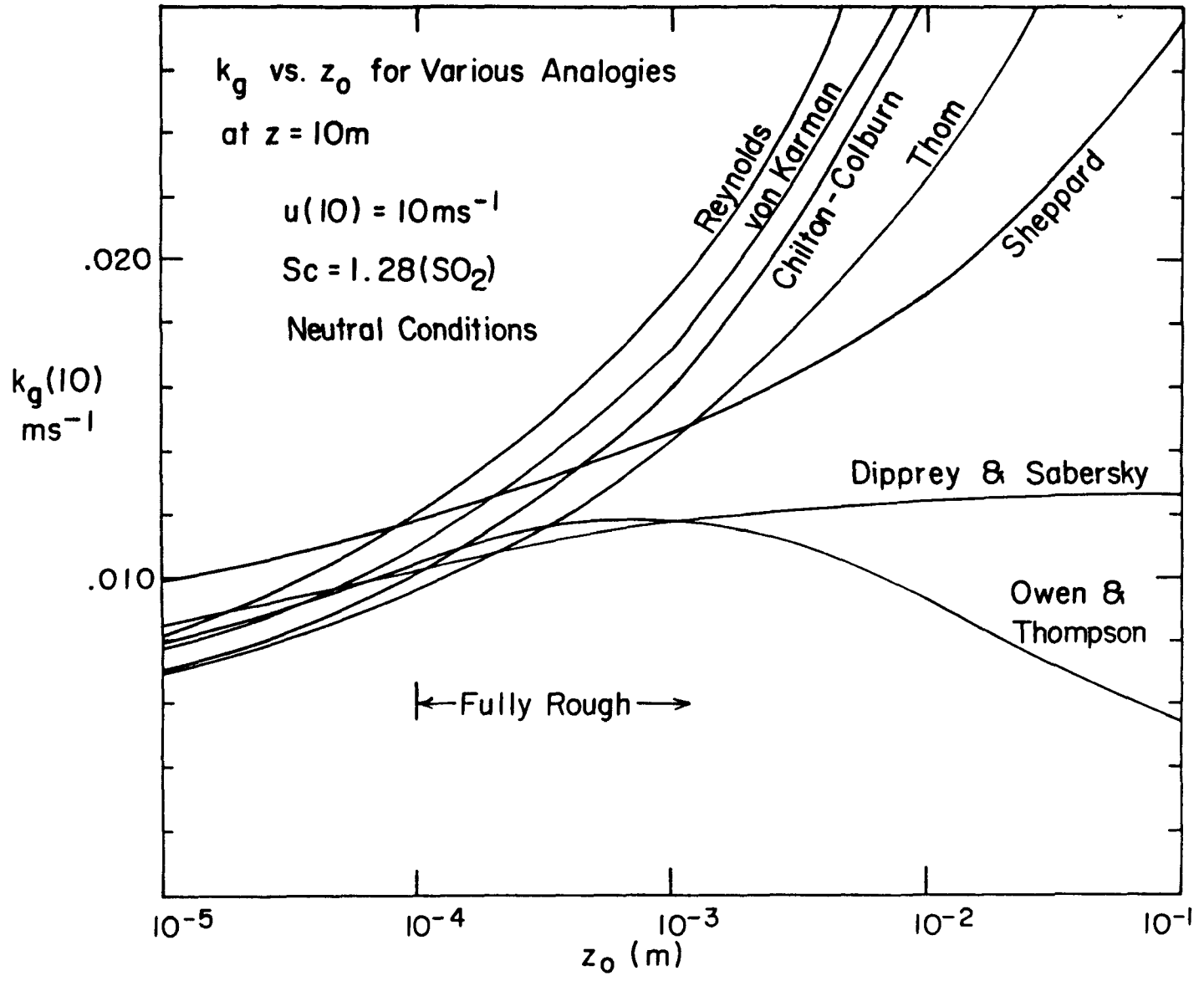

Figure 1. Mass transfer coefficient correlations.

To use this model, only the friction velocity in the air at the free liquid surface, the depth z' in the liquid phase at which the concentration is known, and the temperatures of both phases are required. The friction velocity is obtained as described earlier. The temperatures enable the estimation of the physical properties, and k is the von Kármán constant.

Data with which to compare Equation 14 are few, and most of those that do exist are inadequate for this purpose in one way or another. Comparisons with some of the better defined data are given below. Liss (1973), measuring the desorption of oxygen in a wind-water tunnel, obtained values of about a factor of 2 lower than those predicted by Equation 14. Probably the most reliable field data are those of Broecker and Peng (1971) and Peng et al. (1974), who measured the efflux of radon 222 from the Atlantic and Pacific oceans. The field data fall about a factor of 3 above the predictions of Equation 14. Work is continuing to reconcile the remaining discrepancies. Nevertheless, the agreement appears satisfactory inasmuch as the models mentioned here are the only predictive models known to the author.

OVERVIEW

The importance of accounting for natural sources and sinks of atmospheric pollutants in air-quality simulation models was discussed. Several removal processes were described and illustrated with significant examples from the literature. Some indication of the state of development of quantitative understanding of each process was given. Emphasis was then placed on those mechanisms active at the earth's surface. The principles of modeling mass transfer at interfaces were presented and discussed in the context of common practice. In particular, for the important case of pollutant transport across an atmosphere-water interface, a brief evaluation of methods of predicting gas and liquid phase mass transfer coefficients was attempted.

ACKNOWLEDGMENTS

The author wishes to acknowledge continuing technical input from the members of the Select Research Group in Air Pollution Meteorology. In particular, recognition of the contributions to parts of this paper by graduate students Karen H. Rasmussen, Lawrence B. Hausheer, and Wayne J. Brtko is made.

Special appreciation is extended to the U.S. Environmental Protection Agency for its financial support of this project via Grant No. 800397, administered through the Center for Air Environment Studies and the Department of Meteorology of The Pennsylvania State University.

NOMENCLATURE

B^{-1}	Measure of deviation from Reynolds analogy, dimensionless
b	Proportionality coefficient, dimensionless
C_A	Point solute concentration, $\mu g/m^3$
C_D	Drag coefficient, dimensionless
C_g	Atmospheric pollutant concentration, $\mu g/m^3$
$C_g(0)$	Atmospheric pollutant concentration at gas-liquid interface, $\mu g/m^3$
$C_g(z)$	Atmospheric pollutant concentration at height z, $\mu g/m^3$
$C_\ell(0)$	Pollutant concentration in liquid phase at gas-liquid interface, $\mu g/m^3$
$C_\ell(z')$	Pollutant concentration in liquid phase at depth z', $\mu g/m^3$
D	Molecular diffusivity of pollutant through medium of interest, m^2/s
F(0)	Interfacial flux of pollutant, $\mu g/m^2$ s
$F_g(0)$	Flux of pollutant leaving gas phase at interface, $\mu g/m^2$ s
$F_\ell(0)$	Flux of pollutant entering liquid phase at interface, $\mu g/m^2$ s
g	Acceleration of gravity, m/s
H	Henry's Law constant, $\mu g/m^3$ of gas per $\mu g/m^3$ of liquid
k	von Kármán constant equal to 0.4, dimensionless
$k_g(10)$	Gas phase mass transfer coefficient for 10 m, m/s

$k_g(z)$	Gas phase mass transfer coefficient for height z, m/s
$k_\ell(z')$	Liquid phase mass transfer coefficient for depth z', m/s
n_A	Mass flux of A with respect to stationary coordinates, $\mu g/m^2$ s
Re_o	Roughness Reynolds number $u_* z_o/\nu$, dimensionless
S_c	Schmidt number ν/D, dimensionless
u(10)	Gas phase velocity at 10 m, m/s
u(z)	Gas phase velocity at height z, m/s
u_*	Gas phase friction velocity $\sqrt{\tau_o/\rho}$, m/s
v_A	Velocity of species A with respect to stationary coordinates, m/s
v_g	Deposition velocity, m/s
z	Height above earth's surface, m
z'	Depth beneath water surface, m
z_o	Roughness height, m

Greek Letters

μ	Absolute viscosity of phase of interest, kg/m s
ν	Kinematic viscosity of phase of interest μ/ρ, m^2/s
ρ	Density of phase of interest, kg/m^3
ρ_a	Density of gas phase, kg/m^3
ρ_w	Density of liquid phase, kg/m^3
τ_o	Gas phase shear stress at surface, kg/m s^2

REFERENCES

Altshuller, A. P., and J. J. Bufalini. 1971. Photochemical Aspects of Air Pollution: A Review. Environ. Sci. Tech. 5(1):39-64.

Anthes, R. A. 1978. Meteorological Aspects of Regional-Scale Air-Quality Modeling. In: Select Research Group in Air Pollution Meteorology, Third Annual Progress Report. U.S. Environmental Protection Agency, Research Triangle Park, North Carolina.

Bennett, J. H., A. C. Hill, and D. M. Gates. 1973. A Model for Gaseous Pollutant Sorption by Leaves. J. Air Pollution Control Assoc. 23(11): 957-962.

Bird, R. B., W. E. Stewart, and E. N. Lightfoot. 1960. Transport Phenomena. Wiley, New York.

Broecker, W. S., and T. H. Peng. 1971. The Vertical Distribution of Radon in the Bomex Area. Earth Planet Sci. Letters 11:99-107.

Brtko, W. J. 1976. Mass Transfer at Natural Air-Water Interfaces. M.S. Thesis. The Pennsylvania State University, University Park, Pennsylvania.

Brtko, W. J., and R. L. Kabel. 1976. Pollutant Transfer into Water Bodies. Water, Air, and Soil Pollution 6(1):71-95.

Calder, K. L. 1972. Absorption of Ammonia from Atmospheric Plumes by Natural Water Surfaces. Water, Air, and Soil Pollution 1:375-380.

Charnock, H. 1955. Wind Stress on a Water Surface. Quarterly J. Royal Meteor. Soc. 81:639-640.

Chamberlain, A. C. 1953. Aspects of Travel and Deposition of Aerosol and Vapor Clouds. AERE-HP/R-1261, Great Britain Atomic Energy Research Establishment, Harwell, Berkshire.

Chamberlain, A. C. 1975. Personal communication (30 Sept.).

Chilton, T. H., and A. P. Colburn. 1934. Mass Transfer (Absorption) Coefficients, Prediction from Data on Heat Transfer and Fluid Friction. Ind. Eng. Chem. 26:1183-1187.

Cogbill, C. V., and G. E. Likens. 1974. Acid Precipitation in the Northeastern United States. Water Resources Res. 10(6):1133-1137.

Danckwerts, P. V. 1951. Significance of Liquid-Film Coefficients in Gas Absorption. Ind. Eng. Chem. 43:1460-1467.

Dipprey, D. F., and R. H. Sabersky. 1963. Heat and Momentum Transfer in Smooth and Rough Tubes at Various Prandtl Numbers. Int. J. Heat Mass Transfer 6:329-353.

Forland, E. J., and Y. T. Gjessing. 1975. Snow Contamination from Washout/Rainout and Dry Deposition. Atmos. Environ. 9:339-352.

Friend, J. P. 1976. The Global Atmospheric Nitrogen Cycle and Ozone. Seminar presented in the Department of Meteorology at The Pennsylvania State University, University Park, Pennsylvania (1 April).

Fortescue, G. E., and J. R. A. Pearson. 1967. On Gas Absorption into a Turbulent Liquid. Chem. Eng. Sci. 22:1163-1176.

Hales, J. M. 1972. Fundamentals of the Theory of Gas Scavenging by Rain. Atmos. Environ. 6:635-659.

Hales, J. M., M. T. Dana, and M. A. Wolf. 1973. Advance in the Theory and Modeling of Pollutant Gas Washout. In: Proceedings of the Third International Clean Air Congress. VDI-Verlag GmbH, Düsseldorf, B.R.D.

Hecht, T. A., and J. H. Seinfeld. 1972. Development and Validation of a Generalized Mechanism for Photochemical Smog. Environ. Sci. Tech. 6(1):47-57.

Hicks, B. B. 1973. The Dependence of Bulk Transfer Coefficients Upon Prevailing Meteorological Conditions. Radiological and Environmental Research Annual Report, ANL-8060 Part IV, Argonne National Laboratory, Argonne, Illinois.

Hidy, G. M. 1973. Removal Processes of Gaseous and Particulate Pollutants. In: Chemistry of the Lower Atmosphere, S. I. Rasool, ed. Plenum Press, New York.

Hill, A. C. 1971. Vegetation: A Sink for Atmospheric Pollutants. J. Air Pollution Control Assoc. 21(6):341-346.

Hutchinson, G. L., and F. G. Viets. 1969. Nitrogen Enrichment of Surface Water by Absorption of Ammonia Volatilized from Cattle Feedlots. Science 166:514-515.

Ingersoll, R. B. 1972. The Capacity of the Soil as a Natural Sink for Carbon Monoxide. SRI LSU-1380 CRC A PRAC CAPA 4 68 6, Stanford Research Institute, Menlo Park, California. 43 pp.

Lamont, J. C., and D. S. Scott. 1970. An Eddy Cell Model of Mass Transfer into the Surface of a Turbulent Liquid. AICHE J. 16:513-519.

Liss, P. S. 1973. Processes of Gas Exchange Across an Air-Water Interface. Deep Sea Res. 20:221-238.

Luckat, S. 1973. Die Wirkung von Luftverimreinigungen beim Steinzerfall. Staub-Reinhalt. Luft. 33:283-285.

Miller, J. M., and R. G. de Pena. 1972. Contribution of Scavenged Sulfur Dioxide to the Sulfate Content of Rain Water. J. Geophys. Res. 77(30): 5905-5916.

Molina, M. J., and F. S. Rowland. 1974. Stratospheric Sink for Chlorofluoromethanes: Chlorine Atom-Catalyzed Destruction of Ozone. Nature 249:810-812.

Murphy, T. J. 1975. Concentrations of Phosphorous in Precipitation in the Lake Michigan Basin. In: Proceedings of the IAGLR First Specialty Symposium on Atmospheric Contributions to the Chemistry of Lake Waters, Longford Mills, Ontario, Canada.

Owen, P. R., and W. R. Thomson. 1963. Heat Transfer Across Rough Surfaces. J. Fluid Mech. 15:321-334.

Panofsky, H. A. 1963. Determination of Stress from Wind and Temperature Measurements. Quarterly J. Royal Meteor. Soc. 89:85-94.

Peng, T. H., T. Takahashi, and W. S. Broecker. 1974. Surface Radon Measurements in the North Pacific Ocean. J. Geophys. Res. 79:1772-1780.

Rasmussen, K. H., M. Taheri, and R. L. Kabel. 1974. Sources and Natural Removal Processes for Some Atmospheric Pollutants. EPA-650/4-74-032, U.S. Environmental Protection Agency. 121 pp.

Rasmussen, K. H., M. Taheri, and R. L. Kabel. 1975. Global Emissions and Natural Processes for Removal of Gaseous Pollutants. Water, Air, and Soil Pollution 4:33-64.

Sehmel, G. A. 1975. Experimental Measurements and Predictions of Particle Deposition and Resuspension Rates. Reprint 75-25.2, 68th Annual Meeting of the Air Pollution Control Association, Boston, Massachusetts.

Sheppard, P. A. 1958. Transfer Across the Earth's Surface and Through the Air Above. Quarterly J. Royal Meteor. Soc. 84:205-224.

Shir, C. C., and L. J. Shieh. 1975. Development of an Urban Air Quality Simulation Model with Compatible RAPS Data. EPA-600/4-75-005-a, U.S. Environmental Protection Agency. 147 pp.

Spedding, D. J. 1969. SO_2 Uptake by Limestone. Atmos. Environ. 3:683.

Sutton, O. G. 1953. Micrometeorology. McGraw-Hill, New York.

Thom, A. S. 1972. Momentum, Mass, and Heat Exchange of Vegetation. Quarterly J. Royal Meteor. Soc. 98:124-134.

Twomey, S. 1971. The Composition of Cloud Nuclei. J. Atmos. Sci. 28:377-381.

von Kármán, T. 1934. Aspects of Turbulence Problem. In: Proceedings, Fourth International Congress for Applied Mechanics, Cambridge, England, 3-9 July. pp. 77-83.

OBSERVATIONAL REQUIREMENTS FOR VALIDATION OF AIR POLLUTION METEOROLOGY MODELS

Dennis W. Thomson
Department of Meteorology

INTRODUCTION

Significant advances have been made during the past several years in the development of three-dimensional regional and finer-scale meteorological models. One-dimensional models for both the daytime and nighttime planetary boundary layer may now be run on desk-top calculators and employed routinely for some air-quality predictions (such as passive contaminant concentrations). We now also understand in some detail both the practical potential and limitations of a variety of simplified transport and diffusion models, including box, plume, puff, and particle-in-cell types. Presently, although several extensive (but rather specialized) meteorological and air pollution measurement programs are either in progress or in advanced planning stages, one of the major problems prolonging the development of comprehensive, predictive meteorological models for air pollution applications is the lack of measurements and analyzed data which can be readily used to test and evaluate the models (Anthes, 1978).

Unfortunately, in this case recognizing the need for validation data does not "half solve the problem." The application of conventional "synoptic" data systems and analysis techniques on a regional (or smaller) scale is prohibitively expensive. This is a consequence of the required density, both spatially and temporally, of *in-situ* surface and aerological measurements.

It appears that many of the problems (including fiscal problems) associated with the use of existing operational systems for fine-scale experiments could be solved through appropriate application of sophisticated, continuously-operating remote sounding and — perhaps, on an intermittent basis — instrumented

aircraft observations. With the exceptions of sodar (Sound Detection and Ranging) and path-integrating optical anemometers, however, most of the contemporary remote-probing systems of potential interest are still in the research and developmental stages. Neither these systems nor their users are probably prepared to cope with the operational demands of assembling a set of atmospheric observations of the type which could be used for definitive model validation and intercomparison experiments.

Several excellent review papers and publications exist which summarize the capabilities of many direct sensors (Kaimal, 1975; Johnson and Ruff, 1975) and indirect sounding systems (Derr, 1972; Little, 1972). This paper differs in that I have attempted to recommend the use of specific meteorological observations or measurement systems on the basis of model data requirements rather than system capabilities. Classification of the various models generally follows that of Anthes (1978). No attempt has been made here to review the nature and quality of existing climatological and synoptic observations, for they would presumably be available for use regardless of any particular local (or regional) air pollution meteorology requirements.

GENERAL CONSIDERATIONS

The meteorological measurements required to determine the time rate of change of a passive contaminant are determined, either explicitly or implicitly, by the concentration equation

$$\frac{\partial Q}{\partial t} = - \vec{V}_H \cdot \nabla Q - w\frac{\partial Q}{\partial z} - Q\nabla\cdot\vec{V} - \nabla_H \cdot \overline{\vec{V}'_H Q'} - \frac{\overline{\partial w'Q'}}{\partial z}$$

$$+ \text{ source and removal terms,}$$

in which the mean and turbulent horizontal transport terms are $\vec{V}_H \cdot \nabla Q$ and $\nabla_H \cdot \overline{\vec{V}'_H Q'}$, respectively; and the mean and turbulent vertical transport terms are $w\frac{\partial Q}{\partial z}$ and $\frac{\overline{\partial w'Q'}}{\partial z}$. The remaining term, $Q\nabla\cdot\vec{V}$, is the divergence of the velocity field. Suitable observations of the space- and time-dependent velocity

field are, obviously, of paramount importance. Viewed in this way, the role of other basic meteorological variables (e.g., temperature, pressure, radiation, and moisture) is that of completing the basic set of equations which must be used to determine or predict the mean wind field and turbulent velocity fluctuations. The scalar variables appearing in that set of basic equations, the so-called "primitive equations," include: pressure, temperature, specific humidity, and the latent heats of evaporation and condensation. Ideally, in a complete model all of these variables are specified everywhere within its domain, and on its upper, surface, and four lateral boundaries. In fact, however, a complete set of observations of all the apparently important variables will probably never be realized. The task before us, then, is to determine for a variety of less-than-complete models the minimum number of measurements which can be used and still enable us to make predictions of atmospheric structure and behavior that will aid an air pollution meteorologist.

ONE-DIMENSIONAL MIXING-LAYER MODELS

For most daytime conditions, in the absence of significant advection or subsidence, one-dimensional mixing-layer models are now so refined as to tax the state-of-the-art measurement systems which may be used to acquire model validation data (Tennekes, 1978).

Daytime mixing-layer growth, $H(t)$, may be essentially treated as the result of the time-dependent sensible heat transport, $S_a(t)$, into the lower atmosphere. The initial condition of the lower atmosphere is defined by an early morning temperature profile, $T(z,t_o)$. To a lesser extent, the growth rate also depends upon the variable entrainment rate at the top of the mixing layer. The temperature profile may be adequately determined using either a conventional radiosonde (if the trace is carefully analyzed) or — better yet — one of several new commercial balloon- or kytoon-borne "mini-sondes" (Morris et al., 1975). Either will provide $T(p)$, from which (using the hypsometric relation) $T(z)$ may be calculated.

For studies of mixing-layer climatology, $S_a(t)$ may be sufficiently well specified by a "mean" surface energy balance (Tennekes and van Ulden, 1974).

However, prediction of H(t) on a given day requires precise specification of $S_a(t)$. Recall that

$$S_a(t) = (1-\alpha)R(t) - \varepsilon\sigma T_s^4(t) - E(t) - S_s(t)$$

At a given site the albedo may be estimated or measured (Sellers, 1965; Kondratyev, 1969), and the global radiation then monitored using a pyrometer. Since

$$R_n(t) = (1-\alpha)R(t) - \varepsilon\sigma T_s^4(t)$$

use of a ventilated or dome-type net radiometer to remove uncertainties associated with the albedo and outgoing infrared terms would be preferable. A problem remains, of course, in that local radiation (or energy budget) measurements may not be representative of those for the surrounding area (Dabberdt and Davis, 1974). The relationship between an areal average of $R_n(t)$, which will determine H(t), and observations at a given site can probably be best determined by experimental comparison of observed and predicted H(t) values.

Since the soil heat flux is normally small [$S_s(t) \leq 0.1\ R_n(t)$] and well behaved, it is possible to parameterize it in terms of $R_n(t)$ (Blackadar, 1978). But when a model such as Blackadar's is used, certain corrections should be made (for example, for recent rainfall in a normally dry area).

The most difficult term to specify is E(t). It can easily be fourfold $S_a(t)$, and strongly depends upon factors such as surface and subsurface soil characteristics, vegetative cover, and recent rainfall history. Probably operational measurements of E(t) or $S_a(t)$ by the "eddy correlation" technique $\overline{(w'q', q'T')}$ would, due to the delicacy of available sensors, be prohibitively expensive. For inversion-rise predictions, measurement of the mean vertical dry and wet bulb temperature gradient so that a Penman-type (Sellers, 1965) or Bowen ratio technique may be employed is the best apparent solution. The limitations in these techniques are not likely to give problems during inversion-rise conditions. Highly reliable and sufficiently accurate electronic bridges for thermistor or resistance elements may be built or purchased for

a few hundred dollars — a fraction of the cost of many air-quality monitoring instruments. Given the initial temperature profile and the time-dependent sensible heat flux, an inversion-rise model such as Tennekes' (1973) may then easily be run on a desk-top programmable calculator (Benkley, 1976). Table 1 summarizes data requirements for mixing-layer models and some suggested measurement techniques.

Measurement of H(t), at least to heights of the order of 1 km, may now be routinely performed using the sodar acoustic sounding technique (Russel et al., 1974; Aerovironment, 1976). Several different commercial systems are now available throughout the world. It is only a matter of time before sodar will be as familiar a working tool to the air pollution meteorologist as radar presently is to the severe storms forecaster.

In principle, an additional application of sodar for inversion-rise predictions exists. Using the relationship derived by Wyngaard et al. (1971) for estimating the vertical sensible heat flux from C_T^2 (sensed by a monostatic sodar), it may be possible to obtain $S_a(t)$ as well as H(t) from a sodar system. The two are independent measurements in that $S_a(t)$ is based on signal amplitude at a given range, whereas H(t) is derived from the characteristic rising inversion signature seen on the sodar height-time recordings (Aerovironment, 1976). Evaluation of this technique is presently underway at The Pennsylvania State University.

Much research remains to be done on the modeling of nocturnal and stable planetary boundary layers. Above homogeneous terrain, techniques such as those employed by Blackadar (1978) and Wyngaard (1975) show promise. However, in complex terrain even the simplest meteorological situations will probably require two- or three-dimensional models.

Our qualitative understanding of stable boundary layers has been greatly enhanced during the past 8 to 12 years as a consequence of the wealth of sodar, lidar, and high-resolution radar measurements (e.g., see Ottersten et al., 1973). The stable mixing layer appears characteristically to exhibit either

highly erratic behavior or to regularly include wave-type features. Patches of turbulence, probably generated by shear instability, can generate both upward and downward momentum and heat fluxes. We do not yet know if the quasi-periodic "bursts" of turbulence at arbitrary heights as a consequence of local dynamics in stability are generated at the surface, or are the consequence of (for example) wave motions aloft.

Blackadar (1978) has modeled the evolution of a nocturnal jet. His sensitivity studies show that detailed vertical temperature and wind profile and surface heat flux data would be required if a running model were to be updated with actual observations. In the case of the nocturnal boundary layer, the required sampling frequency at several height levels extending through the jet could be of the order of several minutes. Either sodar or lidar might be used to continuously monitor nocturnal mixing-layer depth (Russel et al., 1974; Thomson, 1975). However, neither system can presently provide all the information necessary to make predictions of its temporal evolution.

TABLE 1. DATA REQUIREMENTS FOR MIXING-LAYER MODELS

Variable	Sensor	Notable Advantages; Disadvantages
$H(t)$	Sodar	Continuous, 1-1.5 km max. height
	Aircraft	Detailed *in-situ* meas.; cost, min. altitude in urban areas
	Helicopter	Maneuverability; cost
	Lidar	Outputs particulate loading; maintenance cost
$T(z,t)$	"Minisonde"	Optimal design
	Radiosonde	Reg. NWS obs.; limited resolution
$R(t)$	Pyrometer	Simple, reliable; solar radiation only
$R_n(t)$	Net radiometer	Fragile
$S_a(t)$, $E(t)$	ΔT, ΔT_w, T_w	Bowen ratio assumption required
$S_s(t)$	Heat flux plates	Subject to corrosion and frost action

BOX MODELS

The concentration of a pollutant predicted by a box model may be written

$$Q = \frac{S}{|\vec{V}| \cdot D \cdot H(t)}$$

where S is the source strength and D the lateral dimension of the box. For climatological predictions of average concentrations, box models do very well (Gifford and Hanna, 1973). If the dynamic response of such a model is also considered (Lettau, 1970; Tennekes, 1978), it can also be successfully applied to a variety of more complicated situations. Obviously, however, a box model breaks down in air stagnation situations when the wind speed falls to 0 or in circumstances in which significant horizontal or vertical gradients are present in any of the independent variables.

From an observational point of view (Table 2), a box model has the advantage that observations from only one location must be representative of the box (typically, urban-scale). Since the flushing time constant is a few hours, measurements on that time scale are sufficient. In the meteorological conditions in which a box model may be applied, $|\vec{V}|$ is a slowly varying parameter, and available surface or winds determined from synoptic analyses will certainly be adequate. The height of the "lid" of the box H(t) may be continuously monitored (using a sodar system) or predicted (using one of the aforementioned models). If a tristatic Doppler sodar system is used, wind speed and direction at, say, 300 m will be continuously available. In fact, since many of the Doppler sodars now include minicomputer processors, if the source term is known, the sodar computer can be programmed to output the model results as well as the meteorological data. Because the meteorological requirements for a box model are minimal, the largest uncertainty in its application will probably be the time-dependent emissions inventory.

GAUSSIAN PLUME MODELS

In steady-state conditions, application of a Gaussian plume model requires only a measurement (Table 3) of the mean wind speed and specification of the

TABLE 2. DATA REQUIREMENTS FOR BOX MODELS

Variable	Sensor	Notable Advantages; Disadvantages
$H(t)$	Sodar	Continuous, 1-1.5 km max. height
	Aircraft	Detailed *in-situ* meas.; cost, min. altitude in urban areas
	Helicopter	Maneuverability; cost
	Lidar	Outputs particulate loading; maintenance cost
$\lvert\vec{V}(z_o,t)\rvert$	Cup anemometer	Reliable, surface obs.
$\theta(z_o,t)$	Wind vane	Reliable, surface obs.
$\vec{V}(z,t)$	Doppler sodar	Continuous; high initial cost
	Pibal	Inconvenient, large rms error
	Radiosonde	High operating costs

appropriate stability category (Turner, 1970). If estimates of diffusion from surface sources are made in conditions including a capping inversion, then its height must, of course, be known also. Normally Pasquill's (1961) key is used to estimate σ_y and σ_z from the surface wind speed and incoming solar radiation or nighttime conditions.

If *in-situ* measurements of σ_y and σ_z are made, they are normally derived from recorded horizontal (θ) and vertical (ϕ) wind direction variations (Slade, 1968). The respective standard deviations, σ_θ and σ_ϕ, may be either visually estimated from a continuous strip chart record or electronically estimated in a high-pass filter "sigma" meter circuit.

One reason for the success of Pasquill's classification scheme is that estimates of σ_y and σ_z derived from local instrument measurements are highly sensitive to site-specific biases. In an urban environment, 100/1 or even 10/1 fetch (particularly independent of direction) rarely exists for wind direction sensors situated within the surface layer.

At the present time, one of the most serious measurement deficiencies in the application of Gaussian plume models is that of poor (or nonexistent) σ_y and σ_z values at altitudes of 150 to 600 m, the effective stack height for the high stacks now in use at many power and large industrial plants. In principle, there is no reason why such measurements could not be made using a Doppler sodar system. Both wind speed (including vertical velocities) and direction, and the variations thereof, may be continuously monitored to heights in excess of 500-700 m with contemporary systems. Experiments for validating sodar-derived σ_y and σ_z estimates for high stack prediction applications could be easily conducted at a large power plant using extended exposure photography of the plume as a diffusion rate reference (Högström, 1964; Slade, 1968). For experimental purposes, it is also possible to obtain detailed plume cross-section data using a lidar operating in a range-height-indicator mode (Johnson, 1971).

TABLE 3. DATA REQUIREMENTS FOR PLUME MODELS

Variable	Sensor	Notable Advantages; Disadvantages
$\lvert\vec{V}(z_o,t)\rvert$	Cup anemometer	Reliable, surface obs.
Insolation or Cloudiness	Trained obs.	Observer-dependent quality
$\sigma_\theta(z_o,t)$, $\sigma_\phi(z_o,t)$	Bivane	In common use; fragile, limited to tower height
	Doppler sodar	Continuous; high initial cost
H(t)	Sodar	Bistatic, C_v^2 sensing, system pref. for interpretation of nocturnal layer structure

LAGRANGIAN PUFF MODELS

The previously discussed models may all be applied using observations from a single location as long as it has been established that the location is representative of the larger region of interest. However, in the case of more complicated models which may be applied to interpretation of regional-scale transport and diffusion, it is necessary to discuss not only the diversity of measurements required at a single point but also the number and siting of network stations or the use of mobile platforms.

In a Lagrangian "puff" model, the center of mass of a puff of pollutants is advected along a trajectory. Thus, determination of the three-dimensional wind field from which trajectories may be computed is essential (Table 4).

TABLE 4. DATA REQUIREMENTS FOR TRAJECTORY AND PUFF MODELS

Variable	Sensor	Notable Advantages; Disadvantages
$\vec{V}(x,y,z,t)$	Radiosonde network	Data analyzed and available; sparse network and only 2 per day
	NWS upper air analyses	Significant local error possible
	Tetroon systems	Outputs traj., cost
$K(x,y,z,t)$	Tetroon systems	Outputs K along traj., cost

In some situations, such as emission from a high stack — when neither stagnation nor rapidly changing meteorological conditions are present — trajectory estimates derived from synoptic meteorological analyses may be adequate. But a puff model is most likely to be applied on a 5- to (perhaps) as much as 400-km scale. Within this domain, underlying terrain characteristics may strongly influence both the direction of the mean flow, such as the veering which is often observed east of the Appalachian mountains, or local diffusivity variations which may result from, for example, orographic convection. At the present time, the use of constant-level balloons (tetroons) is probably the best *in-situ* technique for estimating trajectories on the urban scale (Dickson and Angell, 1968; Angell, 1975; Gage and Jasperson, 1976). It is also possible to infer diffusion coefficients from a constant-level balloon system.

The problem of determining regional-scale trajectory variations or local diffusivity differences using a network of either *in-situ* or remote observations is analogous to that of evaluating the vertical temperature gradient on the basis of two independent mercury-in-glass thermometer readings. In general, in order to minimize systematic and random errors, measurements of any gradient are best achieved by either employing a sensor which detects the gradient directly or by physically moving a single instrument, in this case the tetroons,

from one location to another. The rms errors of pibal or raob wind measurements (World Meteorological Organization, 1971) are comparable to the magnitude of urban- to regional-scale variations. Remote probing systems such as Doppler sodar have, in this case, only the advantage of continuous operation. Variations in the vector wind must still be determined from the difference of two "absolute" measurements.

In some cases, urban and mesoscale gradients also may be measured using an instrumented research aircraft. The advantages and limitations of airborne measurements are discussed in detail in the context of grid-point models.

GRID-POINT DIFFUSION MODELS

In an Eulerian grid-point diffusion model such as Shir and Shieh's (1974), values of the required meteorological variables must be specified (at least initially) at each grid point. Even if it were possible, in principle, to obtain measurements of the required parameters at every grid point (16,800 in Shir and Shieh's model), it would be pointless to do so. Most of the time the mean gradient between adjacent grid points will be well within the noise level of available instruments. Furthermore, a high spatial or temporal density of observations for a region within the domain of the model in which "nothing is happening" can in effect reduce the overall signal-to-noise ratio, since concentration of measurement resources there can divert attention from a feature of interest. In fact, one of the principal advantages of an integrated modeling-measurement program is that a "real-time" model can be used to guide, for example, mobile platforms to specific areas of interest. Lacking a model for guidance, it is generally advisable to concentrate observational systems in those locations which are expected to clearly differ either geographically or temporally.

We note also that, in general, application of a grid-point model does not imply that the required observations must be conventional meteorological parameters such as surface temperature and pressure (Table 5). The latter are required only for truly dynamical models such as Anthes' (1978). Rather, parameters such as stability, eddy diffusivity, and mixing height are the important variables normally used for solving the concentration equation.

Continuous measurement of the mixing height at a number of selected grid points within a mesoscale region could be performed easily (and economically). However, it is not at all clear that continuous, quantitative measurements of eddy diffusivity and atmospheric stability over a significant depth of the mixing layer can be obtained anywhere without costly instrumented tower or indirect sounding installations. For urban- or regional-scale areas, there is presently no alternative to model or statistical parameterization of the diffusion variables. In the event that not even local estimates of these are available, the quantities will have to be approximated on the basis of accumulated experience with surface measurements of pollutants dispersed from local sources or, perhaps, some tracer experiments (Pasquill, 1974).

TABLE 5. DATA REQUIREMENTS FOR GRID-POINT DIFFUSION MODELS

Variable	Sensor	Notable Advantages; Disadvantages
$H(t)$	Sodar	Continuous, 1-1.5 km max. height
	Aircraft	Detailed *in-situ* meas.; cost, min. altitude in urban areas
	Helicopter	Maneuverability; cost
	Lidar	Outputs particulate loading; maintenance cost
$\vec{V}(x,y,z,t)$	Radiosonde network	Data analyzed and available; sparse network and only 2 per day
	NWS upper air analyses	Significant local error possible
	Tetroon systems	Outputs traj., cost
$K(x,y,z,t)$	Parameterized in terms of climatology or submodel	

Presently, an important deterrent to the wider application of remote sounding systems is the difficulty of "inverting" the system outputs into the familiar meteorological variables (such as the vertical temperature profile). In the author's opinion, more attention should be given to seeking solutions to the inversion problem which will result in quantitative estimates of selected

air pollution parameters such as vertical diffusivity. For example, using indirect sensing to estimate the vertical flux of a passive contaminant on the basis of a derived vertical temperature profile could be both difficult and highly prone to error. But the same might easily be done on the basis of a sodar-derived C_T^2 or C_v^2 profile. Then, to obtain adequate flux estimates, a regional-scale experiment might require only a few systems situated at locations representative of the major types of underlying terrain.

GRID-POINT DYNAMICAL MODELS

The logistical magnitude of the measurements problem (Table 6) for initialization of dynamical grid-point models is such that, at least for any "operational" applications, we have little choice other than to rely on automated objective synoptic analysis of surface and upper air network data. In any case, the finer the scale, the less will be the sensitivity of a given forecast to initial conditions (Anthes, 1978). That means, however, that precise monitoring of the time-dependent lateral boundary conditions and adequate measurements of critical parameters at selected interior grid points are essential.

Determination of a state parameter (such as pressure) at every surface boundary grid point is certainly not necessary. In fact, instrument-generated noise or local-terrain-related or nonhydrostatic effects would probably generate artificial, large-amplitude acoustic gravity waves in a running model. However, spatially-representative pressure observations on the scale of terrain smoothing ($4\ \Delta\ x$) could control the error growth rate of the mean geostrophic wind. Pressure and other meteorological sensors suitable for such a network are now available in systems such as the Portable Automated Mesonet (PAM) developed at the National Center for Atmospheric Research.

For regional model test and evaluation programs, lateral boundary measurements of state parameters and winds might be obtained using instrumented aircraft. Assuming a ground speed of 70 m/s, about 2 1/2 hr would be required to make a traverse at a single level along one boundary (600 km). Hence one disadvantage of aircraft for mesoscale observations is that the

measurements time scale does not differ greatly from that of many of the important processes. Use of an aircraft to obtain only vertical temperature and humidity profiles is uneconomical, since the operating costs of a vertical profile to 15,000 ft would be comparable to the launch cost of a conventional radiosonde. If a high altitude (> 30,000-ft) jet research aircraft is available, a single pass along a lateral boundary would require less than 1 hr, and dropsondes (Cole et al., 1973) might be cost-effectively launched to obtain vertical profile measurements.

Still, of all the measurement systems which can be used for *in-situ* aerological observations, instrumented aircraft can provide the most diverse and highest quality data set (Atmospheric Technology, 1973). Temperatures to better than 0.3 K, relative humidities to within better than 5%, and winds to the order of 5 m/s are all well within the state of the art. By appropriately designing flight patterns for an aircraft equipped with an inertial guidance system and gust probe, one can also obtain estimates of derived parameters such as turbulent sensible and latent heat, and momentum fluxes, divergence and vorticity estimates, and highly detailed vertical and horizontal gradients of all the various measured parameters (Lenschow, 1975).

Using an instrumented aircraft, Redford (1976) has shown how the intensity of turbulence at various levels changes upwind, above, and downwind of the St. Louis metropolitan area. The primary limiting factor to, for example, aircraft gradient estimates for studies of model initial-condition or validation, is the natural small-scale heterogeneity of the atmosphere (Godowitch, 1976).

Many of the data-processing routines which are required for essentially real-time processing of conventional surface and upper air synoptic observations have been developed in conjunction with studies related to AFOS (Automation of Field Operations and Services) (Cahir and Norman, 1975) and the NCAR PAM system. However, much work (in both hardware and software) remains to be done before it will be possible to process aircraft and indirect sensing observations in real time for use in a running regional- or finer-scale model. For example, consider just the problem of data transmission. On the urban scale, it is possible to use VHF radio telemetry from an aircraft to a centrally located

TABLE 6. DATA REQUIREMENTS FOR REGIONAL GRID-POINT DYNAMICAL MODELS

Variable	Sensor or System
a) Initial Conditions	
T_g, p and q	
(x,y,z,t_o)	NWS surface + upper air analyses
$\vec{V}(x,y,z,t_o)$	Objective analyses of NWS network data
H(t)	Raob and sodar network
b) Lateral Boundary Conditions	
$P(z_o,t)$	Linear microbarometer array
T, p and q	
(z_n,t)	Aircraft
T, p and q(z)	Dropsondes
$\vec{V}(z,t)$	Raob and sodar (for PBL)
c) Upper Boundary Conditions	
T, p and $\vec{V}$	
(x,y,z,t)	NWS upper air analyses
R(x,y,t)	Satellite and surface obs
$R_n(x,y,t)$	Satellite obs
Clouds	Satellite obs
d) Surface Boundary Conditions	
T, p, q, and $\vec{V}$	
(x,y,z,t)	Mesoscale network such as NCAR PAM
$\alpha(x,y,z)$	Seasonal aircraft reconnaissance
Z_o	Estimated from land-use survey

data receiver which is wired to a computer. On the regional scale, however, use of a satellite relay link may be the only reasonable method for transmitting aircraft observations from any location within the model domain.

Although satellite visible and infrared pictures are tremendously helpful in interpreting meteorological phenomena and processes on all scales — including

air-pollution-related studies (Lyons, 1975) — only one sophisticated interactive satellite data-processing system which might be used for air-pollution-related studies is presently under development. This is the so-called MCIDAS (Smith, 1975) system of the University of Wisconsin Space Science and Engineering Center. The main difficulty in using quantitative satellite data in real time is the problem of translating the photographic images into useful numbers (such as plume trajectories or turbidity coefficients).

To my knowledge, neither air-quality variables nor specific pollutants have yet been integrated into a three-dimensional dynamical meteorological model. Consequently, model validation must be based on predictions of common meteorological variables. Of many possible candidates, the distribution and amount of precipitation is one which is sensitive both to the parameterization of physical processes which are also important to pollutant behavior, and to the accuracy and reliability of the particular computational techniques used. Consequently, quality rain data from either existing or new gauge networks or from improved weather radar observations are essential to progress in air pollution meteorology research. The speed and direction of planetary boundary layer winds may be a second useful verification variable. By using boundary layer winds, perhaps measured continuously with Doppler sodar, verification would be far less sensitive to site-specific observational anomalies and/or to limitations of the particular surface layer parameterization scheme employed in the model.

CONSIDERATIONS FOR THE ORGANIZATION OF MESOSCALE EXPERIMENTS

Many of the specific technical components which must be included in planning a major field experiment are summarized by Johnson and Ruff (1975). But significant progress towards an understanding of mesoscale meteorological and air pollution phenomena does not depend, probably, so much today on organization of a particular experimental program as on the relation of that program to other efforts. The present evolutionary trend in experimental meteorology is toward big programs such as the Global Atmospheric Research Program (GARP), the GARP Atlantic Tropical Experiment, and the National Hail Research Experiment. Although an urban-scale experiment of limited scope such as the St. Louis Regional

Air Pollution Study (RAPS) can (just) be managed by a single government agency, the logistics of future mesoscale experiments are such that multiagency support is probably essential if the effort is not to be subcritical in one or more areas of study.

Alternating hot and cold discussions are currently underway regarding several mesoscale experiments. They include the NOAA Severe Environmental Storms and Mesoscale Experiment; the Electric Power Research Institute Sulfate Regional Experiment; an ERDA multistate MAP3S program; and the EPA successor to RAPS, which is also likely to be concerned with sulfate transportation and transformation problems.

I would suggest that — while each of the above programs may succeed to the extent that there will be limited, specific, useful results — conducting them independently does not represent an optimal use of public resources. If measurements and scientific resources were pooled, the coverage would not only increase in proportion to the number of individual components, but also as a consequence of the interactive (covariance) terms.

In the same sense that successful execution of the GATE field program required the combined expertise and resources of many nations, successful completion of a comprehensive national mesoscale experiment will require the unselfish cooperation of every possible U.S. agency and institution.

NOMENCLATURE

C_T^2	temperature structure parameter
C_v^2	velocity structure parameter
D	lateral dimension of box model
E	atmospheric latent heat flux
H	depth of mixing layer
n	level index
p	pressure
q	specific humidity
Q	contaminant concentration

R	global radiation
R_n	net radiation
S	source strength
S_a	atmospheric sensible heat flux
S_s	soil sensible heat flux
t	time
t_o	initial time
T	air temperature
T_s	soil surface temperature
$\vec{V}$	wind
$\vec{V}_H$	horizontal wind
w	vertical veloctiy
z	height
z_o	aerodynamic roughness length
x	albedo
ε	emissivity
θ	direction of horizontal wind
σ	Stefan-Boltzmann constant
σ_y	horizontal dispersion coefficient
σ_z	vertical dispersion coefficient
ϕ	direction of vertical wind

REFERENCES

Aerovironment. 1976. Monostatic Acoustic Radar. Aerovironment, Inc., Pasadena, California.

Angell, J. K. 1975. The Use of Tetroons for Probing the Atmospheric Boundary Layer. Atmos. Tech. 7:38-43.

Anthes, R. A. 1978. Meteorological Aspects of Regional-Scale Air-Quality Monitoring. In: Select Research Group in Air Pollution Meteorology, Third Annual Progress Report. U.S. Environmental Protection Agency, Research Triangle Park, North Carolina.

Atmospheric Technology. 1973. Issue on NCAR Research Aviation Facility.

Benkley, C. 1976. Studies of Planetary Boundary Layer Growth Using Sodar Validation. M.S. Thesis. The Pennsylvania State University, University Park, Pennsylvania.

Blackadar, A. K. 1978. High-Resolution Models of the Planetary Boundary Layer. In: Select Research Group in Air Pollution Meteorology, Third Annual Progress Report. U.S. Environmental Protection Agency, Research Triangle Park, North Carolina.

Cahir, J. J., and J. M. Norman. 1975. A Forecaster-Initiated Real-Time Cross Section Analysis for AFOS. Report 5-35290 to the National Weather Service, The Pennsylvania State University, University Park, Pennsylvania.

Cole, H. L., S. Rossby, and P. K. Govind. 1973. The NCAR Wind-Finding Dropsonde. Atmos. Tech. 2:19-24.

Dabberdt, W. F., and P. A. Davis. 1974. Determination of Energetic Characteristics of Urban-Rural Surfaces in the Greater St. Louis Area. Paper presented at Symposium on Atmospheric Diffusion and Air Pollution, American Meteorological Society, Santa Barbara, California, 9-13 September.

Derr, V. E. 1972. Remote Probing of the Troposphere. C55.602.T75, U.S. Government Printing Office, Washington, D.C.

Dickson, C. R., and J. K. Angell. 1968. Eddy Velocities in the Planetary Boundary Layer as Obtained from Tetroon Flights at Idaho Falls. J. Appl. Meteor. 7:986-993.

Gage, K. S., and W. H. Jasperson. 1976. Diffusion Coefficients Estimated from Turbulence Data Measured by the METRAC Positioning System in Minneapolis Field Test. In: Proceedings, Third Symposium on Atmospheric Turbulence, Diffusion, and Air Quality, Raleigh, North Carolina, 19-22 October.

Gifford, F. A., and S. R. Hanna. 1973. Modeling Urban Air Pollution. Atmos. Environ. 7:131-136.

Godowitch, J. M. 1976. Case Studies of Aircraft and Helicopter Temperature Measurements over St. Louis, MO during RAPS. M.S. Thesis. The Pennsylvania State University, University Park, Pennsylvania.

Högström, U. 1964. An Experimental Study on Atmospheric Diffusion. Tellus 16:205-251.

Johnson, W. B. 1971. Lidar Measurements of Plume Diffusion and Aerosol Structure. In: Proceedings, Conference on Air Pollution Meteorology, American Meteorological Society, Raleigh, North Carolina, April.

Johnson, W. B., and R. E. Ruff. 1975. Observational Systems and Techniques in Air Pollution Meteorology. In: Lectures on Air Pollution and Environmental Impact Analyses. American Meteorological Society, Boston, Massachusetts.

Kaimal, J. C. 1975. Sensors and Techniques for Direct Measurement of Turbulent Fluxes and Profiles in the Atmospheric Surface Layer. Atmos. Tech. 7:7-14.

Kondratyev, K. Y. 1969. Radiation in the Atmosphere. Academic Press, New York.

Lenschow, D. H. 1975. Use of Aircraft for Probing the Atmospheric Boundary Layer. Atmos. Tech. 7:44-49.

Lettau, H. H. 1970. Physical and Meteorological Basis for Mathematical Models of Urban Diffusion Processes. In: Proceedings of the Symposium on Multiple-Source Urban Diffusion Models, A. C. Stern, ed. APCO Publication AP-86, U.S. Environmental Protection Agency, Research Triangle Park, North Carolina.

Little, C. G. 1972. Status of Remote Sensing of the Troposphere. Bull. Amer. Meteor. Soc. 53(10):936-949.

Lyons, W. A. 1975. Turbulent Diffusion and Pollutant Transport in Shoreline Environments. In: Lectures on Air Pollution and Environmental Impact Analyses. American Meteorological Society, Boston, Massachusetts.

Morris, A. L., D. B. Call, and R. B. McBeth. 1975. A Small Tethered Balloon Sounding System. Bull. Amer. Meteor. Soc. 56:964-969.

Ottersten, H., K. R. Hardy, and C. G. Little. 1973. Radar and Sodar Probing of Waves and Turbulence in Statistically Stable Clear-Air Layers. Boundary Layer Meteor. 4:47-89.

Pasquill, F. 1961. The Estimation of the Dispersion of Windborne Material. Meteor. Mag. 90(1063):33-49.

Pasquill, F. 1974. Atmospheric Diffusion. Wiley, New York.

Redford, T. G. 1976. Airborne Measurements of Atmospheric Turbulence in the St. Louis Metropolitan Area during RAPS. M.S. Thesis. The Pennsylvania State University, University Park, Pennsylvania.

Russel, P. B., E. E. Uthe, F. L. Ludwig, and N. A. Shaw. 1974. A Comparison of Atmospheric Structure as Observed with Monostatic Acoustic Sounder and Lidar Techniques. J. Geophys. Res. 79:5555-5566.

Sellers, W. D. 1965. Physical Climatology. University of Chicago Press, Chicago, Illinois.

Shir, C. C., and L. J. Shieh. 1974. A Generalized Urban Air Pollution Model and Its Applications to the Study of the SO_2 Distribution in the St. Louis Metropolitan Area. J. Appl. Meteor. 13:185-204.

Slade, D. H. 1968. Meteorology and Atmospheric Energy. TIO-24190, FTSTI, Springfield, Virginia.

Smith, E. 1975. The MCIDAS System. GE-13, IEEE Trans. Geos. Elect.

Tennekes, H. 1973. A Model for the Dynamics of the Inversion Above a Convective Boundary Layer. J. Atmos. Sci. 30:558-567.

Tennekes, H. 1978. The Effects of Mixing-Height Variability on Air-Quality Simulation Models. In: Select Research Group in Air Pollution Meteorology, Third Annual Progress Report. U.S. Environmental Protection Agency, Research Triangle Park, North Carolina.

Tennekes, H., and A. P. van Ulden. 1974. Short-Term Forecasts of Temperature and Mixing Height on Sunny Days. In: Proceedings, Symposium on Atmospheric Diffusion and Air Pollution, American Meteorological Society, Santa Barbara, California, 9-13 September.

Thomson, D. W. 1975. Acdar Meteorology: The Application and Interpretation of Atmospheric Acoustic Sounding Measurements. In: Proceedings, Third Symposium on Meteorological Observation and Instrumentation, American Meteorological Society, Washington, D.C., 10-13 February.

Turner, D. B. 1970. Workbook of Atmospheric Dispersion Estimates. PHS-999-AP-26, U.S. Environmental Protection Agency, Research Triangle Park, North Carolina. 88 pp.

World Meteorological Organization. 1971. Guide to Meteorological Instrument and Observing Practices. WMO No. 8, TP. 3, World Meteorological Organization, Geneva, Switzerland.

Wyngaard, J. C. 1975. Modeling the Planetary Boundary Layer - Extension to the Stable Case. Boundary Layer Meteor. 9:441-460.

Wyngaard, J. C., Y. Izumi, and S. A. Collins. 1971. Behavior of the Refractive Index Structure Parameters Near the Ground. J. Opt. Soc. Amer. 61(12):1646-1650.

TECHNICAL REPORT DATA
(Please read Instructions on the reverse before completing)

1. REPORT NO.	2.	3. RECIPIENT'S ACCESSION NO.
EPA-600/4-78-049		

4. TITLE AND SUBTITLE	5. REPORT DATE
SELECT RESEARCH GROUP IN AIR POLLUTION METEOROLOGY Third Progress Report	August 1978 6. PERFORMING ORGANIZATION CODE

7. AUTHOR(S)	8. PERFORMING ORGANIZATION REPORT NO.
R. Anthes, A. Blackadar, R. Kabel, J. Lumley, H. Tennekes and D. Thompson	

9. PERFORMING ORGANIZATION NAME AND ADDRESS	10. PROGRAM ELEMENT NO.
Dept. of Meteorology and Center for Air Environment Studies. The Pennsylvania State University University Park, Pennsylvania 16802	1AA603 AB-02 (FY-78) 11. CONTRACT/GRANT NO. R-800297

12. SPONSORING AGENCY NAME AND ADDRESS	13. TYPE OF REPORT AND PERIOD COVERED
Environmental Sciences Research Laboratory - RTP, NC Office of Research and Development U.S. Environmental Protection Agency Research Triangle Park, North Carolina 27711	Interim 10/74 - 10/76 14. SPONSORING AGENCY CODE EPA/600/09

15. SUPPLEMENTARY NOTES

16. ABSTRACT

Six individual investigators, who have conducted different but related meteorological research, present in-depth technical reviews of their work. Prime conclusions are that (1) a scale analysis shows that different models are necessary for meteorological processes on urban, regional and global scales; (2) for high resolution models of the nocturnal planetary boundary layer, K theory models are very efficient, realistic and useful; (3) the mixing height has a significant effect on climatology models; (4) second moment closure methods are useful for convective situations, properly testing counter gradient fluxes; (5) natural sources and pollutants acting at the surface of the earth are important for air quality simulation models; and (6) a combination of conventional micrometeorological and acoustic sounder techniques are sufficient for verifying locally applied inversion use, box, and regional scale modles, and urban and regional models require a variety of in situ and remote observation.

17. KEY WORDS AND DOCUMENT ANALYSIS

a. DESCRIPTORS	b. IDENTIFIERS/OPEN ENDED TERMS	c. COSATI Field/Group
* Air pollution * Meteorology * Mathematical models * Boundary layer		13B 04B 04A 12A 20D

18. DISTRIBUTION STATEMENT	19. SECURITY CLASS *(This Report)*	21. NO. OF PAGES
RELEASE TO PUBLIC	UNCLASSIFIED	232
	20. SECURITY CLASS *(This page)*	22. PRICE
	UNCLASSIFIED	

EPA Form 2220-1 (9-73)

U.S. ENVIRONMENTAL PROTECTION AGENCY
Office of Research and Development
Environmental Research Information Center
Cincinnati, Ohio 45268

OFFICIAL BUSINESS
PENALTY FOR PRIVATE USE, $300
AN EQUAL OPPORTUNITY EMPLOYER

POSTAGE AND FEES PAID
U S ENVIRONMENTAL PROTECTION AGENCY
EPA-335

If your address is incorrect, please change on the above label tear off, and return to the above address.
If you do not desire to continue receiving these technical reports, CHECK HERE ☐, tear off label, and return it to the above address,

EPA-600/4-78-049